Gaseous hydrocarbon cycling and lipid biogeochemistry in cold and hot seep sediments

Dissertation

zur Erlangung des Doktorgrades

der Naturwissenschaften

- Dr. rer. nat. -

Am Fachbereich Geowissenschaften

der Universität Bremen

vorgelegt von

Min Song

Bremen

June 2020

The presented study was conducted from December 2015 to June 2020 in the Organic Geochemistry research group at the MARUM- Center for Marine Environmental Sciences and Department of Geosciences, University of Bremen, under the supervision of Prof. Dr. Kai-Uwe Hinrichs and Dr. Florence Schubotz. Min Song was further supported by the China Scholarship Council (CSC).

1. reviewer: Prof. Dr. Kai-Uwe Hinrichs

2. reviewer: Prof. Dr. Lorenz Schwark

Dissertation colloquium: July 22, 2020

“There is a cave- and there is a way out.”

Plato’s allegory of the Cave in *Republic*-

Frank Wilczek, “*A Beautiful Question: Finding Nature's Deep Design*”

Contents

Abstract

The release of hydrocarbon gases at the seafloor is a rich energy source for chemosynthetic ecosystems, but can also impact the climate when entering the atmosphere. The overall objective of this thesis was to explore the formation and degradation pathways of hydrocarbon gases in marine sediments and to characterize the involved microorganism in these processes. Two contrasting seep systems were explored for this purpose: the cold, methane-laden US Atlantic Margin (USAM) sediments and the hot, methane and higher hydrocarbon impregnated hydrothermal sediments of the Guaymas Basin.

Stable carbon isotopic composition ($\delta^{13}C$) of hydrocarbons are commonly used to determine their origin. Hydrocarbon gases in hydrothermal sediments of the Guaymas Basin exhibited unusual isotope patterns. While methane had $\delta^{13}C$ values typical for a thermogenic origin, higher hydrocarbons were notably enriched in ^{13}C and displayed an isotope pattern that is reversed relative to thermogenic gases, i.e. $\delta^{13}C$ ethane > $\delta^{13}C$ propane > $\delta^{13}C$ *n*-butane > $\delta^{13}C$ *n*-pentane. We therefore hypothesized an alternative formation process for these hydrocarbons by catalytic reduction of volatile fatty acids (VFAs), which were isotopically enriched due to prior equilibration of their carboxyl carbon with dissolved inorganic carbon under high temperatures. This hypothesis was confirmed by hydrous pyrolysis experiments at 350°C and 400 bar, which demonstrated the proposed pathway in two steps: (*i*) carboxyl carbon exchange of VFAs with ^{13}C-bicarbonate and (*ii*) formation of ^{13}C-labeled ethane and propane from the reduction of 2-^{13}C-acetate, where each reaction was governed by the abundance of H_2. Gibbs free energy computations indicate that reduction of acetate to ethane is more favorable over propane under environmental conditions prevailing in the Guaymas Basin subsurface.

In order to explore the microbial regulation of methane and higher hydrocarbons in the sediments, intact polar lipid (IPL) biomarkers were used as the tool to evaluate microbial imprint and community structure at the USAM and the Guaymas Basin. At the USAM, the diversity and abundance of archaeal IPLs were closely linked to the *in situ* microbial community composition and was well-constrained by methane flux and organic carbon content. (*i*) At a site with high methane flux, archaeal IPLs were dominated by diagnostic lipid biomarkers for anaerobic methanotroph archaea (ANME), these including mono- and diglycosidic glycerols dialkyl glycerol tetraethers (1G- and 2G-GDGTs) with 0 to 2 cyclopentane rings, as

well as archaeol- and hydroxyarchaeol-based glycosidic and phospholipids. (*ii*) At a site with lower methane flux and high organic matter content, the recently identified glycosidic butanetriol dibiphytanyl glycerol tetraether and pentanetriol dibiphytanyl glycerol tetraether were more abundant in the archaeal lipid pool. These lipids were closely related to benthic archaeal groups including Miscellaneous Crenarchaeotal Group, Marine Benthic Group-B and Thermoprofundales, indicating that heterotrophic processes prevailed over methanotrophy. (*iii*) At a site with low methane flux and low organic carbon content, IPL concentrations were extremely low, indicating only small contributions from sedimentary microorganisms.

In the hydrothermal sediments of Guaymas Basin (3 to 70 °C), archaeol-based IPLs generally occurred in surface sediments, whereas 2G-GDGTs increased with depth, indicating different zonation of ANME communities, from respective ANME-2 and ANME-1. In cool sediments 2G-GDGTs were dominated by GDGT-2, whereas in hydrothermally heated sediments GDGT-4 was more predominant pointing to respective mesophilic and thermophilic ANME-1 imprints. Moreover, abundance of glycerol monoalkyl glycerol tetraethers (GMGT)-based lipids was substantially elevated in hydrothermally heated sediments, indicating *in situ* production by thermophilic archaea. In these sediments isotopic evidence also pointed to the microbial consumption of ethane, propane and butane. The recently identified overly branched (OB-), isoprenoid-branched (IB-) and scarcely branched (SB-) GDGTs were for the first time detected in hydrothermal sediments. The abundance of OB-GDGTs increased with temperature and significantly correlated with GMGTs, suggesting *in situ* production by yet unknown thermophilic microorganisms. In general, temperature appears to be the primary controlling factor on the distribution and composition of microbial ether lipids. Adaptive strategies to elevated temperatures include a higher degree of cyclization, which reduces membrane fluidity and proton permeability; the extra covalent bond between the two alkyl chains in GMGT and the addition of methyl groups in OB-GDGTs may further strengthen cell membranes to withstand thermal stress.

Zusammenfassung

Die Freisetzung gasförmiger Kohlenwasserstoffe am Ozeanboden ist eine reichhaltige Energiequelle für chemosynthetische Ökosysteme und kann darüber hinaus bei Eintritt in die Atmosphäre das Klima beeinflussen. Das übergeordnete Ziel dieser Arbeit war es Bildungs -und Abbauwege gasförmiger Kohlenwasserstoffe in marinen Sedimenten zu ergründen und die in diese Prozesse involvierten Mikroorganismen zu charakterisieren. Zwei gegensätzliche Seep Systeme wurden zu diesem Zweck untersucht: Die kalten, methanhaltigen Sedimente des US Atlantic Margins (USAM), sowie die heißen, Methan und höhere kohlenwasserstoffhaltigen hydrothermalen Sedimente des Guaymas Beckens.

Die Zusammensetzung stabiler Kohlenstoffisotope ($\delta^{13}C$) von Kohlenwasserstoffen wird gewöhnlich genutzt um deren Ursprung zu bestimmen. Gasförmige Kohlenwasserstoffe in hydrothermalen Sedimenten des Guaymas Beckens zeigten ungewöhnliche Isotopenmuster. Während Methan für Gase thermogenen Ursprungs typische $\delta^{13}C$ Werte aufwies, waren höhere Kohlenwasserstoffe deutlich angereichert in dem schweren Isotop ^{13}C und zeigten ein umgekehrtes Isotopenmuster im Vergleich zu thermogenen Gasen, d.h. $\delta^{13}C$ Ethan > $\delta^{13}C$ Propan > $\delta^{13}C$ *n*-Butan > $\delta^{13}C$ *n*-Pentan. Daher schlugen wir einen alternativen Bildungsprozess für diese Kohlenwasserstoffe durch katalytische Reduktion von kurzkettigen Fettsäuren (VFAs) vor, welche durch vorherige Äquilibrierung des Kohlenstoffs der Carboxygruppe mit gelöstem anorganischem Kohlenstoff unter hohen Temperaturen isotopisch angereichert wurden. Diese Hypothese wurde mit wässrigen Pyrolyseexperimenten bei 350°C und 400 bar bestätigt, in einem zweistufigen Reaktionsablauf: (*i*) Austausch des Kohlenstoffs der Carboxygruppe von VFAs mit ^{13}C-Bikarbonat und (*ii*) Bildung von ^{13}C-angereichertem Ethan und Propan aus der Reduktion von 2-^{13}C-Acetat, wobei jede Reaktion durch die Abundanz von H_2 reguliert wird. Berechnungen der Gibbs Energie weisen darauf hin, dass die Reduktion von Acetat zu Ethan statt Propan unter den vorherrschenden Umweltbedingen im Ozeanboden des Guaymas Beckens energetisch begünstigt wird.

Um die mikrobielle Regulation von Methan und höheren Kohlenwasserstoffen in den Sedimenten zu untersuchen, wurden Biomarker intakter polarer Lipide (IPL) genutzt um die mikrobielle Prägung und die mikrobielle Gemeinschaft am USAM und im Guaymas Becken zu evaluieren. Am USAM waren Diversität und Abundanz von archaeelen IPL eng mit der Zusammensetzung der *in situ* mikrobiellen Gemeinschaft

verknüpft und waren abhängig von Methanfluss und Gehalt an organischem Kohlenstoff. (*i*) Am Standort mit hohem Methanfluss wurden archaeele IPLs von anaerobe methanotrophe Archaeen (ANME)-diagnostische Lipidbiomarkern dominiert, welche mono- und diglycosidische Glycerol und-Dialkylglycerol-Tetraether (1G- und 2G-GDGTs) Lipide mit 0 bis 2 Cyclopentanringen, sowie Archaeol- und Hydroxyarchaeol-basierte Glycerol und Phospholipide miteinschließen. (*ii*) Am Standort mit niedrigerem Methanfluss und hohem Organikgehalt machten die kürzlich identifizierten glykosidischen Butantriol-Dibiphytanyl Glycerol Tetraether und Pentantriol Dibiphytanyl Glycerol Tetraether einen höheren Anteil der archaeelen Lipide aus. Diese Lipide standen eng im Zusammenhang mit benthischen archaeelen Gruppen, einschließlich der Miscellaneous Crenarchaeotal Group, der Marine Benthic Group-B und Thermoprofundales, was darauf hinweist, dass überwiegend heterotrophe Prozesse statt Methanotrophie vorherrschten. (*iii*) An Standorten mit niedrigem Methanfluss und niedrigem Organikgehalt waren die IPL-Konzentrationen sehr niedrig, was auf einen nur geringen Beitrag im Sediment lebender Mikroorganismen zum Lipidfundus hinweist.

In den hydrothermalen Sedimenten des Guaymas-Beckens (3 bis 70°C) traten Archaeol-basierte IPLs generell in Oberflächensedimenten auf, während 2G-GDGTs mit zunehmender Sedimenttiefe zunahmen, was eine unterschiedliche Zonierung von ANME Gemeinschaften der entsprechenden ANME-2 und ANME-1 anzeigt. In kalten Sedimenten wurden 2G-GDGTs durch GDGT-2 dominiert, während in hydrothermal erhitzen Sedimenten GDGT-4 überwiegte, was auf die Präsenz der entsprechenden mesophilen und thermophilen ANME-1 hindeutet. Darüber hinaus war die Abundanz von Lipiden mit dem Grundgerüst Glycerol Monoalkyl Glycerol Tetraethern (GMGT) in hydrothermal erhitzen Sedimenten deutlich erhöht, was auf eine *in situ* Produktion durch thermophile Archaeen hinweist. In diesen Sedimenten deuteten Isotopenmuster außerdem auf mikrobiellen Konsum von Ethan, Propan und Butan hin. Die kürzlich identifizierten übermäßig verzweigten (OB-), isoprenoidverzweigten (IB-) und wenig verzweigten (SB-) GDGTs wurden erstmals in hydrothermalen Sedimenten nachgewiesen. Die Abundanz von OB-GDGTs nahm mit erhöhter Temperatur zu und korrelierte signifikant mit GMGTs, was auf eine *in situ* Produktion durch noch unbekannte thermophile Organismen hinweist. Die Temperatur scheint generell der primäre Kontrollfaktor für die Verteilung und Zusammensetzung von mikrobiellen Etherlipiden zu sein. Adaptive Strategien gegenüber erhöhten Temperaturen beinhalten höhere Zyklisierungsgrade, was die Membranfluidität und die Protonenpermeabilität verringert; außerdem können die zusätzliche kovalente Bindung zwischen den beiden Alkylketten von GMGT und zusätzliche Methylgruppen in OB-GDGTs Zellmembranen gegenüber thermischer Belastung widerstandsfähiger machen.

Acknowledgements

For me, the four and a half years of PhD life is an excellent exploration of not only science and nature, but also of myself as a human being, a journey of realizing who I am, and what I can be. It has to be acknowledged that particularly at the end of this journey, I recalled again and again of Frodo Baggins' path to Mount Doom. As one can imagine, without the help and support of Sam, and all the other buddies, Frodo wouldn't be able to make it! I am not saying that I am doing something as great as Frodo does, I just have to acknowledge the power of kindness, friendship and love, which I've been given unconditionally by people around me. Without you, this would not have happened!

A special thanks to Lorenz Schwark for agreeing to be my second reviewer. I hope you will find this thesis worthwhile to read.

Kai, thanks for giving me the opportunity to join your fantastic working group in the first place. I believe that was a life-changing moment for me. Thank you for being so open-minded, patient and kind. I enjoyed those many discussion meetings, where we exchanged ideas which felt like...playing ping pong games. From you, the best supervisor I can imagine, I learned the most important skill of thinking thoroughly and independently as a scientist. Thank you for always taking my ideas seriously, from which I gained much self-confidence, another equally important ability for a scientist. Thank you for this invaluable gift!

Florence, my second supervisor- I know no language good enough to express my gratitude to you! Flo, thank you for always being there, not only as a supervisor for my study but also as my spiritual mentor. From the first days you enthusiastically introduced me into the labs, patiently tutored me on identifying lipids, up until the final days of contributing your time and ideas unconditionally on the papers and the thesis. Thank you for always remembering to encourage and cheer me up! I admired your enthusiasm for science, your optimistic attitude towards difficulties and your great patience for your students!

Thanks Andreas and Gunter for being my thesis committee members. Thank you Andreas for introducing me to the fantastic Guaymas Basin. I enjoyed our discussion meetings as much as our little coffee chats. Thank you Gunter for spending the nice time together on *Atlantis*, and for providing your ideas during my committee meetings.

Thank you to all the Hinrichs Lab members: Xavi, Jenny, Yvonne, Evert, Heidi, Julius for keeping the lab running smoothly and efficiently, and being there ready to help whenever I approached. Thank you Sarah, Igor, Bernhard, Qing-Zeng, Vicente, Sandra, Lisa, Rebecca, Ceng-Ling, Susanne, Marcus, Martin, Lars, Verena, Tiffany, Lukas, Niro, Stani and many other former members and Master students not listed here for creating such a wonderful and inspiring working atmosphere. Thank you to all my co-authors on my papers. Kevin, thank you for being such an encouraging person!

I would also like to thank my former and current office mates and friends. Matthias, it was truly fun having shared the office with you. Sandra, I miss your little funny drawings, our silly jokes and particularly the unbelievably tasty vegan food you made! Not to forget our big trip to China in the near future. Lisa, I already miss our spontaneous two-days-one-night vacation and our swimming sessions. I would love to do

it again! A very special thanks to my other office mate Jonas for being my best friend and my love. With you besides me, I know I can beat any difficulties I may encounter in life. At the same time, I would also like to thank your lovely family, for always making me feel welcome. Thanks to my former landlord Dehning for trying to teach me German (…I will pick it up…soon I guess). Thank you, Ute, Wilhelm and Lukas, for hosting me in your house for the past year. You've always been nice and caring, and regarded me as one family member. I appreciate it!

Many thanks are sent to my bouldering buddies: Oli, Manu, Xavi, Bernhard, Vicente, Christian, Wojciech...for hanging out and having fun after work in those good old days! An outdoor climbing should do one day.

Many thanks also go to my friends in China and my family. Thank you for your love and support. Thanks China Scholarship Council supported me for my four-years study.

谢谢丽妮一直是我最知心的朋友， 以及像姐姐一样的存在。谢谢妈妈爸爸一直以来的支持和理解，你们永远是我心中最重要的人。最后，谢谢所有关心支持我的朋友们！

List of Figures

List of Tables

CHAPTER I

General Introduction

Earth's morphology is constantly shaped by plate tectonics. As a consequence, some of the most unusual features are found on the seafloor, including hydrothermal vents and cold seeps (Fig. I.1) Hydrothermal vents occur along mid-oceanic ridges, where hot magma is convected from mantle towards the surface causing seafloor spreading. Seawater that is circulated through the crust is expelled as hot fluids rich in sulfur, metals, hydrogen and hydrocarbons at temperatures of up to 350 to 400 °C. By contrast, cold seeps are frequently found at convergent continental margins, where subduction of the oceanic plate underneath the less dense continental plate results in compression and geothermal alteration of deep sediments and ultimately the release of gases and fluids. Hydrothermal vents have been considered as the "window into the seafloor" (Deming and Baross, 1993) and are frequently regarded as crucibles for life's origin, whereas cold seeps are found to be the largest reservoir for methane, a greenhouse gas that is much more effective than CO_2 in the atmosphere (cf. Wuebbles and Hayhoe, 2002).

This thesis will take a closer look at sources and sinks of hydrocarbon gases, from methane through pentane, in different vent and seep settings, and the microbial communities involved in their cycling. Hydrocarbon gas has a large impact on Earth system processes including but not limited to global carbon cycling, climate change and gas deposits. Although hydrocarbon gas has been the focus of many studies mainly pertaining to petroleum exploration, novel formation pathways (Kelley, 1996; Lollar et al., 2002; Proskurowski et al., 2008) and alterations after formation (e.g., Cruse and Seewald, 2010; Kniemeyer et al., 2007) have been proposed throughout past years. Some ideal locations for in-depth investigations of the formation and consumption of these compounds are the cold seeps and hydrothermal vents. These settings often host substantial amount of natural gas formed from tightly linked physical, chemical and biological processes.

This introduction section firstly describes hydrothermal vent and cold seep systems, then discusses the various sources and types, as well as alteration and formation of hydrocarbon gases in the marine environment. This is followed by an introduction of the research areas, the Guaymas Basin hydrothermal

vent and the US Atlantic margin cold seep system. Lastly, the research approach of using lipid biomarkers to characterize microbial community composition is outlined.

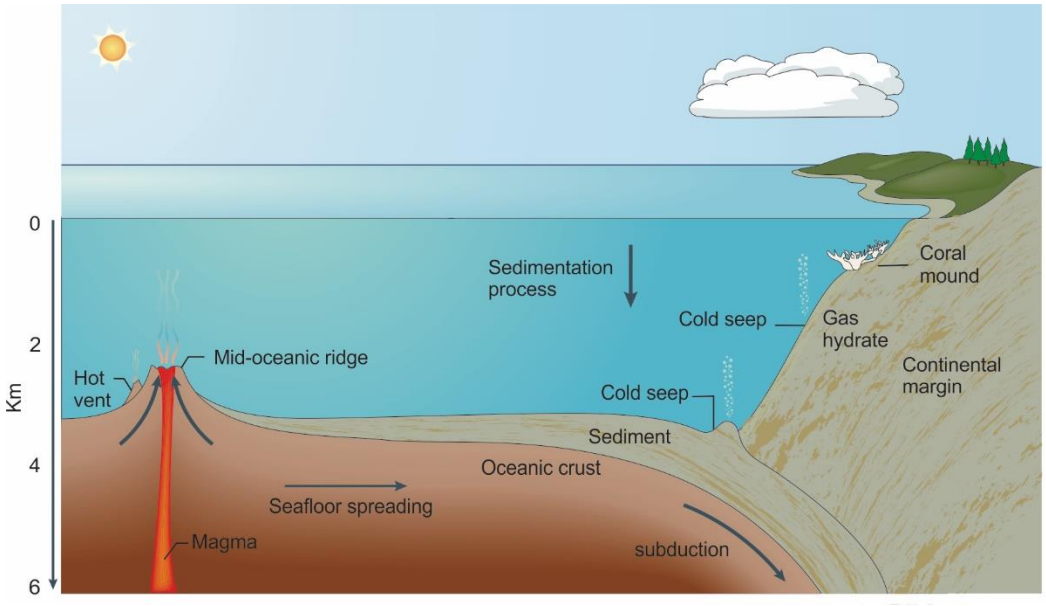

Figure I.1. Schematic overview of seafloor structures, showing a mid-oceanic ridge where hydrothermal vents are located, a subduction zone and a continental margin where cold seeps occur. Figure adopted from Jørgensen and Boetius (2007).

I.1. COLD AND HOT SEEPS IN THE MARINE ENVIRONMENT

I.1.1. Hydrothermal vents

In 1977, scientists discovered the first submarine hydrothermal system at the Galapagos Rift (Corliss et al., 1979), which has fundamentally changed our view of the dark ocean and its role in the global Earth system and biogeochemical cycles. The seafloor was historically thought to be uniform in composition and a scarcely populated desert-like environment, owing to its remoteness from photosynthetic ecosystems. In contrast to this, highly productive and densely populated benthic communities of giant tube worms, clams and microbial biofilms were found to live within the hydrothermal vent areas (Corliss et al., 1979). The hydrothermal ecosystem is sustained by microorganisms as primary producers that thrive on chemical energy derived from water-rock reactions instead of photosynthesis. Hydrothermal fluids are rich in varying amounts of H_2, H_2S, CH_4 and higher hydrocarbons (cf. Deborah S. Kelley et al., 2002), which are potent electron donors to sustain chemosynthetic life. These microorganisms form the basis of a flourishing ecosystem, thereby allowing hydrothermal vent settings to become one of the most eminent biological oases in the dark submarine environment.

So far, more than 500 vent fields have been documented and it is suggested that ~900 more vent fields remain to be discovered (Beaulieu et al., 2013; Beaulieu et al., 2015). Submarine hydrothermal vents often occur at or near tectonic and/or volcanic boundaries, including mid-ocean ridges, volcanic arcs and back-arc spreading centers where magmatic heat sources drive the hydrothermal circulation (e.g., Michael et al., 2003; Dunn and Martinez, 2011; Nakagawa et al., 2006; Teske et al., 2016). There are generally two kinds of hydrothermal vents on the seafloor: the black smoker type and the white smoker type. Black smoker vents are frequently discovered on mid-ocean ridges driven by a magma-chamber that resides below seafloor spreading zones. Here, hot hydrothermal fluids with temperatures up to approximately 350-400°C are typically acidic and rich in dissolved metals, sulfur species and silica; as hot fluids mix with cool seawater on the seafloor, large amounts of sulfide minerals precipitate resulting in the dark color of the fluids, and build up the chimney-like structures around the vent. By contrast, white smoker vents occur off-axis of the mid-ocean ridge with cooler fluids (250-300°C) than those emitted by black smokers. White smoker type hydrothermal vents are driven by the exergonic process of serpentinization rather than the circulation of magma. A notable example is the Lost City hydrothermal vent field in the central Atlantic Ocean (Kelley et al., 2005). Hydrothermal fluids of white smokers are alkaline, they precipitate silica and barium or calcium sulfates following mixing with seawater, thereby giving rise to the white color of the precipitates forming the chimneys. The interactions between alkaline hot fluids and seawater are suggested to have provided favorable conditions for the emergence of life (cf. Martin et al., 2008).

I.1.2. Cold seeps

Cold seeps, first identified at the Florida Escarpment in the northern Gulf of Mexico (Paull et al., 1984), represent another biological oases with dense benthic fauna, similar to those found at hot vents, sustained by chemical energy on the dark seafloor. Unlike hydrothermal vents, cold seeps are emitting methane-rich gases and fluids out of the seafloor at near ambient temperatures, driven by a variety of geophysical processes such as plate subduction, salt diapirism or dissociation of methane hydrates that cause over pressuring in the source beds. Gas seepage forms unique features on the seafloor such as mud volcanoes, pockmarks and methane seeps, where fluidized muds and/or gas-charged fluids are discharged out of the seafloor (Milkov, 2000; Dando et al., 1991; Skarke et al., 2014).

Under certain high pressure and low temperature conditions, gas (mainly methane) saturation in sedimentary pore water results in gas hydrate formation. Submarine gas hydrates are estimated to sequesters approximately 500-2,500 Gt of total methane carbon globally (Milkov, 2004). This makes them one of the most abundant unconventional energy resources on Earth. Meanwhile, gas hydrates are susceptible to global

warming and can alternatively become a powerful trigger for climate change if largely dissociated (Hinrichs et al., 2003; Biastoch et al., 2011). Thus, understanding the fate of methane in cold seep settings are of essential importance to better understand and predict climate feedbacks.

I.2. CYCLING OF HYDROCARBON GASES IN MARINE SEDIMENTS

I.2.1. Sources of hydrocarbon gases

Our knowledge on the formation of natural gas was initially obtained from petroleum exploration studies. According to conventional wisdom, natural gas is mostly sourced from microbially-mediated diagenesis or thermal conversion of organic matter in sedimentary rocks as a function of thermal maturity (Claypool and Kvenvolden, 1983). While methane is the most abundant component in natural gas, and is mainly formed by biological processes in marine sediments, the higher hydrocarbons are conventionally assigned to a thermogenic origin (e.g., Prinzhofer and Huc, 1995).

Biogenic methane is produced by methanogenic archaea which are anaerobes and can live in a wide temperature range (Valentine and Boone, 2000). In the marine environment, methanogens typically utilize H_2 and CO_2 as energy sources, while other substrates including acetate and methylated compounds (methanol, methylamines, or methanethiol) are also used (cf. Whitman et al., 2006). Biogenic methane can further be produced by other organisms than methanogens, a recent study reported Cyanobacteria as notable contributors to methane production in the upper ocean (Bižić et al., 2020). By comparison, biological formation of higher hydrocarbons in marine sediments is less common. Microbial ethanogenesis and propanogenesis have been reported in cold and deeply buried sediments, where stable carbon isotope analysis and thermodynamic calculations indicated microbial reduction of acetate as the formation pathway for ethane, while a third carbon is incorporated from pore water dissolved inorganic carbon for the formation of propane (Hinrichs et al., 2006).

Abiotic sourced methane and other light hydrocarbons have been identified at different settings on Earth, in particular in seafloor hydrothermal systems. Here, water-rock interactions involving Fischer-Tropsch-type reactions (Proskurowski et al., 2008), reduction of carbon dioxide that occurs during magma cooling (Kelley, 1996), and crystalline rocks from continental crust (Lollar et al., 2002) have been suggested as possible mechanisms involved in the abiotic formation of hydrocarbon gases..

Stable carbon isotope compositions ($\delta^{13}C$) of hydrocarbon gases have proven as a powerful tool to aid in distinguishing their sources (e.g., Whiticar, 1999; Wang et al., 2015). It was found that microbially sourced hydrocarbons are dominated by methane with abundance ratios of $C_1/(C_2+C_3)$ greater than 1000

and the $\delta^{13}C_1$ values lower than -55‰ (Bernard et al., 1976). Typically, thermogenic gases consist of a higher abundance of C_{2+} hydrocarbons (Hunt, 1984; Claypool and Kvenvolden, 1983) and the $\delta^{13}C_1$ values are more positive (> -60 to -40‰, Schoell, 1988). As ^{12}C-^{12}C bonds from the source organic compounds are kinetically more readily cleaved relative to ^{13}C-^{12}C bonds, thermogenic hydrocarbon gases become more enriched in ^{13}C with increasing molecular weight: $\delta^{13}C_1 < \delta^{13}C_2 < \delta^{13}C_3 < \delta^{13}C_4 < \delta^{13}C_5$ (Clayton, 1991). This isotopic distribution pattern is observed in many field and laboratory observations and theoretical models of kinetic isotope effects on the thermal alteration of organic matter (cf. Peters and Moldowan, 1993). In contrast, abiotic gases from reduction of carbon dioxide are generally characterized by an "inversed" isotope pattern relative to thermogenic gases, as more ^{12}C-^{12}C bonds are present in higher hydrocarbons with longer chain length (e.g., Proskurowski et al., 2008; Lollar et al., 2002).

I.2.2. Microbial oxidation of methane and higher hydrocarbons

Microbial methane oxidation. In the ocean, vast amounts of methane migrating upwards from deeper sediment strata is consumed by aerobic and anaerobic methane oxidizing microorganisms. The anaerobic methane oxidation (AOM) is estimated to oxidize 90% of the methane produced in marine sediments and therefore represents a major sink for methane in marine environment (Reeburgh, 2007; Knittel and Boetius, 2009). AOM often occurs at the so-called sulfate methane transition zones (SMTZ) in sediments, where upwardly migrating methane meets with downwardly penetrating sulfate-containing seawater. Sulfate-dependent AOM can be expressed in the net reaction of $CH_4 + SO_4^{2-} \rightarrow HCO_3^- + HS^- + H_2O$. The process of AOM was initially suggested by geochemical observations (Barnes and Goldberg, 1976). After twenty years, the responsible microorganisms- anaerobic methanotrophic (ANME) archaea and their associated sulfate-reducing bacteria (SRB)- were discovered in gas-hydrate-bearing seeps by molecular and isotopic analysis (Hinrichs et al., 1999; Elvert et al., 1999) and an ANME/SRB consortium was visualized by fluorescence *in situ* hybridization analysis (Fig. I.2A; Boetius et al., 2000).

To date, it is well-known that AOM in marine environments is mediated by three distinct clusters of Euryarchaeota, namely, ANME-1, ANME-2 and ANME-3, which form microbial consortia with different sulfate-reducing bacteria (Knittel et al., 2019). ANME-2 and ANME-3 are phylogenetically affiliated with the methanogenic order Methanosarcinales, whereas ANME-1 form a separate order Methanophagales (Adam et al., 2017). ANME-2 clades are typically in association with SRB related to the *Desulfosarcina/Desulfococcus* group (DSS; Schreiber et al., 2010). Direct interspecies electron transfer between the ANME-2 and associated Deltaproteobacteria was suggested to be the coupling mechanism for the syntrophic groups (McGlynn et al., 2015). ANME-3 clades are generally found in association with the

SRB that are closely related to the *Desulfobulbus* (Niemann et al., 2006; Lösekann et al., 2007). The ANME-1 clusters may occur as single cells or form consortia with SRB of the DSS group (e.g., Reitner et al., 2005).

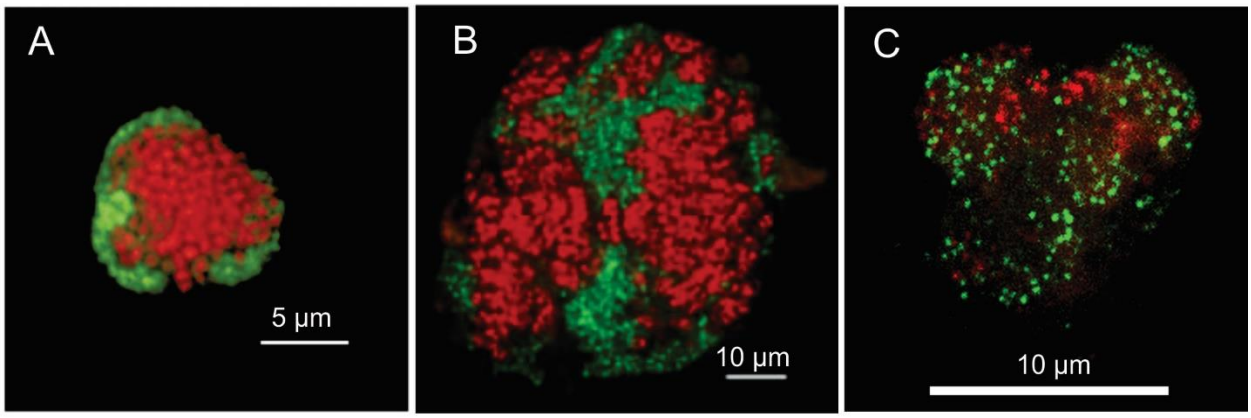

Figure I.2. Examples of archaeal/bacterial consortia that oxidize hydrocarbon gases anaerobically. A. Laser scanning micrograph of syntrophic ANME archaea (red) and sulfate-reducing bacteria (green) that perform AOM, figure from Boetius et al. (2000); B. Laser-scanning micrograph of associated GoM-Arc1 archaeal clade (red) and "*Ca.* Desulfofervidus" bacteria (green) that oxidize ethane anaerobically at 50 °C, figure from Hahn et al. (2020); C. Fluorescence micrographs of microbial consortia of GoM-Arch87 archaea (red) and HotSeep-1 bacteria (green) that oxidize butane anaerobically at 50 °C, figure from Laso-Pérez et al. (2016).

Apart from methane-laden sediments and cold seeps, AOM was also identified in methane-rich hydrothermal sediments of the Guaymas Basin through 16S rRNA and lipids analysis (Teske et al., 2002; Schouten et al., 2003), profoundly expanding our understanding of the role of AOM in both cool and hot environments. Most recent studies from the Guaymas Basin hydrothermal sediments further indicate that AOM can occur at temperatures up to 70-80 °C (McKay et al., 2016). Thermophilic AOM is carried out by thermophilic ANME-1 archaeal lineage in association with the deltaproteobacterial *Ca*. Desulfofervidus (formerly referred to as "HotSeep-1; Holler et al., 2011; Krukenberg et al., 2016). The corresponding consortia were found capable of direct electron exchange via intercellular nanowire-like structures (Wegener et al., 2015). Stable-isotope-probing experiments revealed autotrophy as the major carbon assimilation pathway for ANME-1 archaea (Kellermann et al., 2012). Optimal growth of these AOM communities was at temperatures of 50-60°C (Holler et al., 2011; Wegener et al., 2015), and the AOM process could be detected *in situ* at temperatures up to ca. 70 to 80°C (McKay et al., 2016).

The global distribution of marine ANME clades and SRB groups is not only governed by methane availability, but also other environmental factors, such as sediment depth and seafloor temperature (Ruff et al., 2015). AOM is mostly found as sulfate-dependent process because sulfate is the most abundant electron acceptor in marine sediments, yet other energetically more favorable electron acceptors such as iron or manganese are also being used at some sites (e.g., Beal et al., 2009; Aromokeye et al., 2020).

While ANMEs typically dominate archaeal clades at methane-rich sediments, a high diversity of other uncultured microbial assemblages is also found. These often comprise Thermoprofundales (formerly called Marine Benthic Group-D; Biddle et al., 2012; Kubo et al., 2012; Yoshinaga et al., 2015) and the Miscellaneous Crenarchaeotal Group (MCG; Kubo et al., 2012), which are widely detected in non-seep sedimentary settings (e.g., Kubo et al., 2012; Lloyd et al., 2013). Two members of MCG have been shown to hold genes necessary for methane metabolism (Evans et al., 2015), and key genes of methane activation (methyl coenzyme M reductases) are shared among specific Crenarchaeota (Dombrowski et al., 2018). Taken together this suggests the potential for more archaeal lineages to contribute to methane cycling at seep sites.

Microbial oxidation of higher hydrocarbons. In comparison to AOM, anaerobic utilization of higher hydrocarbon gases in marine sediments is less well documented. From Gulf of Mexico cold seeps and Guaymas Basin hydrothermal vents, pure cultures of sulfate reducers that grow on propane or *n*-butane at low to high temperatures (12°C, 28°C, 60 °C) were obtained (Kniemeyer et al., 2007). Meantime, cold-adapted ethane-oxidizing SRB were harder to isolate due to their slow growth rates (Kniemeyer et al., 2007). More recently, geochemical profiles in Guaymas Basin sediments displayed ^{13}C-enrichments in C_{2+} hydrocarbons suggesting their anaerobic oxidation by microorganisms (Dowell et al., 2016). Laso-Pérez et al. (2016) isolated a thermophilic consortium of archaeal *Ca*. Syntrophoarchaeum in association with *Ca.* Desulfofervidus auxilii of the HotSeep-1 sulfate-reducing bacterial group (Krukenberg et al., 2016) from Guaymas Basin hydrothermal sediments that are capable of growing on *n*-butane (Fig. I.2C). Ethane is presumed to be the chemically most inert hydrocarbon gas under anaerobic conditions with extremely slow microbial utilization (cf. Widdel and Grundmann, 2010). Until most recently, isolates able to oxidize ethane anaerobically were obtained from Gulf of Mexico cold seep sediments (*Ca.* Argoarchaeum ethanivorans' in association with members of sulfate-reducing Deltaproteobacteria; Chen et al., 2019). Shortly after that, another isolates were obtained from the Guaymas Basin hydrothermal sediments (*Ca.* Ethanoperedens, former GoM-Arc1, in association with *Ca.* Desulfofervidus auxilii; Hahn et al., 2020; Fig. I.2B).

Recent metagenomic studies of Guaymas Basin sediments suggest that some ANME-1 archaea are also able to anaerobically oxidize alkanes other than methane. Metagenomic reconstructions detected the unusual coenzyme M reductases in Helarchaeota, a new lineage of the Asgardarchaeota, indicating that these archaea are capable of short-chain hydrocarbon oxidation (Seitz et al., 2019). Altogether our view on the microbial utilization of hydrocarbon gases is currently expanding at a rapid pace.

I.3. RESEARCH SITES

I.3.1. Guaymas Basin- an organic-rich hydrothermal system

The Guaymas Basin is located in the central Gulf of California at a water depth of ca. 2000 m. It is part of a rift system that links to the East Pacific Rise to the South and the San Andreas Fault in the North (Lonsdale, 1985). It is a young marginal rift basin formed during approximately the past 3.5 Myr by ocean floor spreading at a rate of 6 cm yr^{-1} (Moore, 1973; Einsele et al., 1980; Lonsdale and Lawver, 1980). The Guaymas Basin contains a central depression which is divided into two overlapping spreading segments, the northern and southern troughs, owing to right-lateral North America-Pacific plate motion (Minster and Jordan, 1978). As opposed to commonly observed bare lava hydrothermal vent systems along the mid-oceanic ridge, the Guaymas Basin seafloor spreading center is buried by up to hundreds of meters of organic-rich, predominately diatomaceous sediments. This is resulted from a very high sedimentation rate (1-2 mm/year)- owing to high biological productivity in overlying waters- and a large terrigenous input (Calvert, 1966). Shallow magmatic sill intrusions into overlying unconsolidated sediments create a dynamic environment with great thermal and chemical gradients that constrain the biogeochemical cycling of sedimentary carbon and other elements.

Shallow magmatic sill intrusions into the organic-rich sediments lead to thermocatalytical alteration of sedimentary organic matter that releases large amounts of gaseous hydrocarbons (Simoneit and Galimov, 1984; Simoneit et al., 1988), complex petroleum compounds (Didyk and Simoneit, 1989; Peter et al., 1991; Simoneit and Kawka, 1987; Simoneit et al., 1990; Simoneit et al., 1979), short-chain fatty acids (Martens, 1990) and ammonia (Von Damm et al., 1985). Hydrothermal fluids rich in hydrocarbons migrate through fissures towards the sediment surface (Einsele et al., 1980; Simoneit, 1990; Peter et al., 1991), sustaining highly diverse microbial communities in the surface sediments. These microorganisms catalyze a multitude of processes include anaerobic methane and C_{2+} hydrocarbon oxidation (Teske et al., 2002; McKay et al., 2016; Dowell et al., 2016), sulfate reduction (Jørgensen et al., 1990; Jørgensen et al., 1992; Meyer et al., 2013) and methanogenesis (Dhillon et al., 2005). Therefore, the interplay of geochemical, thermal and microbial forces that mobilize and assimilate carbon in the Guaymas Basin sediments provides a promising system for in-depth investigations of anaerobic hydrocarbon transformation, the diversity and the evolution of hydrocarbon-degrading microorganisms and pathways (Teske et al., 2014).

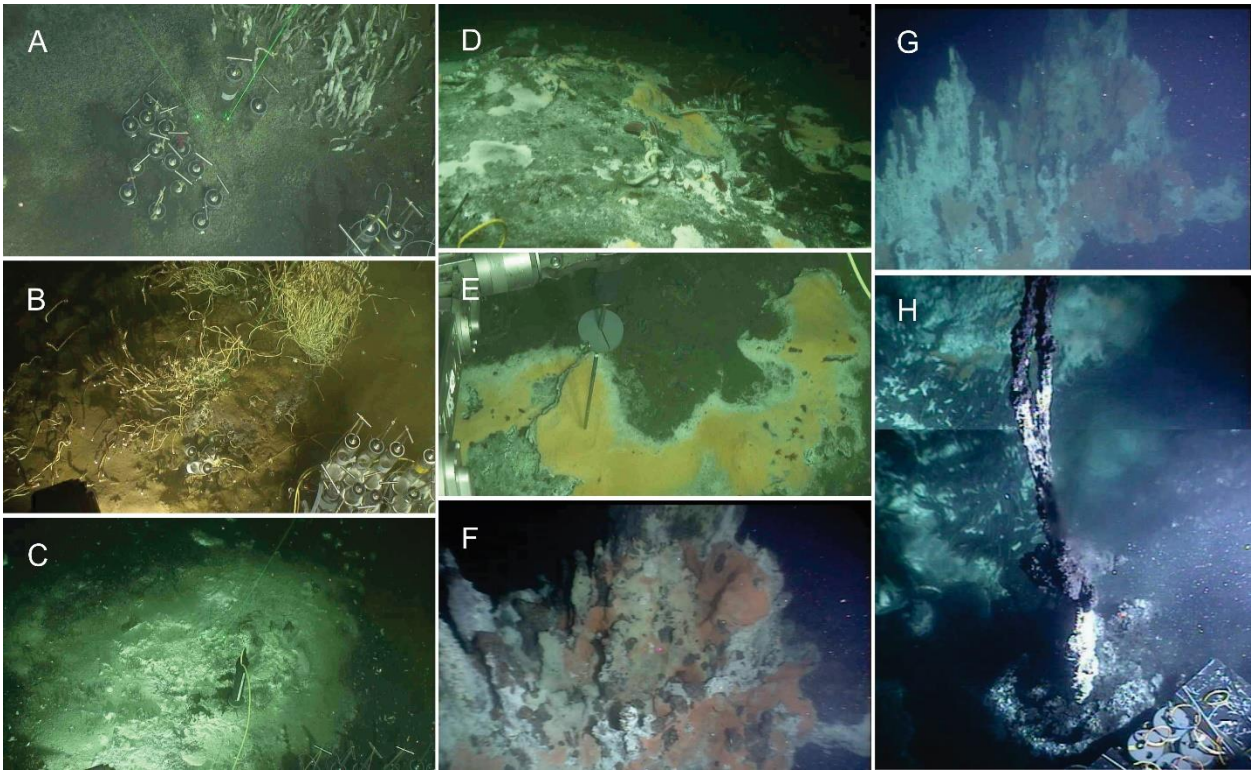

Figure I.3. Image gallery at the Guaymas Basin. **A.** Octopus Mound (*Alvin* Dive 4867, 18 December 2016, GMT 17:17:57); **B.** Ring Vent (*Alvin* Dive 4864, 15 December 2016, GMT 17:11:40); **C.** Northern Tower (*Alvin* Dive 4871, 23 December 2016, GMT 20:57:03); **D.** Ultra Mound (*Alvin* Dive 4869, 21 December 2016, GMT 17:39:29); **E.** Mat Mount Massif (*Alvin* Dive 4863, 14 December 2016, GMT 17:57:27); **F.** Notre Dome (*Alvin* Dive 4573, 04 December 2009, GMT 19:40:57); **G.** Cathedral Hill (*Alvin* Dive 4573, 04 December 2009, GMT 19:35:27); **H.** Rebecca's Roost (*Alvin* Dive 4574, 5 December 2009, composite image of a peripheral thin chimney: upper portion at GMT 20:27:11,lower portion at GMT 20:26.41). Photographs courtesy of Woods Hole Oceanographic Institution, from RV *Atlantis* cruise AT 37-06 and AT15-56.

Early expeditions at the Guaymas Basin include Deep Sea Drilling Project (DSDP) Leg 64 in 1978, which aimed to investigate the young ocean crust and associated rifting and hydrothermal activity (Kelts et al., 1982), substantially improved our understanding of the hydrothermal and geochemical processes driven by igneous intrusion into sediments (Curray et al., 1979; 1982; Einsele et al., 1980). A lot of studies since have contributed to our understanding of the formation of hydrocarbon gases and hydrothermal petroleum. The $\delta^{13}C$-CH_4 data suggested an admixture of thermogenic and microbial gas with the largest proportion of thermogenic gas near the sills (Simoneit et al., 1988). At the time, $\delta^{13}C$ values of C_2-C_5 hydrocarbons were not obtained, but they were suggested to be of thermogenic origin based on correlation plots of $C_1/(C_2 + C_3)$ vs. $\delta^{13}C$-CH_4 (Simoneit and Galimov, 1984; Simoneit et al., 1988).

The hydrothermalism of Guaymas Basin varies both temporally, controlled by the lifespan of the host sill, and spatially, with on-axis and off-axis systems, representing key end-member environments (Teske et al., 2019). Apart from on-axis locations, active magmatic intrusion into sediments was also reported to

occur broadly to more than 40 km off axis (Lizarralde et al., 2011). These sites evolved over thousands of years as magma freezes into sills and the system cools and switches into cold seeps over time (Lizarralde et al., 2011; Geilert et al., 2018). With the aid of the submersible HOV *Alvin* many of the hydrothermal features in the southern trough have been investigated over many years, while the cold seep areas have been only targeted more recently (Fig. I.3. A&B). Both the cold and hydrothermally influenced sediments, mounds, chimneys, microbial mats and vent fauna form a complex hydrothermal landscape on the seafloor, closely reflecting the subsurface hydrothermal circulations (Fig. I.3. C-H; Lonsdale and Becker, 1985; Teske et al., 2016).

I.3.2. US Atlantic Margin- a methane-hydrate-bearing seep system

The northern US Atlantic margin (USAM) is located off shore of the Eastern North America. A recent survey detected hundreds of cold seeps on the USAM between water depths of 100 and 1000 m with estimated methane fluxes of 15-90 Mg yr^{-1}. This finding implies that many major seeps are yet to be discovered along global continental margins (Skarke et al., 2014). The destabilization of gas hydrate on the margin is suspected to be the cause of this release (Phrampus and Hornbach, 2012), but a more likely source is from expulsion of fluids from compaction of sediments that accumulated during the late Pleistocene (Prouty et al., 2016). With recent recognition that gas expulsion is a prevalent process on active (Riedel et al., 2018) and passive margins (Skarke et al., 2014), a better understanding of the controls on methane emission is needed to predict how climate change will affect the production of methane in marine sediments and its release from the seafloor.

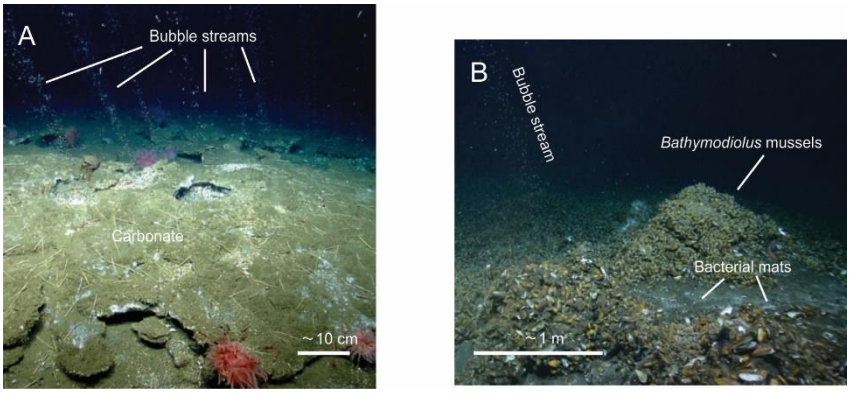

Figure I.4. Seafloor images at upper-slope and deep-water seep sites at the US Atlantic margin. Figures from Skarke et al. (2014).

Investigating sedimentary methane dynamics along the northern USAM is an ideal opportunity to evaluate the biogeochemical mechanisms that regulate the transfer of methane from the seafloor and into

the ocean. Gas plumes at the northern USAM were traced up to hundreds of meters above the sea floor (Fig. I.4) with methane concentrations up to 100-200 nM (Skarke et al., 2014; Weinstein et al., 2016). A recent study reported rapid oxidation of methane in the oxic water column (Leonte et al., 2017), however, knowledge on methane turnover in the sediments at USAM is still limited.

The methane seeps of the US Atlantic margin represent an ideal counterpart to the well-studied cold and hot seep ecosystems of the Guaymas Basin, as they likely harbor similar AOM communities, but ones that are not influenced by drastic changes in temperature. In addition, differences in whole community composition can be expected as microorganisms living in the Guyamas Basin are influenced by the presence of higher hydrocarbon gases and oil, while at the USAM the carbon metabolism of communities is likely solely fueled by methane and total organic carbon in the sediments.

I.4. LIPID BIOGEOCHEMISTRY IN HYDROCARBON SEEP SETTINGS

I.4.1. Function and structure of membrane lipids

A common feature to all living cells is the presence of a cytoplasmic membrane. The structure of the cytoplasmic membrane is commonly described using the fluid mosaic model (Singer and Nicolson, 1972; Nicolson, 2014). Accordingly, the cytoplasmic membrane is considered as a matrix made up of a polar lipid bilayer with embedded proteins, and other components such as carbohydrates and sterols or hopanols (Fig. I.5). The membrane components are able to flow and change position, while maintaining the basic integrity of the membrane. The polar membrane lipids consist of a hydrophobic and a hydrophilic part. The tendency of the hydrophobic ends to self-associate and keep away from the water, and the hydrophilic moieties to interact with aqueous environments, is the physical basis for the formation of membrane bilayer. Essentially, polar membrane lipid bilayers function primarily as a barrier that partitions the inner cytoplastic compartment from the outside environment (van Meer et al., 2008). It also provides a semipermeable barrier that controls the flux of ions and molecules across the membrane and helps to maintain the proton and ion gradients that are essential for energy conservation, cellular signaling and other activities (Madigan et al., 1997).

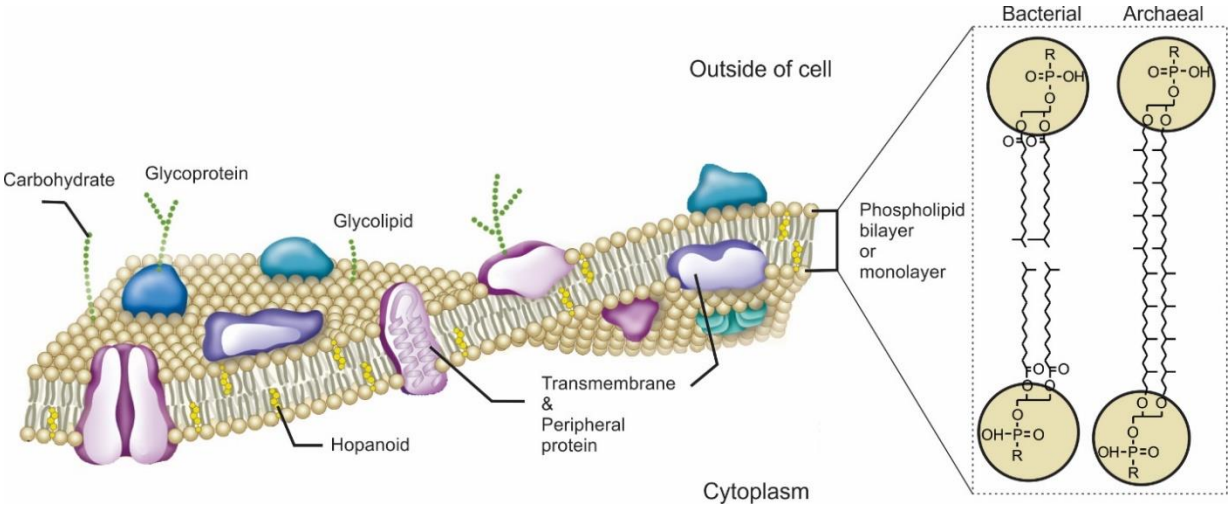

Figure I.5. Schematic structure of a bacterial cytoplasmic membrane. Membrane is made up of a polar lipid bilayer with embedded proteins, and other components such as carbohydrates and hopanoid. Note that hopanoids are not found in archaeal cells. An enlarged figure at the right side shows the structure of the bilayer-forming polar lipids, with a head group (yellow circle), and two side chains forming bilayer (typically in a bacterial cell) or monolayer membrane (typically in archaeal cell). More information on the lipid structure can be found in Figure I.8 and in the main text. This figure is modified after OpenStax (2020).

In addition to the barrier function, polar membrane lipids can adopt various fluid and solid phases depending on their structure. While saturated hydrocarbon chains tend to exist in solid-like phases, short and unsaturated hydrocarbon chains tend to be enriched in liquid phases (van Meer et al., 2008). Meanwhile, the embedded steroids or hopanoids, together with the bilayer-forming lipids, can modulate the molecular order of fluid membranes (van Meer et al., 2008; Sáenz et al., 2015). Consequently, the solid phase provides a high order in the membrane while the fluid phase assures high translational mobility of the membrane (van Meer et al., 2008). These properties of membrane lipids- both bilayer-forming polar lipids and embedded sterols or hopanoids- are essential for the cell to be adaptive in response to environmental changes, such as temperature, pH and salinity. For example, fluorescence probe studies showed that membrane lipids of thermoacidophilic *S. acidocaldarius* were rigid and tightly packed at low temperature, but possessed appreciable membrane fluidity at temperatures close to the minimum growth temperature of ca. 50°C (Khan and Chong, 2000).

I.4.2. Membrane polar lipids as taxomonic biomarkers

One remarkable property of membrane lipids is their fundamental difference in chemical structure among Archaea, Bacteria and Eukarya- the tree domains of life based on small subunit rRNA sequences (Fig. I.6; Woese et al., 1990; Kates et al., 1993; Langworthy, 1982; Koga et al., 1993). The non-bilayer-forming sterols are found within all eukaryotic cells (Benveniste, 1986), whereas hopanols are produced by

many members of bacteria (Kannenberg and Poralla, 1999). More striking is the difference in bilayer-forming polar lipids among different domains of life. The common chemical structure of polar membrane lipids is a glycerol backbone to which a polar, hydrophilic head group as well as two apolar, hydrophobic side chains are attached. The most critical distinction between archaeal and bacterial/eukaryotic polar membrane lipids is the stereochemical structure of the glycerol backbones (Fig. I.6B): while both the bacterial and eukaryotic backbones have *sn*-glycerol-3-phosphate (G-3-P), the archaeal backbone has *sn*-glycerol-1-phosphate (G-1-P). This is attributed to the presence of G-1-P dehydrogenase in archaea and G-3-P dehydrogenase in bacteria and eukaryotes (Koga et al., 1998). Typically, two fatty acyl chains are bound at the *sn*-1 and *sn*-2 position via ester linkage to the glycerol moiety in Bacteria and Eukarya, whereas two isoprenoid chains are bound at the *sn*-2 and *sn*-3 positions via ether linkage to the glycerol in Archaea.

Although bacterial and eukaryotic lipids are more similar in their chemical structure compared to archaeal lipids, there are differences in the carbon chain length and degree of unsaturation and methylation in their fatty acyl chains. The eukaryotic fatty acids are usually even carbon numbered and polyunsaturated (e.g., Guschina and Harwood, 2006), whereas bacterial fatty acids have on average shorter chain lengths, a lower degree of unsaturation, and can be penultimate (iso) or ante-penultimate (anteiso) methyl-branched (Fulco, 1983; Kaneda, 1991). Archaeal isoprenoid chains commonly comprise diphytanyl diethers (also known as archaeol) and/or biphytanyl tetraethers (Koga and Morii, 2005), with the biphytanyl groups bound to two glycerol backbones at each end (also known as glycerol dibiphytanyl or dialkyl glycerol tetraethers; GDGTs). Therefore, archaeal membrane lipids can form both bilayers (in the case of archaeol) or membrane-spanning monolayers (in the case of GDGT). Exceptions to above described generalizations, for instance, membrane-spanning branched GDGTs lipids with non-isoprenoidal hydrocarbon chains (e.g., GDGT-III; Fig. I.6C) were assigned to bacterial sources, as they have bacterial 1,2-di-O-alkyl-*sn*-glycerol stereoconfiguration (Weijers et al., 2006a). Additionally, ether-linked lipids, e.g., acylether glycerol and diether glycerol phospholipids, were also found in sulfate-reducing bacteria (Fig. I.6C; e.g., Rütters et al., 2001; Sturt et al., 2004).

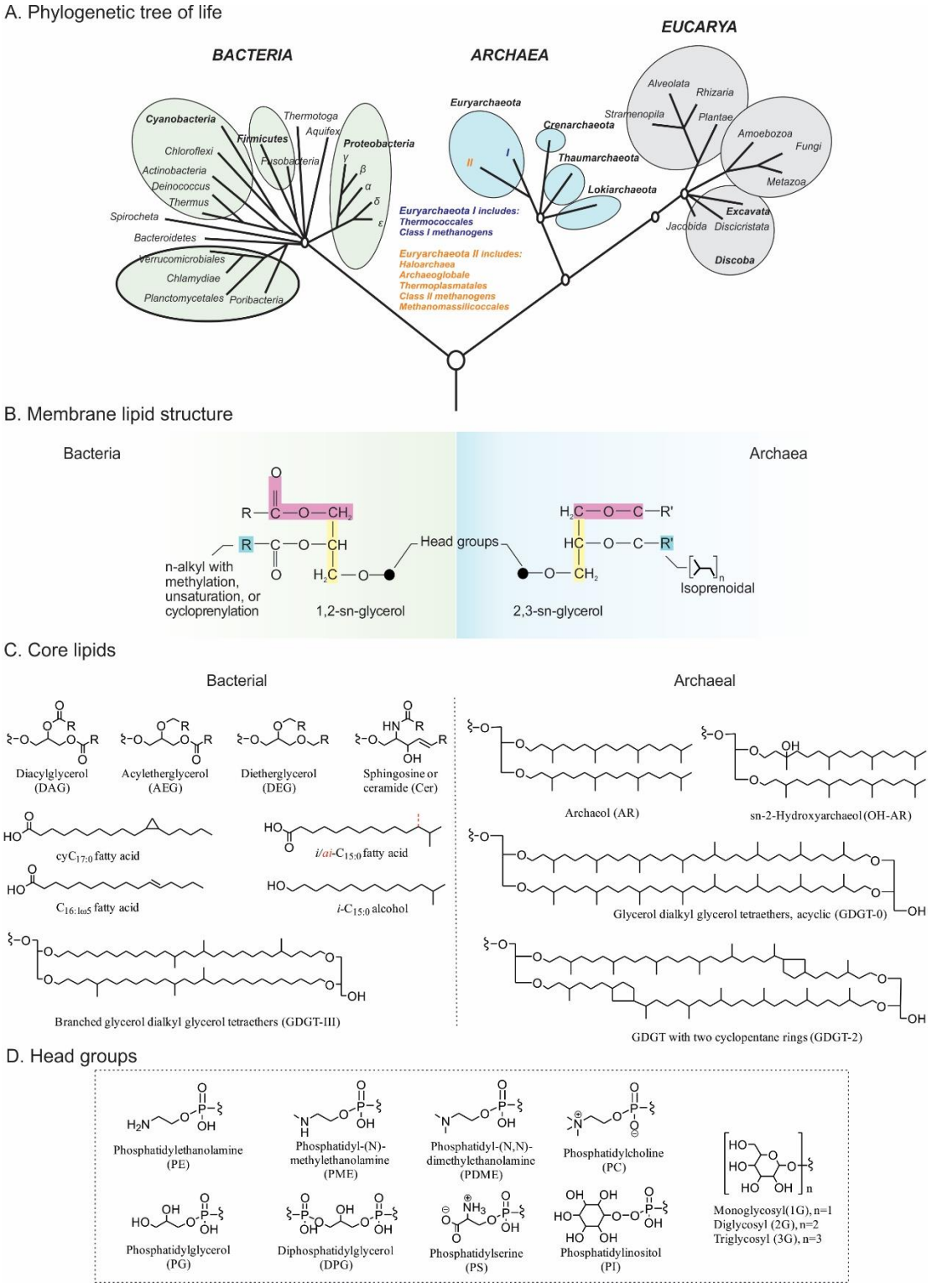

Figure I.6. Membrane lipid structures found in bacterial and archaeal cells. A. Phylogenetic tree of life showing the three domains of life updated from Woese et al. (1990) and modified after Forterre (2015). B. The basic chemical structures of bacterial/eukaryotic and archaeal membrane lipids, the characteristic differences are highlighted in colors (adopted from Valentine, 2007). C. Examples of bacterial and archaeal core lipids. D. Structures of head groups commonly found in microbial intact polar lipids.

Nonetheless, the stereochemical difference of glycerol backbones for the three domains of life are fundamental (Koga et al., 1998). Ultimately, the general characteristic distinction in membrane lipid structure sets up the stage for the development of using lipids as diagnostic biomarker. Owing to the high chemical stability of the hydrocarbon-based structure of lipids, most of the characteristic structures preserve after cell decay, providing specific information about the organisms or processes that made them (Peters and Moldowan, 1993). The past decades have witnessed an immense growth and expansion of lipid biomarker-based techniques (e.g., Hopmans et al., 2000; Sturt et al., 2004; Liu et al., 2012; Zhu et al., 2014b). Lipid biomarkers have been successfully used in developing proxies for reconstructing sea water temperatures and carbon isotope excursions in geological history (Schouten et al., 2002; Elling et al., 2019).

Since the development of HPLC-MS techniques that enable direct measurements of intact polar membrane lipids (IPLs; Sturt et al., 2004), it has become clear that structural information on both the head groups and core lipids of IPLs provides insightful information on the source organisms. The head groups are typically phosphate-based, but glycosidic-, amino- or sulfate-based head groups are also commonly found (Dembitsky, 1996; Hölzl and Dörmann, 2007). An example of the most dominant head groups in nature can be found in Fig. I.6D. Next to gene-based techniques, membrane IPLs become complementary informative, culture independent biomarkers for identifying the distribution and biogeochemical imprint of microbial communities in natural environments. IPLs are thought to be labile compounds which tend to lose their head groups through hydrolysis rapidly after cell death (White et al., 1979; Harvey et al., 1986). Thereby, they are often used as biomarkers for living cells and for identifying their biogechemical imprints (e.g., Rossel et al., 2011; Schubotz et al., 2018; Becker et al., 2018). More insight has been obtained regarding the chemical stability of different types of IPLs. While ester-linked lipids are found to be susceptible to rapid degradation upon cell death, ether-linked lipids may be preserved in non-dynamic sediments over geological time periods (e.g., Xie et al., 2013). Such selective degradation in different environmental settings needs to be considered when applying IPLs as biomarkers for living organisms. Nonetheless, microbial IPLs can provide 'snapshots' of the *in situ* community structure and biogeochemical processes in more active systems (e.g., Biddle et al., 2006; Rossel et al., 2008). Additionally, isotopic composition of IPLs can provide information on the microbial carbon flow (Schubotz et al., 2011; Meador et al., 2015).

I.4.3. Thermal adaptation of the microbial lipid membranes

Bacteria and Archaea have evolved different adaptation mechanisms to cope with changing environmental conditions such as temperature. In principle, lipid membranes function effectively in a liquid

crystalline state, which provides a functional matrix for multiple biochemical processes while maintaining a high permeability barrier for ions and solutes (cf. Koga, 2012). Consequently, cells modify their lipid composition to maintain membrane permeability and fluidity under different temperatures.

The fluidity of membranes depends on the membrane's phase-transition temperature, which is defined as the temperature at which a membrane shifts between the liquid crystalline phase and the rigid gel phase (Eze, 1991). The phase-transition temperatures for archaeal lipid membranes are reportedly very low (below 0 °C), owing to the highly branched isoprenoid hydrocarbon chains in archaeal lipids (Koga, 2012). Consequently, archaeal membranes can maintain liquid crystalline phase while maintaining low permeability under wide biological temperature ranges (Elferink et al., 1994). In contrast, bacterial fatty acyl ester phospholipid membranes express much higher phase-transition temperatures, which are reportedly 40-50 °C depending on their chain length, number of double bonds and the methyl branching position (cf. Koga, 2012). Consequently, bacteria maintain a proper level of permeability and fluidity at temperatures only just above their phase transition temperatures. Therefore, a rapid modification of lipids in bacterial membrane in response to temperature change is required.

As to bacterial membranes, the permeability of bacterial fatty acyl ester lipids increases drastically with increasing temperatures (Yamauchi et al., 1993). Therefore, in order to keep a low permeability while maintaining a fluid phase of the membrane, Bacteria have to response quickly to temperature change by regulating the degrees of unsaturation and methylation in membrane fatty acids. These modifications often cause shifts in ratios of lipid types and/or their hydrocarbon moieties. For instance, it was observed in bacterial cultures that unsaturation in fatty acids increased with decreasing growth temperature (Shigeo et al., 1972). Relative abundance of iso- and anteiso-fatty acids increased with respective increasing and decreasing growth temperatures (Oshima and Miyagawa, 1974).

As to archaeal membranes, their isoprenoid chains realize the state of a high permeability barrier and a liquid crystalline phase throughout the entire biological temperature range (Elferink et al., 1994). In thermophilic archaea, the most common core lipid is the membrane spanning tetraether lipid (i.e. GDGT). GDGTs form monolayers that are highly stable due to a restricted motility of the hydrocarbon chains (Siliakus et al., 2017). Increased cyclopentane ring number in GDGTs with temperature has been observed in membranes of cultured thermoacidophilic archaea (De Rosa et al., 1980; Gliozzi et al., 1983; Uda et al., 2001). This relationship between GDGT cyclization and temperature is the basis for the marine paleotemperature proxy TEX_{86} (e.g., Schouten et al., 2013). The incorporation of cyclopentane rings may raise the transition temperature of the membrane (Gliozzi et al., 1983). However, not all thermophilic archaea employ the same strategies. For example, Thermococcales strains grown at 85 °C are dominated

by GDGTs without cyclopentane rings (GDGT-0, Sugai et al., 2004). A more recent study suggested the cyclization in GDGTs of the thermoacidophile *Sulfolobus acidocaldarius* is also controlled by energy flux (Zhou et al., 2019).

Another common lipid found in thermophilic archaea is the glycerol monoalkyl glycerol tetraether (GMGT; also often referred to as H-shaped GDGT), which contains a covalent bond between the two isoprenoid chains. GMGT with up to four cyclopentane rings are often found in cultivated isolates of thermophiles such as hyperthermophilic methanogens (Morii et al., 1998), members of the Thermococcales (Sugai et al., 2004); thermoacidophilic Euryarchaeota (Schouten et al., 2008), hyperthermophilic Crenarchaeota (Knappy et al., 2011), as well as in samples from hydrothermal vent environments (e.g., Jaeschke et al., 2012; Lincoln et al., 2013; Sollich et al., 2017). The extra covalent bond between the two alkyl chains in GMGT is suggested to further reduce membrane permeability under thermal stress (Knappy et al., 2011; Sollich et al., 2017).

I.4.4. Membrane lipid biomarkers associated with microbial hydrocarbon oxidation

Since the initial evidence for microbial AOM in both cold seep and hydrothermal vent environments (Hinrichs et al., 1999; Teske et al., 2002), membrane lipids are frequently used for evaluating microbial oxidation of hydrocarbons. To date, lipid biomarkers for ANME archaea are well characterized. For instance, diglycosidic glycerol dialkyl glycerol tetraethers (2G-GDGTs) are found to be produced by ANME-1 clades; whereas ANME-2 and ANME-3 clades preferably produce archaeol (AR) and hydroxyarchaeol (OH-AR) bonded with phosphate-based head groups (Rossel et al., 2008). These diagnostic biomarkers provide further information on the distribution of ANME clades in the environment. Such that diagnostic lipid biomarkers for ANME-1 dominate over those for ANME-2 and -3 groups under higher temperatures and less oxidizing conditions (Rossel et al., 2011). Additionally, while GDGTs associated with ANME-1 archaea from cold hydrocarbon seeps contain abundant one to three pentacyclic rings (GDGT-1 to GDGT-3), thermophilic ANME-1 are dominated by GDGT-4 (Schouten et al., 2003; Holler et al., 2011).

Sulfate-reducing bacteria (SRB) usually associate with ANME archaea and are the other major players in AOM. Phospholipids with phosphatidylethanolamine (PE), phosphatidylglycerol (PG), diphosphatidylglycerol (DPG) and phosphatidyl-(N)-methylethanolamine (PME) head groups are found to be diagnostic for AOM-related SRB (Rossel et al., 2008). As many other membrane lipids, these IPLs can have multiple source organisms besides AOM-related SRB. However, since AOM-related SRB usually produce isotopically lighter lipids owing to carbon assimilation from methane-derived carbon (i.e.

isotopically depleted CO_2), these lipids can be used in conjunction with isotope information to assign diagnostic sources. Using this technique some of these phospholipids were also shown to be produced by other SRB that are not involved in AOM but in other heterotrophic processes, such as petroleum degradation (Schubotz et al., 2011). Additionally, as observed in geochemical profiles, sulfate reduction is often unbalanced with the AOM process (Joye et al., 2004) and it was shown that SRB are further involved in degradation of higher hydrocarbon gases, such as propane and butane (Kniemeyer et al., 2007; Jaekel et al., 2013).

A better understanding of not only the source organisms but also the formation pathways for membrane lipids is important for the application of these biomarkers in environmental studies. Stable-isotope-probing experiments have proven to be useful: with the addition of ^{13}C-labeled substrates, the carbon flow for microbial groups can be easily traced. In a study by Kellermann et al. (2012), an enrichment of syntrophic ANME-1 and HotSeep-1 sulfate-reducing bacteria were incubated with unlabeled methane and ^{13}C-labeled dissolved inorganic carbon (DIC). It was observed that this enrichment assimilated DIC for lipid synthesis while oxidizing methane for energy. This finding is striking as ^{13}C-depleted archaeal lipids had until then been attributed to the direct transfer of ^{13}C-depleted methane carbon into lipid biosynthesis. Consequently, the large range in isotopic compositions in putative ANME lipids relative to methane observed at cold seeps could be a result of the existence of widespread ANME archaea that predominantly assimilate CO_2 (Kellermann et al., 2012).

Recent advances in the analysis of IPLs (Sturt et al., 2004; Zhu et al., 2013a; Wörmer et al., 2013) and their core lipid derivatives (Knappy et al., 2009; Liu et al., 2012; Becker et al., 2013) further expanded the catalogue of microbial biomarkers and enhanced the ability to pinpoint the presence of microbial groups and identify their metabolic modes (e.g., Biddle et al., 2006; Schubotz et al., 2011; Meador et al., 2015). For instance, recently identified IPLs with unassigned source organisms were found to be abundant in both methane-rich and deep subsurface sediments, these include glycosidic unsaturated GDGTs (unsGDGTs) (Zhu et al., 2014b), butanetriol dibiphytanyl glycerol tetraether (BDGT) and pentanetriol dibiphytanyl glycerol tetraether (PDGT) lipids (Zhu et al., 2014a). Thermoplasmatales-related archaea were suggested to be the source organism for unsGDGTs at seep sites (Yoshinaga et al., 2015), while BDGT and PDGT lipids seem to have multiple sources including methanogens (Becker et al., 2016; Coffinet et al., 2019), benthic archaeal members of the MCG (Meador et al., 2015), or unknown heterotrophic archaea (Coffinet et al., 2019). Parallel investigation of membrane lipids and nucleic acids, in combination with isotope analysis for specific lipids will eventually resolve the source and function of these lipids, as well as the metabolic pathway of the microbial groups in nature.

In comparison to microbial oxidation of methane, the anaerobic metabolic cycling of higher hydrocarbons is still poorly understood. In recent years, sulfate-reducing bacteria (Kniemeyer et al., 2007), as well as archaeal and SRB consortia that are capable of higher hydrocarbon gas degradation have been successfully isolated from cold seep and hydrothermal vent sediments (Laso-Pérez et al., 2016; Hahn et al., 2020). To date, the corresponding lipid composition for SRB and archaeal groups involved in higher hydrocarbon oxidation have not yet been explored.

CHAPTER II

Scope and Outline

II.1. THESIS OBJECTIVES

The overall objective of this thesis is to expand our knowledge on the sources and sinks of hydrocarbon gases and to explore lipid signatures of microorganisms involved in their cycling. To this end, two contrasting seep systems are investigated: the cold, methane dominated US Atlantic Margin sediments versus the hot, higher hydrocarbon-impregnated Guaymas Basin sediments. Hydrocarbon gas formation and degradation pathways are investigated by isotopic and experimental approaches, while the microbial imprint is characterized by means of intact polar lipid (IPL) analyses, which provide insights into community structure and adaptation of specific microbial groups to prevailing environmental conditions.

Chapter III examines the sources of hydrocarbon gases in Guaymas Basin hydrothermal sediments. Hydrothermally heated sediments in the Guaymas Basin are often considered as time-lapse analogue to petroleum systems. Higher hydrocarbons in Guaymas Basin hydrothermal sediments are historically thought to be of thermogenic origin. However, the isotope signatures ($\delta^{13}C$) of higher hydrocarbons were until now not assessed. In this study, we examined the $\delta^{13}C$ of gaseous hydrocarbons in a large set of sediment samples from the Guaymas Basin spanning the temperature range of 3 to 180 °C. We observed an unusual isotopic relationship for higher hydrocarbon gases that is inconsistent with thermogenic or known abiotic sources. The research question of this study was:

- *What is the formation pathway of higher hydrocarbon gases in organic-rich hydrothermal sediments of the Guaymas Basin?*

Chapter IV explores the biogeochemical mechanisms that regulate the transfer of methane from the seafloor and into the ocean at the US Atlantic Margin (USAM). Recently, massive gas expulsion was observed at the northern USAM. A better understanding of how climate change will affect the production of methane in marine sediments and its release from the seafloor is required. In this study, we used archaeal and bacterial IPL biomarkers in conjunction with 16S rRNA gene sequencing and geochemistry analysis to

investigate the microbial imprint and community structure in USAM sediments under different methane fluxes. The research questions were:

- *How are sedimentary microbial IPL signatures shaped by methane flux and other geochemical conditions?*
- *Can we assign the source organisms for some of the recently identified IPLs that often occur in methane-rich sediments?*

Chapter V investigates the microbial lipid signatures in the hot and higher hydrocarbon impregnated sediments from the Guaymas Basin. The Guaymas Basin hydrothermal sediments are characterized by steep and fluctuating thermal and chemical gradients. Highly diverse microbial communities occur in near surface sediments and catalyze anaerobic microbial processes, including the oxidation of methane and short-chain hydrocarbons. In this study I analyzed the intact and core lipids from six push cores with *in situ* temperatures ranging from 3 to 70 °C with the aim to investigate microbial community response under dynamic and extreme environmental conditions. The research questions were:

- *What are diagnostic lipid signatures for the anaerobic oxidation of hydrocarbon gases?*
- *How is microbial ether lipid composition impacted by temperature?*

II.2. CONTRIBUTIONS TO PUBLICATIONS

As first author

Chapter III: Formation of non-methane hydrocarbon gases via abiotic reduction of volatile fatty acids in hydrothermal sediments

Min Song, Florence Schubotz, Matthias Y. Kellermann, Christian T. Hansen, Wolfgang Bach, Andreas P. Teske, Kai-Uwe Hinrichs

Submitted to *Proceedings of the National Academy of Sciences*, in revision

I designed the research with Florence Schubotz, Andreas P. Teske and Kai-Uwe Hinrichs. I collected samples during the expedition to the Guaymas Basin in 2016, and measured the concentration and isotopic composition of hydrocarbon gases in sediments. I combined these data with data conducted by Matthias Y. Kellermann from two former expeditions. I analyzed these data and prepared figures for discussion with Florence Schubotz, Matthias Y. Kellermann, Andreas P. Teske and Kai-Uwe Hinrichs. Kai-Uwe Hinrichs came up with the hypothesis. In order to test the hypothesis, I, Kai-Uwe Hinrichs, Christian T. Hansen and Wolfgang Bach designed the hydrous pyrolysis experiments. I and Christian T. Hansen performed the experiments. I performed sample measurements and data analysis from the experiments with input from Christian T. Hansen. I wrote the first draft, which was firstly revised by Florence Schubotz and Kai-Uwe Hinrichs. The manuscript was then finalized with inputs from all other co-authors.

Chapter IV: Geochemical constraints on microbial intact polar lipid diversity in methane-laden sediments of the northern US Atlantic Margin

Min Song, Florence Schubotz, Kevin W. Becker, Michael F. Graw, Frederick S. Colwell, John W. Pohlman, Kai-Uwe Hinrichs

In preparation for *Environmental Microbiology*

John W. Pohlman collected the samples and initiated the collaboration. I, Florence Schubotz, Kevin W. Becker, John W. Pohlman and Kai-Uwe Hinrichs designed the research. I measured and analyzed archaeal and bacterial lipids, with the quantification of bacterial lipids being partly contributed by Patrick Agu. John W. Pohlman provided the geochemical data, Michael F. Graw and Frederick S. Colwell provided the

operational taxonomic unit data. I performed the statistical analyses. I defined the story-line of this paper, with inputs from Florence Schubotz and Kai-Uwe Hinrichs. I wrote the first draft, which was firstly revised by Florence Schubotz and Kai-Uwe Hinrichs. The manuscript was then finalized with inputs from Kevin W. Becker, John W. Pohlman and other co-authors.

Chapter V: Microbial ether lipid biogeochemistry in hydrothermal sediments of the Guaymas Basin

Min Song, Florence Schubotz, Gunter Wegener, Andreas P. Teske, Kai-Uwe Hinrichs

In preparation for *Geochimica et Cosmochimica Acta*

I designed the research with Florence Schubotz, Andreas P. Teske and Kai-Uwe Hinrichs. I collected the samples during the expedition to the Guaymas Basin. I measured the samples and analyzed the lipid data. I measured the geochemical data except for *in stu* temperatures and sulfate/sulfide concentrations, which were measured by the submersible *Alvin* and by Gunter Wegener, respectively. I defined the story-line of this paper, with inputs from Florence Schubotz, Andreas P. Teske and Kai-Uwe Hinrichs. I wrote the first draft, which was substantially revised by Florence Schubotz. The manuscript was finalized with inputs from all co-authors.

As co-author

Chapter VII: Generation and utilization of volatile fatty acids and alcohols in hydrothermally altered sediments in the Guaymas Basin, Gulf of California

Guang-Chao Zhuang, Andrew Montgomery, Vladimir A. Samarkin, Min Song, Jiarui Liu, Florence Schubotz, Andreas Teske, Kai-Uwe Hinrichs, and Samantha B. Joye

Published in *Geophysical Research Letters*, 46. https://doi.org/10.1029/2018GL081284

This chapter is presented as an abstract. Here, I measured and analyzed the concentration and isotopic composition of volatile fatty acids and alcohols. This project is closely related to my PhD thesis: (i) the role of volatile fatty acids in the formation of hydrocarbon gases at the Guaymas Basin was evaluated in Chapter III; (ii) the source of microbial ether lipids in hydrothermal sediments of Guaymas Basin was investigated in Chapter V. As demonstrated in this paper, volatile fatty acids and alcohols are important carbon sources for microorganisms, thereby are potentially related to the distribution of lipid biomarkers. Therefore, it is meaningful to investigate the fate of these compounds in hydrothermal sediments in the Guaymas Basin.

CHAPTER III

Formation of non-methane hydrocarbon gases via abiotic reduction of volatile fatty acids in hydrothermal sediments

Min Song[a,1], Florence Schubotz[a], Matthias Y. Kellermann[a,2], Christian T. Hansen[a], Wolfgang Bach[a], Andreas P. Teske[b], Kai-Uwe Hinrichs[a,1]

Submitted to *Proceedings of the National Academy of Sciences*, in revision

[a]MARUM-Center for Marine Environmental Sciences and Department of Geosciences, University of Bremen, D-28359 Bremen, Germany; [b]Department of Marine Sciences, University of North Carolina at Chapel Hill, Chapel Hill, NC 27599-3300, USA

[1]To whom correspondence should be addressed: msong@uni-bremen.de or khinrichs@uni-bremen.de

[2]Present address: Carl von Ossietzky Universität Oldenburg, Institute for Chemistry and Biology of the Marine Environment (ICBM), D-26382 Wilhelmshaven, Germany

ABSTRACT

A mechanistic understanding of formation pathways of gaseous hydrocarbons is relevant for disciplines such as atmospheric chemistry, geology and astrobiology. The molecular and intermolecular patterns of stable carbon isotopic compositions ($\delta^{13}C$) of hydrocarbons are commonly used to distinguish biological, thermogenic and abiotic sources. Here we report unusual intermolecular isotope patterns of non-methane hydrocarbons in hydrothermally heated sediments of the Guaymas Basin; these patterns are inconsistent with the known formation processes of non-methane hydrocarbons. Non-methane hydrocarbons are notably ^{13}C-enriched relative to sedimentary organic matter and display an isotope pattern that is reversed relative to thermogenic gases, i.e., $\delta^{13}C$ ethane > $\delta^{13}C$ propane > $\delta^{13}C$ *n*-butane > $\delta^{13}C$ *n*-pentane. We hypothesized that this pattern results from abiotic reduction of volatile fatty acids (VFAs), which were isotopically enriched due to their prior equilibration of the carboxyl carbon with dissolved inorganic carbon. This hypothesis was confirmed by hydrous pyrolysis experiments with isotopically labeled substrates at 350 °C and 400 bar that demonstrated (I) the exchange of carboxyl carbon of VFAs with ^{13}C-bicarbonate and (II) the formation of ^{13}C-enriched ethane and propane by the reduction of 2-^{13}C-acetate, where formation of either compound appears to be governed by the abundance of H_2. Gibbs free energy computations indicate that reduction of acetate to ethane is indeed exergonic under environmental conditions of the Guaymas Basin subsurface. Collectively, our results reveal a novel abiotic formation pathway for non-methane hydrocarbons. This process may be widespread under organic-rich geothermal conditions and could impact isotopic compositions in sediments and petroleum systems.

SIGNIFICANCE

Non-methane, gaseous hydrocarbons are typically formed in geothermally heated subsurface sediments by cracking of larger precursor molecules. However, this pathway cannot account for the occurrence of C_2-C_5 hydrocarbons in hydrothermally impacted sediments of the Guaymas Basin, a sedimentary model system for extremely rapid formation of petroleum-like compounds. Here C_2-C_5 hydrocarbons are unusually enriched in ^{13}C and the intermolecular pattern of isotopic composition is opposite to that found in conventional petroleum systems. Using isotope tracer experiments at temperatures and pressures pertinent to hydrothermal conditions, we show that these hydrocarbons can be formed by reduction of the corresponding organic acids, whose carboxylic groups were isotopically equilibrated with the dissolved inorganic carbon pool. Our findings revealed a novel formation pathway for natural gases.

III.1. INTRODUCTION

Gaseous hydrocarbons (C_1-C_5) are widespread in marine sediments (Bernard et al., 1976; Claypool and Kvenvolden, 1983; Welhan and Lupton, 1987) where they may fuel chemosynthetic ecosystems or zones of intense microbial activity at or below the seafloor. Three principal sources exist for these compounds: biological processes that turn small carbon-bearing compounds into methane (Whiticar et al., 1986**)** and, in smaller quantities, its higher homologues (Hinrichs et al., 2006), thermal cracking of kerogen **(**Tissot et al., 1987**),** and abiotic production (Etiope and Schoell, 2014). Stable isotopic compositions ($\delta^{13}C$) of hydrocarbon gases are powerful tools that aid distinguishing these sources (Whiticar, 1999,Wang et al., 2015). Intermolecular carbon isotopic patterns within the homologous series of gaseous hydrocarbons likewise have diagnostic value: $\delta^{13}C$ values of thermogenic gases, formed from thermal cracking of kerogen, increase with carbon number (e.g., Chung et al., 1988; Prinzhofer and Huc, 1995; cf. Supp. Fig. III.1). By contrast, abiogenic hydrocarbons formed via Fischer-Tropsch type (FTT) reduction of aqueous CO_2 (e.g., ref. Proskurowski et al., 2008; cf. Supp. Fig. III.1B) or from polymerization of methane (Lollar et al., 2002; cf. Supp. Fig. III.1C) are increasingly depleted in ^{13}C with increasing carbon number, resulting in an inverse isotope trend compared to thermogenic production. Accordingly, methane formed via FTT reactions is typically isotopically enriched in ^{13}C (less negative values) relative to thermogenic methane (cf. Supp. Fig. III.1A, B), while non-methane hydrocarbons formed by polymerization of methane are substantially depleted in ^{13}C relative to those formed by FTT reactions and thermogenic processes (cf. Supp. Fig. III.1A, C). Lastly, biogenic methane is generally ^{13}C-depleted relative to methane from other sources (Whiticar et al., 1986). For ethane, a biological formation pathway involving the reduction of acetate and - in the case of propane - incorporation of dissolved inorganic carbon was suggested (Hinrichs et al., 2006; cf. Supp. Fig. III.1D).

In this study we investigated gaseous hydrocarbons in over 230 samples of both hydrothermally-heated and cold sediments from the Guaymas Basin and observed unusual intermolecular carbon isotopic patterns for ethane, propane, *n*-butane, and *n*-pentane; these patterns are inconsistent with any of the above described pathways. The Guaymas Basin is a unique locality where rapid deposition of organic-rich sediments combined with hot basaltic sill intrusions into the unconsolidated sediments results in rapid heating of young, immature organic matter. This causes the generation of large amounts of complex petroleum-like compounds (Didyk and Simoneit, 1989; Peter et al., 1991; Simoneit and Kawka, 1987; Simoneit et al., 1990; Simoneit et al., 1979), gaseous hydrocarbons (Simoneit and Galimov, 1984; Simoneit et al., 1988), volatile fatty acids (VFAs) (Martens, 1990) and ammonia (Von Damm et al., 1985), which migrate upwards with the hydrothermal fluids to fuel a flourishing seafloor ecosystem (Teske et al., 2014). A detailed description

of subsurface hydrothermal circulation and associated habitats including most of the research sites of this study has been previously provided (Teske et al., 2016). At all sites we observed high amounts of hydrocarbon gases.

Given the unusual intermolecular isotopic patterns of C_2 to C_5 hydrocarbons, we explored the potential for an alternative formation pathway involving reduction of organic acids and prior equilibration of their carboxyl groups with ambient dissolved inorganic carbon (DIC). We conducted sequential hydrous pyrolysis experiments amended with ^{13}C-labeled DIC and acetate to assess if this pathway can produce and explain the observed isotope pattern.

III.2. RESULTS AND DISCUSSION

Samples were retrieved from Guaymas Basin sediments at 11 different sites (Supp. Fig. III. 2) spanning temperatures from 3 °C at the sediment surface to 180 °C at 40 to 50 centimeters below seafloor (cmbsf) (Supp. Table III.1 and Supp. Fig. III.3). Except for the off-axis site Octopus Mound located at the central seep (Geilert et al., 2018), the remaining 10 research sites were located in the southern trough, which is hydrothermally highly active (Williams et al., 1979). While most of these sites were clustered within ~500-m-distance, Northern Tower Site 2 and Site 3 were located further north in the trough (Supp. Fig. III.2).

III.2.1. Microbial overprint of isotopic compositions from deeply sourced gases

A large fraction of the hydrocarbon gases is formed in the deep subsurface, where basaltic sill intrusions result in thermogenic degradation of immature organic matter (Simoneit et al., 1988). The stable carbon isotopic compositions (δ^{13}C) from samples obtained in the temperature range of ~150 to 180 °C (Fig. III.1) is most characteristic of this deeply sourced gas, because it has presumably not been impacted by biological processes, as frequently observed in colder sediments (see below). At these high temperatures, methane carries a typical thermogenic signal (-42.8±0.4‰, mean±SD, n=8), consistent with methane δ^{13}C values reported at deeply buried sills (Simoneit et al., 1986). The C_2-C_5 hydrocarbons exhibit unusually ^{13}C-enriched isotopic compositions and an isotope pattern that is neither conform with a traditional thermogenic origin nor known abiogenic production (Fig. III.1; Supp. Table III.2, cf. next section).

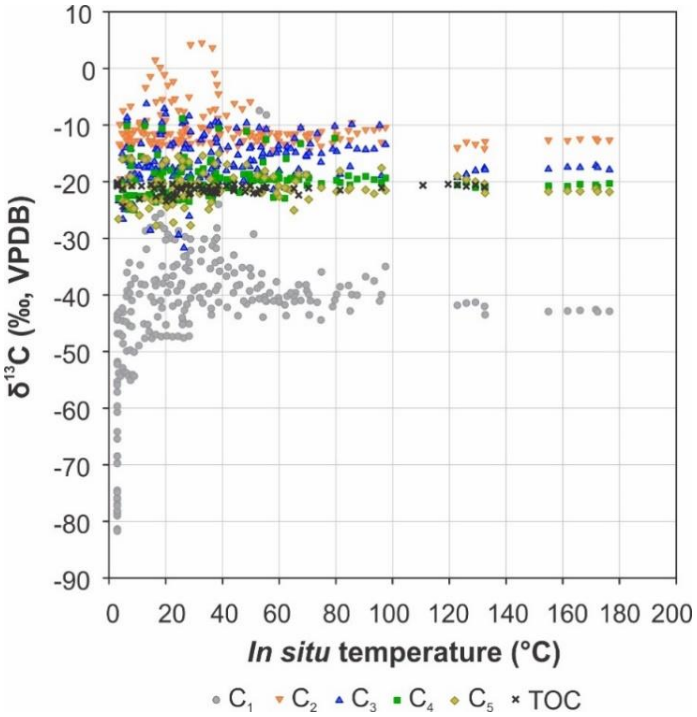

Figure III.1. Carbon isotopic compositions ($\delta^{13}C$) of C_1-C_5 hydrocarbons and TOC in a wide range of *in situ* temperatures at the Guaymas Basin. Samples were retrieved from Guaymas Basin sediments at 11 different sites (cf. Supp. Table III.1). Data from a small fraction of samples (17 out of 236) was published previously (Dowell et al., 2016; cf. Supp. Table III.2).

At *in situ* temperatures of 3 to 60 °C, exuberant microbial activity is commonly observed in Guaymas Basin sediments (McKay et al., 2016). Within this temperature range $\delta^{13}C_1$ values spanned a wide range from -81.7 to -7.5‰. The most negative values strongly suggest the activity of biological methanogenesis while the least negative values probably result from the activity of anaerobic methane-oxidizing communities in cooler surface sediments (cf. McKay et al., 2016; Teske et al., 2002; Holler et al., 2011). The microbially sourced admixtures of methane are also indicated by the abundance ratios of $C_1/(C_2+C_3)$ (Bernard et al., 1976). At the central seep site Octopus Mound, where *in situ* temperatures in the sediment core did not exceed 3 °C, $C_1/(C_2+C_3)$ ratios (319±137, mean±SD, n=24) and relatively negative $\delta^{13}C_1$ values (-81.7 to -55.3‰) indicated admixtures of methane from microbial sources. Likewise, $\delta^{13}C$ of non-methane hydrocarbons showed notable, mostly positive, deviations from the deeply sourced values observed at temperatures above 150 °C. For example, $\delta^{13}C_2$, $\delta^{13}C_3$, $\delta^{13}C_4$ and $\delta^{13}C_5$ reached respective values as high as +4.5‰, -6.3‰, -8.9‰ and -15.0‰. We attribute these deviations to isotopic fractionation induced by biologically mediated oxidation, consistent with the presence and activity of hydrocarbon-oxidizing microbes in the shallower hydrothermally warmed sediments of the Guaymas Basin (Kniemeyer et al., 2007; Laso-Pérez et al., 2016; Seitz et al., 2019), including anaerobic methane-oxidizing communities (e.g., refs. Biddle et al., 2012; Holler et al., 2011; Teske et al., 2002). Although ethane is presumed to be the chemically

most inert hydrocarbon gas under anaerobic conditions with extremely slow microbial utilization (Widdel and Grundmann, 2010), extraordinary ^{13}C-enriched ethane values of up to +4.5‰ at one sediment core (4484-6) from the Mat Mound site, which is situated below 40 °C, indicates microbial oxidation as prominent process. Evidence is accumulating that archaea are capable of anaerobic ethane degradation under sulfate-reducing conditions at mesophilic to thermophilic temperatures (Adams et al., 2013; Dowell et al., 2016; Laso-Pérez et al., 2019) as found in the Guaymas Basin. Likewise, propane and *n*-butane were recently demonstrated to be readily utilized by both bacterial and archaeal communities (e.g., refs. Kniemeyer et al., 2007; Laso-Pérez et al., 2016; Seitz et al., 2019).

III.2.2. Unusual hydrocarbon gas isotope pattern in the Guaymas Basin

Above 80 °C, which has been proposed as the upper thermal limit for hydrocarbon-degrading microbes in subsurface hydrocarbon reservoirs (Head et al., 2003), $\delta^{13}C_1$ values exhibited a narrower range between -44.4 and -34.3‰, and $C_1/(C_2+C_3)$ ratios were between 2 and 102. This trend points to a diminished impact of microbial processes on the methane pool and to a predominantly thermogenic origin of methane at these elevated temperatures, as reported previously (Simoneit et al., 1986). Also, $\delta^{13}C$ values for the other hydrocarbon gases were relatively uniform compared to those at lower temperatures. In particular, propane and ethane $\delta^{13}C$ values ranged between -19.3‰ to -7.2‰ and thus were notably enriched in ^{13}C relative to the surrounding total organic carbon (TOC) values ($\delta^{13}C_{TOC}$: -21.9‰ to -20.4‰).

We defined the averaged isotopic compositions of hydrocarbons detected in samples with *in situ* temperatures > 80 °C as hydrothermal endmember values, which are only minimally impacted by microbial processes (Fig. III.1; Supp. Fig. III.1E). The averaged values for samples above 80 °C were -40.5±2.7‰ (mean±SD, n=28) for methane, -11.7±1.8‰ (mean±SD, n=28) for ethane, -15.3±3.1‰ (mean±SD, n=28) for propane, -19.6±1.9‰ (mean±SD, n=24) for *n*-butane, and -20.5±1.6‰ (mean±SD, n=22) for *n*-pentane. This pattern of isotope values of C_{2+} hydrocarbons (Supp. Fig. III.1E) is reversed relative to the conventional pattern of hydrocarbon gases formed by thermogenic degradation of kerogen (Supp. Fig. III.1A, ref. Prinzhofer and Huc, 1995). Similar reversed isotope patterns for hydrocarbon gases have been reported before in other geologic settings and were explained as a result of, for example, FTT reactions (Supp. Fig. III.1B, ref. Proskurowski et al., 2008) or methane polymerization (Supp. Fig. III.1C, ref. Lollar et al., 2002). However, these scenarios are not applicable to our system as $\delta^{13}C_1$ values are substantially lower than those predicted for FTT reactions and are more consistent with a thermogenic origin (Simoneit et al., 1986). Furthermore, non-methane hydrocarbons are enriched in ^{13}C relative to products of methane polymerization (Lollar et al., 2002).

Given these inconsistencies with known hydrocarbon gas formation pathways, we explored whether post-genetic processes may have affected the isotopic compositions of the gases. Apart from microbially mediated oxidation, which presumably is unimportant at temperatures > 80 °C (cf. ref. McKay et al., 2016, Head et al., 2003), another possible mechanism is abiotic oxidation. An analogous mechanism has been invoked for hydrothermal fluids from the Main Endeavour Field (Cruse and Seewald, 2010) where isotope patterns of methane, ethane and propane resembled those observed in this study. At that site, stepwise oxidation of ethane and propane was proposed to explain the ^{13}C-enrichment. This process ultimately leads to an isotopic reversal for ethane and propane, but also to the production of methane that is isotopically lighter (more negative $\delta^{13}C_1$ values) than its precursor but still heavier than methane of either thermogenic or methanogenic origin. As a consequence of this post-genetic oxidation, $C_1/(C_2+C_3)$ ratios increase as the $\delta^{13}C$ values of methane, ethane and propane become heavier (Cruse and Seewald, 2006, 2010). However, such a trend was not observed in the Guaymas Basin sediments. Instead, at *in situ* temperatures < 80 °C an increase in $C_1/(C_2+C_3)$ ratio was accompanied by both low and high $\delta^{13}C_1$ values that revealed the impact of methanogenesis and methanotrophy, respectively, while at temperatures > 80 °C, $\delta^{13}C_1$ values remained invariable independently of the $C_1/(C_2+C_3)$ ratios (Supp. Fig. III.4A). Similarly, no significant relationship between the $C_1/(C_2+C_3)$ ratios and $\delta^{13}C_2$ or $\delta^{13}C_3$ values was observed (Supp. Fig. III.4 B and C).

III.2.3. Experimental evidence for *n*-alkane synthesis through organic acid reduction

After excluding known pathways of biogenic and abiogenic production, thermogenic degradation of kerogen and post-genetic oxidation as causes for the unusual hydrocarbon gas isotope signatures at Guaymas Basin, we consider reduction of organic acids to *n*-alkanes as potential mechanism to generate C_2 to C_{2+n} hydrocarbons, which could exhibit the observed isotope pattern. This potential pathway is supported by a report of a reversed isotope pattern in the suite of volatile fatty acids (VFAs), from acetic acid through valeric acid in oil field waters of the San Joaquin Basin (Franks et al., 2001), which resembled that of the corresponding hydrocarbons in our study (Fig. III.2). In that study, the $\delta^{13}C$ value in the acid components increased with decreasing molecular weight and was generally higher than their syngenetic oils (Franks et al., 2001). The authors suggested that exchange of the carboxylic carbon of VFAs and the isotopically heavier pool of dissolved inorganic carbon (DIC) was the cause of ^{13}C enrichment in the acid (Franks et al., 2001).

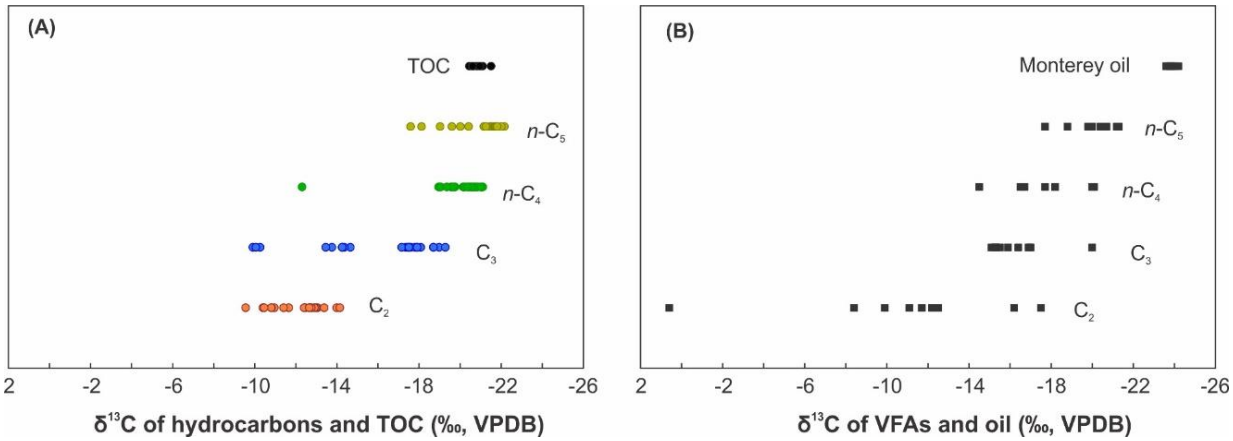

Figure III.2. Comparison of isotopic patterns of C_2-C_5 hydrocarbons from the Guaymas Basin and the corresponding VFAs in oil field waters from the San Joaquin Basin. (A) $\delta^{13}C$ values of non-methane hydrocarbons, ethane through *n*-pentane (C_2-C_5) and TOC at Guaymas Basin in this study at *in situ* temperatures > 80 °C, data were collected from 30 samples of the following sampling sites: Mat Mound (data from three samples from this site was published previously; ref. 38; cf. Supp. Table III.2), T-logger mat/Marker 14, Megamat, INSINC Mat I and Cathedral Hill/Marker 24 where *in situ* temperatures were > 80 °C, see Supp. Table III.2 for details; (B) $\delta^{13}C$ values of VFAs, acetic acid through *n*-valeric acid (C_2-C_5) and their coproduced oil from oil field waters of the San Joaquin Basin at temperatures of 96-135 °C, data were taken from Franks et al. (2001).

In light of this observation, we explored whether reduction of VFAs could be an alternative formation pathway for hydrocarbons within hydrothermal sediments of the Guaymas Basin as this process would lead to isotopically heavy C_2-C_5 hydrocarbons and a reversed isotope pattern. Both, high abundance of VFAs (Martens, 1990) and H_2-rich hydrothermal fluids (Welhan and Lupton, 1987, Von Damm et al., 2005) at Guaymas Basin provide favorable conditions for this reaction. These reactions may take place at substantially higher temperatures than those observed in the sampled shallow cores, e.g., in the subsurface in the vicinity of sill intrusions. This is consistent with ^{14}C-dating of petroleum-like compounds (Peter et al., 1991) and methane (Pearson et al., 2005) in the Guaymas Basin, which place the reaction zone to at least 30-60 m sediment depth.

In order to test the hypothesis, involving both exchange of carboxylic carbon atoms of VFAs with bicarbonate and reduction of VFAs to hydrocarbons at high temperatures, we conducted three hydrous pyrolysis experiments. For this, we mixed hydrothermally affected sediment retrieved from the Megamat II site (core 4861-36) with artificial seawater (cf. ref. Kester et al., 1967) at an initial fluid/sediment ratio of 7 and heated the mixture to 350 °C at 400 bars. In experiment I (Fig. III.3, Supp. Table III.3), ^{13}C-labeled bicarbonate (~9,300‰) and unlabeled VFAs (acetate through valerate, with $\delta^{13}C$ between -40 and -20‰) were added to the seawater. After 24 hours, highly ^{13}C-labeled VFAs ranging from 209 to 979‰ were observed, while $\delta^{13}C_{DIC}$ dropped to ~2,400‰. Isotopic exchange of carboxylic carbons of VFAs and DIC proceeded rapidly, forming a reversed isotope pattern for VFAs in accordance with the proportionally

decreasing contribution of carboxylic carbon with increasing carbon chain length (Fig. III.3A, Supp. Table III.3). This experimental result confirms that carboxylic carbon exchanges between organic acids and dissolved inorganic carbon proceed under hydrothermal conditions (Reaction 1).

$$CH_3(CH_2)_n{}^{12}COOH + {}^{13}CO_2\,(aq) \rightleftharpoons CH_3(CH_2)_n{}^{13}COOH + {}^{12}CO_2\,(aq) \qquad \textbf{[1]}$$

n = 0 to 3, representing acetic acid through valeric acid.

In the next experiments, ^{13}C-2-sodium acetate was added together with either 10 mM (experiment II) or 100 mM (experiment III) of sodium formate using the same experimental set-up and sample material as in experiment I. Formate was added as source for H_2 generation to create the required reducing conditions (McCollom and Seewald, 2003a). H_2 concentration remained at micromolar and millimolar levels in experimental fluid samples after addition of 10 mM and 100 mM formate, respectively (Supp. Table III.4). After 72 hours, we detected the formation of ^{13}C-enriched ethane, with $\delta^{13}C$ values of 3.1‰ and 25.4‰ in experiments II and III, respectively (Supp. Fig. III.5 and Supp. Table III.4). These results indicate the formation of ethane from the reduction of acetate, as demonstrated in Reaction 2.

$$\underset{\text{Acetic acid}}{{}^{13}CH_3COOH} + 3H_2\,(aq) \longrightarrow \underset{\text{Ethane}}{{}^{13}CH_3CH_3} + 2H_2O \qquad \textbf{[2]}$$

In addition, ^{13}C-labeled propane was observed (Supp. Fig. III.5 and Table III.4), which was likely formed according to Reaction 3, a reaction previously suggested to occur during biological propane formation (Hinrichs et al., 2006). Consistent with this reductive carbon-chain-elongation of acetate, other byproducts and/or potential intermediates formed included ^{13}C-labeled acetone and propionate (Supp. Fig. III. 6 and Table III.5).

$$\underset{\text{Acetic acid}}{{}^{13}CH_3COOH} + CO_2(aq) + 6H_2 \longrightarrow \underset{\text{Propane}}{{}^{13}CH_3CH_2CH_3} + 4H_2O \qquad \textbf{[3]}$$

Fig. III.3B shows the $\delta^{13}C$ values of ethane and propane in both experiments after 72 hours with addition of either 10 mM or 100 mM formate. More label was incorporated into ethane and propane under more reducing conditions, consistent with the kinetics of VFA reduction depending on the H_2 concentration. Assuming a closed system with isotopic compositions of acetate (4,000‰) and ethane (-30‰, derived from Experiment I without reducing conditions, cf. Supp. Table III.3) defining the two endmembers, isotopic mass balance - based on the $\delta^{13}C$ values of 3.1‰ and 25.4‰ for ethane after 72 hours (cf. Supp. Table III.4) - indicates that 0.8% (experiment II) and 1.4% (experiment III) of the ethane pool was derived from the conversion of acetate under moderately and strongly reducing conditions, respectively. By comparison, for

propane formation under these conditions, assuming the isotopic compositions of acetate (4,000‰), DIC (0‰) and propane (-30‰, derived from Experiment I under non-reducing conditions, cf. Supp. Table III.3) as endmembers, as much as 2.1% (experiment II) and 8.1% (experiment III) of the propane pool, with respective $\delta^{13}C$ values of 13‰ and 135‰ (cf. Supp. Table III.4), was derived from the conversion of acetate. The substantially higher relative increase of propane formation (4-fold) compared to ethane (2-fold) under strongly reducing conditions suggests that propane is the preferentially formed product at high hydrogen concentrations, in analogy to earlier suggestions for its biological formation (Hinrichs et al., 2006).

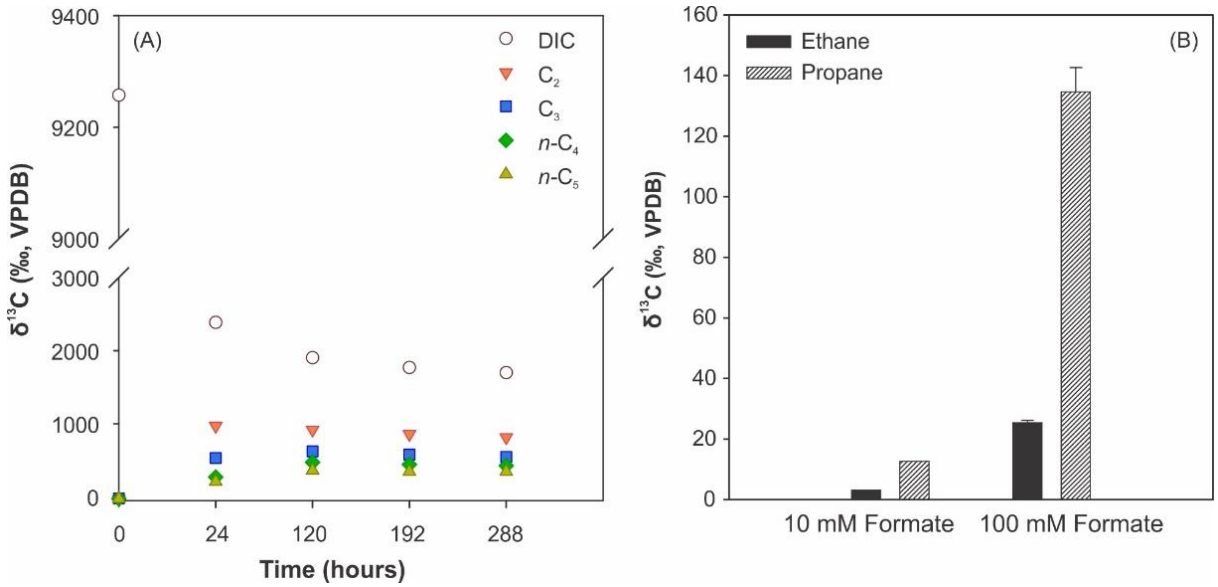

Figure III.3. Results from hydrous pyrolysis experiments with Guaymas Basin sediments after addition of ^{13}C-labeled tracers. (A) $\delta^{13}C$ values of DIC and VFAs, acetate up to valerate (C_2-C_5), during the Experiment I at 350 °C and 400 bar with addition of 10% ^{13}C-labeled DIC (9257‰) and unlabeled C_2-C_5 VFAs; (B) $\delta^{13}C$ values of ethane and propane over 72 hours during the Experiment II at 350 °C and 400 bar, with addition of ^{13}C-2-sodium acetate, and 10 mM and 100 mM formate as additional source of H_2 to create highly reducing conditions.

Experiments II and III have demonstrated that, the reduction of VFAs to hydrocarbons may proceed under the experimental conditions applied to Guaymas Basin sediment. However, our experiments also demonstrate that under highly reducing conditions, chain elongation according to Reaction 3 may compete with the simple reduction according to Reaction 2. Due to the incorporation of additional DIC-derived carbon atoms (with less negative $\delta^{13}C$ values; cf. ref. Simoneit and Galimov, 1984), Reaction 3 would result in an opposite isotopic pattern with propane being ^{13}C enriched relative to ethane; since this trend is not observed this reaction is probably not dominant under the conditions in the Guaymas Basin subsurface. By analogy, a corresponding argument can possibly be made for the higher hydrocarbons *n*-butane and *n*-pentane, for which the isotopic pattern can only be explained by a minimal role of carbon-chain elongation from lower carbon-numbered carboxylic acid precursors according to Reaction 3.

In order to constrain the environmental conditions favoring Reaction 2 over Reaction 3, we calculated the Gibbs free energy yields (Δ_rG) for these two reactions. The thermodynamic model was designed to mimic the conditions found in Guaymas Basin hydrothermal sediments (e.g., refs. Simoneit, 1985, Martens, 1990), i.e., p = 200 bar, pH = 6, [DIC] = 10 mM, and Δ_rG of ethanogenesis and propanogenesis were derived for a range of H_2 concentrations and reaction temperatures (Fig. III.4). Modeling results indicate that propane formation according to Reaction 3 is favored at higher H_2 concentrations and lower temperatures, while ethane formation becomes thermodynamically favorable with increasing temperature and at moderate H_2 concentrations. Under the assumption that Reaction 2 and corresponding reactions for the higher homologues have caused the isotopic relationships of hydrocarbon gases in Guaymas Basin (cf. Fig. III.2), we can thus constrain their formation environment to hot hydrothermal subsurface sediments (ref. Peter et al., 1991; Fig. III.4; $[H_2] < 10$ mM, T > 250 °C).

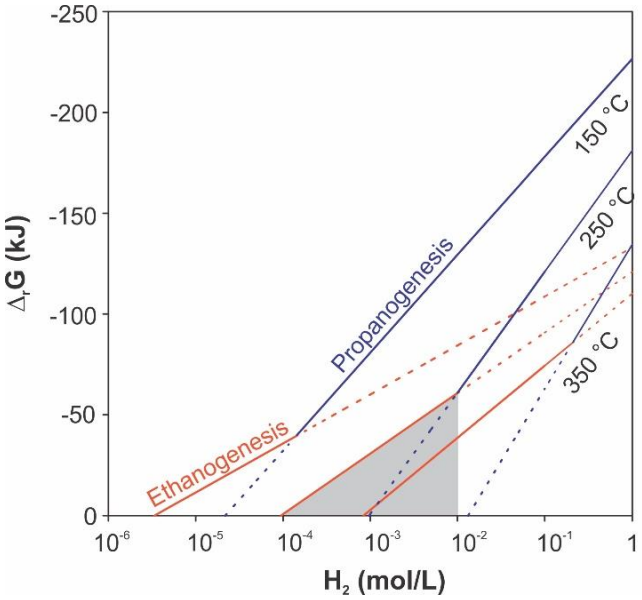

Figure III.4. Energy yields of hydrocarbon formation from acetate. Gibbs free energy (ΔrG) yields of ethanogenesis (orange line, Reaction 2) and propanogenesis (blue line, Reaction 3) as a function of H_2 concentrations at temperatures from 150 to 350 °C, assuming approximate *in situ* conditions in Guaymas Basin hydrothermal sediments: p = 200 bar, pH = 6, [DIC] = 10 mM, [acetate] = 1 mM, [ethane] = 0.1 mM, [propane] = 0.1 mM. Solid line refers preferential reaction, while dashed line refers less preferential reaction under specific conditions of temperature and H_2 concentration. With decreasing H_2 concentrations in the reaction zone, ethanogenesis becomes thermodynamically more favorable than propanogenesis. Under hydrothermal conditions pertinent to the reaction zone, i.e., T > 250 °C and $[H_2] < 10$ mM (shaded gray area), ethanogenesis is thermodynamically more favorable.

Collectively, our results indicate a two-step reaction mechanism involving carboxyl carbon exchange and abiotic reduction of VFAs as a novel formation pathway of non-methane hydrocarbon gases in reducing hydrothermal sediments. In such a system, ongoing hydrothermal decomposition of sedimentary organic matter results in significant generation of organic acids, which incorporate inorganic carbon through rapid carbon exchange with dissolved inorganic carbon under high temperature conditions. Continuous reduction

of organic acids to non-methane hydrocarbon gases then ultimately results in the unusual systematic isotope pattern observed at the Guaymas Basin. While thermogenic gases may also be formed via conventional cracking of kerogen, their isotopic signals are overprinted by these reductive processes. It is conceivable that this process occurs in similar sedimentary systems, thus its effects on isotopic compositions of non-methane hydrocarbon gases should be taken into consideration.

III.3. MATERIALS AND METHODS

Twenty-two push cores were collected from hydrothermally active and inactive sediments by deep-sea submersible *Alvin* at 11 sites (Supp. Table III.1) during three expeditions conducted by the R/V *Atlantis* in the Guaymas Basin in 2008, 2009 and 2016. Before sampling, temperature profiles at the sampling site were recorded using *Alvin*'s external heat-flow probe as described elsewhere (McKay et al., 2012).

III.3.1. Hydrocarbon gases

2-5 mL of fresh sediment were taken within 4 hours after core recovery by a head-cut syringe in 2 cm intervals and placed in headspace vials containing 5 mL of 1 M NaOH solution, crimp sealed with butyl rubber septa and stored upside down at -20 °C for further analysis. Mixtures in headspace vials were homogenized by gently shaking overnight in room temperature. Concentrations of hydrocarbon gases were defined by Trace gas chromatograph (GC) equipped with a flame ionization detector (FID). A carboxen 1006 PLOT column (30 m × 0.32 mm, SUPELCO) was equipped for analysis of methane with temperature set at 40 °C (held for 6 min). A AT-Q column (30 m × 0.32 mm, Alltech) was applied for the analysis of C_2-C_5 higher alkanes, with a temperature program of 60 °C (held for 1 min) to 240 °C (held for 7 min) at a rate of 40 °C/min. The molar fraction of hydrocarbon gases was calculated by injection of known quantities of hydrocarbon gas standards.

The determination of stable carbon isotope ratios of hydrocarbon gases was performed by GC coupled to Delta Plus XP isotope ratio mass spectrometer via a combustion interface-III (all from ThermoFinnigan GmbH, Bremen, Germany). The applied column and temperature program were identical to those for the concentration measurements. The internal precision was ± 0.5‰. Stable carbon isotope ratios were reported in $\delta^{13}C$ notation (per mil, ‰) relative to the Vienna Peedee Belemnite Standard (VPDB), with $\delta^{13}C = (R_{sample}-R_{VPDB})/R_{VPDB} * 10^3$, where $R= {}^{13}C/{}^{12}C$ and $R_{VPDB} = 0.0112372 \pm 2.9 * 10^{-6}$.

III.3.2. Porewater geochemistry

Porewater was obtained by Rhizon samplers at 1-cm intervals upon core retrieval onboard. Samples for VFA analysis were stored at -20 °C. 2 mL vials were filled with porewater and stored at 4 °C for further DIC analysis. The concentration and $\delta^{13}C$ values of VFAs were analyzed onshore by isotope ratio monitoring liquid chromatography/mass spectrometry (irm-LC/MS) as described previously (Heuer et al., 2006). The internal precision was < 1‰. Carbon isotopic compositions of DIC were defined using a Delta Ray Isotope Ratio Infrared Spectrometer (IRIS) equipped with Universal Reference Interface (URI) Connect and autosampler (Thermo Fisher Scientific, Germany) as described previously (Aepfler et al., 2019). The internal precision was < 0.2‰.

III.3.3. Total organic carbon (TOC)

Approximately one gram of freeze-dried sediment was decalcified and analyzed with continuous-flow elemental analyzer-isotope ratio mass spectrometer (EA-IRMS) for the content and isotopic compositions of TOC. The internal precision is ±0.1‰.

III.3.4. Hydrous pyrolysis experiments

Three hydrous pyrolysis experiments were conducted utilizing a customized Dickson-type flexible reaction cell setup (Parr Instruments). As reactants, 20-25 g of sediment (initial porewater/sediment mass ratio of ~1:1) from core 4861-36 (retrieved from Megamat II) and approximately 70 g of artificial seawater (Kester et al., 1967) were transferred into a gold reaction cell ($V_{total} \approx 100$ mL), to set the initial fluid/sediment ratio to 3.5. Pressure in all experiments were set to 400 bars. Temperature was set to 250-350 °C. Experiments were performed for total of 288 hours (Experiment I), 408 hours (Experiment II) and 72 hours (Experiment II). Fluid sample was taken to fill up a 1.5 mL vial and stored upside down for DIC isotopic composition measurement; ~1 mL of fluid was taken for VFA concentration and isotopic composition measurements; 1-2 mL of fluid were taken for measurements of concentrations and isotopic compositions of hydrocarbon gases. The instrumental methods are same as described before. 1-2.5 mL of fluid were taken for H_2 concentration measurements; after certain time of equilibration between fluid and headspace, gas in headspace of a 5-mL-syringe was directly injected to a GC equipped with thermal conductivity detector (TCD).

III.3.5. Thermodynamic calculations

The standard Gibbs free energies of reaction ($\Delta_r G^0$) was calculated using SUPCRT92 (Johnson et al., 1992, Dick, 2019) for a pressure of 250 bar and variable temperatures. The free energies of reactions ($\Delta_r G$), as shown in Fig. III.4, were calculated according to $\Delta_r G = \Delta_r G^0 + 2.303\ R\ T \log Q$, where R is the universal gas constant, T is temperature in Kelvin, and Q is the activity quotient of the reactants and reaction products, assuming [acetate] = 1 mM, [ethane] = [propane] = 0.1 mM, [DIC] = 10 mM, pH = 6. Equations 5 and 6 were used to calculate the respective Q values for ethanogenesis and propanogenesis. Here, [acetate] and [HCO_3^-] were corrected for actual concentrations under thermodynamic equilibrium using Eqs. 7 and 8.

$$Q = \frac{[ethane]}{[acetate] \times [H_2]^3 \times [H^+]} \qquad [5]$$

$$Q = \frac{[propane]}{[acetate] \times [H_2]^6 \times [HCO_3^-] \times [H^+]} \qquad [6]$$

$$\log K = \frac{[acetic\ acid]}{[acetate] \times [H^+]} \qquad [7]$$

$$\log K = \frac{[CO_{2,aq}]}{[HCO_3^-] \times [H^+]} \qquad [8]$$

ACKNOWLEDGEMENTS

We deeply appreciate the captain and crew of R/V Atlantis and the HOV *Alvin* team for their expert support, and the scientific party for sample recovery and documentary of *Alvin* dives during the cruise AT15-40, AT15-56 and AT37-06, funded by NSF (OCE-0647633 and OCE-1357238). Substantial technical support throughout the project from Jenny Wendt and Xavier Prieto Mollar is acknowledged. We thank Heidi Taubner and Jessica Arndt for their assistance in DIC isotope measurements and Gunter Wegener and Karen G. Lloyd for providing the sulfate data. Alexander Diehl is acknowledged for his help with the H_2 gas analysis. This study was supported by the Deutsche Forschungsgemeinschaft (DFG, German Research Foundation) under Germany's Excellence Strategy - EXC-2077 - 390741603. Min Song was sponsored by the China Scholarship Council (CSC) and the GLOMAR graduate school. Andreas Teske acknowledges a fellowship of the Hanse Institute of Advanced Studies in Delmenhorst, Germany. All raw data reported for environmental samples are accessible in the Pangaea database at http://doi.pangaea.de/10.1594/PANGAEA.###.

SUPPLEMENTARY INFORMATION

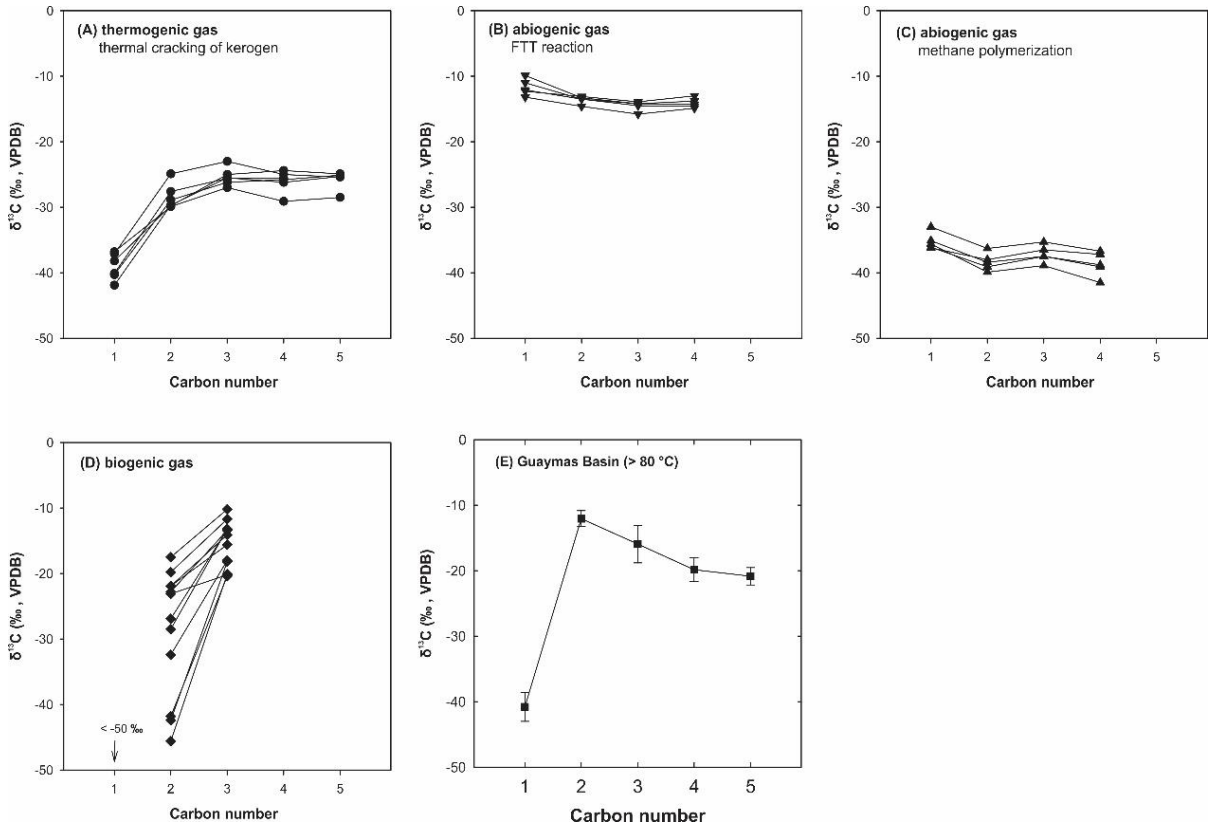

Supplementary Figure III.1. Diverse isotope patterns for hydrocarbon gases observed in nature. This plot shows selected $\delta^{13}C$ values of C_1-C_5 hydrocarbons against carbon number for (A) thermogenic hydrocarbons from Angola and North Sea (ref. Prinzhofer and Huc, 1995), abiotic hydrocarbons formed by (B) either Fischer-Tropsch type (FTT) CO_2 reductions from the Lost City hydrothermal vent field (ref. Proskurowski et al., 2008) or by (C) polymerization of methane precursors from the Kidd Greek mine (ref. Lollar et al., 2002), (D) biogenic hydrocarbons in the deep marine subsurface from the southeastern Pacific (ref. Hinrichs et al., 2006), and (E) average $\delta^{13}C$ values of C_1-C_5 hydrocarbons in Guaymas sediments under *in situ* temperatures > 80 °C: $\delta^{13}C_1$ = -40.8±2.2‰ (mean±SD, n=23), $\delta^{13}C_2$ = -12.1±1.2‰ (mean±SD, n=23), $\delta^{13}C_3$ = -15.9±2.9‰ (mean±SD, n=23), $\delta^{13}C_4$ = -19.9±1.8‰ (mean±SD, n=21), $\delta^{13}C_5$ = -20.9±1.3‰ (mean±SD, n=19).

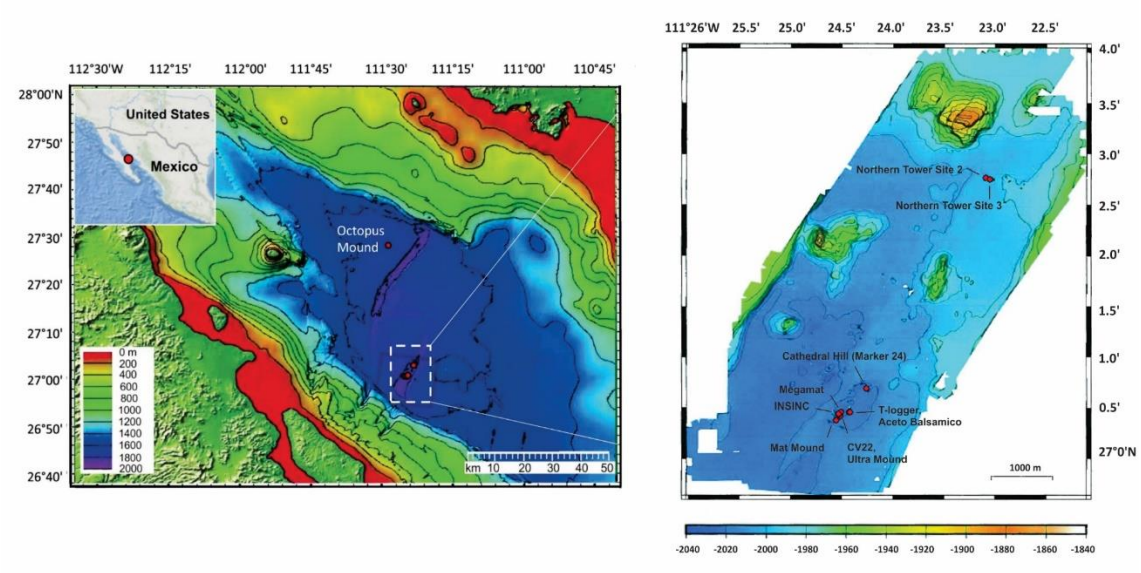

Supplementary Figure III.2. Guaymas Basin map and the 11 sampling locations.

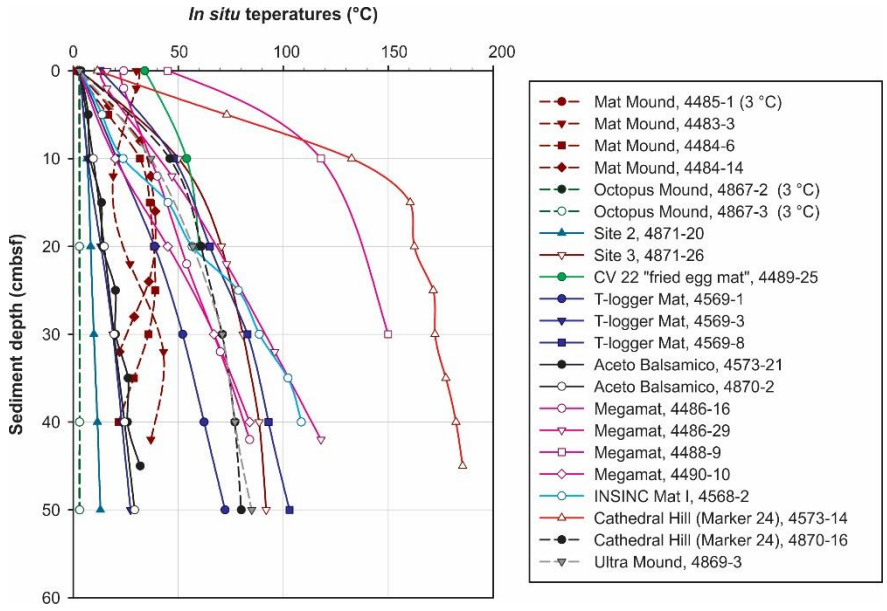

Supplementary Figure III.3. Temperature profiles of 22 sediment cores (reaching down to 50 centimeters below seafloor, cmbsf) retrieved from 11 sites at Guaymas Basin (cf. Supp. Fig. III.2). Temperature profiles for *Alvin* dive numbers 44## and 45## were plotted based on dive reports of the 2008 and 2009 cruises (AT15-40 and AT15-56) and can be referred to ref. McKay et al., 2016, while those for *Alvin* dive number 48## were plotted based on dive reports of the 2016 cruise (AT37-06).

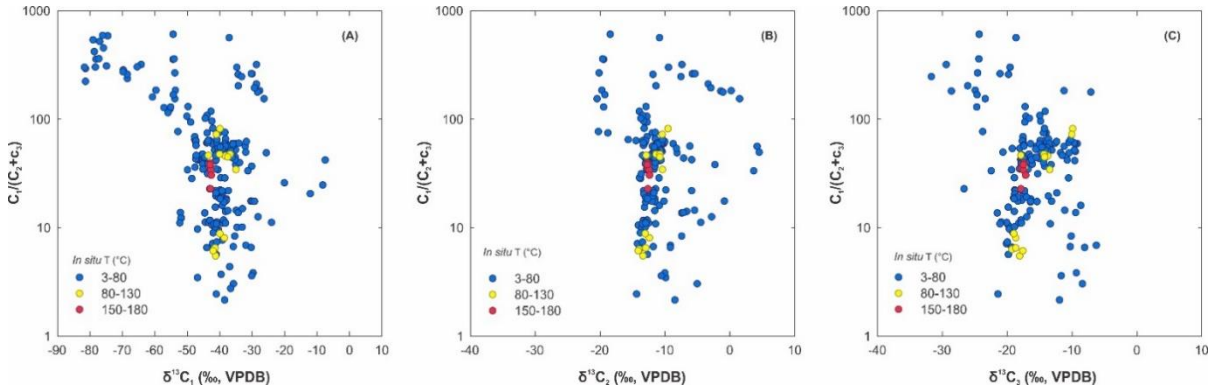

Supplementary Figure III.4. Relationships of $C_1/(C_2+C_3)$ ratios and isotopic compositions of C_1-C_3 hydrocarbons at the Guaymas Basin. Plot shows $C_1/(C_2+C_3)$ ratios against (A) $\delta^{13}C_1$, (B) $\delta^{13}C_2$ and (C) $\delta^{13}C_3$. The dot color reflects *in situ* temperatures ranging from 3 to 180 °C in mixed sediment depths.

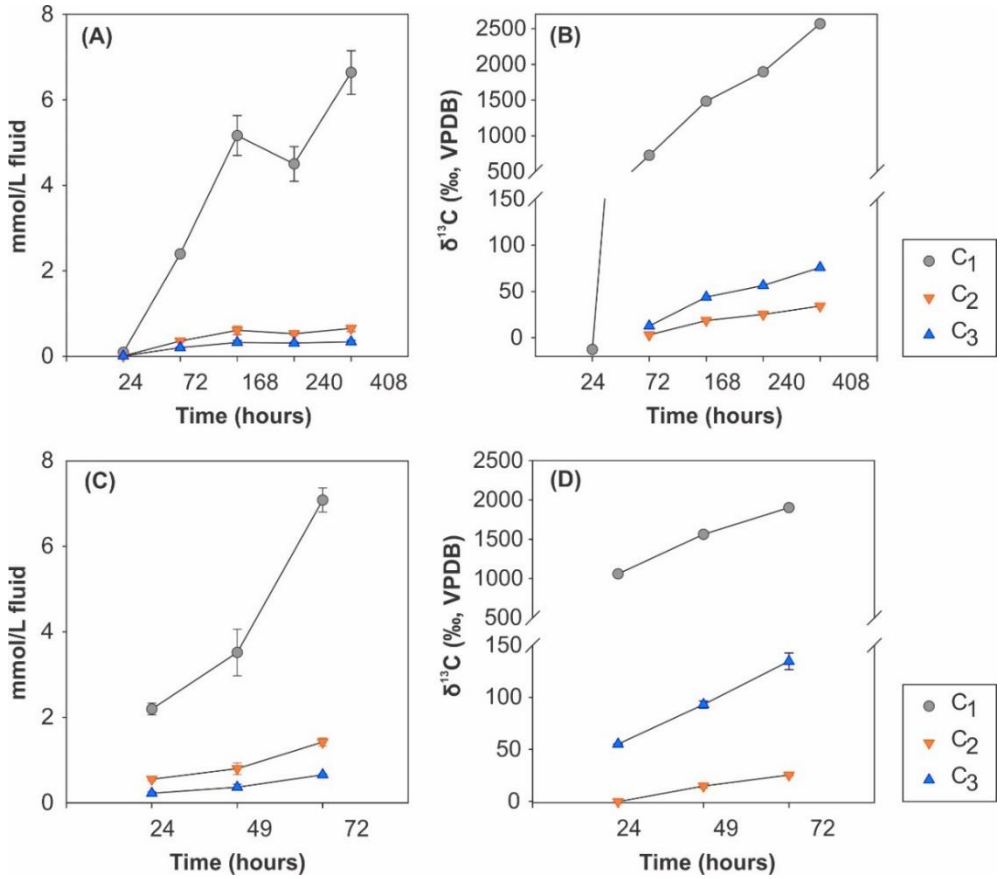

Supplementary Figure III.5. Results from hydrous pyrolysis experiments with Guaymas Basin sediments. Concentration and $\delta^{13}C$ values of methane (C_1, grey circle), ethane (C_2, orange triangle down) and propane (C_3, blue triangle up) with addition of 10 mM sodium formate (A, B) at 250 °C (first 24 hours) and 350 °C (after 24 hours), 400 bar, and those with addition of 100 mM sodium formate (C, D) at 350 °C, 400 bar. Here highly labeled methane was produced through decarboxylation of acetate (McCollom and Seewald, 2003b).

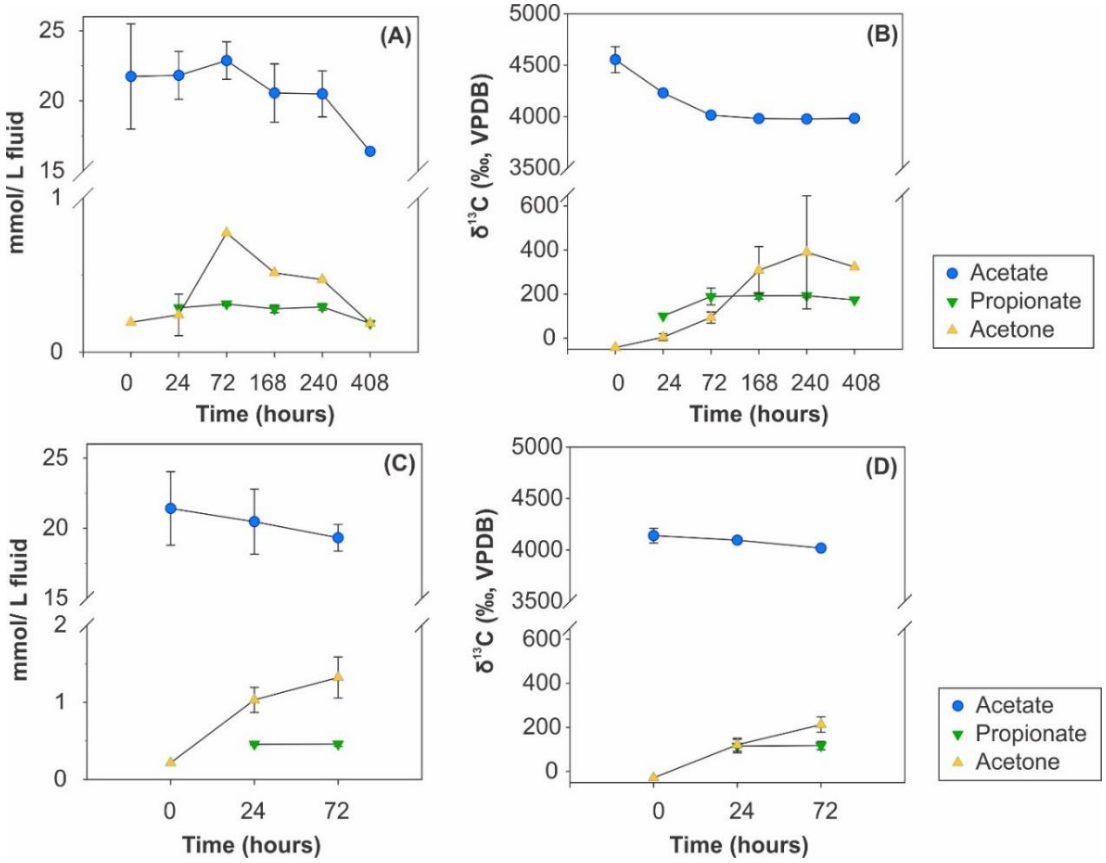

Supplementary Figure III.6. Results from hydrous pyrolysis experiments with Guaymas Basin sediments. Concentration and $\delta^{13}C$ values of acetate (blue circle), propionate (green triangle down) and acetone (yellow triangle up) with addition of 10 mM sodium formate (A, B) at 250 °C (first 24 hours) and 350 °C (after 24 hours), 400 bar, and those with addition of 100 mM sodium formate (C, D) at 350 °C, 400 bar.

Supplementary Table III.1. Metadata from the sampling sites at the Guaymas Basin. Latitude and longitude were checked against published coordinates for 2008/2009 coring locations (Teske et al., 2016), and bathymetries and *Alvin* dive tracks for 2016 coring locations, recorded by AUV *Sentry*.

Location	Latitude (N)	Longitude (W)	Sampling Date	Alvin Dive	Core	Length (cm)	Description and temperature range down to 40 to 50 cm
Mat Mound	27˚00.39’	111˚24.56’	06/12/2008	4483	3	16	Orange mat; 19-43 °C
			07/12/2008	4484	6	21	White mat; 2-39 °C
			07/12/2008	4484	14	13	Orange mat; 21-162 °C
			08/12/2008	4485	1	15	Reference site; ca. 3 °C
Megamat	27˚00.46’	111˚24.51’	09/12/2008	4486	16	19	Outside edge of white *Beggiatoa* mat; 24-84 °C
			09/12/2008	4486	29	21	At edge of white *Beggiatoa* mat; 16-118 °C
			12/12/2008	4488	9	19	Yellow *Beggiatoa* mat; 45-150 °C
			14/12/2008	4490	10	13	White mat, bubbling; 3-84 °C
CV 22 "fried egg mat"	27˚00.43’	111˚24.52’	13/12/2008	4489	25	12	Yellow/white mats; 34-65 °C
INSINC Mat I	27˚00.44’	111˚24.54’	29/11/2009	4568	2	32	No *Beggiatoa*; 3-109 °C
T-logger mat (Marker 14)	27˚00.47’	111˚24.43’	30/11/2009	4569	1	48	Orange/white *Beggiatoa*; 4-72 °C
			30/11/2009	4569	3	52	No *Beggiatoa*; 3-27 °C
			30/11/2009	4569	8	44	Orange *Beggiatoa*; 13-103 °C
Cathedral Hill (Marker 24)	27˚00.69’	111˚24.27’	04/12/2009	4573	14	34	White/gray mat; 11-185 °C
			22/12/2016	4870	16	21	Oil impregnated; 31-74 °C
Aceto Balsamico	27˚00.47’	111˚24.43’	04/12/2009	4573	21	42	Aceto Balsamico mat; 3-32 °C
			22/12/2016	4870	2	48	Aceto Balsamico mat; 5-26 °C
Octopus Mound	27˚28.17’	111˚28.39’	18/12/2016	4867	2	23	Periphery of cold seep; ca. 3 °C
			18/12/2016	4867	3	23	Active cold seep; ca. 3 °C
Ultra Mound	27˚00.45’	111˚24.54’	21/12/2016	4869	3	34	Orange mat; 31-85 °C
Northern Tower site 2	27˚02.77’	111˚23.09’	23/12/2016	4871	20	24	Cool white mat, 5-13 °C
Northern Tower site 3	27˚02.75’	111˚23.05’	23/12/2016	4871	26	28	Hot white mat; 53-97 °C

Supplementary Table III.2. $\delta^{13}C$ values of methane through pentane (C_1-C_5), total organic carbon (TOC) and dissolved inorganic carbon (DIC), abundance ratios of $C_1/(C_2+C_3)$, and TOC content, sulfate concentration, *in situ* temperatures throughout the sediment cores from 12 research sites in this study.

Depth (cmbsf)	T (°C)	TOC (wt%)	$C_1/(C_2+C_3)$	Sulfate (mM)	C_1 (‰)	C_2 (‰)	C_3 (‰)	C_4 (‰)	C_5 (‰)	TOC (‰)	DIC (‰)
					Aceto Balsamico						
					Core 4573-21						
2	5		43.5	10.0	-47.3	-11.5	-15.1		-16.1		-0.2
6	7		47.5	1.8	-45.5	-11.4	-16.7		-15.9		-1.3
10	8		44.2	1.4	-45.6	-11.6	-15.9		-16.1		1.3
14	12		40.0	1.1	-45.2	-11.5	-16.3		-15.9		0.3
18	14		47.7	1.1	-45.3	-11.6	-16.7		-16.0		-0.8
26	20		40.4	1.0	-45.3	-11.7	-16.3		-16.4		3.0
30	20		40.2	1.0	-45.3	-11.8	-16.6	-21.9	-16.2		-4.3
38	26		38.5	1.0	-45.3	-11.8	-16.2	-17.2	-16.3		-0.7
34	26		44.6	1.0	-44.6	-11.6	-16.4	-16.6	-16.4		5.0
42	28		34.6	1.1	-45.2	-11.7	-16.8	-21.4	-16.5		8.9
					Core 4870-2						
1	4		11.7	15.4	-43.0	-13.3					-4.3
3	5		28.4	3.0	-48.6	-13.8					-1.8
5	6		34.2	2.2	-49.9	-12.7					1.3
7	8		131.0	0.5	-49.8	-12.9	-17.2	-23.9			3.1
9	9		106.5	0.3	-50.1	-12.8	-17.1	-22.4			5.1
12	11		94.0	0.4	-49.0	-12.8	-17.3	-22.6			6.9
16	13		64.9	0.4	-47.7	-15.7	-17.5	-22.6	-22.9		8.3
19	14		42.2	0.4	-46.5	-12.8	-17.3	-22.3	-24.7		6.4
21	15		69.2	0.4	-47.7	-12.8	-17.6	-22.3	-23.3		9.1
24	17		42.5		-47.0	-13.0	-17.9	-23.6	-23.3		8.5
28	18		43.1		-47.4	-12.8	-17.7	-22.6	-23.2		6.6
32	20		46.6		-47.3	-13.5	-17.6	-22.9	-24.5		8.4
36	22		61.5		-47.4	-13.1	-17.6	-22.9	-24.0		
40	24		63.1		-47.3	-13.0	-17.7	-23.3	-22.6		
44	26		36.2		-47.6	-12.7	-17.3	-23.1	-22.6		
48	28		57.4		-47.3	-13.3	-17.5	-23.5	-22.5		
					Cathedral Hill, Marker 24						
					Core 4573-14						
2	36		38.9	18.0	-43.6	-13.1	-17.9	-21.0	-21.8		-11.5
6	85		36.1	14.1	-42.9	-12.7	-17.4	-20.6	-21.2		-11.5
10	133		46.5	13.8	-43.5	-12.9	-17.9	-21.1	-22.0		-14.0
14	155		35.0	9.8	-43.0	-12.7	-17.8	-20.8	-21.8		-7.0
18	162		39.4	8.2	-42.9	-12.7	-17.5	-20.9	-21.7		4.4
22	166		34.0	7.8	-42.8	-12.5	-17.5	-20.5	-21.7		-3.8
26	172		30.5	22.0	-42.6	-12.4	-17.2	-20.6	-21.3		-5.2
30	172		38.1	21.0	-43.0	-12.8	-17.5	-21.0	-21.8		-1.7
34	176		22.8	27.9	-42.9	-12.7	-17.9	-20.4	-21.8		-5.2
					Core 4870-16						
1	7		28.9	16.2	-39.7	-13.9	-18.9	-22.4			-9.6
3	16		22.0	15.1	-41.3	-13.3	-18.8	-20.8			-10.8
5	25		15.5	14.1	-41.4	-13.2	-19.8	-20.2	-15.6		-10.3
7	33		10.2	13.3	-41.5	-13.0	-18.9	-20.5	-15.4		-10.1
9	42		7.1	19.4	-42.2	-14.3	-20.1	-19.6	-17.0		-9.0
11	48		5.7	13.8	-41.1	-12.7	-19.8	-18.7			-8.8
13	51		7.4	13.6	-40.9	-13.5	-20.0	-19.8			-7.0
16	55		11.3	13.7	-40.9	-13.0	-20.9	-21.1	-18.1		-4.0
18	58		2.4		-41.1	-14.4	-21.4	-22.8	-19.1		-3.5
21	62		10.9		-41.8	-13.4	-21.1	-22.9	-21.1		-3.3
					CV22 "fried egg mat"						
					Core 4489-25 (sulfate concentrations from adjacent core 4489-28)						
2	38	3.7	17.5	28.5	-30.0	-10.2	-13.2			-21.4	-24.8
5	44	3.7	15.0	30.9	-33.0					-21.6	-25.3

7	48	3.7	25.9	33.0	-20.0				-21.8	-28.9
8.5	51	3.1	17.5	33.5	-29.3	-12.0	-16.4		-22.0	-38.0
9.5	53	3.3	42.1	34.5	-7.5				-21.4	-24.9
11	55	2.6	20.6	33.0	-12.1				-21.1	-1.1
12.5	56	2.6	24.8		-8.2				-21.0	-2.2
					INSINC Mat I					
					Core 4568-2					
1.5	6		59.6	25.9	-36.1	-10.2	-9.2	-10.1		-12.3
4.5	13		50.4	26.0	-38.3	-10.5	-9.5	-10.1	-16.2	-12.5
7.5	19		59.5	23.8	-42.3	-11.0	-9.6	-10.7	-17.1	-12.1
10.5	26		60.6	25.8	-44.0	-11.2	-9.7	-8.9	-17.5	-11.6
13.5	39		41.5	24.5	-41.3	-10.9	-9.6	-10.6	-15.0	-9.0
16.5	49		52.0	28.1	-41.6	-10.7	-9.7	-11.1	-17.0	-8.7
19.5	55		42.1	27.7	-41.2	-10.6	-10.8	-12.6		-7.9
22.5	68		61.4	24.8	-41.0	-10.5	-10.5	-13.3		-10.3
25.5	80		64.9	26.8	-40.9	-10.4	-10.3	-12.3		-8.2
28.5	86		81.9	28.2	-40.0	-9.6	-9.9			-8.6
32.5	95		72.4	24.8	-41.1	-10.5	-10.1			-8.8
					T-logger mat, Marker14					
					Core 4569-1					
1.5	6		75.1	21.9	-40.3	-12.0	-14.0	-15.9		-8.3
4.5	11		58.7	21.3	-38.1	-11.2	-13.3	-15.6		-16.4
7.5	17		75.6	21.2	-38.4	-11.5	-14.3	-18.5		-18.8
10.5	22		65.9	18.4	-38.2	-11.5	-13.7	-18.0		-20.4
13.5	27		59.8	21.8	-35.3	-10.6	-13.5			-21.4
16.5	32		60.2	22.1	-34.1	-10.4	-12.6	-18.6		-21.7
19.5	38		62.3	22.8	-31.8	-10.1	-12.4	-19.8		-21.5
22.5	42		52.3	20.5	-35.1	-10.6	-13.9	-21.1		-15.9
25.5	46		51.9	22.9	-38.2	-11.2	-13.2	-21.9		-22.4
28.5	50		51.1	21.6	-36.7	-11.4	-13.9	-19.8		-21.1
31.5	54		55.1	23.8	-38.3	-11.5	-13.9	-18.8		-21.9
34.5	57		56.8	22.6	-39.7	-11.4	-15.2	-19.6		-20.5
37.5	60		54.3	24.3	-40.5	-11.4	-14.4	-18.7	-20.8	-19.1
40.5	63		50.4		-40.3	-11.6	-13.8	-19.8	-21.2	-18.7
43.5	66		50.8		-39.7	-11.5	-14.9	-19.3	-20.0	-16.5
47.5	70		53.0	22.0	-39.3	-11.7	-15.6	-20.7		-16.3
					Core 4569-3					
1.5	4		3.5	25.4	-46.9	-9.9				-3.7
4.5	5		22.8	27.4	-43.1	-11.5	-26.7	-21.5		-4.8
7.5	6			26.9	-44.8	-11.8	-16.3	-22.8		-7.6
10.5	7		259.2	19.1	-34.3	-11.9	-19.8	-15.9		-13.2
13.5	9		565.0	24.6	-37.1	-10.9	-18.7	-19.7		-14.7
16.5	11		301.3	25.1	-34.7	-9.5	-19.6			-14.9
19.5	13		211.7	22.7	-28.7	-3.4				-15.4
22.5	15		181.9	23.6	-28.1	-1.4	-28.6			-14.8
25.5	16		154.5	23.4	-26.4	1.5				-15.2
28.5	18		183.4		-27.7	0.2	-11.3			-15.6
31.5	20		178.0	22.2	-28.3	-1.1	-7.1			-8.3
34.5	21		194.8	25.1	-29.3	-3.0				-15.7
37.5	22		262.5	22.1	-30.1	-5.8				-16.2
40.5	23		263.0	21.0	-30.3	-5.4	-21.1			-11.8
43.5	25		319.8	24.2	-28.7	-7.4	-29.4			-8.4
48	26		247.6		-33.3	-7.6	-31.7			
52.5	28		203.4		-34.3	-11.4	-26.1	-22.2		
					Core 4569-8					
1.5	18		49.1	25.5	-25.7	-8.2	-11.8	-19.2		-16.0
4.5	29		36.9	22.9	-30.2	-11.6	-14.3	-19.5	-21.7	-22.1
7.5	39		39.8	19.8	-33.9	-11.5	-14.4	-19.4	-21.7	-21.7
10.5	50		44.9	22.3	-35.3	-11.9	-14.1	-19.2	-21.1	-19.2
13.5	54		44.5	22.4	-36.3	-11.7	-15.5	-19.8	-22.0	-30.6
16.5	59		56.6	22.0	-37.7	-11.9	-15.0	-19.7	-22.0	-12.7
19.5	64		51.6	22.9	-39.7	-11.6	-14.2	-19.4	-21.6	-15.5

22.5	70		56.4	27.6	-38.3	-12.0	-15.5	-18.8	-18.8	-9.8
25.5	75		59.1	30.0	-36.0	-11.1	-15.1	-20.4	-21.1	-6.4
28.5	80		55.3	31.7	-39.9	-11.7	-14.7	-19.8	-21.8	-14.1
31.5	85		46.0	29.8	-38.4	-11.0	-13.8	-19.0	-21.5	-8.5
34.5	88		47.7	29.0	-40.1	-11.4	-14.3	-19.6		-25.7
37.5	91		47.7	27.1	-36.8	-10.8	-14.4	-19.1	-21.5	-8.2
40.5	94		44.9		-37.6	-10.8	-14.3	-19.7	-22.2	-23.8
44.5	98		34.4	21.9	-35.0	-10.4	-13.5	-19.4	-21.6	-6.6
					Mat Mound					
					Core 4485-1					
1	3	3.5	12.3		-51.8				-20.8	-17.0
3	3	3.3	13.8		-52.1				-20.7	-21.7
5	3	3.2	12.3		-51.9				-20.7	-40.3
7	3	2.9	11.1		-52.3				-20.5	-38.9
9	3	2.1	6.6		-44.0				-20.2	-38.7
11	3	2.0	9.7		-46.9				-20.2	-40.4
13	3	1.9	11.2		-44.4				-20.3	-40.2
15	3	1.9	11.2		-43.4				-20.4	-22.0
					Core 4483-3					
1.5	30	3.0	7.7		-39.2				-21.2	
4.5	27		10.1		-33.1					
7.5	24	3.4	10.1		-34.7				-22.3	
10.5	21	2.6	3.7		-39.6				-22.6	
13.5	20	2.7	4.4		-36.9				-23.5	
16.5	23	1.7	2.8		-36.6				-23.1	
					Core 4484-14 (ref. Dowell et al., 2016)					
1.5	8	7.3	14.1		-38.2	-6.7	-18.9	-14.2	-19.1	-39.4
4.5	19	7.0	14.5		-34.9	-5.4	-11.1	-20.2	-23.3	-21.9	-35.0
7	28	4.5	3.0		-35.8	-5.0	-8.4	-17.0	-21.7	-22.3	-20.9
9	33	5.0	2.2		-38.5	-8.5	-11.9	-17.7	-18.5	-21.8	-21.5
11	36	4.7	8.4		-35.4	-7.4	-10.1	-16.5	-19.5	-21.9	-28.4
13	38	4.1	13.8		-34.3	-7.2	-9.4	-19.5	-16.9	-21.7	-23.7
					Core 4484-6 (ref. Dowell et al., 2016)					
1	5	6.1	13.7	19.9	-44.6	-7.4	-21.5			-24.4	-38.0
3	11	6.1	22.3	8.4	-39.9	-9.9	-18.8	-22.9	-25.9	-23.1	-36.0
5	17	4.4	22.0	4.3	-37.3	-5.9	-17.8		-27.7	-22.7	-28.8
7	23	3.5	38.1	5.4	-35.1	-2.3	-13.2	-22.5	-27.2	-22.3	-23.1
9	29	2.8	56.2	9.1	-32.2	4.2	-11.2	-21.0	-27.7	-22.0	-33.1
11	33	2.1	49.6	11.8	-32.0	4.5	-20.7			-21.3	-32.8
13	35	2.5	19.3	14.2						-21.6	-20.2
15	37	4.1	33.5		-31.3	3.7	-22.5	-23.2	-21.2	-21.9	-24.6
17	37	2.5	17.6		-30.4	-0.8	-18.4	-20.2	-16.9	-22.0	-27.8
19	38	2.1	12.6		-28.2	-2.8	-17.0	-20.7	-21.8	-22.1	-20.8
21	39	2.1	11.2		-24.0	-4.5	-20.1	-21.8	-21.0		-21.4
					Megamat					
					Core 4486-16 (sulfate concentration values were from ref. Cardman, 2014)					
1	24	2.3	11.1	27.4	-39.3	-12.5	-18.2	-19.2	-20.0	-21.2	-20.1
3	26	3.2	17.8	27.7	-38.0	-12.7	-17.8	-18.3	-20.1	-21.0	-19.6
5	29	3.2	20.4	28.1	-40.6	-13.3	-18.9	-19.5	-20.4	-20.8	-32.4
7	32	2.8	34.2	25.7	-40.5	-12.8	-19.3	-20.8	-22.1	-20.7	-26.3
9	35	2.7	53.8	26.4	-39.8	-10.8	-19.2	-22.5	-24.9	-20.8	-20.9
11	38	2.7	59.5	25.0	-38.5	-8.7	-16.4			-20.7	-15.3
13	41	2.7	53.9	24.7	-36.7	-8.2	-18.0			-20.8	-13.7
15	44	2.7	56.5	23.2	-36.1	-6.2	-17.4			-20.4	-16.7
17	47	2.6	43.8		-35.2	-7.1	-17.5			-20.7	-31.7
19	50	2.6	42.3		-35.3	-5.9	-16.2			-20.8	-14.7
					Core 4486-29 (sulfate concentration values were from ref. Cardman, 2014)					
1	16	2.4	14.4		-37.5	-11.6	-16.5	-18.5	-20.2	-21.3	-15.3
3	19	2.3	18.5	6.1	-38.0	-11.5	-16.4	-18.3	-20.4	-21.3	-3.0
5	25	2.0	17.4	2.6	-38.4	-11.6	-15.4	-18.0	-19.7	-21.3	
7	32	2.0	17.3	2.1	-38.7	-13.0	-16.4	-18.2	-20.1		
9	38	2.0	20.6	2.4	-39.2	-12.2	-17.4	-18.5	-20.6	-21.4	

11	44	2.1	19.2	2.1	-39.7	-12.2	-17.0	-19.8	-19.3	-21.2	-3.9
13	50	2.0	21.9	2.3	-39.3	-11.9	-17.3	-18.7	-21.2		-4.9
15	55	2.0	19.1	2.0	-40.4	-12.5	-18.4	-19.7	-19.3		-11.6
17	60	2.1	34.9	2.4	-41.3	-12.8	-18.1	-19.4	-22.7		-9.4
19	65	1.8	18.8		-40.2	-13.0	-19.0	-19.6	-25.1	-21.2	-4.1
21	70	1.8	18.5		-39.9	-12.7	-18.9	-19.3	-23.1	-21.2	-7.1
				Core 4488-9 (sulfate concentrations from adjacent core 4488-10)							
1	52	4.1	11.8	4.3	-38.8	-12.8	-17.9	-19.7	-18.8	-22.1	-21.7
3	67	3.7	11.0	10.5	-38.2	-13.0	-17.8	-19.6	-18.7	-22.4	-5.9
5	82	4.6	8.1	3.4	-38.6	-12.4	-18.7	-20.2	-18.1	-21.5	-3.0
7	96	3.9	8.8	1.2	-40.0	-13.1	-19.0	-20.1	-17.6	-21.1	-6.0
9	111	3.8		0.3						-20.6	-0.5
11	120	3.2		0.4						-20.4	0.2
13	123	3.1	6.3	0.8	-41.8	-14.0	-19.3	-20.6	-19.0	-20.6	-6.2
15	126	2.9	6.5	1.1	-41.5	-13.0	-18.7	-20.2	-19.6	-20.8	-12.1
17	129	2.9	5.5	1.3	-41.3	-13.4	-18.1	-21.0	-20.0	-20.6	-8.9
19	132	3.0	6.1		-42.0	-14.1	-17.6	-20.7	-20.4	-21.0	-3.3
				Core 4490-10 (sulfate concentrations from adjacent core 4490-12)							
1	5	3.5	10.5	22.8	-42.4	-14.1	-19.8	-20.1	-20.9	-21.3	-20.9
3	8	2.9	9.3	16.5	-41.0	-13.6	-19.2	-20.5	-20.6	-20.7	-6.3
5	12	2.8		9.0						-20.8	-26.4
7	15	2.2	9.5	5.0	-40.4	-13.3	-19.4	-20.7	-20.9	-20.5	-31.3
9	18	2.0	9.7	1.7	-41.1	-13.6	-19.7	-21.0	-20.5	-20.5	-24.3
11	23	2.6	9.0	0.7	-42.0	-13.8	-19.1	-20.7	-21.1	-20.4	-1.5
13	28	2.4	6.6	0.4	-41.7	-13.4	-19.3	-20.6	-21.0	-20.7	-15.0
					Octopus Mound						
					Core 4867-3						
1	3		237.6	29.7	-68.5						-2.2
3	3		160.5	28.9	-60.7						-12.1
5	3		128.1	28.1	-57.2						-21.4
7	3		124.6	26.7	-55.3						-27.7
9	3		115.2	24.9	-55.9						-33.5
11	3		185.1	24.3	-59.7						-40.3
13	3		320.7	23.7	-64.2						-41.4
15	3		304.1	24.0	-65.4						-41.7
17	3		285.3		-69.7						-42.0
19	3		259.7		-68.5						
21	3		309.9		-74.9						
23	3		274.5		-69.8						
					Core 4867-2						
1	3		540.7	30.1	-79.0						-5.1
3	3		588.5	33.3	-74.5						-3.0
5	3		593.6	29.9	-76.1						-5.1
7	3		521.0	31.5	-77.0						-3.2
9	3		302.8	30.8	-78.4						-4.8
11	3		293.3	31.2	-81.4						-2.8
13	3		223.7	30.5	-81.4						-1.8
15	3		421.0	30.8	-78.7						-3.6
17	3		358.6	30.4	-78.1						
19	3		362.2		-77.2						
21	3		454.8		-75.9						
23	3		301.9		-81.7						
	3		540.7		-79.0						-5.1
					Northern Tower Site 2						
					Core 4871-20						
1	3		154.6	13.5	-53.9	-20.5	-23.4	-22.9	-26.6		3.9
3	4		356.9	12.2	-54.4	-19.5					4.6
5	5		77.1		-52.9	-20.3	-23.8	-23.6	-23.4		6.5
7	6		185.1	2.6	-53.7	-19.7	-24.9	-23.6	-23.6		6.9
9	6		267.6		-53.8	-20.2	-24.6	-23.8	-23.7		7.1
12	7		168.5		-54.3	-19.3	-24.6	-24.9	-24.3		
16	8		129.9	0.2	-55.1	-19.5	-24.7	-24.3	-24.2		

20	8	360.6		-54.1	-19.6	-24.4	-24.6	-24.8	
24	9	608.1	0.3	-54.4	-18.5	-24.3	-25.0	-24.7	
				Northern Tower Site 3					
				Core 4871-26					
1	8	63.3	15.2	-43.0	-13.5	-14.2	-17.2		2.8
3	17	74.9	11.2	-43.9	-18.8	-14.4	-15.3	-19.7	4.3
5	27	118.3	10.1	-42.7	-14.0	-14.2	-15.6	-24.7	6.0
7	36	96.1	6.0	-42.4	-13.3	-14.9	-16.1	-23.6	2.1
9	45	31.4	6.1	-43.7	-13.7	-15.3			3.8
12	54	108.4	1.2	-44.0	-13.5	-15.0	-16.5	-21.5	3.1
16	62	60.7	1.1	-43.7	-13.3	-14.9	-15.9		4.7
20	71	63.5	1.1	-43.6	-14.5	-14.9			4.6
24	75	102.0	1.2	-44.4	-13.7	-16.6			3.1
28	79	82.5		-42.1	-13.2	-14.3			3.0
				Ultra Mound					
				Core 4869-3					
1	6	16.1	31.8	-39.3	-10.9	-8.7			-3.3
3	13	6.9	26.6	-31.9	-9.2	-6.3			-11.1
5	20	6.6	19.4	-30.3	-9.2	-8.1			-15.6
7	27	3.8	17.9	-29.7	-10.0	-9.3			-18.8
9	34	3.6	19.0	-30.2	-10.6	-11.7			-18.5
11	39	6.7	20.0	-35.8	-11.8	-10.3			-16.3
14	45	28.8	21.9	-38.4	-10.9	-10.5			-8.0
18	53	48.8	21.4	-40.7	-11.9	-10.5			-2.7
22	60	19.6	20.7	-41.2	-11.9	-13.7			-2.0
26	65	20.9	19.1	-41.2	-11.7	-12.4			
30	71	10.9		-41.1	-11.5	-13.4			
34	73	46.4		-41.3	-12.5	-11.5			

Supplementary Table III.3. Concentration and isotopic compositions of volatile fatty acids (VFAs) and their corresponding carboxyl carbons during hydrous pyrolysis experiment I at 350 °C and 400 bars, with addition of 10% ^{13}C-labeled bicarbonate (DIC) and unlabeled VFAs. Isotopic compositions of hydrocarbon gases produced after 120 hours were shown.

Time, hours	Concentration, mmol/L fluid					δ^{13}C of DIC and VFAs, ‰ vs. VPDB					δ^{13}C of carboxyl carbon in VFAs, ‰ vs. VPDB				δ^{13}C of hydrocarbons, ‰ vs. VPDB			
	DIC	Acetate	Propionate	Butyrate	Valerate	DIC	Acetate	Propionate	Butyrate	Valerate	Acetate	Propionate	Butyrate	Valerate	Ethane	Propane	Butane	Pentane
0	14.4	1.0	0.7	0.8	0.3	9257	-40	-21	-27	-27	-40	-21	-27	-27	n.a.	n.a.	n.a.	n.a.
24	7.9	3.7	0.9	0.7	0.2	2385	979	529	263	209	1998	1628	1133	1154	n.a.	n.a.	n.a.	n.a.
120	6.5	2.7	0.6	0.3	0.08	1903	917	622	472	361	1873	1910	1970	1916	-35.5	-30.5	-29.3	-23.4
192	9.7	1.9	0.4	0.2	0.04	1769	856	581	442	331	1752	1786	1848	1762	n.a.	n.a.	n.a.	n.a.
288	9.3	2.0	0.4	0.2	0.02	1698	816	544	431	335	1672	1674	1804	1782	n.a.	n.a.	n.a.	n.a.

n.a.= not analyzed.

Supplementary Table III.4. Concentrations and isotopic compositions of hydrocarbon gases at 250 to 350 °C, 400 bars in the hydrous pyrolysis experiment II and III, with addition of ^{13}C-labeled acetate and respective 10 mM and 100 mM formate.

Elapsed time (hours)	Concentration (mmol/L fluid)				Isotopic composition (‰ vs. VPDB)		
	H_2	Methane	Ethane	Propane	$\delta^{13}C_{methane}$	$\delta^{13}C_{ethane}$	$\delta^{13}C_{propane}$
Experiment II: Addition of 10 mM sodium formate and ^{13}C-2-sodium acetate at 250 °C* and 400 bars							
24	0.008	0.09	0.01	0.01	-12.7	b.d.	b.d.
Temperature elevated to 350 °C							
72	0.03	2.40	0.36	0.20	727	3.1	13
168	0.03	5.16	0.61	0.32	1484	18.6	44
240	0.04	4.50	0.53	0.31	1895	25.3	56
408	0.04	6.64	0.65	0.34	2569	34.1	76
Experiment III: Addition of 100 mM sodium formate and ^{13}C-2-sodium acetate at 350 °C and 400 bars							
24	n.a.	2.19	0.55	0.22	1059	-0.2	55
49	n.a.	3.52	0.80	0.37	1563	14.8	93
72	11.5	7.08	1.42	0.66	1901	25.4	135

n.a. = not analyzed, b.d. = below detection limit.

* In the experiment II, the fluid-sediment mixture was first heated to 250 °C, in order to minimize the process of acetate decarboxylation.

Supplementary Table III.5. Concentrations and isotopic compositions of volatile fatty acids (VFAs) at 250 to 350 °C, 400 bars, with addition of ^{13}C-labeled acetate and 10 mM or 100 mM formate.

Elapsed time (hours)	mmol/ L fluid				‰ vs. VPDB			
	Formate	Acetate	Propionate	Acetone	$\delta^{13}C_{formate}$	$\delta^{13}C_{acetate}$	$\delta^{13}C_{propionate}$	$\delta^{13}C_{acetone}$
Addition of 10 mM sodium formate and ^{13}C-2-sodium acetate at 250 °C and 400 bars								
0	10.7	21.8	b.d.	0.19	-14.9	4554	b.d.	-42.6
24	b.d.	21.8	101	0.24	b.d.	4231	0.29	4.4
Temperature elevated to 350 °C								
72	b.d.	22.9	189	0.77	b.d.	4014	0.31	94
168	b.d.	20.6	192	0.51	b.d.	3981	0.28	308
240	b.d.	20.5	193	0.47	b.d.	3977	0.29	390
408	b.d.	16.4	173	0.19	b.d.	3983	0.19	323
Addition of 100 mM sodium formate and ^{13}C-2-sodium acetate at 350 °C and 400 bars								
0	103.0	21.4	b.d.	0.22	-17.0	4140	b.d.	-28.5
24	b.d.	20.5	0.46	1.03	b.d.	4095	115	121
72	b.d.	19.3	0.46	1.32	b.d.	4017	118	212

b.d. = below detection limit.

CHAPTER IV

Geochemical constraints on microbial intact polar lipid diversity in methane-laden sediments of the northern US Atlantic Margin

Min Song[a,*], Florence Schubotz[a], Kevin W. Becker[b,1], Michael F. Graw[c], Frederick S. Colwell[c], John W. Pohlman[d], Kai-Uwe Hinrichs[a]

In preparation for *Environmental Microbiology*

[a]MARUM-Center for Marine Environmental Sciences and Department of Geosciences, University of Bremen, Germany; [b]Woods Hole Oceanographic Institution, Woods Hole, MA, USA; [c]Oregon State University, Corvallis, OR, USA; [d]USGS Woods Hole Coastal and Marine Science Center, Woods Hole, MA, USA; [1]Present address: Helmholtz Center for Ocean Research Kiel, Kiel, Germany

*Correspondence: msong@uni-bremen.de

ABSTRACT

Widespread methane seepage from the seafloor along the northern US Atlantic Margin suggests significant quantities of methane and other forms for reduced carbon are returned to the ocean where they contribute to ecosystems, alter ocean chemistry and potentially influence the climate. Central to evaluating the quantitative and ecological significance of this input is a better understanding of the microbial community metabolism of methane in these sediments. Considering that most microbes inhabiting subseafloor sediments remain uncultured, intact polar membrane lipids (IPLs) have become a powerful tool for studying the distribution and activity of microbial communities in methane-rich settings. Here, we investigate the IPL composition in methane-laden and methane-free sediment cores along the northern US Atlantic Margin with the aim of exploring the influence of geochemical conditions on the lipid diversity, and to expand our knowledge of the source organisms for these lipid biomarkers. Our results demonstrate that the archaeal biomarker diversity was closely related to methane flux. High abundances of diglycosidic glycerols dialkyl glycerol tetraethers (2G-GDGTs), phosphatidic archaeols and hydroxyarchaeol (phospho-AR, OH-AR) as well as diglycosidic unsaturated GDGTs (2G-unsGDGTs) were found at sites with high methane flux and these compounds were closely linked to the presence of ANME clades. Such methanotrophic fingerprints were negligible in sediments with moderate methane flux, despite geochemical evidence for the anaerobic oxidation of methane. Instead, comparably high amounts of glycosidic butanetriol dialkyl glycerol tetraethers (1G-BDGT and 2G-BDGT) and glycosidic pentanetriol dialkyl glycerol tetraethers (1G-PDGT) were found. These lipids may be derived from uncultured marine benthic groups that are involved in organic carbon degradation. Under conditions of low methane flux and low organic carbon content, IPL concentrations were extremely low, indicating only small contributions from sedimentary microorganisms. The relative abundance of bacterial phospholipids varied under different geochemical conditions, with phosphatidylethanolamine (PE) of mixed acyl/ether glycerol (AEG) lipids or diacyl glycerol (DAG) lipids and diphosphatidylglycerol (DPG) being diagnostic of AOM-associated sulfate-reducing bacteria, whereas DAG- or diether glycerol (DEG)-based phosphatidyl-(N)-methylethanolamine (PME) were linked with heterotrophic organic matter degrading communities. Furthermore, PE-DEG was linked with members of Chloroflexi and a notable transition of PE-DAG to PE-DEG with depth may indicate ether lipids as an adaptation to the low-energy conditions of the deep biosphere. These findings suggest that the subsurface IPL distribution and quantity closely reflect the structure and activities of *in situ* microbial communities, which are governed by methane flux and sedimentary organic carbon content.

IV.1. INTRODUCTION

Methane is the most abundant hydrocarbon in the atmosphere and an important greenhouse gas. Thus, understanding its sources and sinks is essential for budgeting the global carbon cycle. Methane emissions from the marine environment are insignificant on a global scale (Reeburgh, 2007). However, the recent identification of massive gas seepage at the upper slope of the northern US Atlantic continental margin (USAM) with estimated methane fluxes of 15-90 Mg yr^{-1} implies that many major seeps are yet to be discovered along global continental margins (Skarke et al., 2014). Some gas along the USAM may originate from gas hydrate destabilization (Phrampus and Hornbach, 2012), but a more likely source is from expulsion of fluids from compaction of sediments that accumulated during the late Pleistocene (Prouty et al., 2016). With recent recognition that gas expulsion is a prevalent process on active (Riedel et al., 2018) and passive margins (Skarke et al., 2014), a better understanding of the controls on methane emission is needed to predict how climate change will affect the production of methane in marine sediments and its release from the seafloor.

Investigating sedimentary methane dynamics along the northern USAM is an excellent opportunity to evaluate the biogeochemical mechanisms that regulate the transfer of methane from the seafloor and into the ocean along a passive continental margin. Gas plumes on the northern USAM can be traced up to hundreds of meters above the sea floor (Skarke et al., 2014) and methane concentrations in the waters of Hudson Canyon reached up to 100-200 nM (Skarke et al., 2014; Weinstein et al., 2016). A recent study reported rapid oxidation of methane in the oxic water column (Leonte et al., 2017); however, our knowledge of methane turnover in the sediments of USAM is still limited.

Anaerobic oxidation of methane (AOM) coupled to sulfate reduction is the major biological sink for methane in marine sediments, resulting in the recycling of nearly 90% of methane produced in anoxic marine sediments (Reeburgh, 1996). Molecular and isotopic studies revealed the presence of microbial consortia of anaerobic methanotrophic archaea (ANME) and sulfate-reducing bacteria (SRB), which are the major players of AOM in methane-rich sediments (Hinrichs et al., 1999; Boetius et al., 2000). Over the past decade there have been considerable advances for knowledge about the process of AOM and its corresponding microorganisms. For example, nitrate (Haroon et al., 2013), iron and manganese (e.g., Beal et al., 2009; Aromokeye et al., 2020) have been identified as alternative electron acceptors for AOM. The global distribution and diversity of marine ANME clades and SRB groups have been well-defined (Ruff et al., 2015). Methanotrophic pathways of ANME are better understood (e.g., Meyerdierks et al., 2010; Wang et al., 2014). Also, ANME and their partner SRB are found to capable of direct electron transfer (e.g.,

McGlynn et al., 2015; Wegener et al., 2015). Additionally, the diversity and evolution of other methane-metabolizing microorganisms are detected (Evans et al., 2015).

While ANMEs typically dominate archaeal clades at methane seeps, a high diversity of other uncultured microbial assemblages is also found. These include Thermoprofundales (formerly called Marine Benthic Group-D) and the Miscellaneous Crenarchaeotal Group (MCG), which are also widely detected in non-seep sedimentary setting (e.g., Kubo et al., 2012; Lloyd et al., 2013). Two members of MCG have been shown to hold genes necessary for methane metabolism (Evans et al., 2015), suggesting previously unrecognized archaeal lineages may contribute to methane cycling at seep settings. In addition, subsurface microbial communities are often faced with energy stress as their activities are largely dependent on electron donor and acceptor availability as well as other geochemical conditions (cf. Orcutt et al., 2013). Those microbes adapted to energy stress often employ diverse mechanisms to cope with energy or nutrient limiting conditions, including significant modifications of their membrane lipid composition and other biomolecules (Valentine, 2007; Hoehler and Jørgensen, 2013; Schubotz, 2018). Overall, however, the biogeochemical constraints on the distribution and diversity of microorganisms in dynamic seep settings remains poorly understood.

Intact polar membrane lipids (IPLs) have served as complementary tool to study active microbial communities next to gene-based investigations (Sturt et al., 2004; Biddle et al., 2006). IPLs can provide broad scale chemotaxonomic information (Rossel et al., 2008), give insights on adaptive strategies (cf. Schubotz, 2019) and metabolic processes of the indigenous microorganisms through their isotopic compositions (Schubotz et al., 2011; Schubotz et al., 2015). IPLs have been successfully used to distinguish the major ANME groups in seep sediments: ANME-1 mainly comprise diglycosidic glycerol dibiphytanyl glycerol tetraether (2G-GDGT), while ANME-2 and ANME-3 are abundant in archaeol (AR) and hydroxyarchaeol (OH-AR) based phospholipids (Rossel et al., 2008; 2011). In addition, it was observed that phospholipids with phosphatidylethanolamine (PE), phosphatidylglycerol (PG), diphosphatidylglycerol (DPG) and phosphatidyl-(N)-methylethanolamine (PME) head groups are dominant in seep sediments and thus may be attributed to AOM-related SRB (Rossel et al., 2008), although some of the phospholipids were also shown to be involved in non-AOM related heterotrophic processes (Schubotz et al., 2011).

Recently identified IPLs found to be abundant in both methane-rich and deep subsurface sediments include glycosidic unsaturated GDGTs (unsGDGTs) (Zhu et al., 2014b), butanetriol dibiphytanyl glycerol tetraether (BDGT) and pentanetriol dibiphytanyl glycerol tetraether (PDGT) lipids (Zhu et al., 2014a). *Thermoplasmatales*-related archaea were suggested to be the source organism for unsGDGTs at seep sites

(Yoshinaga et al., 2015), while BDGT and PDGT lipids seem to have multiple sources including methanogens (Becker et al., 2016; Coffinet et al., 2019), benthic archaeal members of the MCG (Meador et al., 2015) or unknown heterotrophic archaea (Coffinet et al., 2019). Nonetheless, more detailed investigations are required to better understand the sources of these newly identified IPLs.

In this study, we investigated the diversity of archaeal and bacterial IPLs from the northern USAM, including three methane-laden and one methane-free sediment cores, By relating the IPL compositions to the biogeochemical setting and comparing them to phylogenetic assignments based on 16S rRNA gene abundance, we were able to (i) identify the geochemical constraints on lipid biomarker abundances and diversity across different type localities, and (ii) assess the source microorganisms for recently identified IPLs.

IV.2. MATERIALS AND METHODS

IV.2.1. Sampling sites, geochemistry analysis

In September 2015, sediment core samples from four sites on the USAM were collected during expedition HRS15-12 aboard the R/V Hugh R. Sharp: 1) An 880 cm long piston core (PC11) from the Tiki Line; 2) An 867 cm long piston core (PC16) and its corresponding 82 cm trigger core (TC16) from Hudson Canyon; 3) A 34 cm long multicore (MUC5) from Chincoteague Seep, and 4) An 18 cm long multicore (MUC10) collected upslope of Chincoteague Seep (herein referred to as Chincoteague slope) (Fig. IV.1; Supp. Table IV.1). For a description of the geologic setting for the Tiki Line core PC11, see seismic reflection profile "Tiki2011" in Brothers et al. (2014). TC16/PC16 was situated in an area of active seafloor gas emissions updip of the upper gas hydrate stability limit in the upper Hudson Canyon. The Chincoteague Seep site (MUC5) is a deeper water setting (1055 m) with sufficient methane flux to support extensive beds of bathymodiolin mussels (Turner et al., 2020). The Chincoteague slope site (MUC 10) is a control site proximal to the active MUC5 site, but with minimial methane flux.

After recovery, multicores (MUC) were split into 2-3 cm intervals and subsampled. The piston cores (PC) and trigger core (TC) were cut into 1 m sections and sub-sampled at 10 cm intervals. The subsamples were either processed for geochemical analyses on-board or stored at -20 °C for later microbiological and lipid analyses. Samples for methane concentration and stable carbon isotope measurements were collected from the geochemistry subsample as 5 cm^3 sediment plugs and stored in 20 mL serum vials sealed with 1-cm-thick butyl rubber septa. At the same time, samples for porosity (as % water volume) and elemental/stable carbon isotope analysis were collected (e.g., Pohlman et al., 2013). Porewaters from the

PC and TC were extracted by pressure-squeezing (~3 bar) and were filter-sterilized with 0.45 μm Acrodisc polyethersulphone (PES) syringe filters (Pall Corporation). Porewaters from the MUC were collected with Rhizon samplers equipped with a 0.2 μm filtration tip.

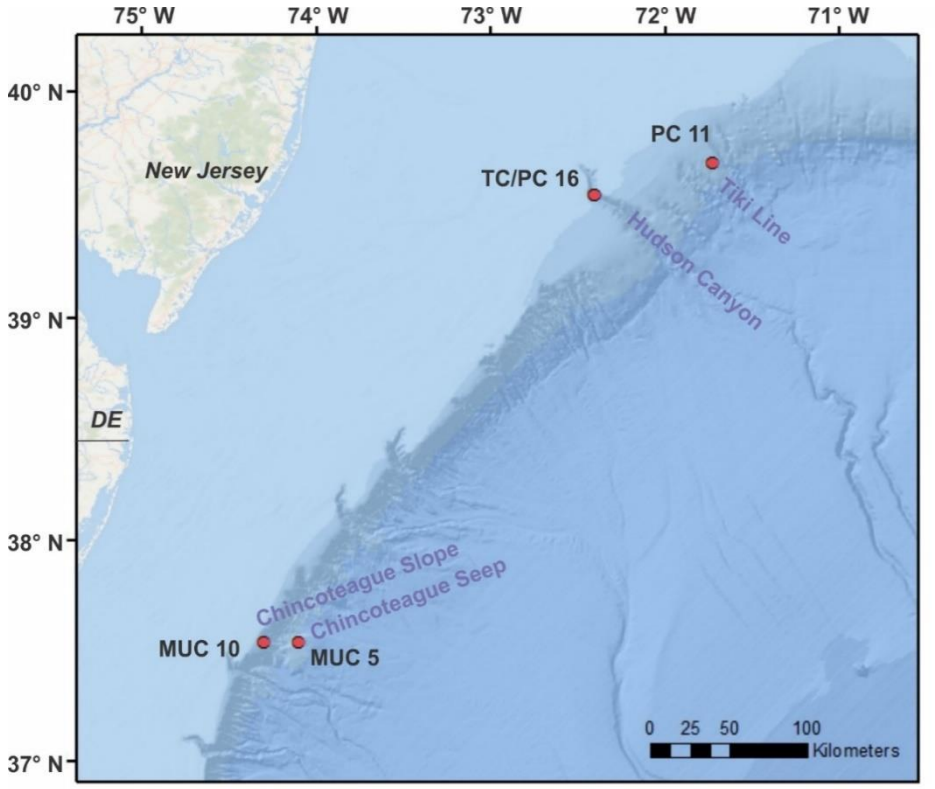

Figure IV.1. Sampling locations of sediment cores collected for this study at the US Atlantic margin: MUC 10 was recovered at Chincoteague Slope, MUC 5 at Chincoteague Seep, TC 16 and PC 16 at Hudson Canyon, and PC 11 at Tiki Line (Basemap sources: Esri, GEBCO, NOAA, National Geographic, DeLorme, HERE, Geonames.org, and other contributors).

Gas analysis. Headspace methane concentrations were determined using a Shimadzu 14-A gas chromatograph (GC) equipped with a flame ionization detector (FID). The gases were isothermally (50 °C) separated with a Poraplot-Q stainless steel column (8 ft x 1/8" OD) packed with 60/80 mesh and quantified against certified gas standards. Headspace concentrations were converted to dissolved concentrations using an established method Magen et al., 2014. The stable carbon isotope composition of methane ($\delta^{13}C_{CH4}$) from the headspace of the serum vials was determined using the USGS Discrete Sample Introduction Module - Cavity Ring-Down Spectroscopy (DSIM-CRDS) system and are reported relative to the Vienna Pee Dee Belemnite (VPDB) standard, as described by Pohlman et al. (In Prep). To confirm the accuracy of the DSIM-CRDS method, several samples were also analyzed by gas chromatography-combustion-isotope ratio mass spectrometrey (GC-C-IRMS) using a Thermo-Finnigan DELTA^{Plus} XL isotope ratio mass

spectrometer (IRMS) coupled to an Agilent 6890 Gas Chromatograph (GC) via a Finnigan GCCIII combustion interface.

Porewater analysis. Total sulfides were quantified with a single wavelength spectrophotometer (670 nM) on-board using the methylene blue method originally described by Cline (1969) and adapted for small volumes of porewater. Sulfate concentrations were determined using a Metrohm 881 Compact Plus ion chromatograph (IC) equipped with a Metrosep A Supp 5-250 anion column. Peak areas for sulfate were quantified against equivalently diluted (101:1) International Association for the Physical Sciences of the Oceans (IAPSO) standard. DIC concentrations were determined with a Model 5011 UIC coulometer and quantified relative to a sea water certified reference material (CRM). CO_2 liberated from DIC by the addition of 85% phosphoric acid in the headspace of a 2 ml septa-sealed serum vial was analyzed for $\delta^{13}C$ by GC-C-IRMS.

Sediment analysis. Concentrations and $\delta^{13}C$ values of total organic carbon (TOC) were measured at the Woods Hole Organic Mass Spectrometry Facility using a Carlo Erba Model 1108 elemental analyzer interfaced to a DeltaPlus Isotope Ratio Mass Spectrometer. The samples were weighed in pre-cleaned silver cups. After weighing, samples were exposed to an HCl rich atmosphere to release most of the carbonate. After gaseous acidification, each sample was further acidified with 2N HCl until all signs of CO_2 production ceased. Samples were then dried in a warm oven prior to analysis.

IV.2.2. Intact polar lipids analysis

Total lipid extracts (TLEs) are yielded from 10 to 15 g of freeze-dried sediments from five sediment cores and a total of 44 samples using a modified Bligh-Dyer method after Sturt et al. (2004) and Schubotz et al. (2011). In brief, after addition of 2 µg of internal standard (di-C_{21}-phosphatidylcholine, Avanti Polar Lipids), samples were ultrasonically extracted (10 min) using a mixture of DCM:MeOH:buffer (1:2:0.8; v/v) in four steps. For the first two steps a phosphate buffer (50 mmol L^{-1} of $K_2HPO_4^{-1}$ at pH 7.4) was used and a trichloroacetic acid buffer (50 g L^{-1}, pH 2) was used for the last two steps. After each extraction step the centrifuged (10 min at 1250 rpm) supernatants were combined in a separatory funnel. Equal amounts of DCM and water were added to the mixture to a final ratio of DCM:MeOH:buffer at 1:1:0.8 (v/v). The separated organic phase was subsequently washed three times with MilliQ water, gently evaporated to dryness under a stream of nitrogen and stored as TLE at -20 °C until further analysis.

Intact polar lipids (IPLs) were identified and quantified by ultra-high pressure liquid chromatography-electrospray ionization-tandem mass spectrometry (UHPLC-ESI-MS^2) using hydrophilic interaction

chromatography (HILIC) and reversed phased (RP) chromatography as described in Wörmer et al. (2013) and Zhu et al. (2013a). While the HILIC method was used for identifying and quantifying bacterial IPLs and archaeol-based archaeal IPLs, the RP analysis was used for intact and core GDGTs, BDGTs and PDGTs as this methods obtains information on ring distributions (Zhu et al., 2013a; Zhu et al., 2014b).

For the HILIC analysis a Dionex Ultimate 3000 UHPLC instrument was equipped with a Waters Acquity UPLC BEH Amide column (1.7 µm, 2.1 x 150 mm, Waters Corporation, Eschborn, Germany) and coupled to a Bruker maXis ultra-high resolution quadrupole time-of-flight (qTOF) mass spectrometer via an electrospray ionization (ESI) source. IPLs were eluted using the following gradient: 99% A (MeCN:dichloromethane, 75/25, 0.01% HCO_2H, 0.01% ammonium hydroxide) and 1% B (MeOH:H_2O, 50/50, 0.4% HCO_2H, 0.4% NH_{3aq}) for 2.5 min, ramping to 5% B at 4 min, 25% B at 22.5 min and 40% B at 26.5 min, held for 1 min and equilibrated to initial conditions for 8 min (Wörmer et al., 2013). Measurements were performed in positive and negative ionization mode with a scan range of *m/z* 150 to 2000 and using data-dependent fragmentation. Compounds were identified according to their exact masses, retention times and fragmentation patterns compared to what has been reported in the literature (Rossel et al., 2011; Schubotz et al., 2011; Yoshinaga et al., 2011). The mass spectrometer was set to a resolving power of 27,000 at m/z 1222, and every analysis was mass calibrated by loop injections of a calibration standard and correction by lock mass, leadingtoamassaccuracyofbetterthan1to 3ppm (cf. Becker et al., 2013). Integration of peaks was performed on extracted ion chromatograms using an isolation width of +/- 10 mDa and included the $[M+H]^+$, $[M+NH_4]^+$ and $[M+Na]^+$ ions where applicable, doubly charged ions were included in the integration.

For the RP analysis a Dionex Ultimate 3000RS UHPLC was equipped with an ACE3 C_{18} column (3 µm, 2.1 x 150 mm, Advanced Chromatography Technologies Ltd, Aberdeen, Scotland) connected to an ABSciEX QTRAP4500 Triple Quadrupole/Ion Trap MS (UHPLC-Triple Quad-MS) via a Turbolon ESI source. For elution the following gradient was used: 100% A (MeOH/HCO_2H/14.8 M $NH_{3aq.}$, 100/0.04/0.1) held for 10 min, ramped to 24% B (isopropanol/HCO_2H/14.8 M $NH_{3aq.}$,100/0.04/0.1) and held for 5 min, gradient to 65% B and held for 55 min, gradient to 90% B and held for 14 min, then equilibrated to initial conditions for 15 min (Zhu et al., 2013b). Multiple reaction monitoring (MRM) transitions were applied according to those described in Evans et al. (2017).

IPL concentrations for HILIC and RP analyses were calculated from the relative response of the analyte compared to the internal standard and reported as lipids per TOC. Due to the lack of commercially available standards for some of the analyzed lipid classes, varying response factors of these could not be accounted

for and thus IPL concentrations are considered semi-quantitative (for an overview on applied response factors see Supp. Table IV.2).

IV.2.3. Statistical analysis

Distance-based redundancy analysis. Distance-based redundancy analysis (db-RDA) was performed to evaluate the effect of geochemical conditions on the microbial IPL composition in samples. Db-RDA is a method for carrying out constrained ordinations on data using non-Euclidean distance measures (cf. Borcard et al., 2018). The db-RDA was carried out by the function 'capscale' in R, which processed the data in three steps: first, a distance matrix of IPL abundance in samples was calculated using the Bray-Curtis distance measure, then a principle coordinates analysis (PCoA) was performed on the matrix, the eigenvalues obtained in the PCoA were combined with the RDA, which evaluate the linear relationships between the response data (IPL abundance) and the explanatory variables (geochemical parameters). Environmental fit was calculated with all of the explanatory variables (geochemical parameters), and line vectors indicated the direction of each parameter on the ordination. The resulting variance inflation factors (VIFs) for the significant explanatory variables were below 15.

Correlation network analysis. Analyses on the abundance of archaeal and bacterial OTUs (operational taxonomic units clustered at 97% sequence) was conducted in another study by Graw, 2017. In this paper, we used correlation network analysis (cf. Probst et al., 2020) to correlate the IPL abundance with the corresponding OTUs data measured in the same samples by Graw, 2017. Specifically, relationship between the relative abundance of IPLs and the relative abundance of microbial genes (both were Hellinger transformed) was evaluated using Pearson's correlation. Only lipids and microbial genes were considered if they were identified in more than half of the samples from a sediment core. Resulting p-values underwent false positive correction using the Bonferroni procedure (Bonferroni-corrected p-value < 0.001). Pair-wise connections of lipid-to-organism with Pearson's $r > 0.6$ were used to construct a network using the software Cytoscape (cf. Batushansky et al., 2016).

IV.3. RESULTS

IV.3.1. Geochemistry

The investigated sites in this study are located off the coast of southern New England (Tiki Line, Hudson Canyon) and the Mid-Atlantic regions (Chincoteague Seep and Chincoteague Slope). At the Chincoteague

Slope, no methane flux was detected therefore it is regarded as a background site. By contrast, diffusive methane flux was detected at Chincoteague Seep, Hudson Canyon and Tiki Line.

Chincoteague Seep. The highest methane concentration (3.4±3.0 mM, mean±S.E., n=14) was observed at the Chincoteague Seep (Supp. Fig. IV.1A). The carbon isotopic composition of methane ($\delta^{13}C_{CH4}$) ranged between -90.0‰ and -36.4‰, and generally increased towards the sediment surface. Sulfate concentrations decreased sharply with depth, the downward depletion of sulfate overlapped with the upward depletion of methane at 7-15 cm below seafloor (cmbsf). At this shallow sulfate-methane transition zone (SMTZ), high concentrations of sulfide were detected, which peaked at concentrations of 18.3 mM slightly above the SMTZ. The porewater DIC concentrations ranged between 3.3 and 18.9 mM. DIC was most depleted in ^{13}C compared to the other sites, with $\delta^{13}C$ values as low as -55.5‰ in the SMTZ. Meanwhile, the most ^{13}C-depleted bulk sedimentary TOC was also detected at this site with an average value of -29.1±1.5‰ (mean±S.E., n=14), which decreased with depth and was most negative beneath the SMTZ. The TOC content was 0.6±0.1 wt.% (mean±S.E., n=14).

Hudson Canyon. The overall methane concentrations at Hudson Canyon (Supp. Fig. IV.1B) were lower than that at Chincoteague Seep but higher than at Tiki Line. Methane concentrations averaged at 0.3±0.5 mM (mean±S.E., n=8) in the shallow core TC 16 and at 1.9±1.1 mM (mean±S.E., n=15) in the deep core PC 16. In PC 16, $\delta^{13}C_{CH4}$ values increased from -88.9‰ to -73.5‰ from the core bottom to the surface; in TC 16, $\delta^{13}C_{CH4}$ values were particularly low at the core bottom (-92.8‰), but increased toward the upper sediment layer. Sulfate decreased with depth but was not completely consumed at the bottom of the trigger core TC 16. At PC 16, sulfate was depleted at a depth of around 132 cmbsf. This suggests that at Hudson Canyon the SMTZ can extend widely from ca. 60 to 130 cmbsf. Meanwhile, sulfide concentrations increased with depth up to 10.4 mM in TC 16. Its peak concentration of 9.2 mM was detected at 32 cm in PC 16. The highest concentration of porewater DIC was observed at Hudson Canyon, where it increased with depth and ranged from 5.2 to 82.2 mM. The most ^{13}C-enriched DIC with $\delta^{13}C$ values up to +11.5‰ was observed beneath the SMTZ in PC 16, while more negative $\delta^{13}C_{DIC}$ values were observed within the SMTZ in both cores of TC 16 and PC 16. The sedimentary TOC content at Hudson Canyon was almost five-fold of that at the Chincoteague Seep, with average values of 2.6±0.1 wt.% (mean±S.E., n=8) in TC 16, and 2.5±0.2 wt.% in PC 16 (mean±S.E., n=14). $\delta^{13}C_{TOC}$ values were constant at around -21.0‰ throughout the core and more positive than those at the Chincoteague Seep.

Tiki Line. The site Tiki Line (Supp. Fig. IV.1C) had relatively low methane concentrations (0.4±0.4 mM, mean±S.E., n=10) and the lowest TOC contents of all sites (0.4±0.1 wt.%, mean±S.E., n=10). $\delta^{13}C$ values of CH_4 were more negative (-107.0±0.4‰, mean±S.E., n=5) than those at Chincoteague Seep and

Hudson Canyon. The $\delta^{13}C_{TOC}$ values were constant at around -23.0‰. The sulfate penetration depth was down to ca. 375 cmbsf, coinciding with a SMTZ. This SMTZ was at much greater depth compared to the other two methane-rich sites. Note that the exact location for SMTZ cannot be defined due to low sampling resolution. Sulfide concentrations were below the detection limit. DIC concentrations increased with depth and ranged from 5.4 to 13.9 mM. The $\delta^{13}C_{DIC}$ values decreased from ca. -5‰ at the surface to as low as -30.5‰ at the SMTZ.

Reference site Chincoteague Slope. The Chincoteague Slope site was regarded as a reference site because there was no methane detected at this location (Supp. Fig. IV.1E). Sulfate concentrations were constantly high throughout the sediment core. In contrast to the other sites, DIC concentrations at the reference site decreased sharply with depth from 11.6 mM to below 3 mM. The $\delta^{13}C_{DIC}$ values were constant at around 0.3‰. TOC concentrations averaged at (0.6±0.1 wt.%, mean±S.E., n=9) and $\delta^{13}C_{TOC}$ values were invariable at around -22.0‰.

IV.3.2. Distribution of microbial IPLs among sites

In agreement with the distinct geochemical profiles for the four sites, the distribution of archaeal and bacterial IPLs within the sediments differed notably from one another (Figs. IV.2 and IV.3). The archaeal IPLs were largely dominated by the contributions of GDGT based IPLs, consisting of monoglycosidic (1G-) and diglycosidic (2G-) GDGT and their monohydroxylated counterparts of 1G-OH-GDGT and 2G-OH-GDGT. These four compounds together comprised 69% to 95% of the total archaeal IPLs (Fig. IV.2), we thereby refer to them as "major" archaeal IPLs and depict them separately from the remaining "minor" archaeal IPLs. The relative abundances of major and minor archaeal IPLs are displayed in Fig. IV.2, along with the respective total concentrations (Fig. IV.2). In the case of bacterial IPLs, we only showed the relative abundance of predominating IPL classes, which mostly comprised > 95% of the total bacterial IPLs, together with their total concentrations (Fig. IV.3). In both figures, the IPL data from the deep PC 16 and its corresponding shallow core TC 16 at the Hudson Canyon were combined.

Archaeal IPLs. The major archaeal IPLs at Tiki Line, Hudson Canyon and the reference site were dominated by 1G-GDGT, followed by 2G-GDGT and 2G-OH-GDGT. By contrast, at Chincoteague Seep, the major archaeal IPLs were exceptionally abundant in 2G-GDGT, followed by 1G-GDGT, while relative contributions of intact OH-GDGTs were low (Fig. IV.2A and Supp. Fig. IV.2). As shown in Fig. IV.2A, the total concentrations of the major archaeal IPLs were mostly in the range of 5 to 15 µg/g TOC at Hudson Canyon and Chincoteague Seep. By contrast, the concentrations of these compounds were constantly below 0.5 µg/g TOC at Tiki Line. At the reference site, the already low abundances of these compounds (< 3 µg/g

TOC) decreased below 1 μg/g TOC within the top 10 cmbsf. While GDGT-0 and GDGT-5 constantly dominate the 1G-GDGT pool at all sites, 1G-GDGT-2 together with 2G-GDGT-1 and 2G-GDGT-2 were particularly abundant at Chincoteague Seep (Fig. IV.2A). The total concentration of minor archaeal IPLs were highest at Chincoteague Seep, they increased with depth and peaked within and below the SMTZ (around 3 μg/g TOC), while the total concentrations of minor archaeal IPLs were constantly below 0.5 μg/g TOC at Hudson Canyon; below 0.02 μg/g TOC at the Tiki Line and below 0.1 μg/g TOC at the reference site.

At the Chincoteague Seep AR and OH-AR based IPLs including 1G-AR, 1G-OH-AR and 2G-AR were particularly abundant among the minor archaeal IPLs, together with relatively high abundances of PG-AR, PG-OH-AR, PE-AR, phosphatidylinositol (PI-) OH-AR, phosphatidylserine (PS-) OH-AR. Additionally, notable PG-GDGT and 2PG-GDGT, as well as recently identified unsGDGT with 1G and 2G head groups were also detected at this site. At the Hudson Canyon, intact AR except for PI-AR, were negligible among the minor archaeal IPLs. This site was instead dominated by BDGT and PDGT based IPLs, i.e., 1G-BDGT, 2G-BDGT and 1G-PDGT; In addition, glycerol dialkanol diethers (GDD) with 1G head group, and 3G-GDGT were abundant, along with minor contribution of hexose phosphohexose (HPH-) GDGT.

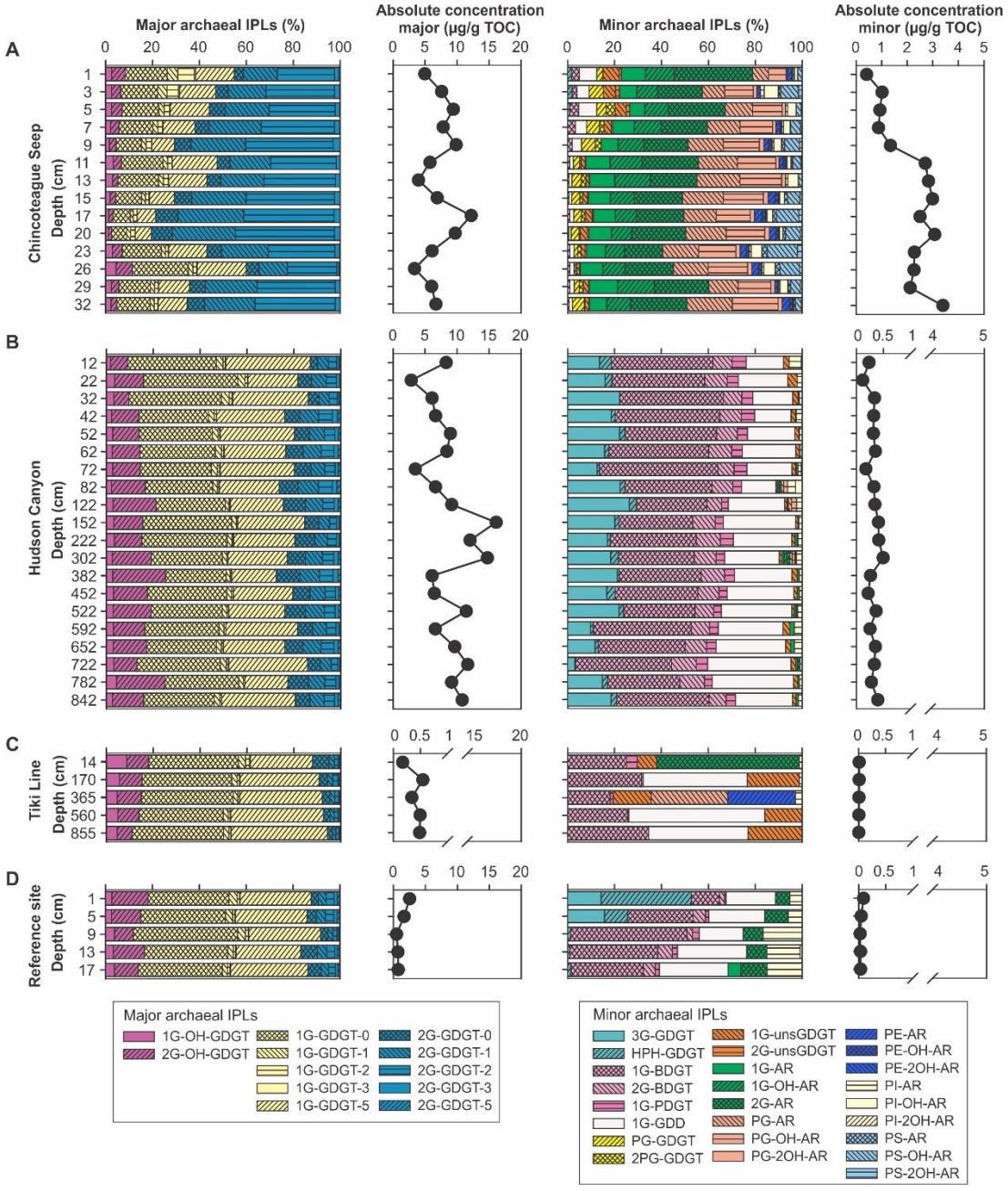

Figure IV.2. Relative and absolute concentrations of major and minor archaeal IPLs at studied sites of US Atlantic Margin. A. Chincoteague Seep, B. Hudson Canyon, C. Tiki Line, D. Chincoteague Slope (Reference site).

At Tiki Line, 1G-BDGT was relatively abundant among the minor archaeal IPLs at all depths, while 2G-AR dominated the top 14 cm. The relative abundance of PE-AR and PG-AR were particularly high within the depth of sulfate penetration (365 cm). Relative abundance of 1G-GDD and 1G-unsGDGT were elevated at the depths in between. At the reference site Chincoteague Slope, notable contributions of HPH-GDGT and 3G-GDGT were observed among the minor archaeal IPL at the surface, which decreased sharply

with depth. Relatively high contribution of 1G-BDGT, 1G-GDD, 2G-AR and PI-AR were observed throughout the deeper sediments.

Bacterial IPLs. Only major bacterial IPL classes, which comprised more than 95% of bacterial IPLs, are shown in Fig. IV.3. The highest concentration of bacterial IPLs was detected at the Chincoteague Seep (5-22 μg/g TOC), followed by the reference site (1-15 μg/g TOC) and the Hudson Canyon (0.1-7 μg/g TOC). Tiki Line had lowest bacterial IPL concentrations (< 0.3 μg/g TOC). At all studied sites, the abundance of bacterial IPLs peaked at the surface layer and steeply decreased with sediment depth.

In comparison to archaeal IPLs, bacterial IPLs were more diverse both between sites and within sites throughout the sediment depth. At the Chincoteague Seep, contributions of DPG were constantly high and decreased with depth with exception of a peak within the SMTZ at 13 cmbsf. Relative abundances of diacylglycerol (DAG) lipids with PE and PG head groups (PE-DAG and PG-DAG), decreased with depth, while that of PE derivatives of mixed acyl/ether glycerol (AEG) and dietherglycerol (DEG) lipids (PE-AEG and PE-DEG) increased with depth (Fig. IV.3A). At the Hudson Canyon, the distribution of bacterial IPLs differed significantly with increasing depth (Fig. IV.3B): relative abundance of DPG was ~50% in depths within and above the SMTZ (< 82 cm), but decreased to negligible contents at greater depth. A similar trend was observed in the relative abundance of both phosphatidylcholine (PC-) DAG and PE-DAG, which decreased with depth. By contrast, relative contribution of PE-DEG increased abruptly from below 30% (< 82 cm) to above 60% at greater depth (> 122 cm); relative abundance PME-DAG and PME-DEG increased with depth. Notably, the relative contributions of PME-DAG and PME-DEG were minor at shallower sediment depth of Hudson Canyon as well as throughout the sediment core at the Chincoteague Seep.

At the Tiki Line, bacterial IPLs were overwhelmingly dominated by PE-DEG and PC-DAG (Fig. IV.3C). Bacterial IPLs at the reference site were dominated by DAG based PG, PC and PE lipids, as well as PE-DEG, which increased with depth (Fig. IV.3D).

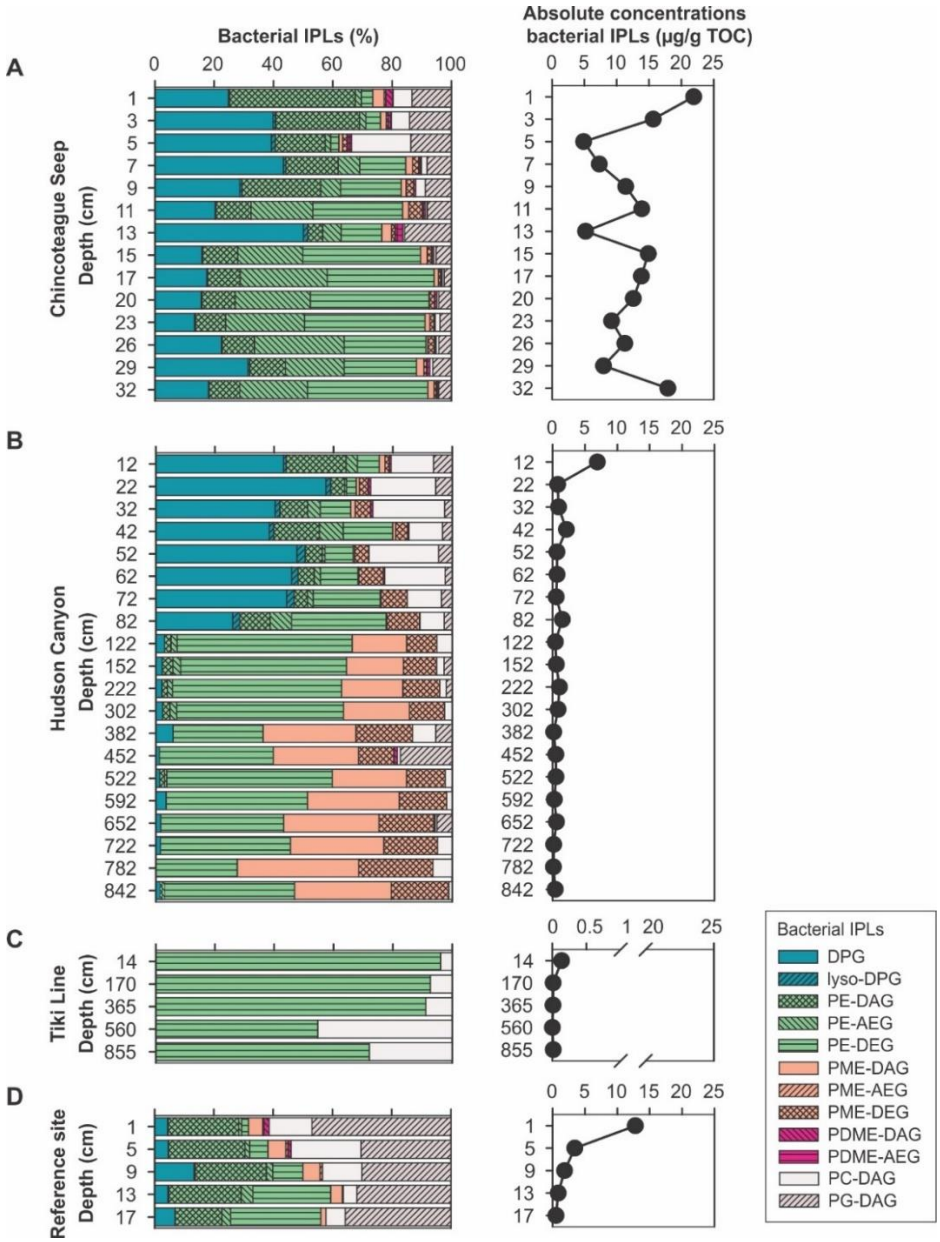

Figure IV.3. Relative and absolute concentrations of bacterial IPLs at sites. A. Chincoteague Seep, B. Hudson Canyon, C. Tiki Line, D. reference site Chincoteague Slope. Note that only major bacterial IPLs (< 95% of total) are shown.

IV.4. DISCUSSION

IV.4.1. Distinct geochemical regimes in USAM sediments

A primarily microbial source for methane at all three methane-laden sites (Tiki Line, Hudson Canyon and Chincoteague Seep) is indicated by highly negative $\delta^{13}C_{CH4}$ values (-107.1‰ to -70.8‰, see Supp. Fig. IV.1) in greater sediment depth (cf. Whiticar et al., 1986). The different depths of the SMTZ in the sediment

cores indicates variable degrees of methane fluxes at each site, whereby a shallower SMTZ indicates high methane flux (Borowski et al., 1996). Consequently, the highest methane flux occurred at Chincoteague Seep (SMTZ at 7-15 cmbsf), while Hudson Canyon exhibits moderate methane flux (estimated SMTZ: 57-132 cmbsf) and comparably low methane flux is present at Tiki Line (estimated SMTZ: ~ 375 cmbsf).

Tiki Line was characterized by extremely low TOC content and methane flux compared to the other two methane-laden sites (Supp. Fig. IV.1D). The reference site represented a typical non-methane influenced marine sedimentary environment, where no indication of AOM or organotrophic sulfate reduction was observed. Organic carbon remineralization does not seem to play a significant role at this site either, as the $\delta^{13}C_{DIC}$ values consistently carried a typical sea water signal of ~ 0‰ (Supp. Fig. IV.1E).

The presence of SMTZs in the sediments indicates the process of sulfate-dependent anaerobic oxidation of methane (AOM) at all the methane-laden sites. The active process of sulfate reduction was evident by the large amount of sulfide at both Chincoteague Seep and Hudson Canyon. Evidence for AOM within or close to the depth of the SMTZ at these sites was further indicated by the $\delta^{13}C_{CH4}$ and porewater $\delta^{13}C_{DIC}$ profiles; the observed increasing (more positive) values of $\delta^{13}C_{CH4}$ towards the sediment surface result from the preferable oxidation of ^{13}C-depleted methane, while $\delta^{13}C_{DIC}$ were more negative due to the accumulation of ^{13}C-depleted inorganic carbon produced by methane oxidation (Supp. Fig. IV.1; Boetius et al., 2000; Orphan et al., 2001). Notably, significant ^{13}C-depletion in sedimentary TOC (δ^{13}C averaged at -29.1±1.5‰) at Chincoteague Seep further distinguished this site from others. This indicates a significant contribution of ^{13}C-depleted biomass that incorporated methane-derived carbon through AOM (Supp. Fig. IV.1A). This suggests the presence of highly active methanotrophic microbial groups at this site (cf. Hinrichs and Boetius, 2002). By comparison, $\delta^{13}C_{TOC}$ values of Hudson Canyon and Tiki Line indicate negligible accumulation of methanotrophic biomass, as these values were even slightly more positive than those of the reference site (Supp. Fig. IV.1). At Hudson Canyon, the sedimentary TOC content was over four times higher (avg. 2.6 wt.%) than those at the other sites; these high TOC concentrations could also mask an *in situ* methanotrophic signal in the bulk TOC. While TOC concentrations of Hudson Canyon decreased beneath the SMTZ, porewater DIC concentrations increased sharply, which can be explained by predominant DIC production from organic carbon remineralization (e.g., Claypool and Kaplan, 1974). Moreover, the $\delta^{13}C_{DIC}$ values at greater depth (> 132 cm) of Hudson Canyon were particularly positive (up to +11‰; Supp. Fig. IV.1C), suggesting a methanogenic zone below our maximum sampling depth (cf. Claypool and Kaplan, 1974).

Altogether, the geochemical profiles differed greatly between the four investigated sites, especially with regard to methane fluxes and total organic carbon contents. Similarly, lipid composition differed

significantly between these sites. In the following section, we will evaluate connections between the distinct geochemical conditions and the diversity of microbial lipids (Figs. IV.2 and IV.3).

IV.4.2. Factors controlling archaeal IPL composition

Distinction of sedimentary and planktonic sources of archaeal IPLs. The assumed labile nature of IPLs (White et al., 1979; Harvey et al., 1986) has been used in numerous studies to assess the composition and dynamics of living microbial communities in sedimentary environments (e.g., Lipp et al., 2008). However, more recent studies challenged this traditional view and provided a more nuanced picture about the degradation kinetics of different IPL groups (Logemann et al., 2011; Xie et al., 2013; Schouten et al., 2010). While bacterial ester-bound bacterial IPLs still appear to be degraded quickly after sediment deposition, the majority of sedimentary archaeal IPLs may in fact originate from planktonic sources as they are more resistant to degradation than originally expected, questioning the use of these lipids as indicators for living biomass (Logemann et al., 2011; Xie et al., 2013). In particular, monoglycosidic GDGTs with predominantly GDGT-0 and Crenarchaeol (referred as GDGT-5 here) as core lipids as well as glycosidic OH-GDGTs are abundantly present in planktonic Thaumarchaeota (Elling et al., 2017), and these compounds are expected to degrade only slowly in marine sediments (Xie et al., 2013). Biomass from sedimentary archaea has been shown to significantly contribute to the GDGT pool. In particular ring containing GDGTs in AOM settings, for instance, methanotrophic archaea can contribute notable amount of 2G-GDGT with one to three cyclopentane rings in methane-rich sediments (e.g., Rossel et al., 2008). This is the case in Chincoteague Seep sediments, where high methane fluxes occurred, and a substantial contribution of 2G-GDGT with one to two rings to the archaeal IPL pool was observed (Supp. Fig. IV.2).

To evaluate the influence of geochemical conditions on the lipid diversity, we performed statistical db-RDA analysis on the individual major archaeal IPLs, whereby Chincoteague Seep samples showed a distinct grouping (Fig. IV.4A). Chincoteague Seep was ordinated by methane and sulfide, with 2G-GDGT-1 and 2G-GDGT-2, the well-known biomarkers for ANME-1 at marine seeps (Rossel et al., 2008), together with 1G-GDGT-2 being significantly correlated with these two geochemical vectors (Fig. IV.4A), indicating that the high methane flux at this site coupled with the process of sulfate-dependent AOM leaves a distinct imprint on the major archaeal IPL composition.

By contrast, the other two methane-laden sites (Hudson Canyon and Tiki Line) clustered closely with the reference site (Fig. IV.4A). The major archaeal IPLs from Tiki Line samples were ordinated by sulfate concentrations, indicating microbes associated with sulfate reduction being theri dominant source, whereas those from Hudson Canyon (both shallow and deep) sediments were mainly ordinated by concentrations of

TOC, DIC and their isotopic compositions, and to lesser extent by sediment depth (Fig. IV.4A). This implies organisms involved in sedimentary organic carbon remineralization being a likely source for archaeal lipids at Hudson Canyon. Despite an unaccounted contribution from the water column, elevated abundances of 2G-OH-GDGT at Hudson Canyon and 1G-OH-GDGT at Tiki Line compared to the other sites (Fig. IV.2; Supp. Fig. IV.2) may at least partly represent an *in situ* signal, as indicated by the statistical analysis, which showed a positive correlation between 2G-OH-GDGT with 0-2 rings and TOC as well as DIC. Additionally, 1G-OH-GDGT-0 was positively correlated with sulfate (Fig. IV.4A), indicating organisms that involved in sulfate reduction or organic carbon remineralization may contribute to these archaeal lipids. Thus, sedimentary archaea appear to synthesize OH-GDGTs extending their sources beyond planktonic Thaumarchaeota in the marine environment (see also section 4.4).

Sedimentary sources of minor archaeal IPLs. We have additionally detected numerous archaeal IPLs that are clearly associated with active archaeal communities in the investigated sediments. These compound groups include diverse glycosidic and phospho-ARs and OH-ARs (Fig. IV.2A), which have been linked to ANME-2 in methane-rich sediments (Rossel et al., 2008; 2011). Our statistical db-RDA analysis strongly supports these earlier findings as the intact ARs showed a significant positive correlation with methane and sulfide concentrations. This was particularly true for Chincoteague Seep (Fig. IV.4B) and indicates active sulfate-dependent AOM communities at this site. This assignment is in line with findings by Graw (2017)), who detected predominantly methanotrophic archaea dominated by ANME-2 and ANME-1 (> 70% of total archaeal OTUs; Supp. Table IV.3). Hence, combined lipid, geochemical and genetic data point to the process of sulfate-dependent AOM dominating at Chincoteague Seep, which were mostly performed by ANME-1 and ANME-2 clades.

The recently identified 1G- and 2G-unsGDGTs (Zhu et al., 2014b) comprised notable amounts of the minor archaeal IPLs at Chincoteague Seep (Fig. IV.2A), while 1G-unsGDGT contributed substantially to the minor archaeal lipid pool of Tiki Line (Fig. IV.2B). These lipids are mainly found in anoxic environments (Zhu et al., 2014b; Zhu et al., 2016) and have been suggested to be sourced from Thermoplasmatales-related archaea that were found to assimilate 13C-depleted carbon in a sedimentary AOM setting at the Pakistan continental margin (Yoshinaga et al., 2015). Our statistical evaluation showed that 2G-unsGDGT clustered with other potential AOM biomarkers at the Chincoteague Seep, while 1G-unsGDGT was the only compound clustering directly with Tiki Line samples (Fig. IV.4B). This indicates different sources for unsGDGTs according to head group, with 2G-unsGDGT being most likely affiliated to the process of AOM.

By contrast to major archaeal IPLs, minor archaeal IPLs of sediments from Tiki Line showed distinct clustering compared to the other sites and was ordinated by sediment depth (Fig. IV.4B). The 1G-unsGDGT and 1G-GDD were closely grouped with Tiki Line samples and positively correlated with sediment depth (Fig. IV.4B). While 1G-unsGDGT have been previously suggested to be sourced from Thermoplasmatales-related archaea (Yoshinaga et al., 2015), the biological sources of 1G-GDD are not well-understood, but they have been reported in cultures of Thaumarchaea (Meador et al., 2014; Elling et al., 2017), the extremely acidophilic Cuniculiplasma divulgatum (Golyshina et al., 2016) as well as in diverse natural environments ranging from estuarine to hot spring sediments (Meador et al., 2014). Analysis on 16S rRNA genes revealed that Tiki Line was uniquely dominated by the Hadesarchaea (formerly called the South-African Gold Mine Miscellaneous Euryarchaeal Group), along with notable contribution of MBG-B, MCG-15 (formerly Group C3), and Thermoprofundales/Deep Sea Hydrothermal Vent Group (DHVEG-1) (Supp. Table IV.3). Hadesarchaea are reported to hold genes involving in CO and H2 oxidation (or H2 production), with potential coupling to nitrite reduction (Baker et al., 2016). Whether any of these organisms might be a potential source for these lipids will be further evaluated in section 4.4. Another abundant minor archaeal IPL at the Tiki Line was the recently identified 1G-BDGT (Fig. IV.2C). Since this lipid contributed significantly to the minor archaeal IPL pools of both the reference site (Fig. IV.2D) and the Hudson Canyon (Fig. IV.2B), it does not show distinct pattern in the statistical analysis.

Statistical analysis on minor archaeal IPLs showed that the Hudson Canyon samples from both shallow and deep sediments clustered with the reference site (Fig. IV.4B), which were mainly ordinated by concentrations of TOC, DIC and their isotopic compositions. The same pattern has been observed for the major archaeal IPLs further supports a primary influence of sedimentary organic carbon remineralization processes at Hudson Canyon. Glycosidic BDGTs and PDGTs were among the lipids that grouped with Hudson Canyon samples and positively correlated with the geochemical variables that ordinated Hudson Canyon samples (Fig. IV.4B). These IPLs were abundant in the minor archaeal IPL pool at all depths of Hudson Canyon, with 51±6.0% (mean±SD; n=20) of all minor archaeal IPLs (Fig. IV.2B). Recently, some light has been shed into potential sources of these compounds, which include marine benthic groups such as the MCG (Meador et al., 2015), methanogens of the order Methanomassiliicoccales (Becker et al., 2016) and unidentified methanogens and heterotrophic archaea (Coffinet et al., 2019). Indeed, such sources would be in line with archaeal 16S genes found at Hudson Canyon, which were dominated by such benthic archaeal groups as MCG-15 and Thermoprofundales/DHVEG-1), followed by Marine Benthic Group-B (MBG-B; Supp. Table IV.3; Graw, 2017). Other deep biosphere settings dominated by MCG include anoxic organic-rich and hydrate-bearing environments (Inagaki et al., 2006), and deeply buried SMTZs (Biddle et al., 2006). Although no pure cultures of MCG have been established yet (Gagen et al., 2013), metagenomic

evidence suggested they are heterotrophs involved in the degradation of peptides (Lloyd et al., 2013) and aromatic compounds (Meng et al., 2014) as well as in metabolism of methane (Evans et al., 2015). Together, our data suggested glycosidic BDGT and PDGT may be produced by some of the uncultured benthic archaea that are involved in the degradation of organic matter and methanogenesis.

Despite of a clear geochemical indication for AOM at Hudson Canyon, we only detected minor contribution of ANME-diagnostic biomarkers, which, in contrast, were dominated the Chincoteague Seep (Fig. IV.2A). Instead, the archaeal IPL distribution was rather uniform with depth (Fig. IV.2B). This was supported by16S rRNA gene analysis, which showed that ANMEs only comprised a minor fraction of the microbial community at Hudson Canyon (Supp. Table IV.3). The 16S rRNA gene data support our interpretation that archaeal IPLs at Hudson Canyon are predominantly sourced from organisms involved in organic carbon remineralization.

At the reference site, HPH-GDGT was particularly abundant within the minor IPL pool of the surface layer (Fig. IV.2D); HPH-GDGT, a specific biomarker for Thaumarchaeota (Schouten et al., 2008; Elling et al., 2017), decreased sharply with depth (Fig. IV.2D). This is in accordance with the relatively high abundance of Marine Group I, in particular Candidatus Nitrosopumilus at the surface, which was swiftly replaced by MCG-15, Thermoprofundales/DHVEG-1 and MBG-B within the surface 5 cm of sediments (Graw, 2017). The corresponding increase in glycosidic BDGT and PDGT among the minor archaeal IPLs explains the close clustering of Hudson Canyon and the reference site during db-RDA analysis of minor IPLs (Fig. IV.4B).

Altogether, our lipid data suggests that the diversity of archaeal IPLs at the different study areas are mainly constrained by the methane flux or the organic carbon content, or a combination of both for Hudson Canyon. Specifically, under conditions with high methane fluxes, IPLs diagnostic for methanotrophic archaea dominated the lipids pool indicating a highly active AOM. In contrast, in organic-rich sediments with low methane fluxes, the archaeal IPL composition suggests the predominance of heterotrophic benthic archaeal groups, while carbon-starved condition was associated with very low *in situ* archaeal IPL production.

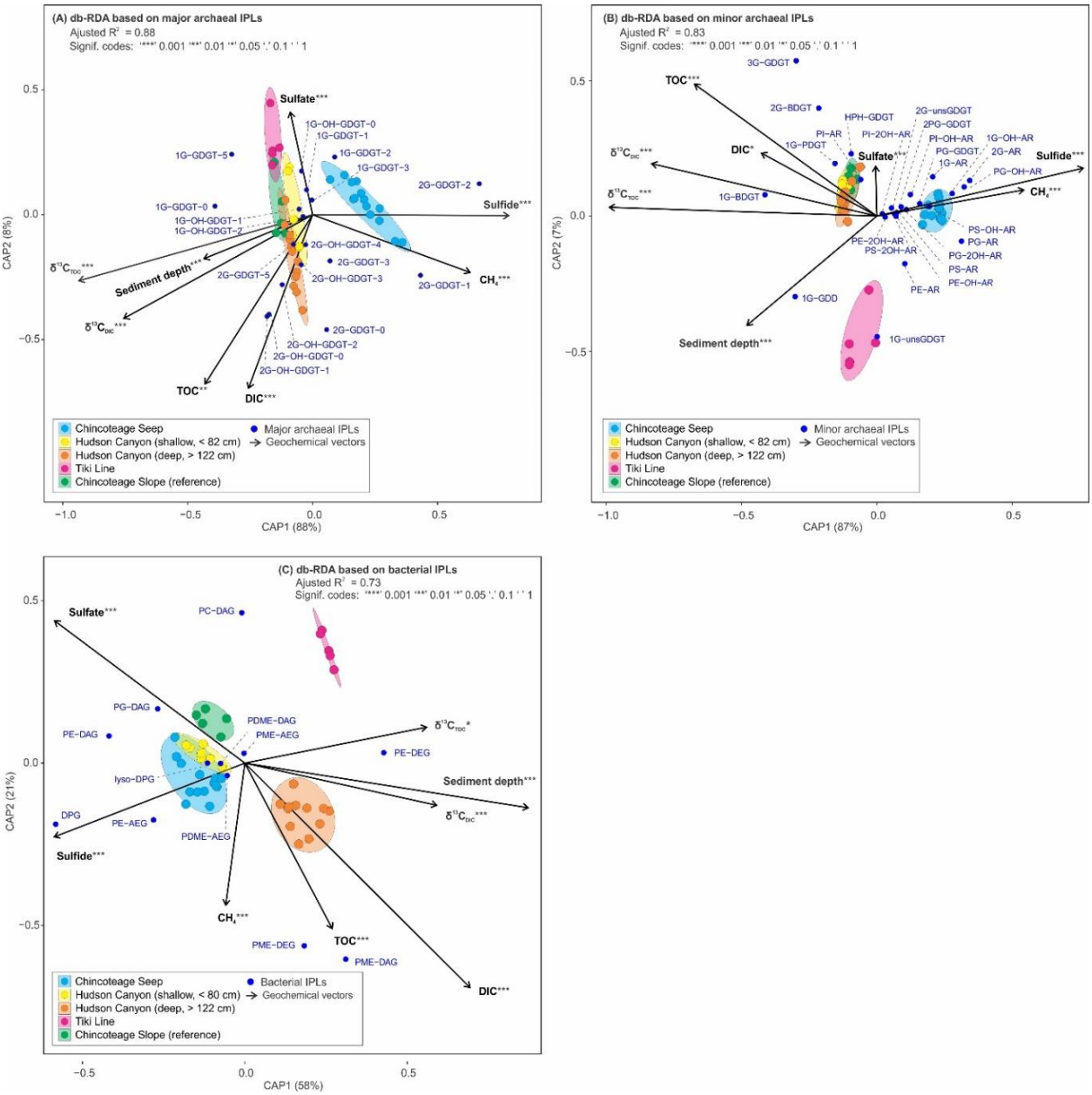

Figure IV.4. Distance based redundancy analysis (db-RDA) on (A) major archaeal IPLs, (B) minor archaeal IPLs, and (C) bacterial IPLs at the four study sites, Chincoteague Seep (blue), Hudson Canyon (yellow and organge), Tiki Line (pink) and reference site Chincoteague Slope (green). Note that the Hudson Canyon is depicted by two colors, yellow for the shallow sediments (< 82 cm) and orange for deeper sediments (> 122 cm). Archaeal and bacterial IPLs are depicted as blue dots. Environmental parameters are fitted to the ordination and represented as solid lines with arrows indicating the direction of increase relative to the other geochemical parameters on the ordination.

IV.4.3. Distinct bacterial IPL composition constrained by geochemical conditions

The bacterial IPLs showed significant differences both among sites and with sediment depth at each site (Fig. IV.3), which resulted in distinct clustering of the investigated sites in our statistical analysis (Fig.

IV.4C). The AOM-dominated Chincoteague Seep grouped closely to the shallower sediments of Hudson Canyon, whereas Tiki Line, the reference site and the deeper sediments of Hudson Canyon (> 122 cm) clustered separately (Fig. IV.4C). Both Chincoteague Seep and the shallow Hudson Canyon samples were ordinated by sulfate and sulfide concentrations (Fig. IV.4C), in accordance with the relatively high sulfate concentrations and active sulfate reduction in these sediments (Fig. S1A, B). Samples from the deeper sediments of Hudson Canyon were ordinated by DIC concentration and sediment depth, as well as to lesser degree by TOC and methane concentrations, as well as $\delta^{13}C$ of DIC and TOC (Fig. IV.4C). This supports that this depth horizon was primarily governed by organic carbon remineralization and methanogenesis, in line with our observations from the archaeal lipid biomarkers. The Tiki Line samples were not significantly ordinated by geochemical parameters (Fig. IV.4C), suggesting a less active environment that corroborates with the extremely low lipid contents at this site (Fig. IV.3C).

The most abundant bacterial IPL at all study sites was PE with either DAG, AEG or DEG core lipids. While PE-DAG was more abundant in surface sediments, contributions of PE-AEG and PE-DEG increased in the AOM-active sediments with PE-DEG being most abundant in the deeper samples (Fig. IV.3). The high abundance of PE-AEG at the Chincoteague Seep suggests an origin from AOM-associated SRB. This is supported by culture studies, which showed that PE-AEG derivatives contributed significantly to total phospholipids in Desulfosarcina variabilis (Rütters et al., 2001), a cultured representative of the AOM syntrophic group Desulfosarcina/Desulfoccocus (DSS) (Boetius et al., 2000). Furthermore, previous studies have demonstrated the presence of strongly ^{13}C-depleted monoalkyl glycerol ethers (MAGE) in methane-rich sediments, thereby attributing MAGE to AOM-associated SRB which assimilate methane-derived carbon (e.g., Hinrichs et al., 2000; Orphan et al., 2001; Elvert et al., 2005). These MAGE lipids were at least partially derived from the PE-AEG, as they were particularly abundant in methane-rich sediments (e.g., Sturt et al., 2004; Rossel et al., 2011, and this study). This assignment is in accordance with our statistical analysis, which clustered PE-AEG with the AOM-active Chincoteague Seep and the shallower sediments of Hudson Canyon where sulfate reduction was most active, and showed its positive correlation with sulfide and methane (Fig. IV.4). Additionally, 16S rRNA gene analysis showed that Deltaproteobacteria contribute largely to the OTUs of Chincoteague Seep sediments (Supp. Table IV.3; Graw, 2017). We therefore conclude that in USAM sediments PE-AEG were predominantly produced by SRB that were partly involved in AOM.

PE-DEG showed increasing relative abundances with sediment depth and it was the dominant bacterial lipid below the SMTZ sediments of Hudson Canyon and Chincoteague Seep (Fig. IV.3). While DEG core lipids were previously attributed to AOM-associated SRB due to their strong ^{13}C-depletions (e.g., Hinrichs et al., 2000; Pancost et al., 2001; Elvert et al., 2005) and they have been found to be the major phospholipid

in cultures of thermophilic and mesophilic sulfate reducing bacteria (Sturt et al., 2004, Grossi et al., 2015), our results indicate that there is an additional biological source that is not related to AOM-associated SRB. 16S rRNA gene analysis revealed that JS1 group dominated the bacterial community in the deeper sediments of both Hudson Canyon and Chincoteague Seep (Supp. Table IV.3; Graw, 2017), making them the most likely source for PE-DEG lipids in our samples. These bacteria have frequently been found in anoxic, methane-rich sediments, where the organisms may be involved in organic matter degradation associated to methanogenesis (Carr et al., 2015; Oni et al., 2015a). Indeed, our statistical analysis showed that PE-DEG was positively correlated with sediment depth as well as $\delta^{13}C$ values of TOC and DIC (Fig. IV.4C), indicating a connection of these lipids with microbes involved in organic carbon degradation. Notably, PE-DEG accounted for more than 60% of bacterial IPLs in all Tiki Line samples (Fig. IV.3D), which showed a dominance of Dehalococcoidia (phylum Chloroflexi) in 16S rRNA gene abundance (Supp. Table IV.3; Graw, 2017). Dehalococcoidia was reported to be a dominant group in marine subsurface sediments where they were linked to the degradation of more refractory aromatic compounds, CO_2 fixation and fermentation (Wasmund et al., 2014; Oni et al., 2015b). The extremely low abundance of bacterial IPLs at Tiki Line (Fig. IV.3C) indicates very low bacterial biomass at this site, which is likely due to carbon scarcity.

The succession of ester to ether lipids with increasing sediment depth (Supp. Fig. IV.3) has been also observed in former studies (Schröder, 2015; Evans et al., 2017). It might be due to different chemical stability of ether- and ester-bonds as observed in degradation experiments (Logemann et al., 2011); Ester-based lipids are quickly degraded after cell death, while the more stable and rigid ether lipids are remained as fossil compounds. Another possible reason is an exclusive production of ether lipid-based cell membranes in deeper sediments in response to energy stress. The diether structure of PE-DEG may assist in cell resistance in energy-limited environments by reducing cellular maintenance activity (Evans et al., 2017).

DPG was also particularly abundant at Chincoteague Seep and in the shallow sediments of Hudson Canyon, suggestive of its association to SRB, partly involved in AOM (Knoblauch et al., 1999; Schubotz et al., 2011). Statistical analysis confirmed the close associations of DPG with sulfate reduction as it was positively correlated with sulfide concentration (Fig. IV.4C). Similarly, PG-DAG a known lipid of SRB (Knoblauch et al., 1999), was clustered with samples from Chincoteague Seep and the shallow Hudson Canyon, as well as the reference site. It was positively correlated with sulfate and may partly be associated with sulfate reduction.

PME with DAG and DEG derivatives were notably abundant in the methanogenic zone of Hudson Canyon (Fig. IV.3B), while statistical analysis displayed that they were positively correlated with concentrations of DIC, TOC and methane (Fig. IV.4C). Together this suggests that these IPLs were related to microbes involved in methane production and organic carbon degradation. Indeed, PME-DAG was found to be abundant in oil-impregnated surface sediments at other hydrocarbon seeps where it was assigned to heterotrophic oil-degrading bacteria as its $\delta^{13}C$ composition closely resembled that of TOC (Schubotz et al., 2011). In light of this, PME-DAG and its DEG analog may be sourced from bacteria that are involved in the degradation of sedimentary organic matter at the Hudson Canyon.

PDME derived DAG and AEG lipids were among the least abundant compounds in the bacterial IPL pool (Fig. IV.3). A former study suggested heterotrophic bacteria as source of PDME-DAG (Schubotz et al., 2011); our results suggest that PDME lipids may also be connected to AOM-associated sulfate reduction, as they closely clustered with Deltaproteobacteria dominated Chincoteague Seep and shallower sediments of Hudson Canyon, and were correlated with sulfide concentration and to lesser degree to sulfate and methane concentration (Fig. IV.4C). PC-DAG was present in all studied samples (Fig. IV.3) where it was weakly correlated with sulfate concentration (Fig. IV.4C). Former studies suggested that heterotrophic bacteria may be the source organism at hydrocarbon seeps (Schubotz et al., 2011).

IV.4.4. Evaluating biological sources for IPLs

The db-RDA analyses provides insight into the environmental factors that regulate IPL distributions, and enable us to make first assignments of IPLs to detected microorganisms at the geochemically different sites (Graw, 2017). We used additional statistical analysis to further evaluate these assignments of IPLs to microorganisms by performing a correlation network analysis (cf. Probst et al., 2020). This analysis first evaluated the linear relationship between IPLs and 16S gene abundance using Pearson's correlation, and then created lipid-to-organism connections for pairs with significant positive correlations ($r > 0.7$, Bonferroni-corrected p-value < 0.001). These lipid-to-organism pairs then underwent co-occurrence network analysis.

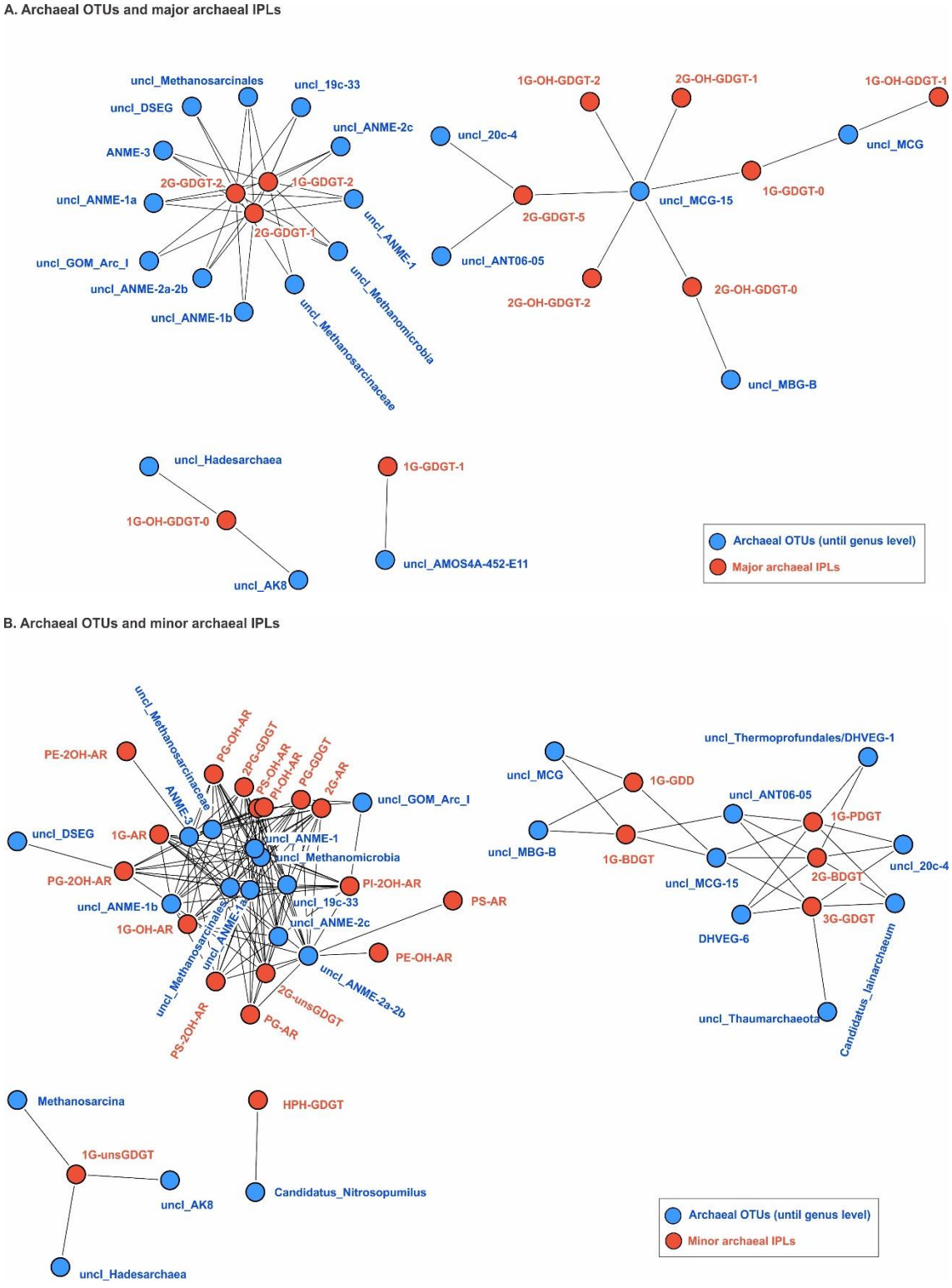

Figure IV.5. Network Pearson's correlation analysis of the relative abundance of (A) major archaeal IPLs and (B) minor archaeal IPLs with archaeal OTUs. Only significantly positive correlations ($r > 0.7$) and Bonferroni-corrected p-value < 0.001 are shown. MCG, Miscellaneous Crenarchaeotal Group; MBG-B, Marine Benthic Group-B; DHVEG, Deep Sea Hydrothermal Vent Group.

Statistical network analysis on the relative abundance of major archaeal IPLs and archaeal OTUs clustered 2G-GDGT-1, 2G-GDGT-2 and 1G-GDGT-2 with ANME-1, -2, and -3 clades and several uncultured methanogens (Fig. IV.5A), suggesting their association with ANMEs in general, and not just ANME-1 as previously suggested (Rossel et al., 2008). In addition, the marine benthic group MCG-15 is possibly an important biological source for 1G-OH-GDGT with 2 rings and 2G-OH-GDGT with 0-2 rings, which explains the co-occurrence of these compounds in the db-RDA analysis with Hudson Canyon samples, where MCG-15 was particularly abundant. This is in agreement with a former hypothesis that such archaeal benthic groups are potential sources for glycosidic and diglycosidic OH-GDGTs (Meador et al., 2015). In addition, 1G-OH-GDGT-0 was correlated with Hadesarchaea, which uniquely dominated the Tiki Line.

Statistical network analysis on the relative abundance of minor archaeal IPLs and archaeal OTUs also largely confirmed previous lipid assignments (Fig. IV.5B). For instance, HPH-GDGT was correlated with Candidatus_Nitrosopumilus, confirming its common use as Thaumarchaeal marker (Schouten et al., 2008; Pitcher et al., 2011; Elling et al., 2017); typical archaeal methanotrophic biomarkers including AR and OH-AR with 1G-, 2G- and phosphate based head groups clustered closely with all three ANME clades as well as other unclassified methanogens, in accordance with a previous survey of wide range of methane seeps (Rossel et al., 2011). Our results suggest that these compounds might be more indicative of active AOM processes rather than specific ANME clades. Furthermore, recently identified IPLs such as 1G-BDGT and 1G-GDD were correlated with MBG-B as well as MCG, in agreement with previous assignments (Meador et al., 2015; Coffinet et al., 2019), while Thermoprofundales/DHVEG-1 seemed to be a potential source for 2G-BDGT and 1G-PDGT, which were also correlated with MCG-15 among other archaeal groups.

Notably, the recently identified 2G-unsGDGT clustered with ANMEs and other methanogens, while 1G-unsGDGT was clustered with both Methanosarcina and Hadesarchaea. This does not support the previous assumption that Thermoplasmatales a dominant source of these lipids (Yoshinaga et al., 2015). However, this study does not exclude Thermoplasmatales or other archaea as possible sources at other sites, but more studies are needed to further constrain the sources of unsGDGTs.

By contrast to archaeal IPLs, network analysis on bacterial IPLs (Fig. IV.6) showed that many of the bacterial IPL classes were affiliated with a multitude of bacterial organisms, suggesting that the chemotaxonomic potential of bacterial phospholipids is lower than that of archaeal lipids. However, some informative relationships were observed. For instance, PE-DAG, PE-AEG, PDME-DAG and DPG clustered together and all correlated with δ-Proteobacteria further solidifying their relationship to sulfate reduction and by inference AOM-related sulfate reduction. Interestingly, PG-DAG, another suggested IPL

derived from SRB (Knoblauch et al., 1999), did not show a correlation with δ-Proteobacteria, but instead correlated with the Acidobacteria and less abundant Proteobacteria, including the Epsilonproteobacteria. Similarly, PME-AEG was correlated with many different but less abundant bacterial groups, including the likely heterotrophic Lentisphaerae and Verrucomicrobia. The widely distributed PC-DAG correlated to a number of abundant bacterial groups, including the Betaproteobacteria, Gammaproteobacteria and Planctomycetes. PC-DAG is not a common bacterial IPL; however, a number of bacteria possess the genetic capacity to synthesize PC, including those that PC is correlated with in our samples (Sohlenkamp et al., 2003).

Notably, both diether-based phospholipids, PE-DEG and PME-DEG clustered separately from the other bacterial IPLs and were associated to distinct bacterial groups. PME-DEG showed correlations with putatively heterotrophic Armatimonadetes, while PE-DEG was correlated with Dehalococcoidia and other less abundant Chloroflexi members as well as uncultured bacteria commonly found in the deep biosphere (OP8, OD1).

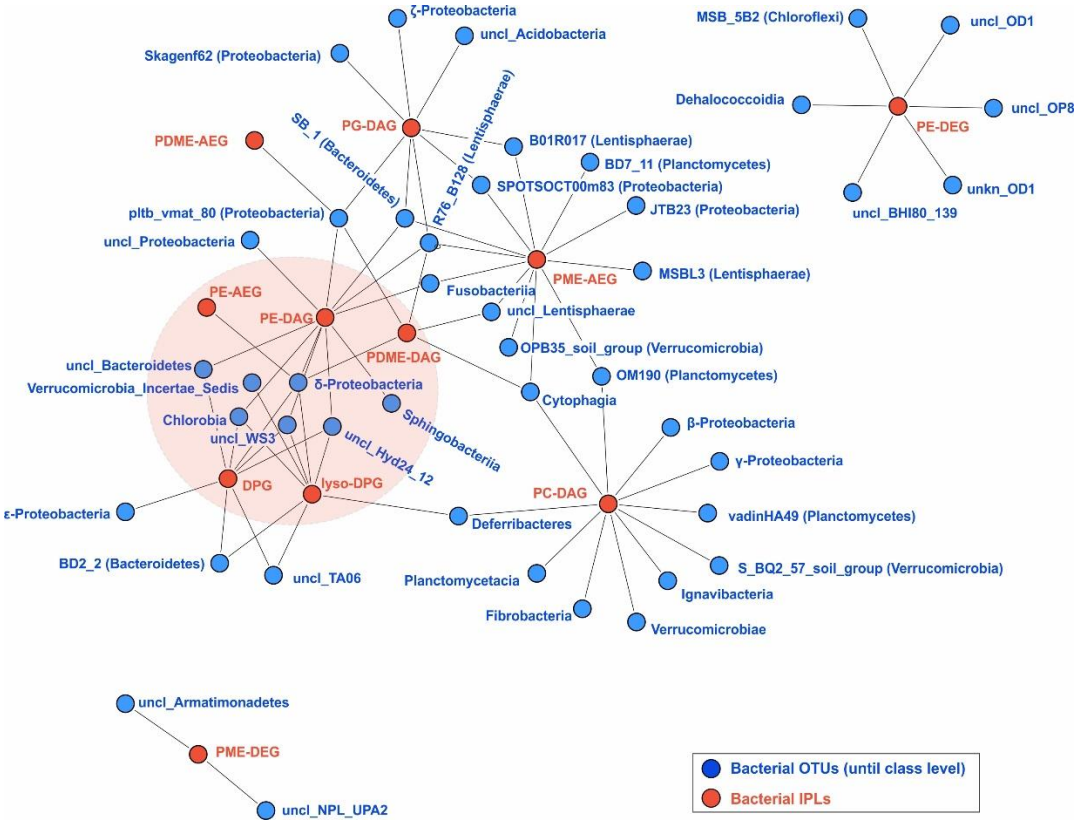

Figure IV.6. Network Pearson's correlation analysis of relative abundance of bacterial IPLs and bacterial OTUs. Only significantly positive correlations ($r > 0.6$) and Bonferroni-corrected p-value < 0.001 are shown. Pink shade highlights the location of δ-Proteobacteria, which include sulfate-reducing bacteria, and its correlated IPLs.

IV.5. SUMMARY AND CONCLUSION

Our study delineates the relative influences of methane- and organic matter-related diagenetic processes on sedimentary IPL signatures from the US Atlantic margin. Insight from this study broadly defines the applicability of these biomarkers as tracers of *in situ* microbial communities and/or processes. A setting with high methane flux and intermediate organic carbon content (Chincoteague Seep) had large amounts of ANME-diagnostic biomarkers including 1G- and 2G-GDGTs with 0 to 2 rings and glycosidic and phosphate based archaeol and hydroxyarchaeols. These compounds clustered closely with ANME-1 and -2 groups and some methanogenic archaea. At a setting with lower methane flux and high organic matter content where heterotrophic processes prevailed over methanotrophy (Hudson Canyon), the recently identified glycosidic BDGT and PDGT were more abundant in the archaeal lipid pool and network correlation analysis confirmed their previously assumed close relationships with benthic archaeal groups including MCG, MBG-B and Thermoprofundales/DHVEG-1. Similarly, 1G and 2G-OH-GDGT with 0 to 2 rings shared close assignments to MCG and were most prominent in sediments with lower methane flux (Hudson Canyon, Tiki Line and the reference site). Additionally, unsaturated GDGTs with 1G and 2G head groups correlated with different organisms, with the 2G-unsGDGT affiliated with methanotrophic groups as suggested previously, 1G-unsGDGT correlated with potentially CO-oxidizing Hadesarchaea, which were most abundant in low methane flux and low organic carbon containing sediments.

Moreover, we showed that the phospholipids PE-DAG, PE-AEG and DPG were particularly abundant in sulfate-reducing sediments and thus have diagnostic potential for the detection of sulfate-reducing bacteria. Statistical analysis furthermore revealed the monoether based PE-AEG as the most specific biomarkers for AOM-associated SRB. PME-DAG and DEG lipids showed closest associations to processes involved in methanogenic organic matter degradation. Diether based PE-DEG lipids increased in abundance with depth while DAG-based lipids decreased showing correlations with Chloroflexi members and other heterotrophic phylogenetic groups, indicating that ether lipids may a prominent adaptive process of bacteria living in the deep biosphere.

Overall, our results indicate that the diversity and abundance of microbial IPLs in studied sediment samples are closely linked to the *in situ* microbial community composition and well-constrained by methane flux and organic carbon content. This implies that specific IPLs may be used as diagnostic markers for fingerprinting processes and/or microbial communities in diverse sedimentary environments, thereby providing insights into the methane and carbon metabolism in marine sediments.

ACKNOWLEDGEMENTS

Samples for this research were provided by the cruise HRS15-12 (R/V Hugh R Sharp). We deeply appreciate the crew and scientists for their support with sample collection. Julius S. Lipp, Xavier Prieto Mollar, Michael Casso and Lee-Gray Boze are thanked for substantial instrumental and technical support. Julius S. Lipp is also appreciated for his assistance on lipid identification and statistical analysis. Patrick Agu is thanked for analysis of part of the bacterial IPLs. Felix J. Elling is thanked for the timely suggestion on the network analysis. This study was supported by the Deutsche Forschungsgemeinschaft, through MARUM-Center for Marine Environmental Sciences, the GLOMAR graduate school (to Min Song). K W. Becker was supported by the Postdoctoral Scholarship Program at Woods Hole Oceanographic Institution & U.S. Geological Survey. Min Song is sponsored by the China Scholarship Council (CSC) and USGS-DOE interagency agreements DE-FE000291, DE-FE0005806, and DE-FE0023495. Any use of trade names is only for descriptive purposes and does not implyt endorsement by the US government.

SUPPLEMENTARY INFORMATION

Supplementary Table IV.1. Description of the sampling sites and sediment cores at the northern US Atlantic margin in this study. PC indicates that a piston corer was used, MUC indicates that a multicorer was used. TC 16 was the gravity core used to trigger PC 16.

Site	Core	Core length (cm)	Latitude (N)	Longitude (W)	Water depth (m)
Tiki Line	PC 11	880	39°41.14’	71°43.72’	685
Hudson Canyon	TC 16	82	39° 32.61’	72°23.99’	541
	PC16	867			
Chincoteague Seep	MUC 5	34	37° 32.45’	74°6.13’	1055
Chincoteague Slope (reference site)	MUC 10	18	37° 32.32’	74°17.91’	366

Supplementary Table IV.2. List of commercially available standards used to determine response factors of intact polar lipids (IPL) in this study. The injection standard di-C_{21}-Phosphatidylcholine was used to evaluate the absolute quantifications of IPLs, after calculating the response factors for IPLs with the standards.

Short ID	Full name	Fatty acid distribution	Company	Used for IPL class (UPLC-qTOF-MS)	Used for IPL class (UHPLC-Triple Quad-MS)
1G-GDGT-0	Main phospholipid (MPL) of Thermoplasma acidophilum		Matreya LLC, USA		1G-GDGT, 1G-unsGDGT, 1G-OH-GDGT, 1G-BDGT, 1G-PDGT, 1G-GDD
2G-GDGT-0	Main phospholipid (MPL) of Thermoplasma acidophilum		Matreya LLC, USA		2G-GDGT, 2G-unsGDGT, 2G-OH-GDGT, HPH-GDGT, 2G-BDGT, 3G-GDGT
1G-AR	Monoglycosidic archaeol		Matreya LLC, USA	1G-AR, 1G-OH-AR	
2G-AR	Diglycosidic archaeol		Matreya LLC, USA	2G-AR, 2G-OH-AR	
PE-AR	1,2-di-O-phytanyl-*sn*-glycero-3-phosphoethanolamine		Matreya LLC, USA	PE-AR, PE-OH-AR, PE-2OH-AR	
C18:1 DPG	1',3'-bis[1,2-dioleoyl-*sn*-glycero-3-phospho]-*sn*-glycerol (sodium salt)	18:1/18:1/18:1/18:1	Avanti Polar Lipids, USA	DPG	
C16:0 PE	1,2-dipalmitoyl-*sn*-glycero-3-phosphoethanolamine	16:0/16:0	Avanti Polar Lipids, USA	PE-DAG, PE-AEG, PE-DEG	
C16:0 PME	1,2-dipalmitoyl-*sn*-glycero-3-phosphoethanolamine-N-methyl	16:0/16:0	Avanti Polar Lipids, USA	PME-DAG, PME-AEG, PME-DEG	
C16:0 PDME	1,2-dipalmitoyl-*sn*-glycero-3-phosphoethanolamine-N,N-dimethyl	16:0/16:0	Avanti Polar Lipids, USA	PDME-DAG, PDME-AEG, PDME-DEG	
C16:0 PG	1,2-dipalmitoyl-*sn*-glycero-3-phospho-(1'-rac-glycerol) (sodium salt)	16:0/16:0	Avanti Polar Lipids, USA	PG-DAG	
C16:0 PC	1,2-dipalmitoyl-*sn*-glycero-3-phosphocholine	16:0/16:0	Avanti Polar Lipids, USA	PC-DAG	

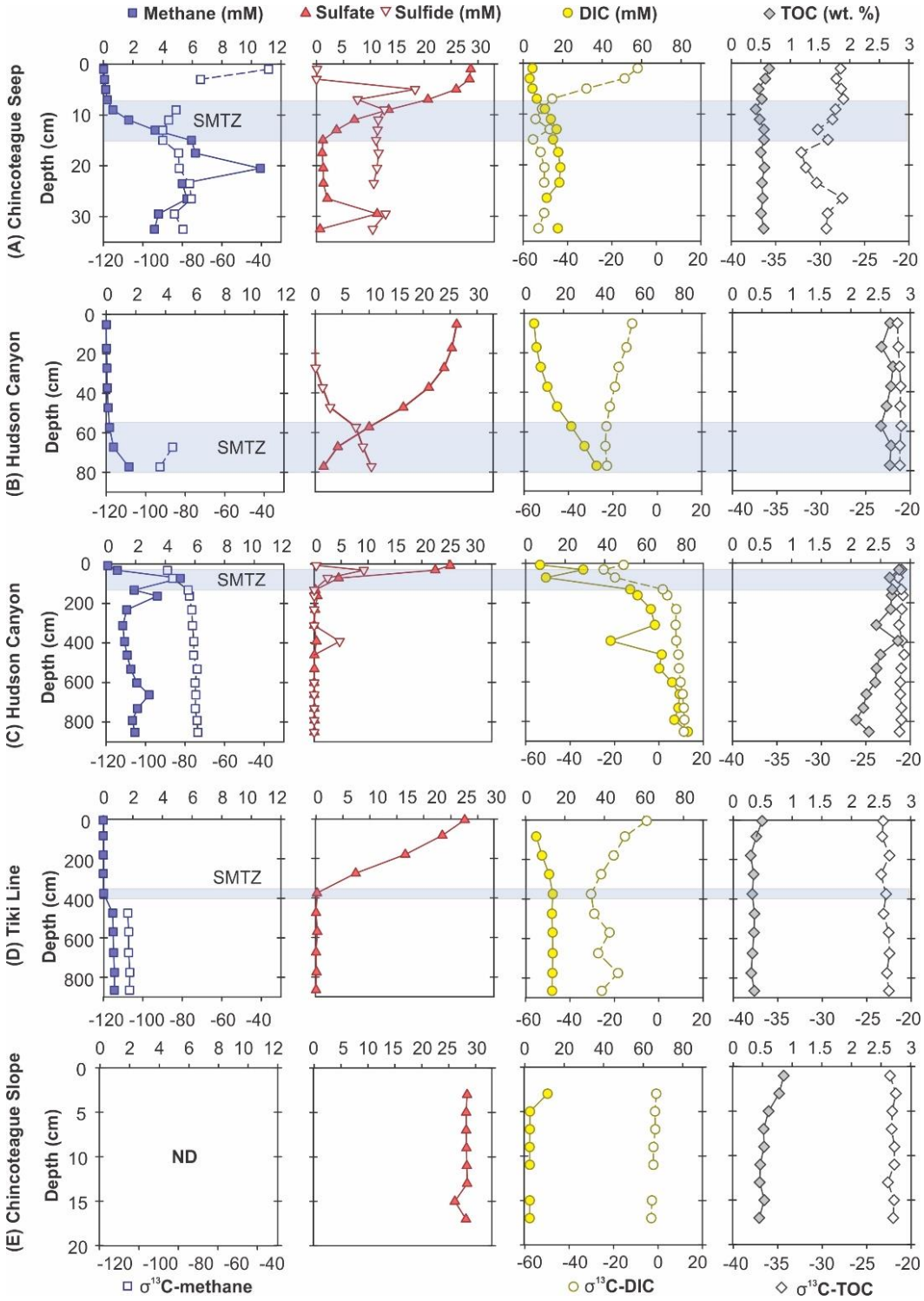

Supplementary Figure IV.1. Geochemistry profiles redrawn from Graw, 2017, i.e. concentration and stable isotopic compositions ($\delta^{13}C$) of methane, concentrations of sulfate and sulfides, concentration and $\delta^{13}C$ values of porewater dissolved inorganic carbon (DIC) and of total organic carbon (TOC) throughout four methane seep sediment columns, (A) Hudson Canyon shallow core TC 16, (B) Hudson Canyon deep core PC 16, (C) Chincoteague Seep MUC 5, (D) Tiki Line PC 11 and (E) the reference site Chincoteague Slope MUC 10. "ND" denotes "not determined".

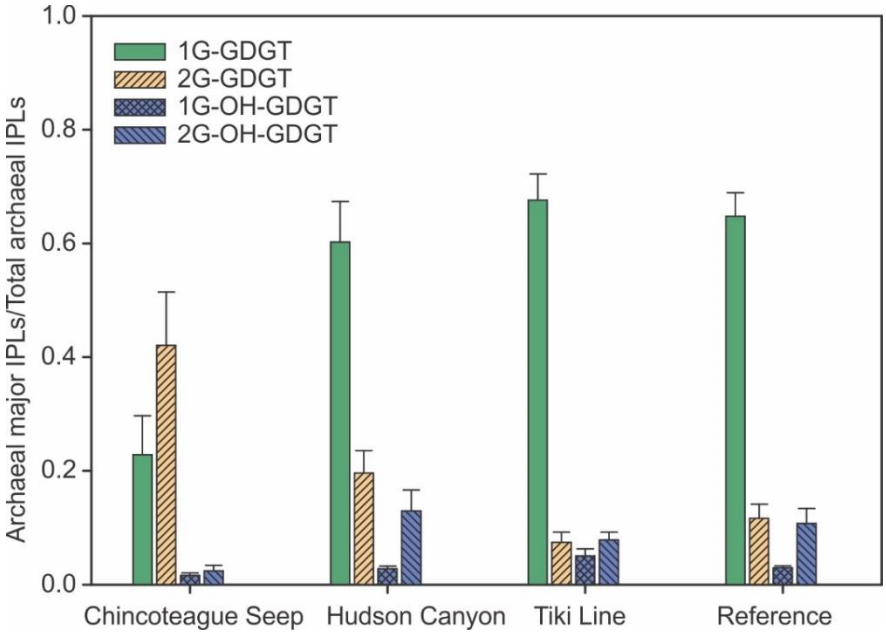

Supplementary Figure IV.2. Relative contribution of archaeal major IPLs, i.e., 1G-GDGT, 2G-GDGT, 1G-OH-GDGT, 2G-OH-GDGT, in the sediment column at each site.

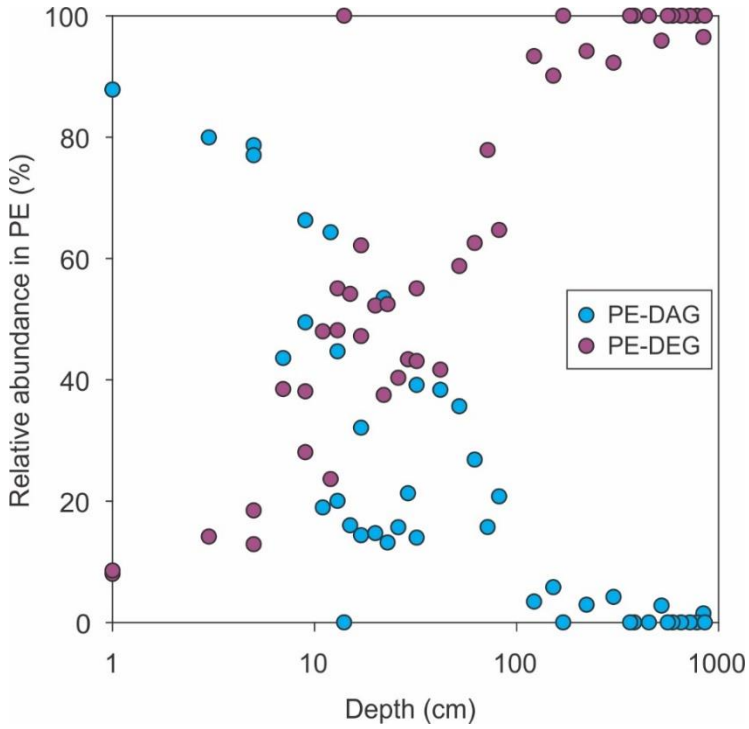

Supplementary Figure IV.3. Relative abundance of PE-DAG and PE-DEG in PE pool with increasing depth.

Supplementary Table IV.3. Relative abundance of most abundant archaeal and bacterial operational taxonomic units (OTUs) in studied samples. OTUs data are from Graw (2017) and shown as mean±SD (number of samples) here. Note that "uncld" refers to "unclassified". MCG, Miscellaneous Crenarchaeotal Group; DHVEG, Deep Sea Hydrothermal Vent Group.

OTUs	Chincoteague Seep	Hudson Canyon (shallow)	Hudson Canyon (deep)	Tiki Line	Reference site
Archaeal OTUs (until genus level)					
uncld_ ANME-1b	22.5±16.3 (7)	0.1±0.2 (7)	4±3 (8)	0.1±0.1 (3)	0±0 (2)
uncld_ ANME-2a-2b	22±7.7 (7)	0.3±0.5 (7)	0.3±0.8 (8)	0±0 (3)	0±0 (2)
uncld_ ANME-2c	34.1±9.7 (7)	0.1±0.2 (7)	0.1±0.2 (8)	0.1±0.1 (3)	0±0 (2)
uncld_ Hadesarchaea	0±0 (7)	0.3±0.1 (7)	0.8±1.3 (8)	40.7±11.2 (3)	0.1±0.1 (2)
uncld_ Thermoprofundales and DHVEG-1	6.9±3.3 (7)	28.8±8.1 (7)	23.5±7.5 (8)	9.5±7 (3)	7.2±10 (2)
uncld_ MCG-15	0.3±0.2 (7)	35.9±2.7 (7)	35.9±9 (8)	17.5±4.5 (3)	18.5±22.3 (2)
uncld_ Marine Benthic Group-B	1.4±0.6 (7)	11.2±4 (7)	24.3±4.6 (8)	19.6±12.9 (3)	6.1±7.2 (2)
Ca. Nitrosopumilus	0±0 (7)	2.1±3.1 (7)	0.5±0.2 (8)	0.6±0.3 (3)	39.9±48.3 (2)
Bacterial OTUs (until class level)					
uncld_Candidate division JS1	44.4±14.1 (8)	4.1±4.1 (7)	54.8±9.2 (8)	12.3±6.6 (3)	0.1±0.1 (2)
Dehalococcoidia	0.8±0.2 (8)	4.7±2.3 (7)	7.5±1.4 (8)	29.4±2.7 (3)	1.5±2 (2)
Deltaproteobacteria	34±4 (8)	30.2±6.4 (7)	5.4±2.6 (8)	6.4±2 (3)	34.8±6.6 (2)
Gammaproteobacteria	1.4±0.6 (8)	8.9±4.7 (7)	0.8±0.3 (8)	1.7±0.8 (3)	18±10.5 (2)

CHAPTER V

Microbial ether lipid biogeochemistry in hydrothermal sediments of the Guaymas Basin

Min Song[a], Florence Schubotz[a], Gunter Wegener[a,b], Andreas P. Teske[c], Kai-Uwe Hinrichs[a]

In preparation for *Geochimica et Cosmochimica Acta*

[a]MARUM-Center for Marine Environmental Sciences and Department of Geosciences, University of Bremen, Germany; [b]Max Planck Institute for Marine Microbiology, Bremen, Germany; [c]Department of Marine Sciences, University of North Carolina at Chapel Hill, Chapel Hill, NC 27599-3300, USA

*Correspondence: msong@uni-bremen.de

ABSTRACT

Guaymas Basin hydrothermal sediments sustain highly active and diverse microbial communities that thrive on the oxidation of hydrocarbons while facing fluctuating thermal and chemical gradients. In this study, we combined lipid biomarker and geochemical analyses in sediments spanning temperatures from 3 to 70 °C to identify lipid signatures related to hydrocarbon degradation at different temperatures. Our results revealed the presence of diagnostic markers for the anaerobic oxidation of methane in both cold and hydrothermally heated sediments. While archaeol based lipid biomarkers diagnostic of ANME-2 archaea dominated cooler surface sediments, diglycosidic glycerol dialkyl glycerol tetraethers (2G-GDGTs) diagnostic of ANME-1 increased with depth and temperature. ANME-1 signature lipids exhibited distinct changes in core lipid ring distribution from a dominance of GDGT-2 to GDGT-4 as a function of temperature, in line with contributions of corresponding mesophilic and thermophilic ANME-1 groups. Moreover, abundance of intact and core H-shaped glycerol monoalkyl glycerol tetraethers (GMGT) was substantially elevated in hydrothermally heated sediments, indicating production by yet unknown thermophilic archaeal groups, with potential contribution of archaeal C_{2+} hydrocarbon degraders. A notable increase of overly-branched GDGTs in hydrothermally heated sediments and their significant relationship with GMGTs suggests *in situ* production by yet unknown thermophilic source organisms. Higher cyclization in both GDGT and GMGT lipids and the increase in the number of methylations in GMGT lipids with temperature suggest lipid adaptation as mechanisms of ether lipid producing organisms to cope with heat and energy stress in the environment.

V.1. INTRODUCTION

The Guaymas Basin hydrothermal sediments are a unique ecosystem where abundant and diverse microbial communities thrive on the cycling of carbon, sulfur and nitrogen, including the oxidation of petroleum hydrocarbons (Teske et al., 2014). The distribution of microbial communities seems to be governed by the provision of energy-rich substrates through hydrothermal mobilization and fluid flow. The Guaymas Basin is located in the Gulf of California (Supp. Fig. V.1) and is a young marginal seafloor spreading center where new igneous crust is buried by up to 500-m-thick layer of organic-rich sediments, derived from highly productive overlying sea water and terrigenous input with sedimentation rates of 1-2 mm yr^{-1} (Calvert, 1966). Magmatic sill intrusions into sediments result in thermocatalytic alteration of the organic matter and substantial migration of hot, hydrocarbon-rich fluids through fissures towards the seafloor (Einsele et al., 1980; Simoneit, 1990; Peter et al., 1991). Mixing of cold and oxygenated bottom water with hydrothermal fluids results in steep and fluctuating thermal and chemical gradients in near surface sediments with highly diverse microbial communities that catalyze anaerobic microbial processes, including oxidation of methane and C_{2+} hydrocarbons (Teske et al., 2002; McKay et al., 2016; Dowell et al., 2016), sulfate reduction (Jørgensen et al., 1990; Jørgensen et al., 1992; Meyer et al., 2013) and methanogenesis (Dhillon et al., 2005). The hydrothermal sediments of the Guaymas Basin therefore provide an ideal system to investigate microbial community response under dynamic and extreme environmental conditions.

The presence of ANME populations in Guaymas Basin sediments was initially evidenced by 16S rRNA sequencing and microbial lipid analysis (Teske et al., 2002; Schouten et al., 2003). Further investigation showed that anaerobic oxidation of methane (AOM) at elevated temperatures at the Guaymas Basin is mediated by ANME-1 in association with the thermophilic sulfate-reducing bacterium Ca. Desulfofervidus (HotSeep-1 clade) (Biddle et al., 2012; Holler et al., 2011; Krukenberg et al., 2016). The corresponding consortia were found capable of direct electron exchange via intercellular nanowire-like structures (Wegener et al., 2015). Optimal growth of AOM communities was measured at temperatures of 50-60°C (Holler et al., 2011; Wegener et al., 2015). The stable carbon isotopic imprint of AOM could be detected *in situ* at temperatures up to ca. 70 to 80°C (McKay et al., 2016), and stable-isotope-probing experiments revealed autotrophy as the major carbon assimilation pathway for ANME-1 archaea (Kellermann et al., 2012). Not only methane, but also short-chain alkanes are oxidized by archaeal/bacterial syntrophic associations in Guaymas Basin (Dowell et al., 2016), including thermophilic ethane-oxidizing Ca. Ethanoperedens (GoM-Arc1clade; Hahn et al., 2020) and the propane and *n*-butane-oxidizing Ca. Syntrophoarchaeum (Laso-Pérez et al., 2016), both forming syntrophic associations with Ca.

Desulfofervidus auxilii of the HotSeep-1 group. Those archaea contain highly divergent variants of methyl-coenzyme M reductases (also described as alkyl coenzyme M reductases; ACR) that enable activation of non-methane alkanes. Besides, mesophilic sulfate reducer BuS5 alone (belonging to the Desulfosarcina/Desulfococcus cluster) is also able to oxidize propane and *n*-butane (Kniemeyer et al., 2007). Assembled genomes (MAGs) suggest that the ACR gene is more widespread in the archaea, including the Hadesarchaeota (Wang et al., 2019; Wang et al., 2020; Borrel et al., 2019). Many of those MAGs derive from the Guaymas Basin. Moreover, even some MAGs of ANME-1 archaea contain the ACR for non-methane alkane activation, and some Crenarchaeota have the genomic capacity of methanogenesis (Dombrowski et al., 2018). Metagenomic reconstructions also detected unusual coenzyme M reductases in Helarchaeota, a new lineage of the Asgardarchaeota, indicating that these archaea are capable of short-chain hydrocarbon oxidation (Seitz et al., 2019). Altogether these studies greatly expanded the possibility of archaeal utilization of hydrocarbons, yet that function needs to be revealed by further investigations.

Next to gene-based methods, membrane lipids serve as informative, culture independent biomarkers for identifying the distribution and biogeochemical imprint of microbial communities in nature. These findings include the existence of microbial AOM in both cold seep and hydrothermal sediments, initially evidenced by parallel co-location of lipid biomarkers and nucleic acids (Hinrichs et al., 1999; Teske et al., 2002). More recent advances in the analysis of intact polar lipids (IPLs; Sturt et al., 2004; Zhu et al., 2013a; Wörmer et al., 2013) and their core lipids (CLs; Knappy et al., 2009; Becker et al., 2013) further expanded the catalogue of microbial biomarkers and enhanced the ability to pinpoint the presence of microbial groups and identify their metabolic modes (e.g., Biddle et al., 2006; Schubotz et al., 2011; Meador et al., 2015). To date, lipid biomarkers for ANME archaea are well characterized; for instance, diglycosidic glycerol dialkyl glycerol tetraethers (2G-GDGTs) and archaeol (AR) based phospholipids are useful biomarkers for ANME-1 and ANME-2 (and/or ANME-3) archaea, and their respective distribution in methane-rich environments (Rossel et al., 2008). Lipid biomarker distribution patterns showed that ANME-1 dominated over ANME-2 and -3 groups with increasing temperatures and reducing conditions (Rossel et al., 2011). However, while lipid signatures for methanotrophs are well-documented, those for the archaeal C_{2+} degraders are still largely unknown.

Membrane lipids also provide information on microbial adaptations to environmental conditions, including changes in temperature, as organisms have to regulate their lipid composition in order to maintain their cell membrane in liquid crystalline phase and to provide a permeability barrier to the outside environment (Koga, 2012). Higher degree of cyclization in GDGTs with temperature has been observed in membranes of cultured thermoacidophilic archaea (De Rosa et al., 1980; Gliozzi et al., 1983; Uda et al.,

2001); this relationship between GDGT cyclization and temperature is the basis for the marine paleotemperature proxy TEX_{86} (e.g., Schouten et al., 2013). This adaptation has been explained by higher thermal transition points of cell membranes composed of GDGTs with cyclopentane rings (Gliozzi et al., 1983) and more recently also as archaeal response to energy availability (Zhou et al., 2019). It has also found that the CLs of ANME-1 archaea from cold hydrocarbon seeps contain abundant GDGT lipids with one to three cyclopentane rings (GDGT-1, GDGT-2 and GDGT-3; see Supp. Fig. V.2A for structures, whereas thermophilic ANME-1 are dominated by GDGT with four cyclopentane rings (GDGT-4; Schouten et al., 2003; Holler et al., 2011). However, not all thermophilic archaea employ the same strategies; for example, Thermococcales strains grown at 85 °C are dominated by GDGTs without cyclopentane rings (GDGT-0, Sugai et al., 2004).

Another interesting group of archaeal lipids are glycerol monoalkyl glycerol tetraethers (GMGTs; also often referred to as H-shaped GDGTs), which contain a covalent bond between the two isoprenoid chains (see Supp. Fig. V.2B for structures). GMGT with up to four cyclopentane rings have been reported in cultivated isolates of hyperthermophilic methanogens (Morii et al., 1998), members of the Thermococcales (Sugai et al., 2004); thermoacidophilic Euryarchaeota (Schouten et al., 2008), hyperthermophilic Crenarchaeota (Knappy et al., 2011), as well as in samples from hydrothermal vent environments (e.g., Jaeschke et al., 2012; Lincoln et al., 2013; Sollich et al., 2017). Often these compounds are found with additional methyl groups located in the monoalkyl side chains (see Supp. Fig. V.2B for structure), and their concentrations were also observed to increase with temperature (Sollich et al., 2017). Consequently, the occurrence of GMGT and its methylated derivatives were suggested to assist in reducing membrane fluidity and proton permeability to cope with high temperatures (Knappy et al., 2011; Sollich et al., 2017). In the hydrothermal sediments of the Guaymas Basin additional GMGT-related lipids were observed, which have been attributed as degradation products of GMGTs (Liu et al., 2016). These compounds include the so called H-shaped tetrols and tetraacids (H-tetrols and H-tetraacids; see Supp. Fig. V.2B for structures), the latter are frequently observed to clog oil pipelines during production (Lutnaes et al., 2006). The mechanism of their formation is still unclear.

It is well known that archaea modify their membrane lipid composition to cope with stress conditions including high temperature, acidity, salinity or low energy availability (Valentine, 2007; Koga, 2012). Most of these dependencies are based on culture experiments and do not take into account complex interactions of multiple microbial groups and fluctuating environmental conditions. In this study, we therefore investigated changes in the composition of archaeal intact and core lipids in Guaymas Basin sediments impacted at varying degree by hydrothermal activity, ranging in temperature from 4 to 70 °C. We examined how microbial ether lipid composition is related to temperature and sought to identify biomarkers from

anaerobic degraders of methane and C_{2+} hydrocarbons. Furthermore, we extended our ether lipid investigations to branched GDGTs from bacterial sources (Weijers et al., 2006a), including the more recently identified compounds, such as the overly branched (OB-), isoprenoid-branched (IB-) and scarcely branched (SB-) GDGTs (see Supp. Fig. V.2D for structures) to further understand their biological sources and production in marine sediments.

V.2. MATERIALS AND METHODS

V.2.1. Sampling sites and geochemistry analyses

Push core from hydrothermally-heated sediments of the Guaymas Basin (Gulf of California) were collected during RV *Atlantis* cruise AT37-06 with HOV *Alvin* in December 2016 (). Samples derived from the southern Guaymas Basin spreading center and at the off-axis Central Seep site on the northwestern Guaymas flanks that are approximately equidistant from the Sonora and Baja California coasts (Table V.1; Supp. Figure V.1; Teske et al., 2016; Geilert et al., 2018). The Octopus Mound is a carbonate-dominated seafloor mound at the Central Seep location where hydrothermal circulation has ceased several thousands of years ago (Geilert et al., 2018). The Mat Mound Massif is an extensive cluster of hydrothermal mounds and edifices surrounded by hot hydrothermal sediments and microbial mats, it had been probed from different angles on previous cruises (e.g., Dowell et al., 2016); hydrothermal samples were collected from the "Ultra Mound" site of this area. The Aceto Balsamico area is located ca. 150 meters west of Mat Mound Massif and contains moderately warm sediments covered with lime-yellow sulfur precipitates and mats of sulfur-oxidizing bacteria (Teske et al., 2016). At Cathedral Hill, ca. 200 meters north of Aceto Balsamico, gradually sloping sediment-covered mounds with extensive microbial mats are topped with hydrothermal edifices (Teske et al., 2016). The Northern Towers area is located ca. 5 km northeast from the other, tightly clustered sites and was not sampled during previous expeditions in 2008/2009 (Teske et al., 2016); it contains relatively few hydrothermal sediments and mats but is dominated by massive, steep hydrothermal chimneys. Parallel push cores were retrieved from five sites that are located on the Southern Trough (Aceto Balsamico, Ultra Mound, Cathedral Hill, Northern Tower Site 2, Northern Tower Site 3) and one off-axis site located on the northern Central Seep of the Guaymas Basin (Octopus Mound) (Table V.1; Supp. Fig. V.1).

Before sampling, temperature profiles at the sampling site were recorded using *Alvin*'s external heat flow temperature probe as described elsewhere (McKay et al., 2012). At each site, two to three parallel cores were collected and sectioned immediately after retrieval (Supp. Table V.1). One core was sub-sectioned into 2- to 4-cm intervals and stored at -20 °C until lipid analysis. Meanwhile, 2-5 mL of fresh

sediment were taken from the same core or from an adjacent core by head-cut syringes in 2-cm intervals and placed in headspace vials containing 5 mL of 1 M NaOH solution, crimp sealed with butyl rubber septa and stored upside down at -20 °C until further gaseous hydrocarbon analysis. Porewater samples were obtained by Rhizon samplers at 1-cm intervals. For sulfate and sulfide, 1 ml of porewater samples were mixed with 50 µL zinc acetate solution (0.5 M) and stored at -20 °C until analysis. 2-mL vials were filled with porewater and stored at 4 °C for dissolved inorganic carbon (DIC) analysis.

Table V.1. Sample location and site description.

Site name	Latitude (N)	Longitude (W)	Sampling date	Core ID		Core length (cm)	Description, notable features
				For lipid analysis	For geochemistry		
Octopus Mound	27˚28.17’	111˚28.39’	18/12/2016	4867-3	4867-3, 4870-30	23	Active cold seep site, methane tubeworms, “fuzzy” sedimentary carpeting formed by worm tubes
Aceto Balsamico	27˚00.47’	111˚24.43’	22/12/2016	4870-28	4870-32	48	Aceto Balsamico, white mat; gas gaps
Ultra Mound	27˚00.45’	111˚24.54’	21/12/2016	4869-3	4869-3, 4869-26	34	Orange mat; degassing
Cathedral Hill	27˚00.71’	111˚24.23’	22/12/2016	4870-30	4870-16, 4870-29	21	White mat, gas gaps, heavily oiled
Northern Tower site 2	27˚02.77’	111˚23.09’	23/12/2016	4871-22	4871-20	24	Cool white mat, gas gaps
Northern Tower site 3	27˚02.75’	111˚23.05’	23/12/2016	4871-28	4871-26, 4871-23	28	Hot white crust, gas gaps

For gaseous hydrocarbon analysis, the mixture in the headspace vials was homogenized by gentle shaking overnight at room temperature. Concentrations of hydrocarbon gases were determined by a ThermoFinnigan Trace gas chromatograph (GC) equipped with a flame ionization detector (FID). Stable carbon isotope ratios of hydrocarbon gases were analyzed by GC coupled to Delta Plus XP isotope ratio mass spectrometer via a combustion III interface (ThermoFinnigan GmbH, Bremen, Germany). A carboxen 1006 PLOT column (30 m × 0.32 mm, SUPELCO) was used for analysis of methane, the program was set to 40 °C and held for 6 min. For the analysis of C_{2+} hydrocarbons, an AT-Q column (30 m × 0.32 mm, Alltech) was used, with the initial temperature set to 60 °C (held for 1 min), ramped up to 240 °C (held for 7 min) at a rate of 40 °C/min. The molar fraction of hydrocarbon gases was calculated by injection of known quantities of hydrocarbon gas standards. Stable carbon isotope ratios were reported in the delta notation (per mil, ‰) relative to the Vienna Peedee Belemnite Standard (VPDB), with $\delta^{13}C = (R_{sample}-R_{VPDB})/R_{VPDB} * 10^3$, where $R= {}^{13}C/{}^{12}C$ and $R_{VPDB} = 0.0112372 \pm 2.9 * 10^{-6}$. The internal precision was ± 0.5‰.

To determine the sulfate concentration, zinc acetate fixed samples were diluted with MilliQ water (1:50, v/v) and were measured by ion chromatography (Metrohm 930 compact IC) against standards with known

sulfate concentrations. To determine sulfide concentration, sample aliquots were 1:5 (v/v) diluted with MilliQ water and measured by a Shimadzu UV-1800 spectrophotometer following Cline (1969).

Carbon isotopic compositions of DIC were determined using a Delta Ray Isotope Ratio Infrared Spectrometer (IRIS) equipped with Universal Reference Interface (URI) Connect and autosampler (Thermo Fisher Scientific, Germany) as described previously (Aepfler et al., 2019). The internal precision was < 0.2‰.

V.2.2. Lipid analysis

The total lipid extracts were obtained by extraction of 20-100 g wet sediments from six sediment cores (29 samples in total). Meanwhile, an aliquot of wet sediment (~1 g) from each sample was used to define the water content of each sample by measuring its weight before and after freeze-drying. Accordingly, the dry weight of each sediment sample used for lipid extraction was calculated.

TLE extraction was according to a modified Bligh-Dyer method after Sturt et al. (2004). Before extraction the samples were spiked with 5 µg of di-C_{21}-phosphatidylcholine as internal standard (Avanti Polar Lipids, USA). Lipid analysis was carried out with a Dionex Ultimate 3000RS ultra-high pressure liquid chromatography (UHPLC) coupled to a Bruker maXis ultra-high resolution quadrupole time-of-flight (qTOF) mass spectrometry (Bruker Daltonik, Bremen, Germany) via an electrospray ionization (ESI) interface for IPL analysis and via an atmospheric pressure chemical ionization (APCI) interface for core lipid separation.

Reversed phase (RP) chromatography was used as described in Zhu et al. (2013a) for identification and quantification of tetraether and glycerol dibiphytanol diethers (GDD)-based IPLs, H-shaped tetrols and acids. An ACE3 C_{18} column (3 µm, 2.1 x 150 mm, Advanced Chromatography Technologies Ltd, Aberdeen, Scotland) was used. The chromatographic gradient was: 100% A (MeOH/HCO_2H/14.8 M $NH_{3aq.}$, 100/0.04/0.1) held for 10 min, ramped to 24% B (isopropanol/HCO_2H/14.8 M $NH_{3aq.}$,100/0.04/0.1) and held for 5 min, gradient to 65% B (55 min), gradient to 90% B (14 min), then equilibrated to initial conditions with 100% A for 15 min (Zhu et al., 2013a).

Hydrophilic interaction chromatography (HILIC) was applied after Wörmer et al. (2013) for detection of archaeol-based IPLs. A Waters Acquity UPLC BEH Amide column (1.7 µm, 2.1 x 150 mm, Waters Corporation, Eschborn, Germany) was used. IPLs were eluted using the following gradient: 99% A (MeCN:dichloromethane, 75/25, 0.01% HCO_2H, 0.01% ammonium hydroxide) and 1% B (MeOH:H_2O,

50/50, 0.4% HCO_2H, 0.4% NH_{3aq}) for 2.5 min, ramping to 5% B at 4 min, 25% B at 22.5 min and 40% B at 26.5 min, held for 1 min and equilibrated to initial conditions for 8 min (Wörmer et al., 2013).

Additionally, ring distributions of diether and tetraether core lipids were determined with UHPLC-MS equipped with an APCI source following Becker et al. (2013). Lipid separation was achieved by two coupled Acquity BEH HILIC amide columns (2.1 x 150 mm, 1.7 µm, Waters, Eschborn, Germany) maintained at 50 °C. This method also ensures that crenarchaeol, a glycerol dialkyl glycerol tetraether (GDGT) uniquely consisting of four cyclopentane plus one cyclohexane rings, can be unequivocally identified apart from its isomer and GDGT-5 (with five cyclopentane rings). Core lipids were eluted using the following gradient with eluent A (*n*-hexane) and B (*n*-hexane/isopropanol, 90:10) at a constant 0.5 mL/min: linear gradient from 3% B to 20% B in 20 min, then increased linearly to 50% B in 15 min, followed by linear gradient to 100% B in 10 min and held for 6 min and equilibrated to initial conditions for 9 min.

An external standard (C_{46} glycerol trialkyl glycerol tetraether) was used for calculating lipid concentrations for the RP ESI and APCI method. Lipid concentrations were calculated by comparing the relative response of the analytes to the internal or external standards. In this study the response factors of different lipid classes were not determined. Thus lipid concentrations are considered semi-quantitative. The final lipid concentrations were reported as lipid mass per gram of dry sediment.

V.2.3. Indices

Ring index (RI; Eq. 1) was calculated for intact and core tetraether lipids with one to four cyclopentane rings (cf. Pearson et al., 2004). Core lipid indices were calculated according to Schouten et al. (2002) and Kim et al. (2010) for the tetraether lipid index TEX_{86} and reconstructed sea surface temperatures (SST) (Eq. 2-4); Zhang et al. (2011) for the methane index (MI; Eq. 5); Hopmans et al. (2004) for the branched and isoprenoid tetraether index (BIT; Eq. 6).

$$RI = \frac{[GDGT-1] + 2*[GDGT-2] + 3*[GDGT-3] + 4*[GDGT-4]}{[GDGT-1] + [GDGT-2] + [GDGT-3] + [GDGT-4]} \quad [1]$$

$$TEX86 = \frac{[GDGT2] + [GDGT3] + [Cren']}{[GDGT1] + [GDGT2] + [GDGT3] + [Cren']} \quad [2]$$

$$TEX_{86}^{H} = logTEX_{86} \quad [3]$$

$$SST = 68.4 * TEX_{86}^{H} + 38.6 \qquad [4]$$

$$MI = \frac{[GDGT1] + [GDGT2] + [GDGT3]}{[GDGT1] + [GDGT2] + [GDGT3] + [Cren] + [Cren']} \qquad [5]$$

$$BIT = \frac{[brGDGTI] + [brGDGTII] + [brGDGTIII]}{[brGDGTI] + [brGDGTII] + [brGDGTIII] + [Cren]} \qquad [6]$$

V.3. RESULTS

V.3.1. Geochemical properties of the sampling sites

***In situ* temperature gradients.** The six sampling sites in the Guaymas Basin showed distinct temperature and chemical gradients. *In situ* temperatures for the surface sediments of the push cores were interpolated between the bottom water temperature and the topmost measurements of Alvin's heat probe, which started to read the temperatures at 10 cm below seafloor. We conservatively assume the sea water/sediment interface temperatures to be around 3 °C, as temperature data from similar sites in past cruises have shown that the surface temperatures were generally below 10 °C and in most cases close to 3 °C (McKay et al., 2012; Teske et al., 2016).

At the Octopus Mound cold seep site, *in situ* temperatures of the sediment were consistently similar to ambient bottom sea water at ~ 3 °C (Fig. V.1A). At Aceto Balsamico (Teske et al., 2016), the *in situ* temperatures of the warm sediments increased gradually from 3 °C at the seafloor to ca. 18 °C at 30 cm. In contrast, temperatures in the two hot hydrothermal sediments at Ultra Mound and Cathedral Hill increased steeply to ca. 71 °C at 30 cm. Sediment samples from Cathedral Hill were found to be heavily oil impregnated. In the Northern Towers area dominated by steep hydrothermal edifices, Northern Tower Site 2 represented a cool sediment site opposite to its hot counterpart Northern Tower Site 3. While *in situ* temperatures in sediments of Site 2 increased gradually from ca. 3 °C at the seafloor to 8 °C at 30 cm, they increased sharply to 57 °C at 30 cm in Site 3 sediments.

Porewater sulfate and sulfide gradients. The Octopus Mound core showed moderate sulfate depletion, most likely due to sulfate reduction as indicated by downcore sulfide accumulation (Fig. V.1B). Sulfide concentrations were variable across the warm and hot hydrothermal cores, apparently reflecting a complex web of biological production, reoxidation and possibly dilution by mixing. At the moderate and warm Aceto Balsamico and Northern Tower sites, sulfate concentrations decreased downcore towards near-complete depletion, as a consequence of microbial sulfate reduction favored by moderate temperatures combined

with the lack of vigorous hydrothermal circulation. In contrast, the hot hydrothermal sites at Ultra Mound and Cathedral Hill showed only partial sulfate depletion, most likely a consequence of hydrothermal circulation and seawater inmixing within the upper sediment layers (Teske et al., 2016) (Fig. V.1B).

Concentration and isotopic compositions of C_1-C_5 hydrocarbons and DIC. The gaseous hydrocarbon concentrations are affected by outgassing and bubble formation during core retrieval to the surface of the unpressurized cores, therefore here only residual porewater concentrations can be reported. Methane was consistently the most abundant hydrocarbon at each site, followed by ethane, propane, butane and pentane, when detectable (Fig. V.1C). Methane concentration of Octopus Mound samples ranged between 0.01 and 0.1 mM, while they were slightly higher in the hydrothermally influenced sediments (Northern Tower Site 2, Site 3, Aceto Balsamico, Ultra Mound and Cathedral Hill), ranging from 0.1 to 1.5 mM with no apparent trend with depth (Fig. V.1C). Ethane concentrations ranged from 1 to 100 μM at the hydrothermally influenced sites, which are several orders of magnitude higher than those from the cold seep Octopus Mound. Concentrations of C_3-C_5 hydrocarbons were generally one to two orders of magnitude lower than those of ethane. The highest hydrocarbon contents were detected in oil impregnated sediments of Cathedral Hill (Fig. V.1C).

Isotopic compositions of methane ($\delta^{13}C_1$) ranged from strongly ^{13}C-depleted biogenic values (-74.9‰) towards ^{13}C enrichment (-29.7‰) previously seen in sediments with active methane-oxidizing archaeal populations (McKay et al., 2016). The lightest methane (near and below -70‰) was found at the bottom and top of the cold seep Octopus Mound core, around a zone of ^{13}C-enriched methane (up to -55.3‰) at approximately 7 cm depth (Fig. V.1D). Intermediate $\delta^{13}C_1$ values ranging from -55.1 to -43.0‰, matching the previously reported range of hydrothermal methane at Guaymas Basin (Welhan and Lupton, 1987), were observed at the two warmer sites Northern Tower Site 2 and Aceto Balsamico, with the latter site exhibiting a sharp ^{13}C-enrichement at the sediment surface. The least negative $\delta^{13}C_1$ values that characterize methane impacted by microbial methane oxidation (-41.3 to -29.7‰) were observed at the hot site Ultra Mound, where ^{13}C-enriched methane was observed at ca. 7 cm (Fig. V.1D). Similarly, $\delta^{13}C_1$ values ranged from -44.0 to -39.7‰ for the remaining two hot sites Northern Tower Site 3 and Cathedral Hill (Fig. V.1D).

$\delta^{13}C$ values for C_2-C_5 hydrocarbons ranged from -20 to -11‰ for ethane, -24 to -10‰ for propane, -24 to -21‰ for butane, and -24 to -18‰ for pentane (Fig. V.1D). In Ultra Mound sediments, $\delta^{13}C$ values for ethane and propane were notably enriched in ^{13}C within the upper 7 cm, roughly coinciding with the depths where ^{13}C-enriched methane was observed. Similarly, ^{13}C-enriched butane and particularly pentane were observed in Cathedral Hill sediments at depths between 5 to 11 cm.

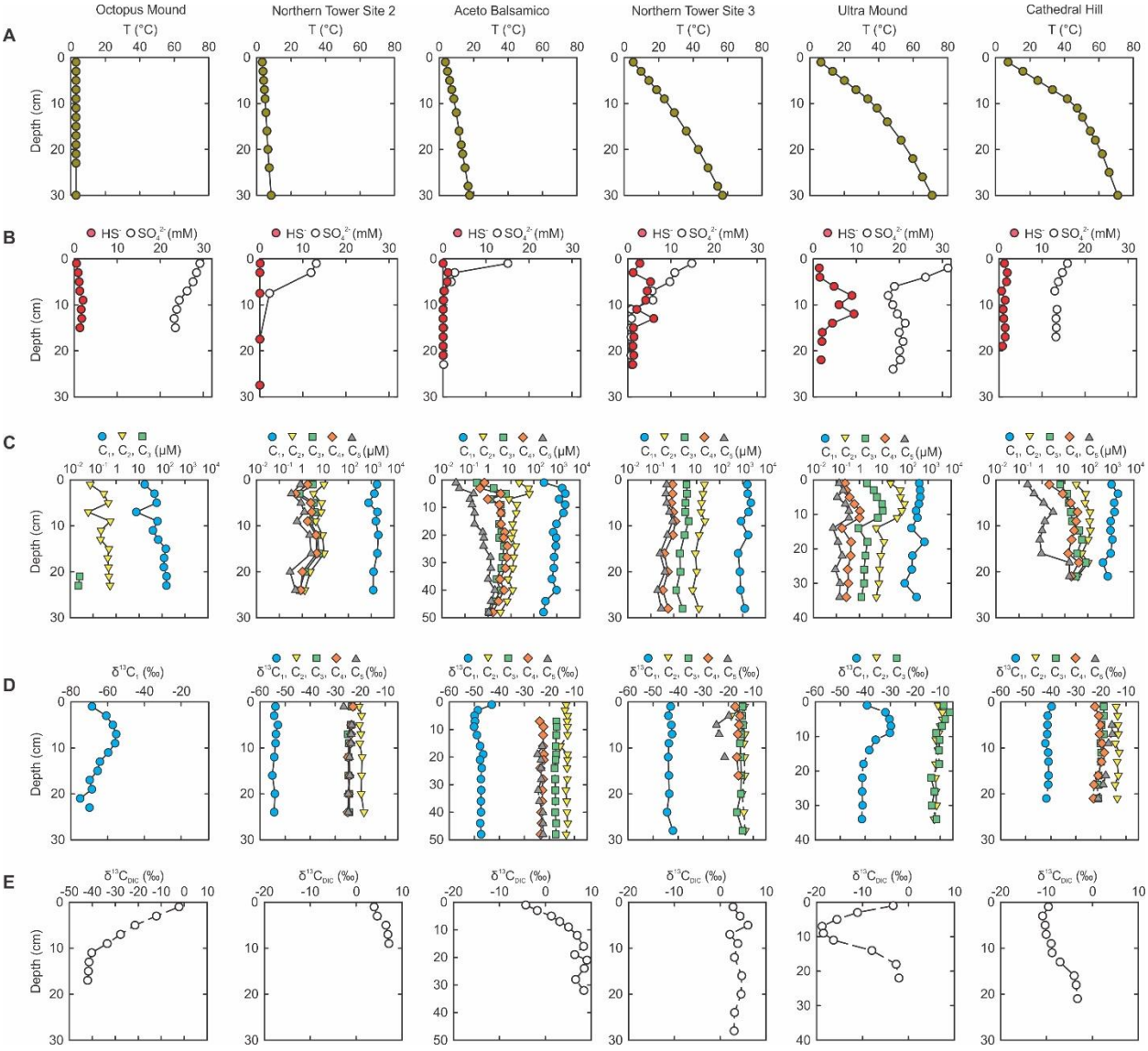

Figure V.1. Geochemical data of the six studied sites. The results are displayed from cool to warm to hot sites. A. Extrapolated temperatures based on data from *Alvin*'s heat-flow probe; B. Sulfate and sulfide concentrations; C. Concentrations of C_1-C_5 hydrocarbons; D. $\delta^{13}C$ values of C_1-C_5 hydrocarbons; E. $\delta^{13}C$ values of dissolved inorganic carbon (DIC).

$\delta^{13}C$ values of DIC were particularly negative at Octopus Mound (-29.1±13.7‰; mean±SD; n=9), Ultra Mound (-10.7±6.5‰; mean±SD; n=9) and Cathedral Hill (-7.6±2.8‰; mean±SD; n=10). At Octopus Mound, $\delta^{13}C_{DIC}$ decreased with depth, whereas at Ultra Mound $\delta^{13}C_{DIC}$ first decreased (from -3‰ to -19‰) with depth until ~ 9 cm, then increased again to -2‰. At Cathedral Hill $\delta^{13}C_{DIC}$ increased gradually with depth (Fig. V.1E). In contrast, $\delta^{13}C_{DIC}$ values were comparably positive at Northern Tower Site 2 (5.8±1.3‰; mean±SD; n=5), Aceto Balsamico (4.8±4.2‰; mean±SD; n=12) and Northern Tower Site 3 (3.8±1.1‰; mean±SD; n=10), with values from the first two sites increasing with depth.

V.3.2. Distribution of microbial lipids

The highest archaeal IPL concentration was observed at the cold seep site Octopus Mound (2.4 µg/g dry weight sediment; DW) at ~ 6 cm, followed by hot sites Ultra Mound (0.4 µg/g DW at ~ 9 cm) and Cathedral Hill (0.3 µg/g DW at ~ 5 cm) and warm site Aceto Balsamico (0.2 µg/g DW at ~ 10 cm). IPL concentrations at the hot Northern Tower Site 3 and cool Site 2 were overall low (< 0.1 and < 0.01 µg/g DW, respectively) (Fig. V.2A). In comparison, total archaeal core lipids (CLs) concentrations were one to three orders of magnitude higher than IPL concentrations in the same samples. The highest CLs concentration was also found at Octopus Mound at ~ 6 cm, whereas CLs concentrations generally decreased with depth at the other sites (Fig. V.2A).

Archaeal intact polar lipids. Among the studied sites, monoglycosidic glycerol dialkyl glycerol tetraether (1G-GDGT) was predominant in most of the sediment layers under cold to hot conditions (Fig. V.2B). 2G-GDGT accounted < 10% of total IPLs at the cold seep Octopus Mound. At the other sites it was only detected in some sediment layers, predominantly in the first 5 cm (10-20% of total IPLs) (Fig. V.2B). In both of the 1G-GDGT and 2G-GDGT pools (Fig. V.3A, B), GDGT-2 and GDGT-1 dominated at the cold seep site Octopus Mound, whereas the contribution of GDGT-4 increased significantly with elevated temperatures in Northern Tower Site 3 sediments and was consistently abundant in Ultra Mound sediments and dominated the surficial sediments of Cathedral Hill. Only very few sediment layers contained detectable amounts of IPLs at Cathedral Hill. We assign this lack in detectability to the high oil content at this site, which probably increased ion suppression during analysis. At the less hydrothermally influenced sites Northern Tower Site 2 and Aceto Balsamico, ring distribution in the 1G-GDGT and 2G-GDGT pools was distinct, at both sites 1G-GDGT pool was dominated by GDGT-0 and GDGT-5 (we expect GDGT-5 to be crenarchaeol according to the retention time reported by Zhu et al., 2014b, however, we have not confirmed this with IPL-derived core lipid measurements), while 2G-GDGT was dominated by GDGT-2 and GDGT-1 (Fig. V.3A, B).

Notable amounts of phosphatidylglycerol (PG-) GDGT were detected in near surface sediments (< 10 cm) of both cold (Octopus Mound, Northern Tower Site 2) and hot sites (Ultra Mound, Cathedral Hill). PG-GDGT also displayed different ring distribution in sediments from cold and hot sites, with GDGT-2 and GDGT-3 dominating in sediments from Octopus Mound and Northern Tower Site 2, whereas GDGT-4 was detected in surface sediments of Cathedral Hill and its relative abundance increased with depth at Ultra Mound (Fig. V.3C).

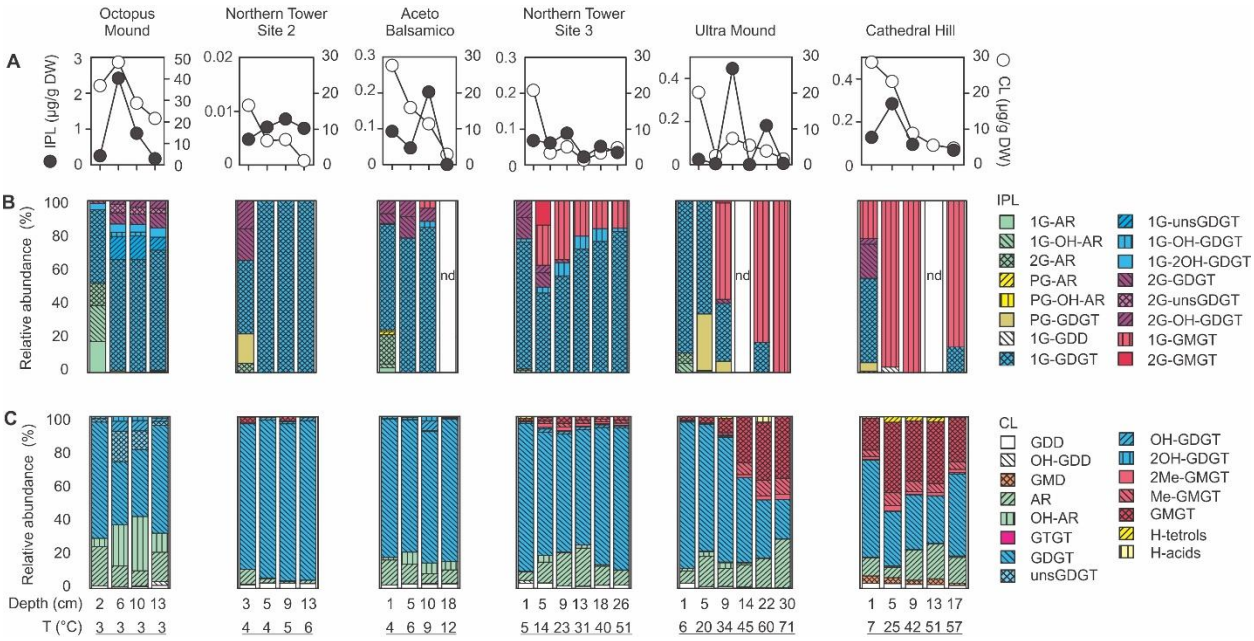

Figure V.2. Distribution of archaeal lipids at studied sites. A. Absolute total concentrations of intact polar lipids (IPLs) and core lipids (CLs), note the different scales between sites; B. Relative abundance of IPLs; C. Relative abundance of CLs among the six studied sites. nd, not detected.

Hydroxylated GDGT (OH-GDGT and 2OH-GDGT) with 1G and 2G head groups were minor lipids detected at some of the sites. While 1G-2OH-GDGT was exclusively present at Octopus Mound, 1G-OH-GDGT was also detected in Aceto Balsamico sediments and found with higher amounts at Northern Tower Site 3; 2G-OH-GDGT was found abundantly in sediments where temperatures exceeded 15 °C with the exception of Ultra Mound. The minor lipid isoprenoid glycerol dibiphytanol diether (GDD) with 1G head group was only detected in Cathedral Hill sediments at 5 cm (Fig. V.2B).

Intact AR and hydroxy (OH-) AR with 1G and 2G head groups were only detected in surface sediments where *in situ* temperatures were below 10 °C. Unsaturated GDGT (unsGDGT) with 1G and 2G head groups were exclusively detected at Octopus Mound. Furthermore, in surface layer of Aceto Balsamico low abundance of PG-AR and PG-OH-AR (together < 3% of total IPLs) were observed.

1G-GMGTs were predominantly detected in sediments from hot sites, and were barely detectable at greater depth of warm site Aceto Balsamico (Fig. V.2B). 1G-GMGT comprised around 20-40% in the deeper layers of Northern Tower Site 3 and overwhelmingly dominated the subsurface sediments of Ultra Mound and Cathedral Hill, where it comprised > 80% of the total IPL pool (Fig. V.2B). 1G-GMGT was detected with up to 4-5 rings, while relative abundance of 1G-GMGT-0 increased with depth at Northern Tower Site 3, 1G-GMGT-4 comprised > 20% at most depths at Northern Tower Site 3 and Ultra Mound and dominated at Cathedral Hill, where it decreased with depth (Fig. V.4A). 1G-GMGT-5 was only detected

in Cathedral Hill at 17 cm. 2G-GMGT (accounting 15% of total IPLs) with up to 3 rings was only detected at 5 cm at Northern Tower Site 3.

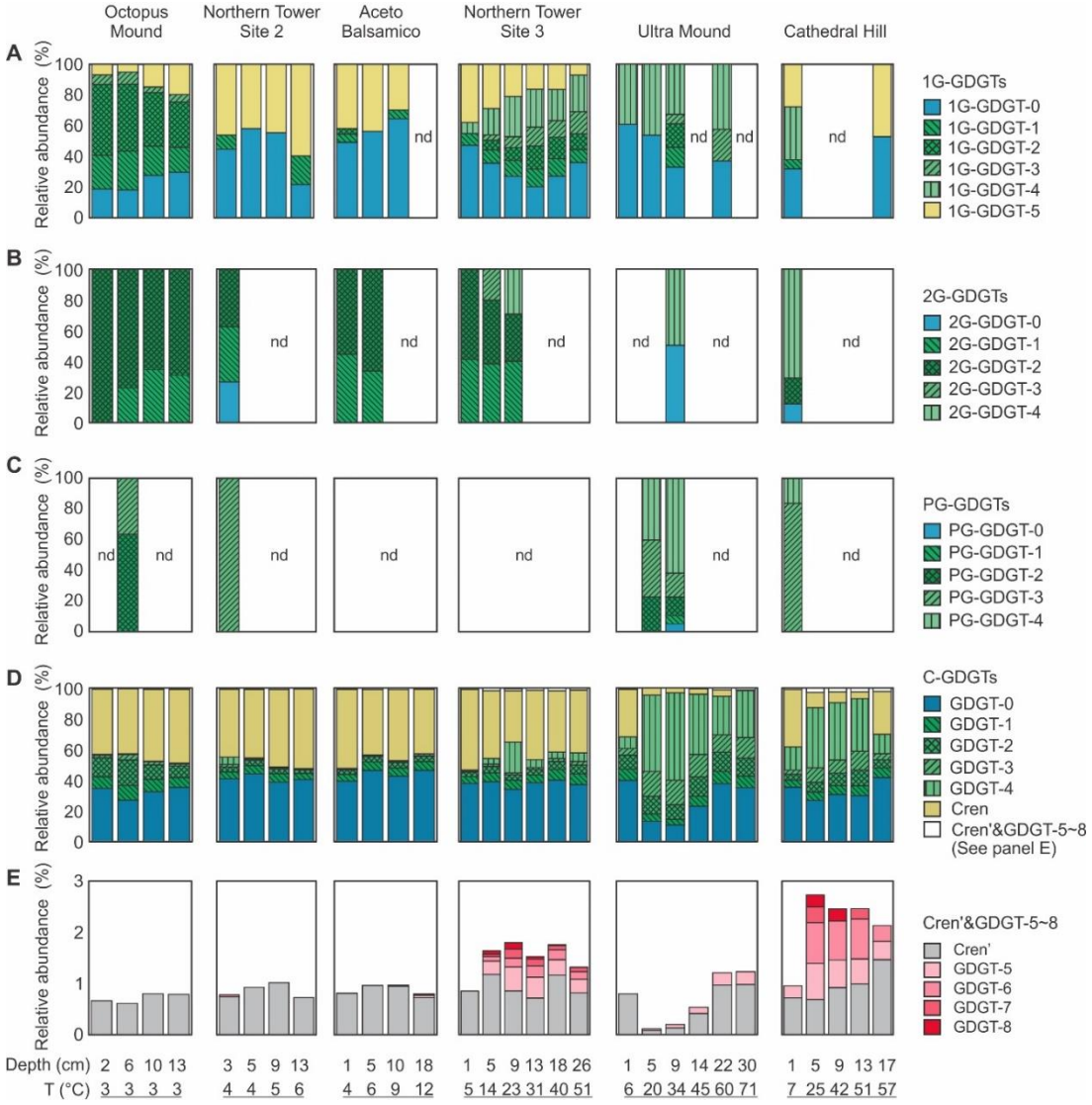

Figure V.3. Relative abundance of intact and core GDGTs among the six studied sites. nd, not detected. A. 1G-GDGTs; B. 2G-GDGTs; C. PG-GDGTs; D. C-GDGTs. E. Cren' and GDGT-5 to GDGT-8.

Archaeal core lipids. Mirroring the IPL distribution, with a shift from intact GDGT to intact GMGT in sediments from low to higher temperatures, core lipids exhibited a similar dominance of GDGT in cold sediments, while GMGT increased with temperature and were particularly abundant at hot sites Ultra Mound and Cathedral Hill (Fig. V.2C). Similarly, the ring distribution of GDGT was also distinct in sediments from cold to hot sites, where GDGT-0 and crenarchaeol (composed of cyclopentane and one cyclohexane rings) dominated the cooler sites Octopus Mound, Northern Tower Site 2 and Aceto Balsamico, and GDGT-4 increased with temperature and became dominant at Ultra Mound and Cathedral

Hill. Notably, relative abundances of GDGT-1 to GDGT-3 were elevated in sediments of both the cold seep site Octopus Mound and the hot sites Ultra Mound and Cathedral Hill. Minor amounts of GDGT-5 (with five cyclopentane rings) were detected in Ultra Mound (< 0.3% of core GDGTs), whereas up to GDGT-8 were detected in sediments of Cathedral Hill and Northern Tower Site 3 (0.2-2% of total GDGTs; Fig. V.3C).

Another abundant core lipid was AR, which varied from 1 to 30% in the core lipid pool with no apparent trend linked to temperature (Fig. V.2C). Additionally, OH-AR and unsGDGT were particularly abundant (up to 20-30% of core lipid pool) at Octopus Mound (Fig. V.2C). Some other detectable minor core lipids include OH-GDGT and 2OH-GDGT, which had relatively high abundances at Octopus Mound and Aceto Balsamico, and were barely detectable at Northern Tower Site 2 and 3. GDD was detected at all sites with low abundance, while OH-GDD was only detected in deeper sediments of Octopus Mound and surficial sediments of Northern Tower Site 3 (Fig. V.2C).

Relative abundance of core GMGT, together with its mono- and di-methylated analogs (Me-GMGT and 2Me-GMGT) increased significantly in sediments from hot sites Ultra Mound and Cathedral Hill, while only minor amounts of these compounds were detected in the third hot site Northern Tower Site 3 (Fig. V.2C). Core GMGT with 0-8 rings were detected at all of the three hot sites (Fig. V.4B), with GMGT-4 (accounting for 30-60% of the GMGT pool) predominating most depths. Relative abundance of GMGT-5 to GMGT-8 were elevated in Cathedral Hill and Northern Tower Site 3 sediments, accounting for 10-40% of the GMGT pool (Fig. V.4B). Analogous to GMGT, Me-GMGT and 2Me-GMGT were also dominated by four rings, whereas contribution of 5-8 rings were more pronounced (Fig. V.4C, D).

Meanwhile, H-shaped glycerol monoalkyl diether (GMD) and H-tetrols with 80 to 82 carbon numbers were detected at these hot sites, and small amount of H-shaped acids (H-acids) were detected at the Ultra Mound where *in situ* temperature was around 60 °C (Fig. V.2C). GMD with up to 8 rings were detected and were mostly dominated by GMD-4 and GMD-0 in Ultra Mound sediments, whereas GMD with 5-8 rings were more abundant at Cathedral Hill (Fig. V.4E). While H-C_{80}-tetrol was dominated by 0-4 rings, the contribution of 5-8 rings increased significantly in H-C_{81}-tetrol and particularly in H-C_{82}-tetrol (Fig. V.4F-H).

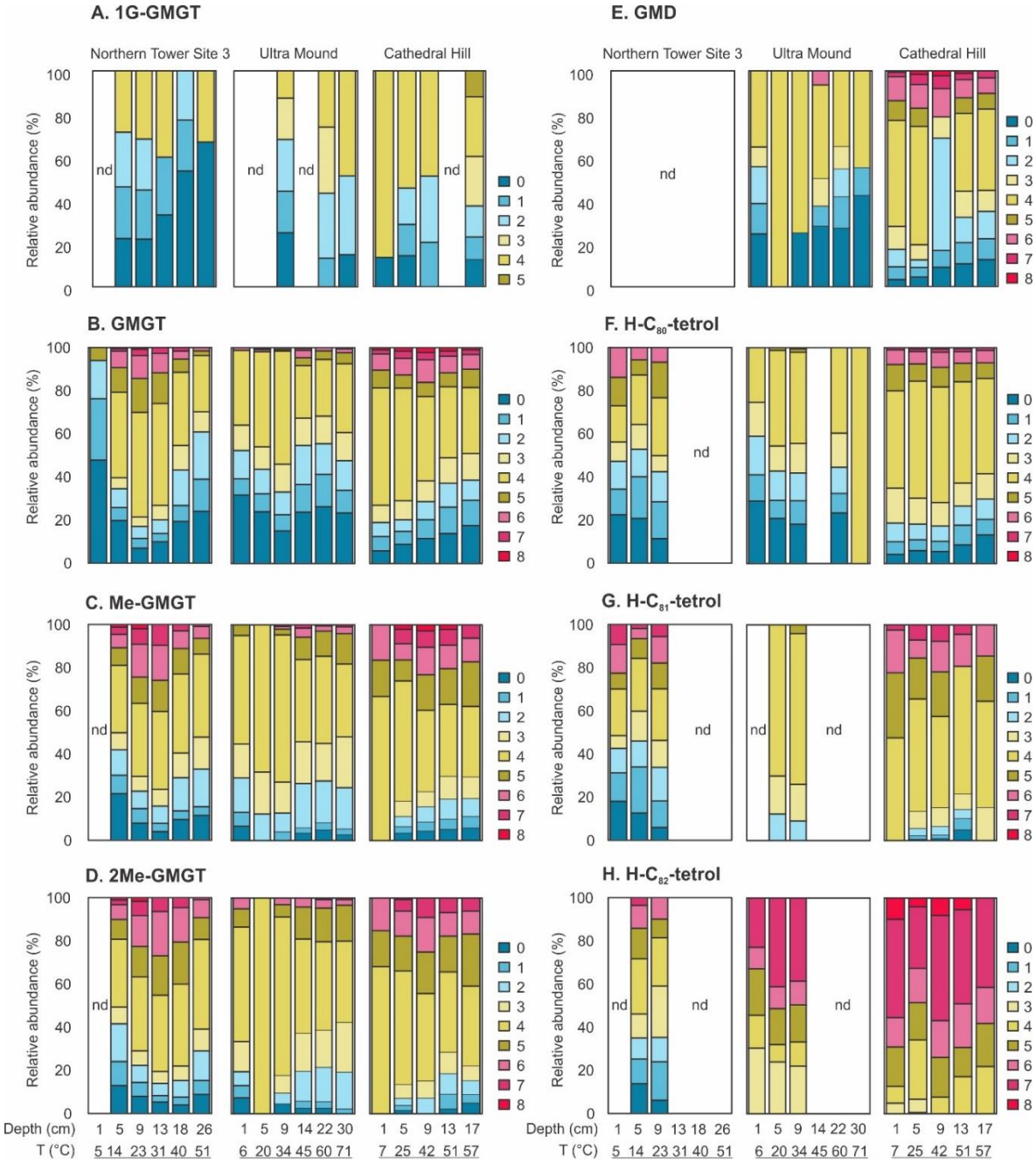

Figure V.4. Relative abundance of H-shaped tetraethers, diether and H-tetrols (A-H) in sediments from the three hot sites Ultra Mound, Cathedral Hill (Marker 24) and Northern Tower Site 3.

Branched GDGTs. The brGDGT and its analogs with higher or lower degrees of methylation, i.e., OB-GDGT and SB-GDGT, as well as IB-GDGT were also detected at all six sites. The total concentrations of these compounds ranged from 0.01 to 1.0 µg/g DW (Fig. V.5A); thus the total branched GDGTs pool equates in size to 1-3% of the archaeal core lipid pool. While brGDGT and IB-GDGT predominated the most of the investigated sites (Octopus Mound, Northern Tower site 2, Aceto Balsamico and Northern

Tower site 3), relative and absolute amounts of OB-GDGT increased at Northern Tower site 3 and dominated the branched GDGT pool at the other two hot sites Ultra Mound and Cathedral Hill (Fig. V.5B).

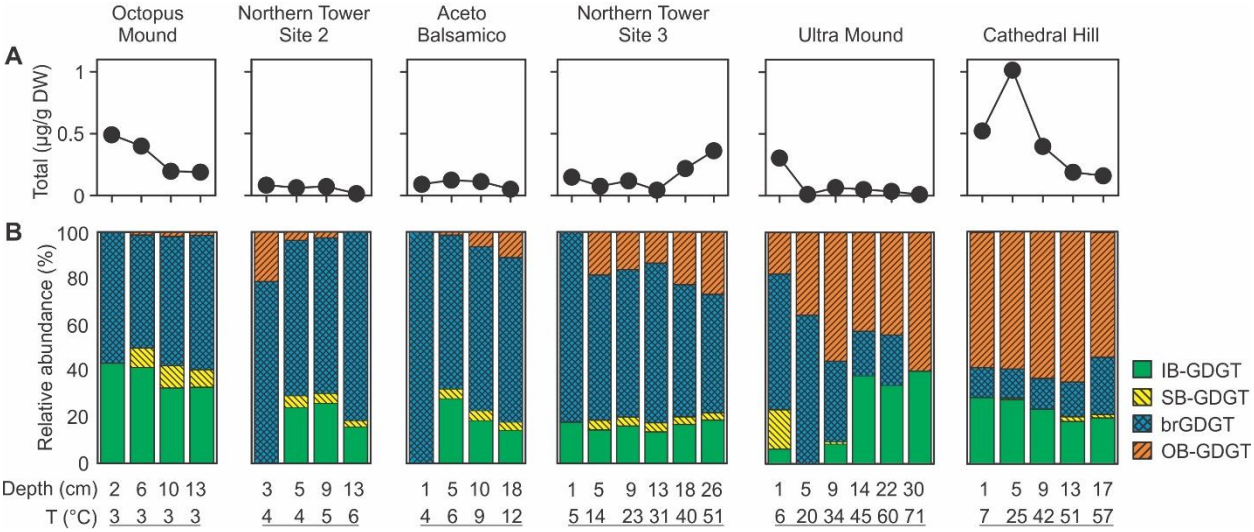

Figure V.5. Absolute and relative abundance of branched GDGTs. A. Absolute total concentrations of branched GDGTs; B. Relative abundance of branched GDGTs.

V.4. DISCUSSION

V.4.1. Archaeal lipid signatures associated with AOM in cold and hot sediments

Microbial oxidation of methane is evidenced by preferential oxidation of ^{12}C-CH_4 to ^{12}C-DIC, leading to local enrichment in residual ^{13}C-CH_4 (less negative $\delta^{13}C_1$ values) co-located with relative depletion of ^{13}C-DIC (more negative $\delta^{13}C_{DIC}$ values). These signatures are conspicuous throughout the Octopus Mound core, at the very surface of Aceto Balsamico, and in the upper 10 cm of the Ultra Mound core (Fig. V.1D and E); the electron acceptor sulfate is available at these locations. Previous studies have identified ANME-1 archaea as the most frequently detected and wide-spread methane-oxidizing microorganisms in Guaymas Basin (Teske et al., 2002; Ruff et al., 2015; McKay et al., 2016; Dowell et al., 2016). The evidence for anaerobic oxidation of methane in these cores implies that the characteristic lipids of ANME-1 archaea should be detectable.

The hydrothermally unaffected cold seep site Octopus Mound showed the highest concentrations of IPL and core lipids. Both reached maximal values at ca. 6 cm where AOM was most active as indicated by the most positive $\delta^{13}C_1$ values (Figs. V.1D; V.2A). Currently we lack the carbon isotopic compositions of individual IPLs, but already the distribution of AOM related biomarkers can provide clues on the distribution of methanotrophic archaea. For instance, in the surface sediments notable amounts of glycosidic

AR and OH-AR suggest the presence of ANME-2 (2011; Rossel et al., 2008; Fig. V.2B). GDGT-2 dominated 2G-GDGT, PG-GDGT as well as 1G-GDGT increased with depth (where in cm) (Figs. V.2B and V.3A-C). Both 2G-GDGT-2 and PG-GGDT-2 are frequently assigned to ANME-1 in methane-rich sediments (Rossel et al., 2011; Song et al., Chapter IV), while higher abundance of 1G-GDGT-2 was also observed to be associated with ANME-1 in AOM active sediments from the Eastern North Atlantic margin (Song et al., Chapter IV). Similarly, the core lipids were dominated by OH-AR and GDGT-2 compared to the other sites (Figs. V.2C and V.3D), reflecting past signals of AOM.

Abundance ratios of IPL/(IPL+CL) for different type of IPLs have been used as indicator for microbial activity in sediment based on the premise that live community members should increase the pool size of IPLs relative to the corresponding CLs (cf. Schröder, 2015). Abundance ratios of AR and OH-AR based IPLs were highest at ~ 1 cm and decreased sharply to below detection limit within the top 5 cm, whereas abundance ratios of intact GDGTs (consisting of 1G, 2G and PG-GDGTs) reached maximal values at ~ 6 cm where AOM was most active (Supp. Fig. V.3A). This suggests that AOM in Octopus Mound sediments is performed by spatially separated ANME-2 and ANME-1 communities, with the former being more active in sulfate-rich surface sediments while the latter is more abundant in greater depth under more reducing conditions, a pattern observed at many other seep sites (e.g., Orphan et al., 2004; Orcutt et al., 2005; Schubotz et al., 2011; Rossel et al., 2011). In addition, intact unsGDGTs and 2OH-GDGTs, which were only detected in the sediments of Octopus Mound, together with intact OH-GDGTs, showed a similar trend as intact GDGTs primarily assigned to ANME-1 (Supp. Fig. V.3A), suggesting *in situ* production of these compounds by AOM related organisms. Specifically, unsGDGTs are frequently detected in anoxic environments (Zhu et al., 2016) and have been associated to AOM in methane-rich sediments (Yoshinaga et al., 2015; Song et al., Chapter IV).

In the warmer site Aceto Balsamico, geochemical profile suggests a combination of advective porewater discharge and AOM in the surface sediments, whereas in deeper layers no sulfate was available to sustain AOM. Consequently, high abundance of 2G-AR was present in the surface sediments, accompanied by minor amounts of 1G-AR, 1G-OH-AR as well as PG-AR and PG-OH-AR (Fig. V.2B), all have been proposed as diagnostic biomarkers for ANME-2 groups in methane-rich sediments (2011; Rossel et al., 2008). Moreover, 2G-GDGT consisting of GDGT-2 and GDGT-1 core lipids were detected in the top 5 cm (Fig. V.3B), suggesting contribution of ANME-1 communities (2011; Rossel et al., 2008) similar to what was observed at Octopus Mound. However, given the overall low abundance of GDGT-1 and GDGT-2 in the core GDGT pool in comparison to that of Octopus Mound (Fig. V.3D), AOM does not seem to play a primary role in these sediments.

In sediments from the hot site Ultra Mound, the concentrations of both intact and core lipids were elevated at around 9 cm coinciding with an AOM hot spot suggested by geochemical profiles (Fig. V.2A; Fig. V.1). Similar to its cooler counterpart sites, the ANME-2 diagnostic biomarkers 1G-OH-AR and 2G-AR were only detectable in the surface sediments (~ 1 cm) whereas relatively high contributions of PG-GDGTs and low amounts of 2G-GDGTs were detected in greater depth (Fig. V.2B). Both PG-GDGTs and 2G-GDGTs contained substantial amounts of GDGT-4 reaching maximal abundance (40 to 60%) at the AOM hot spot depth (~ 9 cm; Fig. V.3B, C). Similarly, both 1G-GDGTs and core GDGTs also showed comparably higher contributions of GDGT-4 than at the other sites (Fig. V.3A. D). This is very likely due to contribution of thermophilic ANME-1 archaea at temperatures > 30 °C, consistent with the presence of GDGT-1 to GDGT-4 and their intact precursors in both hydrothermally heated sediments and thermophilic ANME-1/HotSeep-1 enrichment cultures retrieved from Guaymas Basin (Schouten et al., 2003; Holler et al., 2011; Supp. Fig. V.4). Depth profiles of abundance ratios for intact AR and GDGTs showed similar trends as those from Octopus Mound, with intact AR decreasing rapidly within the first 5 cm of the sediments, limiting the presence of ANME-2 biomarkers to the surface sediments whereas intact GDGTs reached maximal abundance ratio at ~ 9 cm then decreased with depth (Supp. Fig. V.3E). Together these results confirm previously observed depth zonations of surficial ANME-2 communities and deeper thermophilic ANME-1 clusters in Guaymas Basin hydrothermal sediments, and the dominance of ANME-1 in archaeal clone libraries in Guaymas Basin sediments throughout a wide thermal range (Teske et al., 2002; McKay et al., 2016).

The low abundance of 2G-GDGTs in Ultra Mound hydrothermally heated sediments are surprising considering the general abundance of 2G-GDGT at active AOM sites (2011; Rossel et al., 2008) and the predominance of 2G-GDGTs in the ANME-1/HotSeep-1 enrichments (Supp. Fig. V.4; Holler et al., 2011). However, as pointed out by Kellermann et al. (2016) low amounts of 2G-GDGT in the presence of PG-GDGT could indicate a rapidly growing ANME-1 community. In mesophilic ANME-1 enrichments Kellermann et al. (2016) observed a low production rate of 2G-GDGT during their active growth phase, while existing phosphate-based lipids, including PG-GDGT, were replaced by 2G-GDGT during stationary phase. We therefore suggest that the low 2G-GDGT abundances concomitant with high PG-GDGT observed in Ultra Mound sediments are indicative of active and flourishing ANME-1 communities.

While AOM did not seem to be a dominant process at the other sites, signs of AOM occurring in the surface sediments were apparent at cool Northern Tower Site 2 (by the presence of 2G-AR together with PG-GDGT-3 and 2G-GDGTs with 0 to 2 rings), at the hot sites Northern Tower Site 3 (by an increase of 2G-GDGT-4 with elevated temperatures) and Cathedral Hill (by dominance of the 2G-GDGT-4) (Figs. V.2B; V.3B, C). Meanwhile, these sites exhibited a high abundance of 1G-GMGTs, accompanied by the

presence of core GMGTs and methylated GMGTs, which seemed to increase with temperature (Northern Tower Site 3, Ultra Mound and Cathedral Hill) (Fig. V.2B, C). 1G-GMGTs were not present in the thermophilic ANME-1/Hot Seep-1 enrichment (Supp. Fig. V.4), suggesting the presence of additional archaeal groups as sources for these lipids, which is further discussed in the following sections.

V.4.2. Lipid signatures of C_{2+} hydrocarbon oxidation

As previously noted (Dowell et al., 2016, Song et al., Chapter III), non-methane short-chain alkanes in Guaymas Basin show a systematic pattern of decreasing $\delta^{13}C$ values with higher carbon number, from ethane as the heaviest alkane ($\delta^{13}C_2$ ca. -13‰) towards pentane as the lightest measured alkane in this dataset ($\delta^{13}C_5$ ca. -25 ‰). Localized ^{13}C-enrichment for specific alkanes, indicative of biological oxidation, is observed in particular for ethane and propane in the surface layers of the Ultra Mound sediment core, and for butane and pentane at the Cathedral Hill core (Fig. V.1D). At both Northern Tower sites, biological oxidation may have affected propane, butane and pentane (Fig. V.1D). Microbial candidates for these processes include diverse sulfate-reducing bacteria with highly specialized substrate spectra (Kniemeyer et al., 2007), and sulfate reducers growing as syntrophs with thermophilic alkane-oxidizing archaea; the best-studied examples have been isolated from Guaymas Basin sediments (Laso-Pérez et al., 2016; Krukenberg et al., 2016; Hahn et al., 2020). It is reasonable to assume that these bacteria and archaea contribute to the lipid pool as well.

We investigated archaeal enrichment cultures isolated from Guaymas Basin sediments capable of growing on ethane, propane and butane (Hahn et al., 2020; Laso-Pérez et al., 2016; Zehnle, Wegener et al., unpubl. data) on their lipid composition. Some of these cultures grown at 37 °C already contained 1G-GMGT, as well as core GMGT, Me-GMGT, 2Me-GMGT with up to 4 rings, these amounts increased with increasing temperatures. Particularly the propane and butane oxidizing enrichments contained notable amounts of 1G and 2G-GMGT with 0-4 rings at 50 °C (Zehnle, Wegener et al., unpubl. data). The three hot sites- Northern Tower Site 3, Ultra Mound and Cathedral Hill- were notably dominated by intact and core GMGT lipids, accompanied by increasing amounts of Me-GMGT and 2Me-GMGT in greater depths. This suggests that at least a fraction of the GMGT-based lipids from our samples were sourced from archaea that took part in anaerobic degradation of C_{2+} hydrocarbons in the Guaymas Basin hydrothermally heated sediments. Given that such compounds were also detected in greater sediment depths of all three hot sites where no apparent geochemical evidence for hydrocarbon degradation was observed, there may be other archaeal groups that also produced GMGT-based lipids. Or these lipids were formed at an earlier stage,

when short-chain hydrocarbons were still oxidized in the respective horizons and were then preserved in sediments.

V.4.3. Temperature-related distributions of isoprenoidal ether lipids

In order to evaluate the impact of temperature on sedimentary *in situ* produced lipids, we calculated the weighted average ring index (RI; See method, Eq. 1) for GDGT-1 to GDGT-4 based intact and core lipids. The ring index for 1G-GDGTs were between 1.0 and 1.8 at cooler sites and between 2.8 and 3.6 at hotter sites (Supp. Fig. V.5), but did not correlate with temperature (Table V.2). The lack of correlation with recorded temperature, despite the clear distinction between cool and warm sites, is possibly related to the rather short-lived nature of the temperature recording in this dynamic hydrothermal system while the lipid distributions have accumulated over time and thus integrate comparably long periods. Presumably, the hotter sediments host higher proportions of thermophilic archaea and/or, due to the inherent higher fluxes of methane, methanotrophic archaea, which tend to produce higher proportions of cyclic GDGTs.

Core GDGTs reflected contribution from both sedimentary and planktonic inputs, as AOM impacted Octopus Mound and Ultra Mound held elevated abundance of GDGT-2 and/or GDGT-4 (Fig. V.4D) due to methanotrophic biomass, allochthonous crenarchaeol dominated the core GDGT pool of all three cool sites and the hot Northern Tower Site 3 (Fig. V.3D). Increased GDGT-4 accompanied by decreasing crenarchaeol in sediments of the other hot site Cathedral Hill indicates *in situ* contribution possibly including oil-degrading archaeal groups given its high oil content, although intact GDGTs were largely not detected due to oil effect on IPL ionization during analysis. The average ring index values calculated for GDGT-1 to GDGT-4 core lipids were around 1.8 at cooler sites and from 1.7 to 3.1 at hotter sites (Supp. Fig. V.5), and were positively and significantly correlated with temperature (Table V.2). Additionally, minor amounts of GDGT-5 to GDGT-8 were also detected in Northern Tower Site 3 and Cathedral Hill (Fig. V.3E). Together this may indicate archaeal community response to high temperatures as cell membranes composed of GDGTs with more cyclopentane rings have higher thermal transition points (Gliozzi et al., 1983).

Moreover, intact hydroxylated GDGTs (1G-OH-GDGT, 1G-2OH-GDGT and 2G-OH-GDGT), which are also known to be largely produced by Thaumarchaea (Elling et al., 2017), were detected in sediments of cooler sites and surface layer of warmer sites. However, elevated abundance of 1G-OH-GDGT in greater depth of Northern Tower Site 3 at temperatures up to 40 °C (Fig. V.2B) implies a likely *in situ* production by sedimentary archaeal groups. It was found that 1G- and 2G-OH-GDGT were highly correlated with Miscellaneous Crenarchaeotal Group and Marine Benthic Group B in methane-laden sediments (Song et

al., Chapter IV). Given that these benthic archaeal groups were also found abundantly in Guaymas Basin sediments (Biddle et al., 2012), it is not unlikely that they may contribute to the production of both intact GDGTs and OH-GDGTs.

Table V.2. Spearman's rank correlation of temperature and weighted ring distribution of isoprenoidal ether lipids with one to four rings. Compounds that exhibited positive and significant correlations are marked in bold. Significance codes: 0 '***' 0.001 '**' 0.01 '*' 0.05 '.' 0.1 ' ' 1.

	rho	P-value	Significance
1G-GDGT	-0.01	0.9630	
2G-GDGT	-0.48	0.0085	**
GDGT	0.61	0.0004	***
GDD	0.59	0.0007	***
1G-GMGT	0.67	0.0001	***
GMGT	0.47	0.0106	*
Me-GMGT	0.63	0.0003	***
2Me-GMGT	0.55	0.0021	**
GMD	0.45	0.0156	*
H-C_{80}-tetrol	0.48	0.0080	**
H-C_{81}-tetrol	0.29	0.1277	
H-C_{82}-tetrol	0.31	0.0984	.

V.4.4. Temperature-related distributions of H-shaped ether lipids

Concentrations of intact and core GMGTs were notably high at hot sites where temperatures reached up to 70 °C (Fig. V.2B, C). While 1G-GMGT was comprised of core lipids with 0-5 cyclopentane rings, core GMGT, Me-GMGT and 2Me-GMGT with up to 8 rings were detected (Fig. V.4A-D). GMGT with 0 to 4 rings has been reported in cultivated isolates of (hyper-) thermophilic archaea (e.g., Morii et al., 1998; Schouten et al., 2008; Knappy et al., 2011), and from hydrothermal vent environments (e.g., Jaeschke et al., 2012; Lincoln et al., 2013; Sollich et al., 2017). Sollich et al. (2017) also reported on intact GMGT and Me-GMGT with up to four rings and 1G and 2G head groups from shallow water hydrothermal sediments, and noted increasing abundances of these compounds with increasing temperatures from 20 to 100 °C. They suggested that increasing the number of methylations in GDGT and GDMTs are a response to heat stress, which reduces the ion permeability of the archaeal membranes, while the addition of cyclopentane rings may not be temperature-regulated alone. Notably, the intact precursors for methylated GMGTs were not

detected in our samples, also core GMGT was more abundant than its methylated counterparts in our samples (Fig. V.2B, C). One explanation for this could be that currently the source organisms for methylated GMGTs are not as active and the intact counterparts have already been degraded. Alternatively, the source organisms may synthesize the core forms of methylated GMGT, as previously suggested for core GDGTs in marine sediments by way of radioisotope probing experiments (Evans et al., 2019). Our results confirm that the number of methylations and rings in GMGT lipids increase with temperature (Fig. V.4); this observation is consistent with a membrane adjustment in order to cope with increased heat stress as suggested in previous studies (Sollich et al., 2017). This then can also explain the significant positive correlations of relative abundance and ring index between GMGT and its methylated counterparts (Fig. V.6A; Table V.2). Together our results suggest related source organisms for cyclic and methylated GMGTs, the extra covalent bond between the two alkyl chains in GMGT could further reduce membrane fluidity and proton permeability, thereby enabling higher packing densities as suggested in former studies (Knappy et al., 2011; Sollich et al., 2017).

Besides intact and core GMGTs, we also detected known breakdown products of GMGT that were previously found to be abundant in Guaymas Basin sediments (Liu et al., 2016). We found GMD and H-tetrols with 80 to 82 carbons and up to eight cyclopentane rings (Figs. V.2C and V.4) at all of the three hot sites, but most abundant at oil impregnated Cathedral Hill. While it has been suggested that these compounds are most likely produced from the degradation of intact and core GMGT, Me-GMGT and 2Me-GMGT, it is still unclear whether primarily biotic or abiotic processes are involved in their formation (Liu et al., 2016). Spearman's rank correlation analysis showed that relative abundance of GMD correlated positively and significantly with both GMGT, methylated GMGTs and H-tetrols with 80 to 82 carbons (Fig. V.6A), supporting the close connection to these suggested precursor molecules. In addition, H-acids consisting of monoacid, diacid, triacid and tetraacid with 80 carbons were detected in minor amounts in Cathedral Hill and Ultra Mound sediments (Fig. V.2C). H-C_{80}-monoacid correlated with H-tetrols, whereas the other H-acids correlated with one another (Fig. 6A). This is in line with the suggestion that these acids are generated by stepwise oxidation of the four hydroxyl groups in the H-tetrols (Liu et al., 2016).

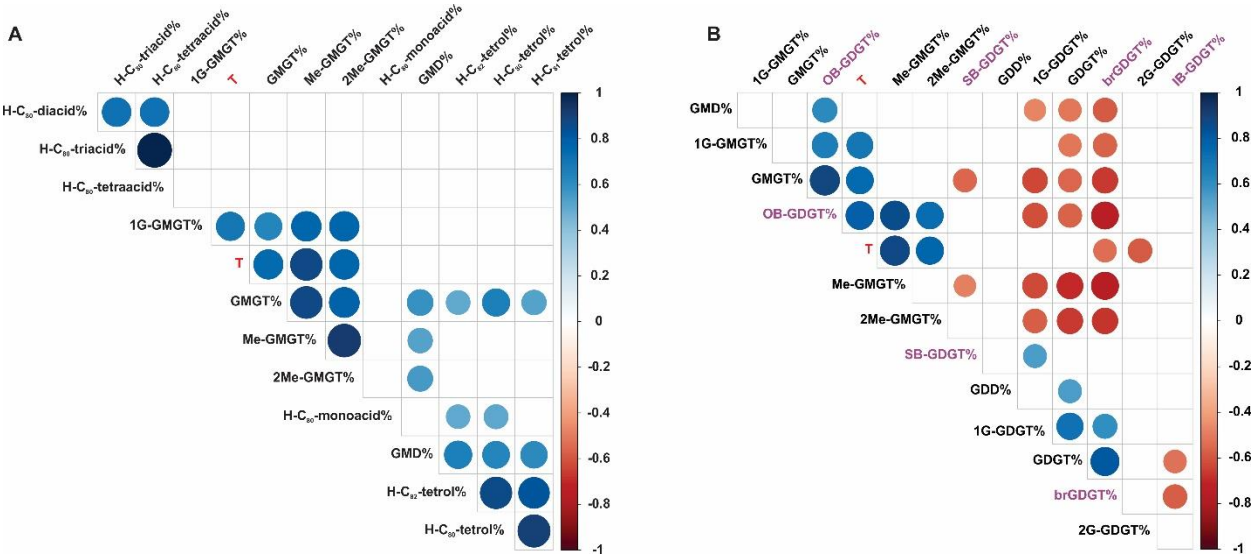

Figure V.6. Spearman's rank correlation of temperature and lipid compounds with P-value < 0.01. A. Significant correlations between temperature and H-shaped isoprenoidal ether lipids and their degradation products; B. Significant correlations between temperature and intact and core H-shaped isoprenoidal ether lipids, isoprenoidal ether lipids, and branched GDGTs. Temperature is highlighted in red, and branched GDGTs are highlighted in violet color.

V.4.5. Temperature-related distributions of branched GDGTs

One unexpected observation was the distribution of branched GDGT (i.e. IB-GDGT, brGDGT, OB-GDGT and SB-GDGT) at cold to hot sediments (Fig. V.5). The presence of brGDGT in marine sediments has been used as an indicator for the contribution of specific terrestrial material as these compounds are very abundant in peat and soils (Schouten et al., 2000; Damsté et al., 2000; Weijers et al., 2006b), where anaerobic soil bacteria are attributed as the source organisms (Weijers et al., 2006a). Recent studies provided evidence for the *in situ* production of brGDGTs in various marine environments (Liu et al., 2012; Xie et al., 2014; Liu et al., 2014), and brGDGTs have also been detected in hydrothermal systems at mid-ocean ridges with no obvious terrigenous inputs (e.g., Hu et al., 2012; Lincoln et al., 2013; Jaeschke et al., 2014). In marine sediments, brGDGT often co-occur with IB-, OB- and SB-GDGTs (Liu et al., 2012). Corresponding IPL precursors of these branched GDGTs were recently identified in marine sediments, thus suggesting *in situ* production of these compounds in the marine environment (Becker, 2015). While IB-GDGT may possess alkyl chains that are characteristic of both archaea (isoprenoidal moiety) and bacteria (methylated alkyl moiety), OB- and SB-GDGT possess non-isoprenoidal side chains with higher or lower degrees of methylation (Liu et al., 2012) than the commonly found brGDGT (Weijers et al., 2007). Therefore, a bacterial source for the SB- and OB-GDGT classes is not unlikely.

Notably, IB-, OB- and SB-GDGTs have only been reported in normal marine settings, which are typically dominated by brGDGT (e.g., Xie et al., 2014; Liu et al., 2014). Although the relative abundance of branched GDGTs in the investigated sediments was in the range of that typically observed in marine sediments (Liu et al., 2012), their distribution is distinct to what has been reported before: relative abundance of OB-GDGTs increase substantially in the hot sediments (Fig. V.5B) and absolute abundances of total branched GDGTs increased twofold at the high temperature sites Cathedral Hill compared to the other sites (Fig. V.5A), indicating *in situ* production of these compounds in Guaymas Basin hydrothermal sediments. Spearman rank's correlation confirmed that OB-GDGT positively correlates to temperatures, while the other three (brGDGT, SB-GDGT and IB-GDGT) have either negative or no correlation with temperature (Fig. V.6B). We interpret this to indicate *in situ* production of OB-GDGTs possibly by thermophilic bacteria especially adapted to the prevailing environmental conditions.

Interestingly, relative abundances of OB-GDGTs were also correlated with GMGT lipids (Fig. V.6B), tentatively suggesting a close relationship between their source organisms. The increased degree of methylation of branched GDGTs was previously suggested to be a microbial adaptation to increasingly harsh redox conditions (Liu et al., 2014), whereas our results suggest their distribution may also be controlled by temperature.

V.4.6. Imprint of benthic activity on the core lipid pool

In non-seep marine sediments where microbial activities are not as high, a large fraction of the detected core GDGTs (and sometimes intact GDGTs) are derived from detrital material of planktonic Thaumarchaeota. These GDGTs are actively applied in paleoenvironmental studies, most prominently using the TEX_{86} paleothermometer, which is based on the observation that Thaumarchaeota change the ring distribution in GDGTs dependent on growth temperature thereby reflecting sea surface temperatures (SST) (see method, Eq. 2-4; Schouten et al., 2002; Kim et al., 2010).

To evaluate to what extent the active sedimentary microbes affect the detrital water column signal that would be reflective of sea surface temperature we compared the calculated SST from the core lipid GDGT distribution using adapted TEX_{86}^{H} (Kim et al., 2010) with the actual satellite-derived annual mean SSTs of the Guaymas Basin (https://www.ospo.noaa.gov/Products/ocean/sst/contour/). As shown in Fig. V.7A, sites Aceto Balsamico, Northern Tower Site 2 and Site 3 exhibited similar ranges of TEX_{86} around 0.5 which all correspond to lower temperatures than the satellite-derived annual mean SST of ca. 20 °C. In contrast, TEX_{86} values of AOM-impacted Octopus Mound, Ultra Mound and less affected Cathedral Hill where as high or higher than the satellite-derived annual mean SST. Deviations of the calculated TEX86 compared

to the measured values can be best explained by benthic production of GDGTs that overprint a detrital water column signal. The low TEX_{86} values in the two cool sites (Aceto Balsamico, Northern Tower Site 2) and the hot Northern Tower Site 3 are mainly governed by the comparably low abundances of cyclic GDGTs compared to the other sites. As was recently suggested by Zhou et al. (2019) the lower amounts of cyclic GDGTs may indicated benthic communities that are thriving at optimal conditions. Notably, ring distributions of intact 1G- and 2G-GDGT lipids show some differences to those of core GDGTs as can be seen by deviations in the calculated ring indices (Supp. Fig. V.5). While this indicates that the core lipid GDGTs represent a mixture of detrital and benthic sources a general trend of increasing ring indices from cold to hot sites for all GDGT species does indicate a significant benthic imprint. While the average ring index values calculated for GDGT-1 to GDGT-4 core lipids were positively and significantly correlated with temperature (Table V.2), the average ring indices for 1G-GDGT showed no correlation and a negative correlation for 2G-GDGT indicating that temperature is not the sole factor in governing ring distributions. For instance, the higher TEX_{86} values (and comparably higher ring indices of the intact GDGTs) at Octopus Mound are reflective of the higher amounts of GDGT-2 present in these sediments due to the activity ANME-1 archaea involved in AOM, while the elevated TEX_{86} values at Ultra Mound and Cathedral Hill can be assigned to the decreased amounts of the crenarchaeol isomer and increased amounts of GDGT-1 to GDGT-3 at these sites due to the *in situ* sedimentary input by thermophilic archaea. Overall these results indicate that benthic GDGT production largely overprints a water column derived past planktonic signal.

The methane index (MI; see method, Eq. 5) was designed to identify the presence of AOM activity in methane-rich sediments by considering the contribution of GDGT-1 to GDGT-3 as diagnostic ANME-1 markers to the overall GDGT pool (Zhang et al., 2011). It was concluded that above a MI of 0.5 TEX_{86} should not be used as above this value sedimentary *in situ* production significantly overprints the water column-derived signal. As expected, Aceto Balsamico, Nortern Tower Site 2 and Site 3 exhibited rather low MI (< 0.3; Fig. V.7B), indicating insignificant contributions of ANME GDGTs. Whereas MI at Octopus Mound peaked to a value of above 0.4 at depth 5 cm, which was within the active AOM zone, indicating sedimentary input of GDGT-2 and GDGT-1 by methanotrophic archaea as discussed in 4.2. In addition, extraordinarily high MI values were observed at the hot sites Ultra Mound and Cathedral Hill, out of which only Ultra Mound was AOM impacted. These high MI values are not only caused by the increase in the number of rings, mainly GDGT-2 and GDGT-3 (GDGT-4 is not considered in the MI) due to increasing contribution of thermophilic archaeal groups, but is mainly a result of the insignificant amounts of crenarchaeol at greater depths at these sites.

Finally we looked into the branched and isoprenoid tetraether (BIT; see method, Eq. 6) index, typically used to assess the input of terrestrial organic material into marine sediments (Hopmans et al., 2004). As

shown in Fig. V.7C, BIT was consistently low in cool and warm sediments from Octopus Mound, Northern Tower Site 2 and Aceto Balsamico (< 0.02), but increased with depth and reached maximal values of 0.1 to 0.3 in hydrothermally-heated sediments. This is analog to observations from the Eastern Lau Spreading Center sediments (Hu et al., 2012), where BIT values were also higher in hydrothermally heated sediments than less affected sediments, supporting the notion that brGDGTs have *in situ* sources in hydrothermal sediments.

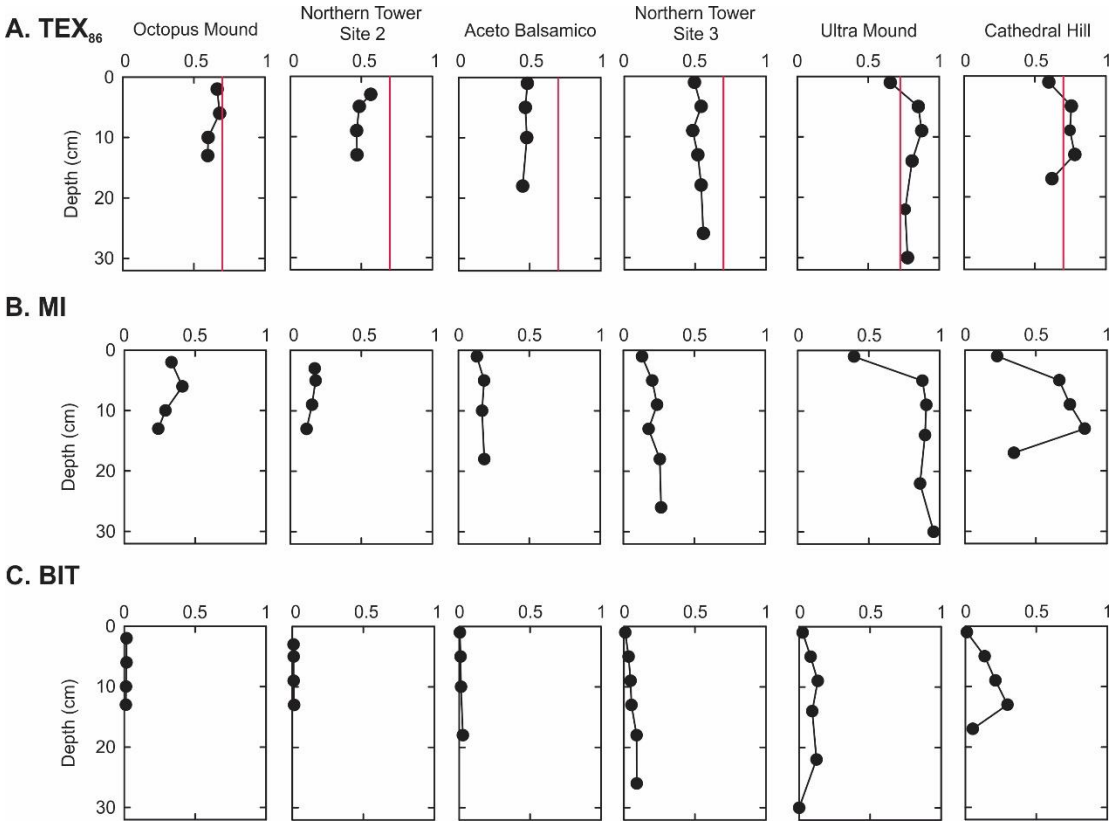

Figure V.7. Calculated indices based on tetraether lipid distribution at the six studied sites. A. TEX86, red line indicates TEX86 values calculated based on satellite-derived annual mean SST (ca. 20 °C) of the Guaymas Basin; B. Methane index (MI); C. Branched and isoprenoid tetraether (BIT) index.

V.5. CONCLUSION

We analyzed microbial intact and core ether lipids from hydrothermal sediments of Guaymas Basin with the aim to evaluate the impact of elevated temperature on lipid composition and to identify lipid signatures related to microbial degradation of methane and C_{2+} hydrocarbons. In cooler and more oxidized surface sediments ANME-2 diagnostic archaeol-based IPL biomarkers dominated whereas ANME-1 diagnostic 2G-GDGTs with GDGT-1 and GDGT-2 core lipids increased in abundance at greater depth. This habitat zonation of ANME communities is well known from other cold seep settings and reflects the affinity of ANME-2 archaea to thrive in more energy-rich environments while ANME-1 communities are better

adapted to low energy environments. With increasing temperature GDGT core lipid compositions shift to a dominance of GDGT-4 both in the IPL and core lipid pools, which we interpret as increased contribution of thermophilic ANME-1. In addition, the abundance of 1G-GMGT with 0 to 4 rings increased substantially in hydrothermally heated sediments, indicating *in situ* production of yet unknown thermophilic archaeal groups. We suggest that some of them are involved in anaerobic C_{2+} hydrocarbon degradation as evidenced by geochemical profiles and lipid distribution in cultured enrichments.

In general, temperature seems to be the primary controlling factor on the distribution and composition of microbial ether lipids. Strong correlations of GMGT-based lipids having up to eight cyclopentane rings with temperature were observed. This is consistent with previous findings that suggested higher cyclization to reduce membrane fluidity and proton permeability, while the extra covalent bond between the two alkyl chains in GMGT may further strengthen cell membranes to withstand thermal stress. We also observed a temperature dependency of bacterially sourced branched GDGTs, indicating *in situ* production of these compounds in hydrothermal sediments. Notable, the number of methylations in the alkyl chains seems to play an important role during adaptation to temperature as relative and absolute abundances of OB-GDGTs increased with temperature. This mirrors observations made for methylations added in GMGT ether lipids, which were speculated to also reduce ion permeability at high temperatures. Notable amounts of GMD and H-tetrols with 80 to 82 rings were present in hydrothermally heated sediments and further support a link of previously observed H-shaped tetraacids to thermophilic archaea.

ACKNOWLEDGEMENTS

Samples for this research were provided by the cruise AT37-06 (R/V Atlantis) which was supported by NSF Biological Oceanography grant 1357238 to Andreas Teske We deeply appreciate the crew and scientists for their support with sample collection. Julius S. Lipp, Jenny Wendt and Xavier Prieto-Mollar are thanked for substantial instrumental and technical support. Matthias Kellermann is acknowledged for providing the lipid analysis data for the ANME-SRB enrichments. This study was supported by the Cluster of Excellence (Deutsche Forschungsgemeinschaft DFG), through MARUM-Center for Marine Environmental Sciences, and the GLOMAR graduate school (to Min Song). Min Song is sponsored by the China Scholarship Council (CSC).

SUPPLEMENTARY INFORMATION

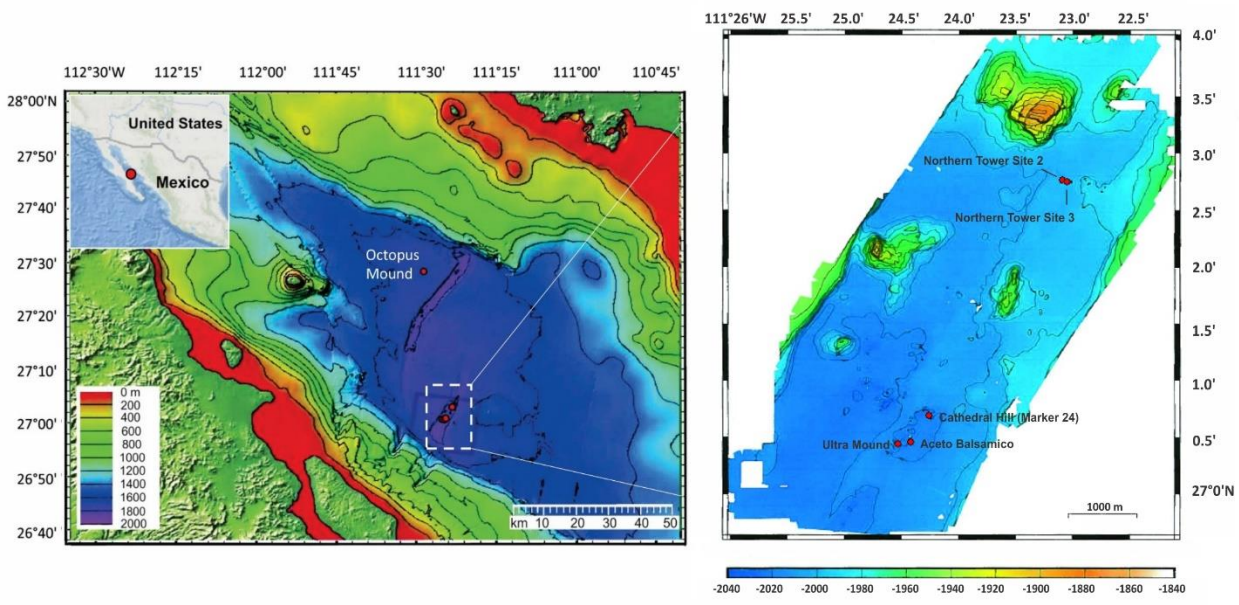

Supplementary Figure V.1. Sampling locations of the six sediment cores collected for this study in the Guaymas Basin.

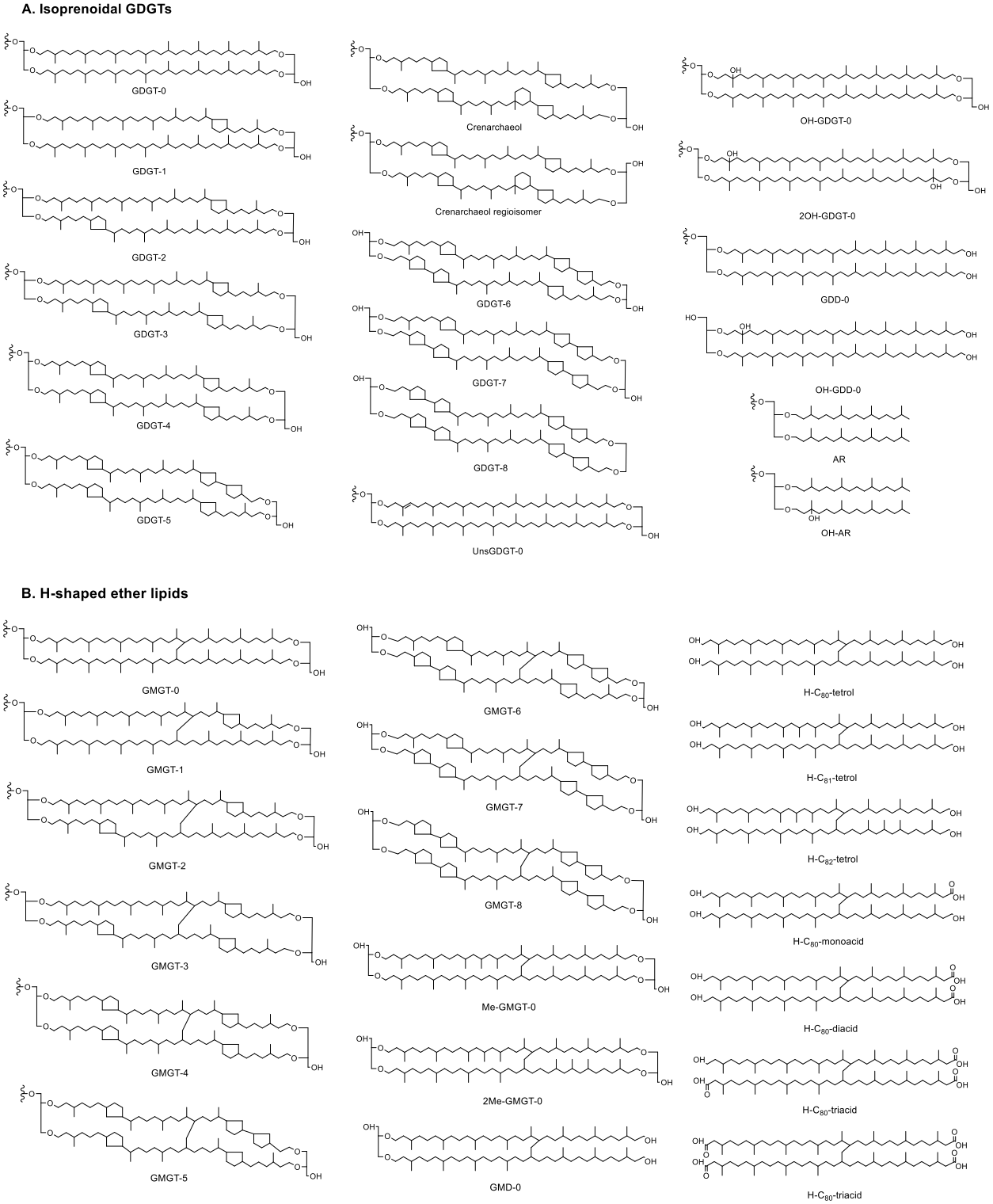
A. Isoprenoidal GDGTs
GDGT-0
GDGT-1
GDGT-2
GDGT-3
GDGT-4
GDGT-5
Crenarchaeol
Crenarchaeol regioisomer
GDGT-6
GDGT-7
GDGT-8
UnsGDGT-0
OH-GDGT-0
2OH-GDGT-0
GDD-0
OH-GDD-0
AR
OH-AR
B. H-shaped ether lipids
GMGT-0
GMGT-1
GMGT-2
GMGT-3
GMGT-4
GMGT-5
GMGT-6
GMGT-7
GMGT-8
Me-GMGT-0
2Me-GMGT-0
GMD-0
H-C80-tetrol
H-C81-tetrol
H-C82-tetrol
H-C80-monoacid
H-C80-diacid
H-C80-triacid
H-C80-triacid
C. Head groups
Phosphatidylglycerol (PG-)
Monoglycosidic (1G-)
Diglycosidic (2G-)

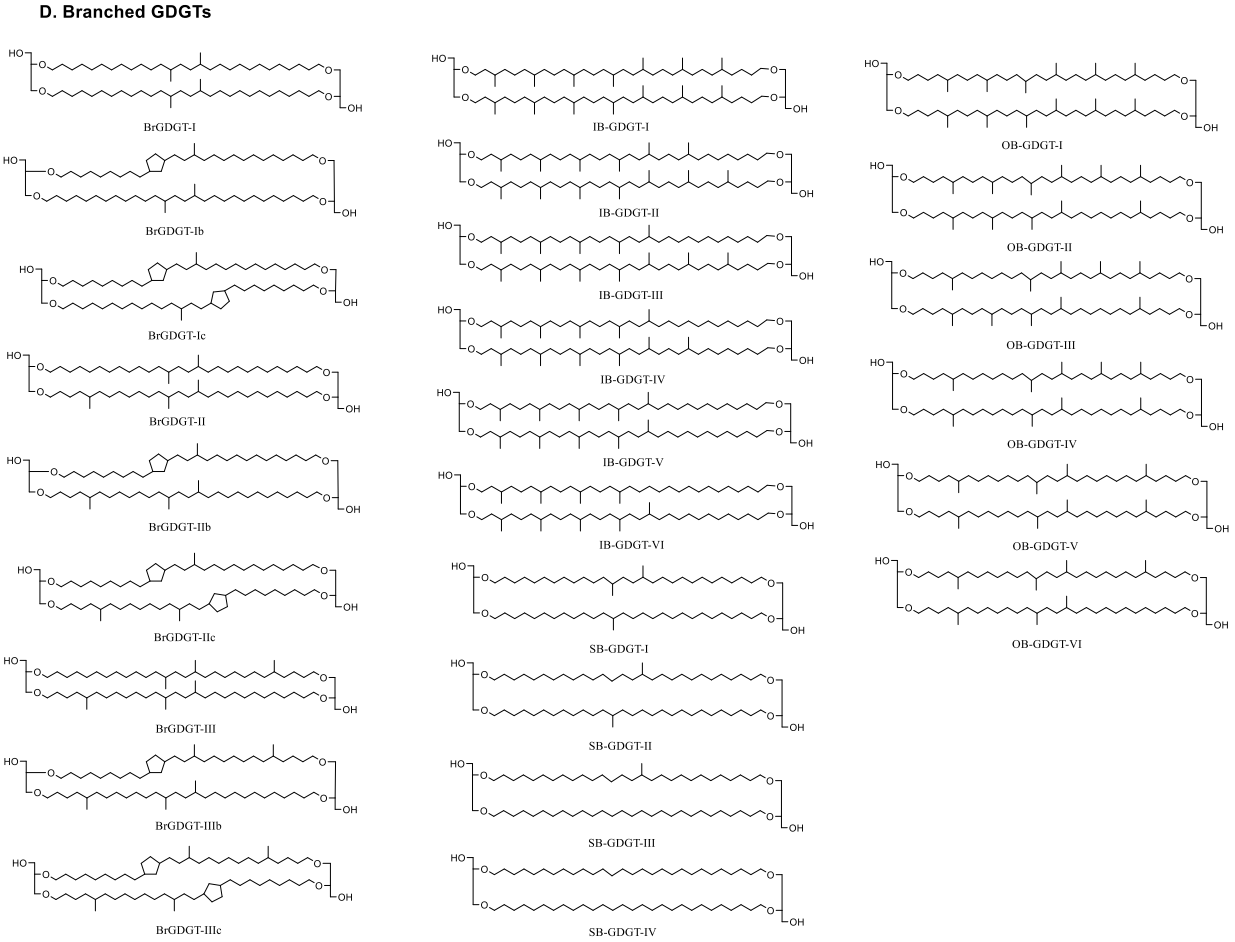

Supplementary Figure V.2. Structures of ether lipids. A. Isoprenoidal GDGTs; B. H-shaped ether lipids; C. Head groups for corresponding IPLs; D. Branched GDGTs.

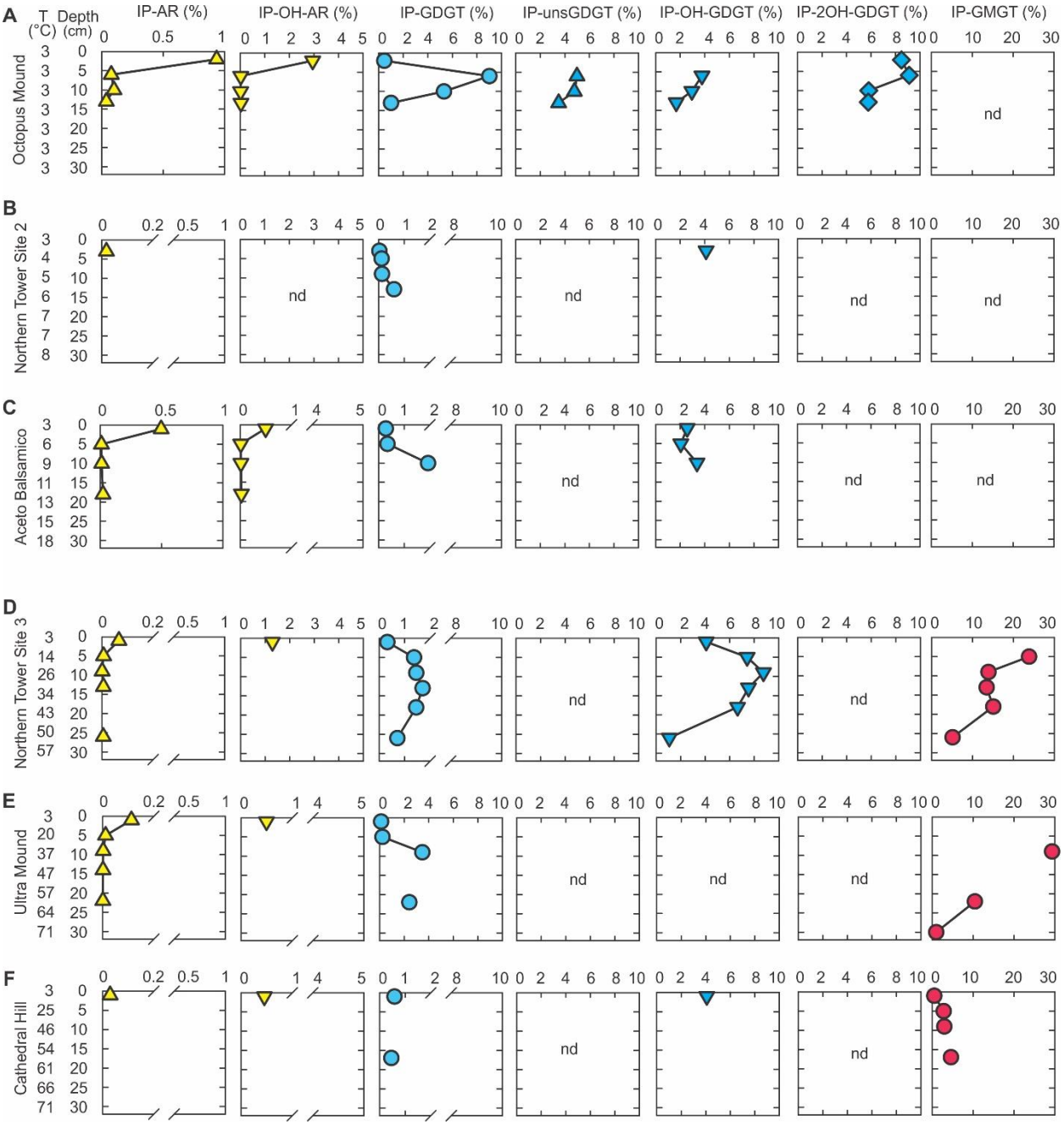

Supplementary Figure V.3. Abundance ratios of IPL/(IPL+CL) for individual lipids, grouped according to studied sites (A-F); nd, not detected.

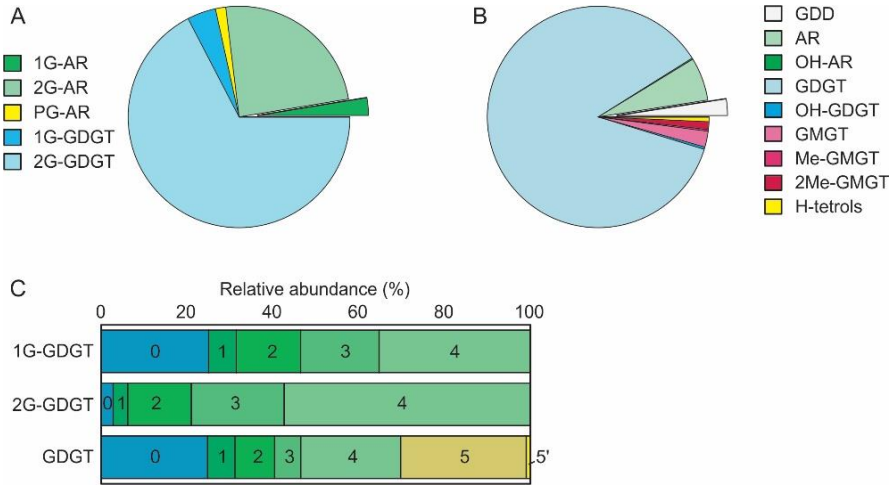

Supplementary Figure V.4. Archaeal lipid composition of ANME-1/HotSeep-1 enrichment culture isolated from Guaymas Basin sediments by Holler et al. (2011). A. Relative abundance of IPLs; B. Relative abundance core lipids; C. Relative abundance of 1G-, 2G- and core GDGTs; numbers refer to cyclopentane rings in GDGT. The culture was grown at 50 °C. Apart from the afore described core GDGTs (Holler et al., 2011), the lipid extract was re-analyzed and additional intact and core lipids are shown here. Abundance ratio of IPL/(IPL+CL) is 12.5%.

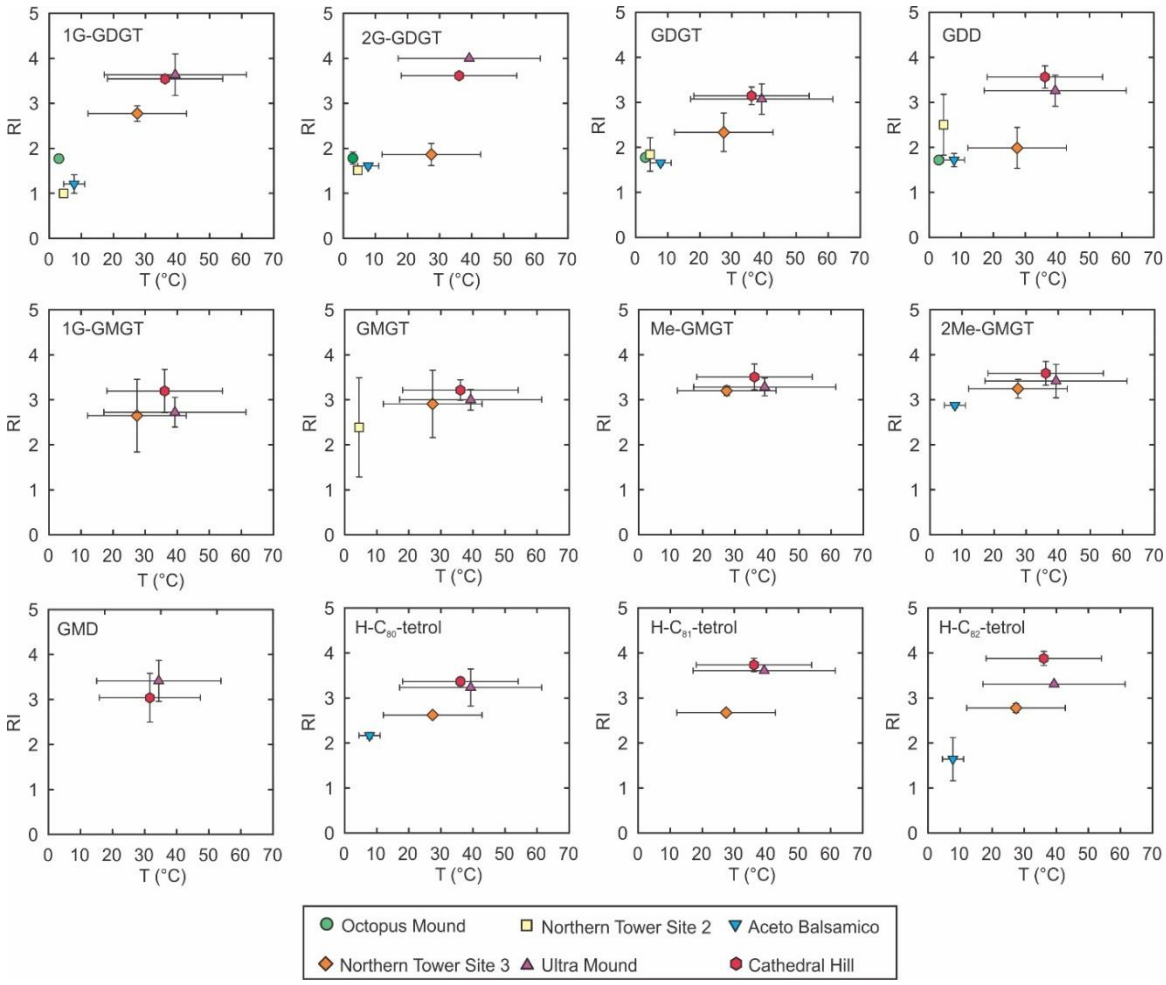

Supplementary Figure V.5. Averaged ring index of lipids with 1 to 4 cyclopentane rings with averaged temperatures in the six studied sediment cores. Error bars: mean±SD.

Supplementary Table V.1. Ring numbers of IPLs detected in the six studied sites.

Site	Depth (cm)	1G-GDGT	2G-GDGT	PG-GDGT	1G-OH-GDGT	2G-OH-GDGT	1G-2OH-GDGT	1G-GDD	1G-GMGT	2G-GMGT
Octopus Mound	2	0-3, 5	2	-	-	-	0	-	-	-
	6	0-3, 5	1, 2	2, 3	0	0-2	0	-	-	-
	10	0-3, 5	1, 2	-	0	0, 1	0	-	-	-
	13	0-3, 5	1, 2	-	0	0, 1	0	-	-	-
Northern Tower Site 2	3	0, 1, 5	0-2	3	-	0-2	-	-	-	-
	5	0, 5	-	-	-	-	-	-	-	-
	9	0, 5	-	-	-	-	-	-	-	-
	13	0, 1, 5	-	-	-	-	-	-	-	-
Aceto Balsamico	1	0-3, 5	1, 2	-	0	0-2	-	-	-	-
	5	0, 5	1, 2	-	-	0-2	-	-	-	-
	10	0, 1, 5	-	-	0, 1	0-2	-	-	0	-
	18	-	-	-	-	-	-	-	-	-
Northern Tower Site 3	1	0, 1, 4, 5	1, 2	-	0	0-2	-	-	-	-
	5	0-5	1-3	-	0-2	0-2	-	-	0-2, 4	0-3
	9	0-5	1, 2, 4	-	0-2	-	-	-	0-2, 4	-
	13	0-5	-	-	0-2	-	-	-	0, 1, 4	-
	18	0-5	-	-	0-2	-	-	-	0-2	-
	26	0-5	-	-	0, 1	-	-	-	0	-
Ultra Mound	1	0, 4	-	-	-	-	-	-	-	-
	5	0, 4	-	2-4	-	-	-	-	-	-
	9	0-4	0, 4	0-4	-	-	-	-	0-4	3
	14	-	-	-	-	-	-	-	-	-
	22	0, 3, 4	-	-	-	-	-	-	1-4	-
	30	-	-	-	-	-	-	-	0, 2, 4	-
Cathedral Hill	1	0, 1, 4, 5	0, 2, 4	3, 4	-	0, 1	-	0	0, 4	-
	5	-	-	-	-	-	-	3-5	0-2, 4	-
	9	-	-	-	-	-	-	0	1, 2, 4	-
	13	-	-	-	-	-	-	0	-	-
	17	0, 5	-	-	-	-	-	0	0-5	-

Supplementary Table V.2. Ring numbers of core ether lipids detected in the six studied sites.

Site	Depth (cm)	GDGT	OH-GDGT	2OH-GDGT	GDD	OH-GDD	GMGT	Me-GMGT	2Me-GMGT	GMD	H-C_{80}-tetrol	H-C_{81}-tetrol	H-C_{82}-tetrol
Octopus Mound	2	0-4, cren, cren'	0-2	0	0-2, 5	0-2	-	-	-	-	-	-	-
	6	0-4, cren, cren'	0-2	0, 5	0-3, 5	0-3	-	-	-	-	-	-	-
	10	0-4, cren, cren'	0-2	0, 5	0-5	0-3, 5	-	-	-	-	-	-	-
	13	0-4, cren, cren'	0-3	0, 5	0-2, 4, 5	0-3	-	-	-	-	-	-	-
Northern Tower Site 2	3	0-4, 6, cren, cren'	0-3	0, 5	0, 1, 4, 5	0-3	0, 2-4, 6	-	4	4	0-4, 6	2-5	
	5	0-4, cren, cren'	0-2	0, 5	0-5	0-3	0	-	-	-	-	-	-
	9	0-4, cren, cren'	0-2	0, 5	0-5	0-2	0-2, 5	-	-	-	-	-	-
	13	0-4, cren, cren'	0-2	5	0-3	0-2	-	-	-	-	-	-	-
Aceto Balsamico	1	0-4, cren, cren'	0-3	0, 5	0-2, 5	0-3	-	-	-	-	0	-	-
	5	0-4, cren, cren'	0-3	0, 5	0-2, 4, 5	0-4	-	-	-	-	0	0	0, 1
	10	0-5, cren, cren'	0-3	0, 5	0-2, 4, 5	0-3	-	-	0, 1, 4	-	0-4	0, 1	0-3
	18	0-5, 7, 8, cren, cren'	0-2	0, 5	0-5	0-3	0, 4	0, 3, 4, 5	0-2, 4, 5	-	0-2, 4	0	0-4
Northern Tower Site 3	1	0-4, cren, cren'	0-3	0, 5	0-2, 5	0-3	0-2, 5	-	-	-	0-6	0-7	-
	5	0-8, cren, cren'	0-3	0, 5	0-5	0-3	0-8	0-8	0-8	0	0-6	0-7	0-7
	9	0-8, cren, cren'	0-3	0, 5	0-5	0-3	0-8	0-8	0-8	-	0-6	0-7	0-6
	13	0-8, cren, cren'	0-2	0, 5	0-2, 4, 5	0-2	0-7	0-7	0-7	-	-	-	-
	18	0-8, cren, cren'	0-2	0, 5	0-5	0-2	0-7	0-7	0-7	-	-	-	-
	26	0-8, cren, cren'	0-3	0, 5	0-5	0-2	0-6	0-7	0-7	-	-	-	-
Ultra Mound	1	0-4, cren, cren'	0-2	-	0-5	0-2	0-4, 6	0-5	0-6	0-4	0-4	-	3-7
	5	0-5, cren, cren'	0-2	-	0-5	0-2	0-4, 6-8	2-4	4	4	0-5	2-4	3-7
	9	0-5, cren, cren'	0-4	0	0-5	0-2	0-8	1-7	0, 2-6	0, 4	0-6	2-5	3-7
	14	0-5, cren, cren'	-	-	0-5	-	0-8	0-7	0-6	0, 1, 3, 4, 6	-	-	-
	22	0-5, cren, cren'	-	-	0-5	-	0-8	0-7	0-7	0-4	0-4	-	-
	30	0-5, cren, cren'	-	-	0, 3, 4	-	0-8	0-7	1-7	0, 1, 4	4	-	-
Cathedral Hill	1	0-5, cren, cren'	0-3	0, 5	0, 3-5	0-2	0-8	4-6	4-6	0-8	0-8	4-7	0, 3-8
	5	0-8, cren, cren'	0-2	0, 5	0-6	0	0-8	0-8	0-8	0-8	0-8	0-7	1, 3-8
	9	0-6, 8, cren, cren'	0, 1	-	0, 1, 3, 4	0	0-8	0-8	2-7	0-3, 6-8	0-8	0-7	4-8
	13	0-7, cren, cren'	1	-	0-5	-	0-8	0-8	0-7	0-8	0-8	0-4, 6, 7	4-8
	17	0-6, cren, cren'	0-2	-	0-5	0-2	0-8	0-7	0-7	0-7	0-7	3-6	4-7

CHAPTER VI
Conclusion and Outlook

VI.1. CONCLUSION

The overall objective of this thesis is to understand the sources and sinks of hydrocarbon gases in cold and hot seep sediments and to explore lipid signatures of microorganisms involved in their cycling. I investigated two contrasting seep systems of the cold, methane-dominated US Atlantic Margin (USAM) and the hot, higher hydrocarbon-impregnated Guaymas Basin sediments.

At the Guaymas Basin, we investigated the cycling of methane and higher hydrocarbon gases and found that at higher temperatures where hydrothermal heating inhibits microbial activity, methane had isotopic signatures that confirmed a thermogenic origin as previously suggested, while higher hydrocarbon gases exhibited an unusual isotope pattern of $\delta^{13}C$ ethane > $\delta^{13}C$ propane > $\delta^{13}C$ *n*-butane > $\delta^{13}C$ *n*-pentane. As this pattern cannot be explained by thermogenic or known abiotic formation pathways, we hypothesized that an alternative formation pathway of abiotic reduction of volatile fatty acids can lead to the observed isotope pattern for these hydrocarbons. We confirmed this hypothesis by hydrous pyrolysis experiments and Gibbs free energy computations. Experiments with addition of isotopically labeled substrates at 350 °C and 400 bar demonstrated (i) the exchange of carboxyl carbon of volatile fatty acids with ^{13}C-bicarbonate and (ii) the formation of ^{13}C-enriched ethane and propane by the reduction of 2-^{13}C-acetate, where formation of either compound appears to be governed by the abundance of H_2. Gibbs free energy computations indicate that reduction of acetate to ethane is indeed exergonic under environmental conditions of the Guaymas Basin subsurface (Chapter III).

At the USAM, we examined the biogeochemical mechanisms that regulate the transfer of methane in the subsurface sediments. We used archaeal and bacterial IPL biomarkers as the tool to evaluate microbial imprint and community structure in methane-laden and methane-free sediments and combined these analyses with statistical evaluations to determine IPL assignments to different phylogenetic groups and/or environmental parameters. The diversity and abundance of microbial IPLs in the studied sediment samples

are closely linked to the *in situ* microbial community composition and well-constrained by methane flux and organic carbon content. (i) A site with high methane flux was dominated by ANME-diagnostic biomarkers including 1G- and 2G-GDGTs with 0 to 2 rings and glycosidic and phosphate-based archaeol and hydroxyarchaeols. (ii) At a setting with lower methane flux and high organic matter content where heterotrophic processes prevailed over methanotrophy, the recently identified glycosidic BDGT and PDGT were more abundant in the archaeal lipid pool, these lipids were closely related to benthic archaeal groups including MCG, MBG-B and Thermoprofundales/DHVEG-1. (iii) Additionally, unsaturated GDGTs with 1G and 2G head groups correlated with distinct organisms, while the 2G-unsGDGT were affiliated with methanotrophic groups as suggested previously, 1G-unsGDGT correlated with Hadesarchaea, which were most abundant in low methane flux and low organic carbon containing sediments. Moreover, we showed that the bacterial sourced phospholipids PE-DAG, PE-AEG and DPG were particularly abundant in sulfate-reducing sediments and thus have diagnostic potential for the detection of AOM-associated sulfate-reducing bacteria. (i) Hereby, PE-AEG is the most specific biomarker for AOM-associated SRB. (ii) PME-DAG and DEG lipids showed closest associations to processes involved in methanogenic organic matter degradation. (iii) PE-DEG lipids increased in abundance with depth while DAG-based lipids decreased showing correlations with Chloroflexi members and other heterotrophic phylogenetic groups, indicating that the biosynthesis of ether lipids may be a prominent adaptive process of bacteria living in the deep biosphere (Chapter IV).

A further study explored the consumption of methane and higher hydrocarbon gases in Guaymas Basin hydrothermal sediments with temperatures that are more susceptible to microbial activity. In near surface sediments with temperatures up to 70 °C where highly diverse microbial communities occur (as evidenced by extensive microbial mats), we found isotopic enrichments in C_1 to C_5 gases pointing to active microbial oxidation of these hydrocarbons. We consequently sought to identify lipid biomarkers related to these processes, and to examine the impact of heat stress on microbial ether lipid composition in these sediments. Our results showed (i) ANME-2 diagnostic archaeol-based IPL biomarkers dominated in cooler and more oxidized surface sediments, whereas ANME-1 diagnostic 2G-GDGTs with GDGT-1 and GDGT-2 core lipids increased in abundance at greater depth. (ii) Thermophilic ANME-1 biomarker 2G-GDGT-4 increased in samples with higher temperatures. (iii) 1G-GMGT with 0 to 4 rings increased substantially in hydrothermally heated sediments, indicating *in situ* production of yet unknown thermophilic archaeal groups and potentially those that were involved in anaerobic C_{2+} hydrocarbon degradation. In general, the succession of GDGT-based lipids to GMGT-based lipids, and higher degree of cyclization in both lipid pools with increasing temperature suggests temperature may be the primary controlling factor on the distribution and composition of microbial ether lipids. Higher degrees of cyclization can reduce membrane

fluidity and proton permeability, while the extra covalent bond between the two alkyl chains of GMGT may further strengthen cell membranes to withstand thermal stress. We also observed a temperature dependency of bacterially sourced branched GDGTs, particularly those with multiple methyl branches, indicating *in situ* production of these compounds in hydrothermal sediments (Chapter V).

VI.2. OUTLOOK

Collectively, this thesis presents an alternative formation pathway for higher hydrocarbon gases in the organic-rich hydrothermal sediments of the Guaymas Basin (Chapter III). This process may be widespread under organic-rich geothermal conditions and could impact isotopic compositions of hydrocarbon gases in sediments and petroleum systems. For future studies it would be interesting to also test the reduction of other short-chain organic acids, i.e., propionate, *n*-butyrate, *n*-valerate using hydrous pyrolysis experiments. An additional experiment without the addition of sediment could provide more information on the reactions of organic acids reduction to corresponding hydrocarbons.

Secondly, this thesis showed that different membrane lipid patterns are related to the anaerobic degradation of methane and higher hydrocarbons under cold, methane-dominated seep sediments and hot, higher hydrocarbon-impregnated hydrothermal sediments. These results refine the applicability of polar membrane lipid biomarkers as tracers of *in situ* microbial communities and/or processes (Chapter IV and V). Further 16S rRNA gene analysis in the sediments of the Guaymas Basin combined with isotope analyses of the unassigned lipids, such as GMGT and OB-GDGT, will shed further light on their sources and function in the environment (Chapter V).

To further elucidate microbial membrane lipid adaptation in response to energy or heat stress (Chapter V), it should be kept on mind that lipid does not function as a single compound in a living cell, but as a membrane functioning and interacting with many other lipid species and membrane components such as proteins, carbohydrates etc. Therefore, techniques such as microscopy and spectroscopy (cf. Lingwood and Simons, 2010) would be promising to reveal dynamic nanoassemblies and functions of membrane lipids in living cells. At the same time, a better understanding on microbial membrane lipid adaptation in response to environmental change can also be obtained by laboratory experiments in isolated cultures, through stable-isotope-probing experiments under controlled temperatures and substrate additions. These techniques can substantially assist in interpreting environmental data.

CHAPTER VII

References

Adam, P.S., Borrel, G., Brochier-Armanet, C. and Gribaldo, S. (2017) The growing tree of Archaea: new perspectives on their diversity, evolution and ecology. The ISME journal 11, 2407-2425.

Adams, M.M., Hoarfrost, A.L., Bose, A., Joye, S.B. and Girguis, P.R. (2013) Anaerobic oxidation of short-chain alkanes in hydrothermal sediments: potential influences on sulfur cycling and microbial diversity. Frontiers in microbiology 4.

Aepfler, R.F., Bühring, S.I. and Elvert, M. (2019) Substrate characteristic bacterial fatty acid production based on amino acid assimilation and transformation in marine sediments. FEMS microbiology ecology 95, fiz131.

Aromokeye, D.A., Kulkarni, A.C., Elvert, M., Wegener, G., Henkel, S., Coffinet, S., Eickhorst, T., Oni, O.E., Richter-Heitmann, T. and Schnakenberg, A. (2020) Rates and microbial players of iron-driven anaerobic oxidation of methane in methanic marine sediments. Frontiers in Microbiology 10, 3041.

Barnes, R. and Goldberg, E. (1976) Methane production and consumption in anoxic marine sediments. Geology 4, 297-300.

Batushansky, A., Toubiana, D. and Fait, A. (2016) Correlation-based network generation, visualization, and analysis as a powerful tool in biological studies: a case study in cancer cell metabolism. BioMed research international 2016.

Beal, E.J., House, C.H. and Orphan, V.J. (2009) Manganese-and iron-dependent marine methane oxidation. Science 325, 184-187.

Beaulieu, S.E., Baker, E.T. and German, C.R. (2015) Where are the undiscovered hydrothermal vents on oceanic spreading ridges? Deep Sea Research Part II: Topical Studies in Oceanography 121, 202-212.

Beaulieu, S.E., Baker, E.T., German, C.R. and Maffei, A. (2013) An authoritative global database for active submarine hydrothermal vent fields. Geochemistry, Geophysics, Geosystems 14, 4892-4905.

Becker, K.W. (2015) Biogeochemical significance and biomarker potential of novel glycerolipids and respiratory qinones in the marine environment, Am Fachbereich Geowissenschaften der Universität Bremen, Bremen.

Becker, K.W., Collins, J.R., Durham, B.P., Groussman, R.D., White, A.E., Fredricks, H.F., Ossolinski, J.E., Repeta, D.J., Carini, P. and Armbrust, E.V. (2018) Daily changes in phytoplankton lipidomes reveal mechanisms of energy storage in the open ocean. Nature communications 9, 5179.

Becker, K.W., Elling, F.J., Yoshinaga, M.Y., Söllinger, A., Urich, T. and Hinrichs, K.-U. (2016) Unusual butane-and pentanetriol-based tetraether lipids in Methanomassiliicoccus luminyensis, a representative of the seventh order of methanogens. Applied and environmental microbiology 82, 4505-4516.

Becker, K.W., Lipp, J.S., Zhu, C., Liu, X.-L. and Hinrichs, K.-U. (2013) An improved method for the analysis of archaeal and bacterial ether core lipids. Organic Geochemistry 61, 34-44.

Benveniste, P. (1986) Sterol biosynthesis. Annual review of plant physiology 37, 275-308.

Bernard, B.B., Brooks, J.M. and Sackett, W.M. (1976) Natural gas seepage in the Gulf of Mexico. Earth and Planetary Science Letters 31, 48-54.

Biastoch, A., Treude, T., Rüpke, L.H., Riebesell, U., Roth, C., Burwicz, E.B., Park, W., Latif, M., Böning, C.W. and Madec, G. (2011) Rising Arctic Ocean temperatures cause gas hydrate destabilization and ocean acidification. Geophysical Research Letters 38.

Biddle, J.F., Cardman, Z., Mendlovitz, H., Albert, D.B., Lloyd, K.G., Boetius, A. and Teske, A. (2012) Anaerobic oxidation of methane at different temperature regimes in Guaymas Basin hydrothermal sediments. The ISME journal 6, 1018-1031.

Biddle, J.F., Lipp, J.S., Lever, M.A., Lloyd, K.G., Sørensen, K.B., Anderson, R., Fredricks, H.F., Elvert, M., Kelly, T.J. and Schrag, D.P. (2006) Heterotrophic Archaea dominate sedimentary subsurface ecosystems off Peru. Proceedings of the National Academy of Sciences of the United States of America 103, 3846-3851.

Bižić, M., Klintzsch, T., Ionescu, D., Hindiyeh, M., Günthel, M., Muro-Pastor, A., Eckert, W., Urich, T., Keppler, F. and Grossart, H.-P. (2020) Aquatic and terrestrial cyanobacteria produce methane. Science Advances 6, eaax5343.

Boetius, A., Ravenschlag, K., Schubert, C.J., Rickert, D., Widdel, F., Gieseke, A., Amann, R., Jørgensen, B.B., Witte, U. and Pfannkuche, O. (2000) A marine microbial consortium apparently mediating anaerobic oxidation of methane. Nature 407, 623-626.

Borcard, D., Gillet, F. and Legendre, P. (2018) Numerical ecology with R. Springer.

Borrel, G., Adam, P.S., McKay, L.J., Chen, L.-X., Sierra-García, I.N., Sieber, C.M., Letourneur, Q., Ghozlane, A., Andersen, G.L. and Li, W.-J. (2019) Wide diversity of methane and short-chain alkane metabolisms in uncultured archaea. Nature microbiology 4, 603-613.

Brothers, D.S., Ruppel, C., Kluesner, J., Brink, U., Chaytor, J.D., Hill, J.C., Andrews, B.D. and Flores, C. (2014) Seabed fluid expulsion along the upper slope and outer shelf of the US Atlantic continental margin. Geophysical Research Letters 41, 96-101.

Calvert, S. (1966) Accumulation of diatomaceous silica in the sediments of the Gulf of California. Geological Society of America Bulletin 77, 569-596.

Cardman, Z. (2014) Active Prokaryotic Communities Along a Thermally and Geochemically Variable Transect in Guaymas Basin Hydrothermal Sediments.

Chen, S.-C., Musat, N., Lechtenfeld, O.J., Paschke, H., Schmidt, M., Said, N., Popp, D., Calabrese, F., Stryhanyuk, H. and Jaekel, U. (2019) Anaerobic oxidation of ethane by archaea from a marine hydrocarbon seep. Nature, 1.

Chung, H., Gormly, J. and Squires, R. (1988) Origin of gaseous hydrocarbons in subsurface environments: theoretical considerations of carbon isotope distribution. Chemical Geology 71, 97-104.

Claypool, G.E. and Kvenvolden, K.A. (1983) Methane and other hydrocarbon gases in marine sediment. Annual Review of Earth and Planetary Sciences 11, 299-327.

Clayton, C. (1991) Carbon isotope fractionation during natural gas generation from kerogen. Marine and petroleum geology 8, 232-240.

Cline, J.D. (1969) Spectrophotometric determination of hydrogen sulfide in natural waters 1. Limnology and Oceanography 14, 454-458.

Coffinet, S., Meador, T.B., Mühlena, L., Becker, K.W., Schröder, J., Zhu, Q.-Z., Lipp, J.S., Heuer, V.B., Crump, M.P. and Hinrichs, K.-U. (2019) Structural elucidation and environmental distributions of butanetriol and pentanetriol dialkyl glycerol tetraethers (BDGTs and PDGTs). Biogeosciences Discussions, 1-17.

Corliss, J.B., Dymond, J., Gordon, L.I., Edmond, J.M., von Herzen, R.P., Ballard, R.D., Green, K., Williams, D., Bainbridge, A. and Crane, K. (1979) Submarine thermal springs on the Galapagos Rift. Science 203, 1073-1083.

Cruse, A.M. and Seewald, J.S. (2006) Geochemistry of low-molecular weight hydrocarbons in hydrothermal fluids from Middle Valley, northern Juan de Fuca Ridge. Geochimica et cosmochimica acta 70, 2073-2092.

Cruse, A.M. and Seewald, J.S. (2010) Low-molecular weight hydrocarbons in vent fluids from the Main Endeavour Field, northern Juan de Fuca Ridge. Geochimica et Cosmochimica Acta 74, 6126-6140.

Curray, J., Moore, D., Aguayo, E., Aubry, M., Einsele, G., Fornari, D., Gieskes, J., Guerrero, J., Kastner, M. and Kelts, K. (1979) Leg 64 seeks evidence on development of basins. Geotimes 24, 18-20.

Curray, J.R. (1982) Initial Reports of the Deep Sea Drilling Project, Vol. 64 [Parts 1 and 2]: Covering Leg 64 of the Cruises of the Drilling Vessel" Glomar Challenger", Mazatlan, Mexico to Long Beach, California, December 1978-January 1979. US Government Printing Office.

Damsté, J.S.S., Hopmans, E.C., Pancost, R.D., Schouten, S. and Geenevasen, J.A. (2000) Newly discovered non-isoprenoid glycerol dialkyl glycerol tetraether lipids in sediments. Chemical Communications, 1683-1684.

Dando, P., Austen, M., Burke Jr, R., Kendall, M., Kennicutt, M., Judd, A., Moore, D., O'Hara, S., Schmalijohann, R. and Southward, A. (1991) Ecology of a North Sea pockmark with an active methane seep. Marine Ecology Progress Series, 49-63.

De Rosa, M., Esposito, E., Gambacorta, A., Nicolaus, B. and Bu'Lock, J.D. (1980) Effects of temperature on ether lipid composition of Caldariella acidophila. Phytochemistry 19, 827-831.

Deborah S. Kelley, John A. Baross, a. and Delaney, J.R. (2002) Volcanoes, Fluids, and Life at Mid-Ocean Ridge Spreading Centers. Annual Review of Earth and Planetary Sciences 30, 385-491.

Dembitsky, V.M. (1996) Betaine ether-linked glycerolipids: chemistry and biology. Progress in lipid research 35, 1-51.

Deming, J.W. and Baross, J.A. (1993) Deep-sea smokers: windows to a subsurface biosphere? Geochimica et Cosmochimica Acta 57, 3219-3230.

Dhillon, A., Lever, M., Lloyd, K.G., Albert, D.B., Sogin, M.L. and Teske, A. (2005) Methanogen diversity evidenced by molecular characterization of methyl coenzyme M reductase A (mcrA) genes in hydrothermal sediments of the Guaymas Basin. Appl. Environ. Microbiol. 71, 4592-4601.

Dick, J.M. (2019) CHNOSZ: Thermodynamic calculations and diagrams for geochemistry. Frontiers in Earth Science 7, 180.

Didyk, B.M. and Simoneit, B.R. (1989) Hydrothermal oil of Guaymas Basin and implications for petroleum formation mechanisms. Nature 342, 65.

Dombrowski, N., Teske, A.P. and Baker, B.J. (2018) Expansive microbial metabolic versatility and biodiversity in dynamic Guaymas Basin hydrothermal sediments. Nature communications 9, 4999.

Dowell, F., Cardman, Z., Dasarathy, S., Kellermann, M.Y., Lipp, J.S., Ruff, S.E., Biddle, J.F., McKay, L.J., MacGregor, B.J. and Lloyd, K.G. (2016) Microbial communities in methane-and short chain alkane-rich hydrothermal sediments of Guaymas Basin. Frontiers in microbiology 7.

Dunn, R.A. and Martinez, F. (2011) Contrasting crustal production and rapid mantle transitions beneath back-arc ridges. Nature 469, 198-202.

Einsele, G., Gieskes, J.M., Curray, J., Moore, D.M., Aguayo, E., Aubry, M.-P., Fornari, D., Guerrero, J., Kastner, M. and Kelts, K. (1980) Intrusion of basaltic sills into highly porous sediments, and resulting hydrothermal activity. Nature 283, 441.

Elferink, M.G., de Wit, J.G., Driessen, A.J. and Konings, W.N. (1994) Stability and proton-permeability of liposomes composed of archaeal tetraether lipids. Biochimica et Biophysica Acta (BBA)-Biomembranes 1193, 247-254.

Elling, F.J., Gottschalk, J., Doeana, K.D., Kusch, S., Hurley, S.J. and Pearson, A. (2019) Archaeal lipid biomarker constraints on the Paleocene-Eocene carbon isotope excursion. Nature communications 10.

Elling, F.J., Könneke, M., Nicol, G.W., Stieglmeier, M., Bayer, B., Spieck, E., de la Torre, J.R., Becker, K.W., Thomm, M. and Prosser, J.I. (2017) Chemotaxonomic characterisation of the thaumarchaeal lipidome. Environmental Microbiology 19, 2681-2700.

Elvert, M., Suess, E. and Whiticar, M.J. (1999) Anaerobic methane oxidation associated with marine gas hydrates: superlight C-isotopes from saturated and unsaturated C20 and C25 irregular isoprenoids. Naturwissenschaften 86, 295-300.

Etiope, G. and Schoell, M. (2014) Abiotic gas: atypical, but not rare. Elements 10, 291-296.

Evans, P.N., Parks, D.H., Chadwick, G.L., Robbins, S.J., Orphan, V.J., Golding, S.D. and Tyson, G.W. (2015) Methane metabolism in the archaeal phylum Bathyarchaeota revealed by genome-centric metagenomics. Science 350, 434-438.

Evans, T.W., Coffinet, S., Könneke, M., Lipp, J.S., Becker, K.W., Elvert, M., Heuer, V. and Hinrichs, K.-U. (2019) Assessing the carbon assimilation and production of benthic archaeal lipid biomarkers using lipid-RIP. Geochimica et Cosmochimica Acta.

Evans, T.W., Wörmer, L., Lever, M.A., Lipp, J.S., Lagostina, L., Lin, Y.-S., Jørgensen, B.B. and Hinrichs, K.-U. (2017) Size and composition of subseafloor microbial community in the Benguela upwelling area examined from intact membrane lipid and DNA analysis. Organic Geochemistry 111, 86-100.

Eze, M.O. (1991) Phase transitions in phospholipid bilayers: Lateral phase separations play vital roles in biomembranes. Biochemical Education 19, 204-208.

Forterre, P. (2015) The universal tree of life: an update. Frontiers in microbiology 6, 717.

Franks, S.G., Dias, R.F., Freeman, K.H., Boles, J.R., Holba, A., Fincannon, A.L. and Jordan, E. (2001) Carbon isotopic composition of organic acids in oil field waters, San Joaquin Basin, California, USA. Geochimica et Cosmochimica Acta 65, 1301-1310.

Fulco, A.J. (1983) Fatty acid metabolism in bacteria. Progress in Lipid Research 22, 133-160.

Geilert, S., Hensen, C., Schmidt, M., Liebetrau, V., Scholz, F., Doll, M., Deng, L., Fiskal, A., Lever, M.A. and Su, C.-C. (2018) On the formation of hydrothermal vents and cold seeps in the Guaymas Basin, Gulf of California. Biogeosciences 15, 5715-5731.

Gliozzi, A., Paoli, G., De Rosa, M. and Gambacorta, A. (1983) Effect of isoprenoid cyclization on the transition temperature of lipids in thermophilic archaebacteria. Biochimica et Biophysica Acta (BBA) - Biomembranes 735, 234-242.

Graw, M.F. (2017) Characterizing drivers of microbial community structure and function in diverse marine sediments. Doctoral dissertation, Oregon State University, Corvallis, OR, USA.

Guschina, I.A. and Harwood, J.L. (2006) Lipids and lipid metabolism in eukaryotic algae. Progress in Lipid Research 45, 160-186.

Hahn, C.J., Laso-Pérez, R., Vulcano, F., Vaziourakis, K.-M., Stokke, R., Steen, I.H., Teske, A., Boetius, A., Liebeke, M., Amann, R., Knittel, K. and Wegener, G. (2020) "Candidatus Ethanoperedens," a Thermophilic Genus of Archaea Mediating the Anaerobic Oxidation of Ethane. mBio 11, e00600-00620.

Haroon, M.F., Hu, S., Shi, Y., Imelfort, M., Keller, J., Hugenholtz, P., Yuan, Z. and Tyson, G.W. (2013) Anaerobic oxidation of methane coupled to nitrate reduction in a novel archaeal lineage. Nature 500, 567-570.

Harvey, H.R., Fallon, R.D. and Patton, J.S. (1986) The effect of organic matter and oxygen on the degradation of bacterial membrane lipids in marine sediments. Geochimica et Cosmochimica Acta 50, 795-804.

Head, I.M., Jones, D.M. and Larter, S.R. (2003) Biological activity in the deep subsurface and the origin of heavy oil. Nature 426, 344-352.

Heuer, V., Elvert, M., Tille, S., Krummen, M., Mollar, X.P., Hmelo, L.R. and Hinrichs, K.U. (2006) Online δ13C analysis of volatile fatty acids in sediment/porewater systems by liquid chromatography‐isotope ratio mass spectrometry. Limnology and Oceanography: Methods 4, 346-357.

Hinrichs, K.-U., Hayes, J.M., Bach, W., Spivack, A.J., Hmelo, L.R., Holm, N.G., Johnson, C.G. and Sylva, S.P. (2006) Biological formation of ethane and propane in the deep marine subsurface. Proceedings of the National Academy of Sciences 103, 14684-14689.

Hinrichs, K.-U., Hayes, J.M., Sylva, S.P., Brewer, P.G. and DeLong, E.F. (1999) Methane-consuming archaebacteria in marine sediments. Nature 398, 802-805.

Hinrichs, K.-U., Hmelo, L.R. and Sylva, S.P. (2003) Molecular fossil record of elevated methane levels in late Pleistocene coastal waters. Science 299, 1214-1217.

Hoehler, T.M. and Jørgensen, B.B. (2013) Microbial life under extreme energy limitation. Nature Reviews Microbiology 11, 83-94.

Holler, T., Widdel, F., Knittel, K., Amann, R., Kellermann, M.Y., Hinrichs, K.-U., Teske, A., Boetius, A. and Wegener, G. (2011) Thermophilic anaerobic oxidation of methane by marine microbial consortia. The ISME journal 5, 1946-1956.

Hölzl, G. and Dörmann, P. (2007) Structure and function of glycoglycerolipids in plants and bacteria. Progress in lipid research 46, 225-243.

Hopmans, E.C., Schouten, S., Pancost, R.D., van der Meer, M.T. and Sinninghe Damsté, J.S. (2000) Analysis of intact tetraether lipids in archaeal cell material and sediments by high performance liquid chromatography/atmospheric pressure chemical ionization mass spectrometry. Rapid Communications in Mass Spectrometry 14, 585-589.

Hopmans, E.C., Weijers, J.W., Schefuß, E., Herfort, L., Sinninghe Damsté, J.S. and Schouten, S. (2004) A novel proxy for terrestrial organic matter in sediments based on branched and isoprenoid tetraether lipids. Earth and Planetary Science Letters 224, 107-116.

Hu, J., Meyers, P.A., Chen, G. and Yang, Q. (2012) Archaeal and bacterial glycerol dialkyl glycerol tetraethers in sediments from the Eastern Lau Spreading Center, South Pacific Ocean. Organic geochemistry 43, 162-167.

Hunt, J.M. (1984) Generation and migration of light hydrocarbons. Science 226, 1265-1270.

Jaekel, U., Musat, N., Adam, B., Kuypers, M., Grundmann, O. and Musat, F. (2013) Anaerobic degradation of propane and butane by sulfate-reducing bacteria enriched from marine hydrocarbon cold seeps. The ISME journal 7, 885-895.

Jaeschke, A., Eickmann, B., Lang, S.Q., Bernasconi, S.M., Strauss, H. and Früh-Green, G.L. (2014) Biosignatures in chimney structures and sediment from the Loki's Castle low-temperature hydrothermal vent field at the Arctic Mid-Ocean Ridge. Extremophiles 18, 545-560.

Jaeschke, A., Jørgensen, S., Bernasconi, S.M., Pedersen, R.B., Thorseth, I.H. and Früh‐Green, G.L. (2012) Microbial diversity of Loki's Castle black smokers at the Arctic Mid‐Ocean Ridge. Geobiology 10, 548-561.

Johnson, J.W., Oelkers, E.H. and Helgeson, H.C. (1992) SUPCRT92: A software package for calculating the standard molal thermodynamic properties of minerals, gases, aqueous species, and reactions from 1 to 5000 bar and 0 to 1000 C. Computers & Geosciences 18, 899-947.

Jørgensen, B.B. and Boetius, A. (2007) Feast and famine—microbial life in the deep-sea bed. Nature Reviews Microbiology 5, nrmicro1745.

Jørgensen, B.B., Isaksen, M.F. and Jannasch, H.W. (1992) Bacterial sulfate reduction above 100 C in deep-sea hydrothermal vent sediments. Science 258, 1756-1757.

Jørgensen, B.B., Zawacki, L.X. and Jannasch, H.W. (1990) Thermophilic bacterial sulfate reduction in deep-sea sediments at the Guaymas Basin hydrothermal vent site (Gulf of California). Deep Sea Research Part A. Oceanographic Research Papers 37, 695-710.

Joye, S.B., Boetius, A., Orcutt, B.N., Montoya, J.P., Schulz, H.N., Erickson, M.J. and Lugo, S.K. (2004) The anaerobic oxidation of methane and sulfate reduction in sediments from Gulf of Mexico cold seeps. Chemical Geology 205, 219-238.

Kaneda, T. (1991) Iso- and anteiso-fatty acids in bacteria: biosynthesis, function, and taxonomic significance. Microbiol Rev 55, 288-302.

Kannenberg, E.L. and Poralla, K. (1999) Hopanoid biosynthesis and function in bacteria. Naturwissenschaften 86, 168-176.

Kates, M., Kushner, D.J. and Matheson, A. (1993) The biochemistry of archaea (archaebacteria). Elsevier.

Kellermann, M.Y., Wegener, G., Elvert, M., Yoshinaga, M.Y., Lin, Y.-S., Holler, T., Mollar, X.P., Knittel, K. and Hinrichs, K.-U. (2012) Autotrophy as a predominant mode of carbon fixation in anaerobic methane-oxidizing microbial communities. Proceedings of the National Academy of Sciences 109, 19321-19326.

Kellermann, M.Y., Yoshinaga, M.Y., Wegener, G., Krukenberg, V. and Hinrichs, K.-U. (2016) Tracing the production and fate of individual archaeal intact polar lipids using stable isotope probing. Organic Geochemistry.

Kelley, D.S. (1996) Methane‐rich fluids in the oceanic crust. Journal of Geophysical Research: Solid Earth 101, 2943-2962.

Kelley, D.S., Karson, J.A., Früh-Green, G.L., Yoerger, D.R., Shank, T.M., Butterfield, D.A., Hayes, J.M., Schrenk, M.O., Olson, E.J. and Proskurowski, G. (2005) A serpentinite-hosted ecosystem: the Lost City hydrothermal field. Science 307, 1428-1434.

Kelts, K., Curray, J.R. and Moore, D.G. (1982) Introduction and explanatory notes. *In* Curray, J.R., Moore, D.G., et al., *Initial Reports of the Deep Sea Drilling Project*, 64: Washington, DC (U.S. Govt. Printing Office), 5–26.

Kester, D.R., Duedall, I.W., Connors, D.N. and Pytkowicz, R.M. (1967) Preparation of artificial seawater 1. Limnology and oceanography 12, 176-179.

Khan, T.K. and Chong, P.L.-G. (2000) Studies of Archaebacterial Bipolar Tetraether Liposomes by Perylene Fluorescence. Biophysical Journal 78, 1390-1399.

Kim, J.-H., Van der Meer, J., Schouten, S., Helmke, P., Willmott, V., Sangiorgi, F., Koç, N., Hopmans, E.C. and Damsté, J.S.S. (2010) New indices and calibrations derived from the distribution of crenarchaeal isoprenoid tetraether lipids: Implications for past sea surface temperature reconstructions. Geochimica et Cosmochimica Acta 74, 4639-4654.

Knappy, C.S., Chong, J.P. and Keely, B.J. (2009) Rapid discrimination of archaeal tetraether lipid cores by liquid chromatography-tandem mass spectrometry. Journal of the American Society for Mass Spectrometry 20, 51-59.

Knappy, C.S., Nunn, C.E., Morgan, H.W. and Keely, B.J. (2011) The major lipid cores of the archaeon Ignisphaera aggregans: implications for the phylogeny and biosynthesis of glycerol monoalkyl glycerol tetraether isoprenoid lipids. Extremophiles 15, 517.

Kniemeyer, O., Musat, F., Sievert, S.M., Knittel, K., Wilkes, H., Blumenberg, M., Michaelis, W., Classen, A., Bolm, C. and Joye, S.B. (2007) Anaerobic oxidation of short-chain hydrocarbons by marine sulphate-reducing bacteria. Nature 449, 898-901.

Knittel, K. and Boetius, A. (2009) Anaerobic oxidation of methane: progress with an unknown process. Annual review of microbiology 63, 311-334.

Knittel, K., Wegener, G. and Boetius, A. (2019) Anaerobic methane oxidizers. Microbial Communities Utilizing Hydrocarbons and Lipids: Members, Metagenomics and Ecophysiology, 1-21.

Koga, Y. (2012) Thermal adaptation of the archaeal and bacterial lipid membranes. Archaea 2012.

Koga, Y., Akagawa-Matsushita, M., Ohga, M. and Nishihara, M. (1993) Taxonomic significance of the distribution of component parts of polar ether lipids in methanogens. Systematic and Applied Microbiology 16, 342-351.

Koga, Y., Kyuragi, T., Nishihara, M. and Sone, N. (1998) Did archaeal and bacterial cells arise independently from noncellular precursors? A hypothesis stating that the advent of membrane phospholipid with enantiomeric glycerophosphate backbones caused the separation of the two lines of descent. Journal of molecular evolution 46, 54-63.

Koga, Y. and Morii, H. (2005) Recent advances in structural research on ether lipids from archaea including comparative and physiological aspects. Bioscience, biotechnology, and biochemistry 69, 2019-2034.

Krukenberg, V., Harding, K., Richter, M., Glöckner, F.O., Gruber‐Vodicka, H.R., Adam, B., Berg, J.S., Knittel, K., Tegetmeyer, H.E. and Boetius, A. (2016) Candidatus Desulfofervidus auxilii, a hydrogenotrophic sulfate‐reducing bacterium involved in the thermophilic anaerobic oxidation of methane. Environmental microbiology 18, 3073-3091.

Kubo, K., Lloyd, K.G., Biddle, J.F., Amann, R., Teske, A. and Knittel, K. (2012) Archaea of the Miscellaneous Crenarchaeotal Group are abundant, diverse and widespread in marine sediments. The ISME journal 6, 1949-1965.

Langworthy, T.A. (1982) Lipids of bacteria living in extreme environments, Current topics in membranes and transport. Elsevier, pp. 45-77.

Laso-Pérez, R., Hahn, C., van Vliet, D.M., Tegetmeyer, H.E., Schubotz, F., Smit, N.T., Pape, T., Sahling, H., Bohrmann, G. and Boetius, A. (2019) Anaerobic Degradation of Non-Methane Alkanes by "Candidatus Methanoliparia" in Hydrocarbon Seeps of the Gulf of Mexico. mBio 10, e01814-01819.

Laso-Pérez, R., Wegener, G., Knittel, K., Widdel, F., Harding, K.J., Krukenberg, V., Meier, D.V., Richter, M., Tegetmeyer, H.E. and Riedel, D. (2016) Thermophilic archaea activate butane via alkyl-coenzyme M formation. Nature 539, 396-401.

Leonte, M., Kessler, J.D., Kellermann, M.Y., Arrington, E.C., Valentine, D.L. and Sylva, S.P. (2017) Rapid rates of aerobic methane oxidation at the feather edge of gas hydrate stability in the waters of Hudson Canyon, US Atlantic Margin. Geochimica et Cosmochimica Acta 204, 375-387.

Lincoln, S.A., Bradley, A.S., Newman, S.A. and Summons, R.E. (2013) Archaeal and bacterial glycerol dialkyl glycerol tetraether lipids in chimneys of the Lost City Hydrothermal Field. Organic geochemistry 60, 45-53.

Lingwood, D. and Simons, K. (2010) Lipid rafts as a membrane-organizing principle. science 327, 46-50.

Liu, X.-L., Birgel, D., Elling, F.J., Sutton, P.A., Lipp, J.S., Zhu, R., Zhang, C., Könneke, M., Peckmann, J. and Rowland, S.J. (2016) From ether to acid: A plausible degradation pathway of glycerol dialkyl glycerol tetraethers. Geochimica et Cosmochimica Acta 183, 138-152.

Liu, X.-L., Zhu, C., Wakeham, S.G. and Hinrichs, K.-U. (2014) In situ production of branched glycerol dialkyl glycerol tetraethers in anoxic marine water columns. Marine Chemistry 166, 1-8.

Liu, X.L., Summons, R.E. and Hinrichs, K.U. (2012) Extending the known range of glycerol ether lipids in the environment: structural assignments based on tandem mass spectral fragmentation patterns. Rapid Communications in Mass Spectrometry 26, 2295-2302.

Lizarralde, D., Soule, S.A., Seewald, J.S. and Proskurowski, G. (2011) Carbon release by off-axis magmatism in a young sedimented spreading centre. Nature Geoscience 4, 50-54.

Lloyd, K.G., Schreiber, L., Petersen, D.G., Kjeldsen, K.U., Lever, M.A., Steen, A.D., Stepanauskas, R., Richter, M., Kleindienst, S. and Lenk, S. (2013) Predominant archaea in marine sediments degrade detrital proteins. Nature 496, 215-218.

Lollar, B.S., Westgate, T., Ward, J., Slater, G. and Lacrampe-Couloume, G. (2002) Abiogenic formation of alkanes in the Earth's crust as a minor source for global hydrocarbon reservoirs. Nature 416, 522-524.

Lonsdale, P. (1985) A transform continental margin rich in hydrocarbons, Gulf of California. AAPG bulletin 69, 1160-1180.

Lonsdale, P. and Becker, K. (1985) Hydrothermal plumes, hot springs, and conductive heat flow in the Southern Trough of Guaymas Basin. Earth and Planetary Science Letters 73, 211-225.

Lonsdale, P. and Lawver, L. (1980) Immature plate boundary zones studied with a submersible in the Gulf of California. Geological Society of America Bulletin 91, 555-569.

Lösekann, T., Knittel, K., Nadalig, T., Fuchs, B., Niemann, H., Boetius, A. and Amann, R. (2007) Diversity and abundance of aerobic and anaerobic methane oxidizers at the Haakon Mosby Mud Volcano, Barents Sea. Appl. Environ. Microbiol. 73, 3348-3362.

Lutnaes, B.F., Brandal, Ø., Sjöblom, J. and Krane, J. (2006) Archaeal C 80 isoprenoid tetraacids responsible for naphthenate deposition in crude oil processing. Organic & biomolecular chemistry 4, 616-620.

Madigan, M.T., Martinko, J.M. and Parker, J. (1997) Brock biology of microorganisms. Prentice hall Upper Saddle River, NJ.

Magen, C., Lapham, L.L., Pohlman, J.W., Marshall, K., Bosman, S., Casso, M. and Chanton, J.P. (2014) A simple headspace equilibration method for measuring dissolved methane. Limnology and Oceanogaphy: Methods 12, 637-650.

Martens, C.S. (1990) Generation of short chain acid anions in hydrothermally altered sediments of the Guaymas Basin, Gulf of California. Applied Geochemistry 5, 71-76.

Martin, W., Baross, J., Kelley, D. and Russell, M.J. (2008) Hydrothermal vents and the origin of life. Nature Reviews Microbiology 6, 805-814.

McCollom, T.M. and Seewald, J.S. (2003a) Experimental constraints on the hydrothermal reactivity of organic acids and acid anions: I. Formic acid and formate. Geochimica et Cosmochimica Acta 67, 3625-3644.

McCollom, T.M. and Seewald, J.S. (2003b) Experimental study of the hydrothermal reactivity of organic acids and acid anions: II. Acetic acid, acetate, and valeric acid. Geochimica et Cosmochimica Acta 67, 3645-3664.

McGlynn, S.E., Chadwick, G.L., Kempes, C.P. and Orphan, V.J. (2015) Single cell activity reveals direct electron transfer in methanotrophic consortia. Nature 526, 531-535.

McKay, L., Klokman, V.W., Mendlovitz, H.P., LaRowe, D.E., Hoer, D.R., Albert, D., Amend, J.P. and Teske, A. (2016) Thermal and geochemical influences on microbial biogeography in the hydrothermal sediments of Guaymas Basin, Gulf of California. Environmental microbiology reports 8, 150-161.

McKay, L.J., MacGregor, B.J., Biddle, J.F., Albert, D.B., Mendlovitz, H.P., Hoer, D.R., Lipp, J.S., Lloyd, K.G. and Teske, A.P. (2012) Spatial heterogeneity and underlying geochemistry of phylogenetically diverse orange and white< i> Beggiatoa</i> mats in Guaymas Basin hydrothermal sediments. Deep Sea Research Part I: Oceanographic Research Papers 67, 21-31.

Meador, T.B., Bowles, M., Lazar, C.S., Zhu, C., Teske, A. and Hinrichs, K.U. (2015) The archaeal lipidome in estuarine sediment dominated by members of the Miscellaneous Crenarchaeotal Group. Environmental microbiology 17, 2441-2458.

Meyer, S., Wegener, G., Lloyd, K.G., Teske, A., Boetius, A. and Ramette, A. (2013) Microbial habitat connectivity across spatial scales and hydrothermal temperature gradients at Guaymas Basin. Frontiers in microbiology 4, 207.

Meyerdierks, A., Kube, M., Kostadinov, I., Teeling, H., Glöckner, F.O., Reinhardt, R. and Amann, R. (2010) Metagenome and mRNA expression analyses of anaerobic methanotrophic archaea of the ANME‐1 group. Environmental microbiology 12, 422-439.

Michael, P., Langmuir, C., Dick, H., Snow, J., Goldstein, S., Graham, D., Lehnert, K., Kurras, G., Jokat, W. and Mühe, R. (2003) Magmatic and amagmatic seafloor generation at the ultraslow-spreading Gakkel ridge, Arctic Ocean. Nature 423, 956-961.

Milkov, A. (2000) Worldwide distribution of submarine mud volcanoes and associated gas hydrates. Marine Geology 167, 29-42.

Milkov, A.V. (2004) Global estimates of hydrate-bound gas in marine sediments: how much is really out there? Earth-Science Reviews 66, 183-197.

Minster, J.B. and Jordan, T.H. (1978) Present‐day plate motions. Journal of Geophysical Research: Solid Earth 83, 5331-5354.

Moore, D.G. (1973) Plate-edge deformation and crustal growth, Gulf of California structural province. Geological Society of America Bulletin 84, 1883-1906.

Morii, H., Eguchi, T., Nishihara, M., Kakinuma, K., König, H. and Koga, Y. (1998) A novel ether core lipid with H-shaped C< sub> 80</sub>-isoprenoid hydrocarbon chain from the hyperthermophilic methanogen< i> Methanothermus fervidus</i>. Biochimica et Biophysica Acta (BBA)-Lipids and Lipid Metabolism 1390, 339-345.

Nakagawa, T., Takai, K., Suzuki, Y., Hirayama, H., Konno, U., Tsunogai, U. and Horikoshi, K. (2006) Geomicrobiological exploration and characterization of a novel deep‐sea hydrothermal system at the TOTO caldera in the Mariana Volcanic Arc. Environmental Microbiology 8, 37-49.

Nicolson, G.L. (2014) The Fluid—Mosaic Model of Membrane Structure: Still relevant to understanding the structure, function and dynamics of biological membranes after more than 40 years. Biochimica et Biophysica Acta (BBA)-Biomembranes 1838, 1451-1466.

Niemann, H., Lösekann, T., de Beer, D., Elvert, M., Nadalig, T., Knittel, K., Amann, R., Sauter, E.J., Schlüter, M. and Klages, M. (2006) Novel microbial communities of the Haakon Mosby mud volcano and their role as a methane sink. Nature 443, 854-858.

OpenStax (2020) Microbiology (OpenStax). https://bio.libretexts.org/link?5285. Licenced under https://creativecommons.org/licenses/by-nc-sa/3.0/us/. Access Date June 8, 2020.

Orcutt, B., Boetius, A., Elvert, M., Samarkin, V. and Joye, S.B. (2005) Molecular biogeochemistry of sulfate reduction, methanogenesis and the anaerobic oxidation of methane at Gulf of Mexico cold seeps. Geochimica et Cosmochimica Acta 69, 4267-4281.

Orcutt, B.N., LaRowe, D.E., Biddle, J.F., Colwell, F.S., Glazer, B.T., Reese, B.K., Kirkpatrick, J.B., Lapham, L.L., Mills, H.J. and Sylvan, J.B. (2013) Microbial activity in the marine deep biosphere: progress and prospects. Frontiers in microbiology 4.

Orphan, V.J., Ussler III, W., Naehr, T.H., House, C.H., Hinrichs, K.-U. and Paull, C.K. (2004) Geological, geochemical, and microbiological heterogeneity of the seafloor around methane vents in the Eel River Basin, offshore California. Chemical Geology 205, 265-289.

Oshima, M. and Miyagawa, A. (1974) Comparative studies on the fatty acid composition of moderately and extremely thermophilic bacteria. Lipids 9, 476-480.

Paull, C.K., Hecker, B., Commeau, R., Freeman-Lynde, R., Neumann, C., Corso, W., Golubic, S., Hook, J., Sikes, E. and Curray, J. (1984) Biological communities at the Florida Escarpment resemble hydrothermal vent taxa. Science 226, 965-967.

Pearson, A., Huang, Z., Ingalls, A., Romanek, C., Wiegel, J., Freeman, K., Smittenberg, R. and Zhang, C. (2004) Nonmarine crenarchaeol in Nevada hot springs. Applied and Environmental Microbiology 70, 5229-5237.

Pearson, A., Seewald, J.S. and Eglinton, T.I. (2005) Bacterial incorporation of relict carbon in the hydrothermal environment of Guaymas Basin. Geochimica et Cosmochimica Acta 69, 5477-5486.

Peter, J., Peltonen, P., Scott, S., Simoneit, B. and Kawka, O. (1991) 14C ages of hydrothermal petroleum and carbonate in Guaymas Basin, Gulf of California: implications for oil generation, expulsion, and migration. Geology 19, 253-256.

Peters, K.E. and Moldowan, J.M. (1993) The biomarker guide: interpreting molecular fossils in petroleum and ancient sediments.

Phrampus, B.J. and Hornbach, M.J. (2012) Recent changes to the Gulf Stream causing widespread gas hydrate destabilization. Nature 490, 527-530.

Pohlman, J.W., Casso, M. and Bergeron, E. (In Prep) Discrete sample introduction module (DSIM) for quantitative and isotopic analysis of gases by cavity ring-down spectroscopy. Environmental Science & Technology.

Pohlman, J.W., Riedel, M., Bauer, J.E., Canuel, E.A., Paull, C.K., Lapham, L., Grabowski, K.S., Coffin, R.B. and Spence, G.D. (2013) Anaerobic methane oxidation in low-organic content methane seep sediments. Geochimica et Cosmochimica Acta 108, 184-201.

Prinzhofer, A.A. and Huc, A.Y. (1995) Genetic and post-genetic molecular and isotopic fractionations in natural gases. Chemical Geology 126, 281-290.

Probst, A.J., Elling, F.J., Castelle, C.J., Zhu, Q., Elvert, M., Birarda, G., Holman, H.-Y.N., Lane, K.R., Ladd, B. and Ryan, M.C. (2020) Lipid analysis of CO 2-rich subsurface aquifers suggests an autotrophy-based deep biosphere with lysolipids enriched in CPR bacteria. The ISME Journal, 1-14.

Proskurowski, G., Lilley, M.D., Seewald, J.S., Früh-Green, G.L., Olson, E.J., Lupton, J.E., Sylva, S.P. and Kelley, D.S. (2008) Abiogenic hydrocarbon production at Lost City hydrothermal field. Science 319, 604-607.

Prouty, N.G., Sahy, D., Ruppel, C.D., Roark, E.B., Condon, D., Brooke, S., Ross, S.W. and Demopoulos, A.W. (2016) Insights into methane dynamics from analysis of authigenic carbonates and chemosynthetic mussels at newly-discovered Atlantic Margin seeps. Earth and Planetary Science Letters 449, 332-344.

Reeburgh, W.S. (1996) "Soft spots" in the global methane budget, Microbial growth on C1 compounds. Springer, pp. 334-342.

Reeburgh, W.S. (2007) Oceanic methane biogeochemistry. Chemical reviews 107, 486-513.

Reitner, J., Peckmann, J., Reimer, A., Schumann, G. and Thiel, V. (2005) Methane-derived carbonate build-ups and associated microbial communities at cold seeps on the lower Crimean shelf (Black Sea). Facies 51, 66-79.

Riedel, M., Scherwath, M., Römer, M., Veloso, M., Heesemann, M. and Spence, G.D. (2018) Distributed natural gas venting offshore along the Cascadia margin. Nature communications 9, 1-14.

Rossel, P.E., Elvert, M., Ramette, A., Boetius, A. and Hinrichs, K.-U. (2011) Factors controlling the distribution of anaerobic methanotrophic communities in marine environments: evidence from intact polar membrane lipids. Geochimica et Cosmochimica Acta 75, 164-184.

Rossel, P.E., Lipp, J.S., Fredricks, H.F., Arnds, J., Boetius, A., Elvert, M. and Hinrichs, K.-U. (2008) Intact polar lipids of anaerobic methanotrophic archaea and associated bacteria. Organic Geochemistry 39, 992-999.

Ruff, S.E., Biddle, J.F., Teske, A.P., Knittel, K., Boetius, A. and Ramette, A. (2015) Global dispersion and local diversification of the methane seep microbiome. Proceedings of the National Academy of Sciences 112, 4015-4020.

Rütters, H., Sass, H., Cypionka, H. and Rullkötter, J. (2001) Monoalkylether phospholipids in the sulfate-reducing bacteria Desulfosarcina variabilis and Desulforhabdus amnigenus. Archives of microbiology 176, 435-442.

Sáenz, J.P., Grosser, D., Bradley, A.S., Lagny, T.J., Lavrynenko, O., Broda, M. and Simons, K. (2015) Hopanoids as functional analogues of cholesterol in bacterial membranes. Proceedings of the National Academy of Sciences 112, 11971-11976.

Schoell, M. (1988) Multiple origins of methane in the earth. Chemical geology 71, 1-10.

Schouten, S., Baas, M., Hopmans, E.C., Reysenbach, A.-L. and Damsté, J.S.S. (2008) Tetraether membrane lipids of Candidatus "Aciduliprofundum boonei", a cultivated obligate thermoacidophilic euryarchaeote from deep-sea hydrothermal vents. Extremophiles 12, 119-124.

Schouten, S., Hopmans, E.C. and Damsté, J.S.S. (2013) The organic geochemistry of glycerol dialkyl glycerol tetraether lipids: a review. Organic geochemistry 54, 19-61.

Schouten, S., Hopmans, E.C., Pancost, R.D. and Damsté, J.S.S. (2000) Widespread occurrence of structurally diverse tetraether membrane lipids: evidence for the ubiquitous presence of low-temperature relatives of hyperthermophiles. Proceedings of the National Academy of Sciences 97, 14421-14426.

Schouten, S., Hopmans, E.C., Schefuß, E. and Sinninghe Damsté, J.S. (2002) Distributional variations in marine crenarchaeotal membrane lipids: a new tool for reconstructing ancient sea water temperatures? Earth and Planetary Science Letters 204, 265-274.

Schouten, S., Wakeham, S.G., Hopmans, E.C. and Damsté, J.S.S. (2003) Biogeochemical evidence that thermophilic archaea mediate the anaerobic oxidation of methane. Applied and environmental microbiology 69, 1680-1686.

Schreiber, L., Holler, T., Knittel, K., Meyerdierks, A. and Amann, R. (2010) Identification of the dominant sulfate‐reducing bacterial partner of anaerobic methanotrophs of the ANME‐2 clade. Environmental microbiology 12, 2327-2340.

Schröder, J.M. (2015) Intact polar lipids in marine sediments: improving analytical protocols and assessing planktonic and benthic sources. Universität Bremen.

Schubotz, F. (2018) Membrane Homeostasis upon Nutrient (C, N, P) Limitation, in: Geiger, O. (Ed.), Biogenesis of Fatty Acids, Lipids and Membranes. Springer International Publishing, Cham, pp. 1-25.

Schubotz, F. (2019) Membrane Homeostasis upon Nutrient (C, N, P) Limitation. Biogenesis of Fatty Acids, Lipids and Membranes, 823-847.

Schubotz, F., Hays, L.E., D'Arcy, R., Gillespie, A., Shock, E.L. and Summons, R.E. (2015) Stable isotope labeling confirms mixotrophic nature of streamer biofilm communities at alkaline hot springs. Frontiers in microbiology 6.

Schubotz, F., Lipp, J.S., Elvert, M. and Hinrichs, K.-U. (2011) Stable carbon isotopic compositions of intact polar lipids reveal complex carbon flow patterns among hydrocarbon degrading microbial communities at the Chapopote asphalt volcano. Geochimica et Cosmochimica Acta 75, 4399-4415.

Schubotz, F., Xie, S., Lipp, J.S., Hinrichs, K.-U. and Wakeham, S.G. (2018) Intact polar lipids in the water column of the eastern tropical North Pacific: abundance and structural variety of non-phosphorus lipids. Biogeosciences 15, 6481-6501.

Seitz, K.W., Dombrowski, N., Eme, L., Spang, A., Lombard, J., Sieber, J.R., Teske, A.P., Ettema, T.J. and Baker, B.J. (2019) Asgard archaea capable of anaerobic hydrocarbon cycling. Nature communications 10, 1-11.

Shigeo, A., Michie, K., Masataka, I. and Makoto, K. (1972) Changes in positional distribution of fatty acids in the phospholipids of Escherichia coli after shift-down in temperature. Biochimica et Biophysica Acta (BBA) - Lipids and Lipid Metabolism 270, 301-306.

Siliakus, M.F., van der Oost, J. and Kengen, S.W.M. (2017) Adaptations of archaeal and bacterial membranes to variations in temperature, pH and pressure. Extremophiles 21, 651-670.

Simoneit, B. and Kawka, O. (1987) Hydrothermal petroleum from diatomites in the Gulf of California. Geological Society, London, Special Publications 26, 217-228.

Simoneit, B., Lonsdale, P., Edmond, J. and Shanks III, W.C. (1990) Deep-water hydrocarbon seeps in Guaymas Basin, Gulf of California. Applied Geochemistry 5, 41-49.

Simoneit, B.R. (1985) Hydrothermal petroleum: genesis, migration, and deposition in Guaymas Basin, Gulf of California. Canadian Journal of Earth Sciences 22, 1919-1929.

Simoneit, B.R. (1990) Petroleum generation, an easy and widespread process in hydrothermal systems: an overview. Applied Geochemistry 5, 3-15.

Simoneit, B.R. and Galimov, E.M. (1984) Geochemistry of interstitial gases in Quaternary sediments of the Gulf of California. Chemical geology 43, 151-166.

Simoneit, B.R., Kawka, O. and Brault, M. (1988) Origin of gases and condensates in the Guaymas Basin hydrothermal system (Gulf of California). Chemical Geology 71, 169-182.

Simoneit, B.R., Mazurek, M., Brenner, S., Crisp, P. and Kaplan, I. (1979) Organic geochemistry of recent sediments from Guaymas Basin, Gulf of California. Deep Sea Research Part A. Oceanographic Research Papers 26, 879-891.

Simoneit, B.R., Summerhayes, C.P. and Meyers, P.A. (1986) Sources and hydrothermal alteration of organic matter in Quaternary sediments: a synthesis of studies from the Central Gulf of California. Marine and petroleum geology 3, 282-297.

Singer, S.J. and Nicolson, G.L. (1972) The fluid mosaic model of the structure of cell membranes. Science 175, 720-731.

Skarke, A., Ruppel, C., Kodis, M., Brothers, D. and Lobecker, E. (2014) Widespread methane leakage from the sea floor on the northern US Atlantic margin, Nature Geoscience.

Sollich, M., Yoshinaga, M.Y., Häusler, S., Price, R.E., Hinrichs, K.-U. and Bühring, S.I. (2017) Heat stress dictates microbial lipid composition along a thermal gradient in marine sediments. Frontiers in microbiology 8, 1550.

Sturt, H.F., Summons, R.E., Smith, K., Elvert, M. and Hinrichs, K.U. (2004) Intact polar membrane lipids in prokaryotes and sediments deciphered by high ‐ performance liquid chromatography/electrospray ionization multistage mass spectrometry—new biomarkers for biogeochemistry and microbial ecology. Rapid Communications in Mass Spectrometry 18, 617-628.

Sugai, A., Uda, I., Itoh, Y.H. and ITOH, T. (2004) The core lipid composition of the 17 strains of hyperthermophilic archaea, Thermococcales. Journal of Oleo Science 53, 41-44.

Teske, A., Callaghan, A.V. and LaRowe, D.E. (2014) Biosphere frontiers of subsurface life in the sedimented hydrothermal system of Guaymas Basin. Frontiers in microbiology 5.

Teske, A., De Beer, D., McKay, L.J., Tivey, M.K., Biddle, J.F., Hoer, D., Lloyd, K.G., Lever, M.A., Røy, H. and Albert, D.B. (2016) The Guaymas Basin hiking guide to hydrothermal mounds, chimneys, and microbial mats: complex seafloor expressions of subsurface hydrothermal circulation. Frontiers in microbiology 7.

Teske, A., Hinrichs, K.-U., Edgcomb, V., de Vera Gomez, A., Kysela, D., Sylva, S.P., Sogin, M.L. and Jannasch, H.W. (2002) Microbial diversity of hydrothermal sediments in the Guaymas Basin: evidence for anaerobic methanotrophic communities. Applied and Environmental Microbiology 68, 1994-2007.

Teske, A., McKay, L.J., Ravelo, A.C., Aiello, I., Mortera, C., Núñez-Useche, F., Canet, C., Chanton, J.P., Brunner, B. and Hensen, C. (2019) Characteristics and Evolution of sill-driven off-axis hydrothermalism in Guaymas Basin–the Ringvent site. Scientific reports 9, 1-16.

Tissot, B.P., Pelet, R. and Ungerer, P. (1987) Thermal history of sedimentary basins, maturation indices, and kinetics of oil and gas generation. AAPG bulletin 71, 1445-1466.

Turner, P.J., Ball, B., Diana, Z., Fariñas-Bermejo, A., Grace, I., McVeigh, D., Powers, M.M., Van Audenhaege, L., Maslakova, S. and Young, C.M. (2020) Methane seeps on the US Atlantic margin and their potential importance to populations of the commercially valuable deep-sea red crab, Chaceon quinquedens. Frontiers in Marine Science 7, 75.

Uda, I., Sugai, A., Itoh, Y.H. and Itoh, T. (2001) Variation in molecular species of polar lipids from Thermoplasma acidophilum depends on growth temperature. Lipids 36, 103-105.

Valentine, D.L. (2007) Adaptations to energy stress dictate the ecology and evolution of the Archaea. Nature Reviews Microbiology 5, 316-323.

Valentine, D.L. and Boone, D.R. (2000) Diversity of methanogens, Journey to Diverse Microbial Worlds. Springer, pp. 289-302.

van Meer, G., Voelker, D.R. and Feigenson, G.W. (2008) Membrane lipids: where they are and how they behave. Nature Reviews Molecular Cell Biology 9, 112-124.

Von Damm, K., Parker, C., Zierenberg, R., Lilley, M., Olson, E., Clague, D. and McClain, J. (2005) The Escanaba Trough, Gorda Ridge hydrothermal system: Temporal stability and subseafloor complexity. Geochimica et Cosmochimica Acta 69, 4971-4984.

Von Damm, K.v., Edmond, J.t. and Grant, B. (1985) Chemistry of submarine hydrothermal solutions at Guaymas Basin, Gulf of California. Geochimica et Cosmochimica Acta 49, 2221-2237.

Wang, D.T., Gruen, D.S., Lollar, B.S., Hinrichs, K.-U., Stewart, L.C., Holden, J.F., Hristov, A.N., Pohlman, J.W., Morrill, P.L. and Könneke, M. (2015) Nonequilibrium clumped isotope signals in microbial methane. Science 348, 428-431.

Wang, F.-P., Zhang, Y., Chen, Y., He, Y., Qi, J., Hinrichs, K.-U., Zhang, X.-X., Xiao, X. and Boon, N. (2014) Methanotrophic archaea possessing diverging methane-oxidizing and electron-transporting pathways. The ISME journal 8, 1069-1078.

Wang, Y., Wegener, G., Hou, J., Wang, F. and Xiao, X. (2019) Expanding anaerobic alkane metabolism in the domain of Archaea. Nature microbiology, 1.

Wang, Y., Wegener, G., Ruff, S.E. and Wang, F. (2020) Methyl/alkyl‐coenzyme M reductase‐based anaerobic alkane oxidation in archaea. Environmental Microbiology.

Wegener, G., Krukenberg, V., Riedel, D., Tegetmeyer, H.E. and Boetius, A. (2015) Intercellular wiring enables electron transfer between methanotrophic archaea and bacteria. Nature 526, 587-590.

Weijers, J.W., Schouten, S., Hopmans, E.C., Geenevasen, J.A., David, O.R., Coleman, J.M., Pancost, R.D. and Sinninghe Damsté, J.S. (2006a) Membrane lipids of mesophilic anaerobic bacteria thriving in peats have typical archaeal traits. Environmental Microbiology 8, 648-657.

Weijers, J.W., Schouten, S., Spaargaren, O.C. and Sinninghe Damsté, J.S. (2006b) Occurrence and distribution of tetraether membrane lipids in soils: Implications for the use of the TEX< sub> 86</sub> proxy and the BIT index. Organic Geochemistry 37, 1680-1693.

Weijers, J.W., Schouten, S., van den Donker, J.C., Hopmans, E.C. and Sinninghe Damsté, J.S. (2007) Environmental controls on bacterial tetraether membrane lipid distribution in soils. Geochimica et Cosmochimica Acta 71, 703-713.

Weinstein, A., Navarrete, L., Ruppel, C., Weber, T.C., Leonte, M., Kellermann, M.Y., Arrington, E.C., Valentine, D.L., Scranton, M.I. and Kessler, J.D. (2016) Determining the flux of methane into H udson C anyon at the edge of methane clathrate hydrate stability. Geochemistry, Geophysics, Geosystems 17, 3882-3892.

Welhan, J. and Lupton, J. (1987) Light hydrocarbon gases in Guaymas Basin hydrothermal fluids: thermogenic versus abiogenic origin. AAPG Bulletin 71, 215-223.

White, D., Davis, W., Nickels, J., King, J. and Bobbie, R. (1979) Determination of the sedimentary microbial biomass by extractible lipid phosphate. Oecologia 40, 51-62.

Whiticar, M.J. (1999) Carbon and hydrogen isotope systematics of bacterial formation and oxidation of methane. Chemical Geology 161, 291-314.

Whiticar, M.J., Faber, E. and Schoell, M. (1986) Biogenic methane formation in marine and freshwater environments: CO2 reduction vs. acetate fermentation—isotope evidence. Geochimica et Cosmochimica Acta 50, 693-709.

Whitman, W.B., Bowen, T.L. and Boone, D.R. (2006) The Methanogenic Bacteria, in: Dworkin, M., Falkow, S., Rosenberg, E., Schleifer, K.-H., Stackebrandt, E. (Eds.), The Prokaryotes: Volume 3: Archaea. Bacteria: Firmicutes, Actinomycetes. Springer New York, New York, NY, pp. 165-207.

Widdel, F. and Grundmann, O. (2010) Biochemistry of the anaerobic degradation of non-methane alkanes, Handbook of Hydrocarbon and Lipid Microbiology. Springer, pp. 909-924.

Williams, D.L., Becker, K., Lawver, L.A. and Von Herzen, R.P. (1979) Heat flow at the spreading centers of the Guaymas Basin, Gulf of California. Journal of Geophysical Research: Solid Earth 84, 6757-6769.

Woese, C.R., Kandler, O. and Wheelis, M.L. (1990) Towards a natural system of organisms: proposal for the domains Archaea, Bacteria, and Eucarya. Proceedings of the National Academy of Sciences 87, 4576-4579.

Wörmer, L., Lipp, J.S., Schröder, J.M. and Hinrichs, K.-U. (2013) Application of two new LC–ESI–MS methods for improved detection of intact polar lipids (IPLs) in environmental samples. Organic Geochemistry 59, 10-21.

Wuebbles, D.J. and Hayhoe, K. (2002) Atmospheric methane and global change. Earth-Science Reviews 57, 177-210.

Xie, S., Lipp, J.S., Wegener, G., Ferdelman, T.G. and Hinrichs, K.-U. (2013) Turnover of microbial lipids in the deep biosphere and growth of benthic archaeal populations. Proceedings of the National Academy of Sciences 110, 6010-6014.

Xie, S., Liu, X.-L., Schubotz, F., Wakeham, S.G. and Hinrichs, K.-U. (2014) Distribution of glycerol ether lipids in the oxygen minimum zone of the Eastern Tropical North Pacific Ocean. Organic Geochemistry 71, 60-71.

Yamauchi, K., Doi, K., Yoshida, Y. and Kinoshita, M. (1993) Archaebacterial lipids: highly proton-impermeable membranes from 1,2-diphytanyl-sn-glycero-3-phosphocoline. Biochimica et Biophysica Acta (BBA) - Biomembranes 1146, 178-182.

Yoshinaga, M.Y., Kellermann, M.Y., Rossel, P.E., Schubotz, F., Lipp, J.S. and Hinrichs, K.U. (2011) Systematic fragmentation patterns of archaeal intact polar lipids by high ‐ performance liquid chromatography/electrospray ionization ion ‐ trap mass spectrometry. Rapid Communications in Mass Spectrometry 25, 3563-3574.

Yoshinaga, M.Y., Lazar, C.S., Elvert, M., Lin, Y.-S., Zhu, C., Heuer, V.B., Teske, A. and Hinrichs, K.-U. (2015) Possible roles of uncultured archaea in carbon cycling in methane-seep sediments. Geochimica et Cosmochimica Acta 164, 35-52.

Zhang, Y.G., Zhang, C.L., Liu, X.-L., Li, L., Hinrichs, K.-U. and Noakes, J.E. (2011) Methane Index: a tetraether archaeal lipid biomarker indicator for detecting the instability of marine gas hydrates. Earth and Planetary Science Letters 307, 525-534.

Zhou, A., Weber, Y., Chiu, B.K., Elling, F.J., Cobban, A.B., Pearson, A. and Leavitt, W.D. (2019) Energy flux controls tetraether lipid cyclization in Sulfolobus acidocaldarius. Environmental microbiology.

Zhu, C., Lipp, J.S., Wörmer, L., Becker, K.W., Schröder, J. and Hinrichs, K.-U. (2013a) Comprehensive glycerol ether lipid fingerprints through a novel reversed phase liquid chromatography–mass spectrometry protocol. Organic Geochemistry 65, 53-62.

Zhu, C., Meador, T.B., Dummann, W. and Hinrichs, K.U. (2014a) Identification of unusual butanetriol dialkyl glycerol tetraether and pentanetriol dialkyl glycerol tetraether lipids in marine sediments. Rapid Communications in Mass Spectrometry 28, 332-338.

Zhu, C., Wakeham, S.G., Elling, F.J., Basse, A., Mollenhauer, G., Versteegh, G.J., Könneke, M. and Hinrichs, K.U. (2016) Stratification of archaeal membrane lipids in the ocean and implications for adaptation and chemotaxonomy of planktonic archaea. Environmental microbiology 18, 4324-4336.

Zhu, C., Yoshinaga, M.Y., Peters, C.A., Liu, X.L., Elvert, M. and Hinrichs, K.U. (2014b) Identification and significance of unsaturated archaeal tetraether lipids in marine sediments. Rapid Communications in Mass Spectrometry 28, 1144-1152.

Zhu, R., Evans, T.W., Wörmer, L., Lin, Y.-S., Zhu, C. and Hinrichs, K.-U. (2013b) Improved sensitivity of sedimentary phospholipid analysis resulting from a novel extract cleanup strategy. Organic Geochemistry 65, 46-52.

CHAPTER VIII

Contribution as Co-author

Generation and utilization of volatile fatty acids and alcohols in hydrothermally altered sediments in the Guaymas Basin, Gulf of California

Guang-Chao Zhuang[1], Andrew Montgomery[1], Vladimir A. Samarkin[1,5], Min Song[2], Jiarui Liu[3], Florence Schubotz[2], Andreas Teske[4], Kai-Uwe Hinrichs[2], and Samantha B. Joye[1]

Published in *Geophysical Research Letters*, 46. https://doi.org/10.1029/2018GL081284

[1]Department of Marine Sciences, University of Georgia, Athens, Georgia, USA, [2]MARUM Center for Marine Environmental Sciences, University of Bremen, Bremen, Germany, [3]State Key Laboratory of Biogeology and Environment Geology, College of Marine Science and Technology, China University of Geosciences, Wuhan, China, [4]Department of Marine Sciences, University of North Carolina at Chapel Hill, Chapel Hill, North Carolina, USA, [5]Deceased

Correspondence: mjoye@uga.edu

ABSTRACT

Volatile fatty acids (VFAs) and alcohols are key intermediates of anaerobic carbon metabolism, yet their biogeochemical cycling remains poorly constrained in hydrothermal systems. We investigated the abundance, stable carbon isotopic composition, and metabolic cycling of VFAs and alcohols to elucidate their generation and utilization pathways in hydrothermally influenced sediments (4 °C to 90 °C) from the Guaymas Basin. Acetate (up to 229 μM) and methanol (up to 37 μM) were abundant in porewaters. The $\delta^{13}C$ values of acetate varied between -35.6‰ and -18.1‰. Carbon isotopic signatures, thermodynamic predictions, and experimental incubations suggested biological sources such as fermentation and acetogenesis for acetate. Acetate and methanol were predominantly consumed by nonmethanogenic processes (e.g., sulfate reduction), as reflected in high oxidation rates versus low methanogenesis rates, and further evidenced through inhibition experiments with molybdate. These results reveal an important role for VFAs and alcohols as energy sources for diverse chemoheterotrophs in organic-rich hydrothermally influenced sediments.

PLAIN LANGUAGE SUMMARY

Hydrothermal systems are unique seafloor habitats that host abundant and diverse microbial communities, but questions remain regarding their energy strategy and metabolic activity. We found that low molecular weight organic compounds such as acetate and methanol were abundant in the hydrothermal sediments of Guaymas Basin. Multiple lines of evidence suggested that these substrates were produced largely via biological pathways. We further investigated the microbial metabolism of acetate and methanol and found that both compounds could be used as an energy source to support various microbial processes in the hydrothermal systems.